HAL open science

Topological Phases and Majorana Fermions

Loïc Herviou

To cite this version:

Loïc Herviou. Topological Phases and Majorana Fermions. Superconductivity [cond-mat.supr-con]. Université Paris Saclay (COmUE), 2017. English. NNT : 2017SACLX036 . tel-01651575

HAL Id: tel-01651575

https://pastel.hal.science/tel-01651575v1

Submitted on 29 Nov 2017

HAL is a multi-disciplinary open access archive for the deposit and dissemination of scientific research documents, whether they are published or not. The documents may come from teaching and research institutions in France or abroad, or from public or private research centers.

L'archive ouverte pluridisciplinaire **HAL**, est destinée au dépôt et à la diffusion de documents scientifiques de niveau recherche, publiés ou non, émanant des établissements d'enseignement et de recherche français ou étrangers, des laboratoires publics ou privés.

NNT : 2017SACLX036

Thèse de doctorat de l'Université Paris-Saclay préparée á l'Ecole Polytechnique

Ecole doctorale n°564
Ecole Doctorale Physique en Île-de-France
Spécialité de doctorat: Physique
par

M. Loïc Herviou

Phases topologiques et Fermions de Majorana

Thèse présentée et soutenue à l'Ecole Polytechnique, le 8 septembre 2017.

Composition du Jury :

M.	Hubert Saleur	Directeur de recherche IPHT, CEA Saclay	(Président du jury)
Mme.	Julia Meyer	Professeur INAC/PHELIQS, Université Grenoble-Alpes	(Rapporteur)
M.	Frank Pollmann	Professeur associé Technical University of Munich	(Rapporteur)
M.	Nicolas Laflorencie	Chargé de recherche LPT, Université Paul Sabatier	(Examinateur)
M.	Philippe Lecheminant	Professeur LPTM, Université Cergy-Pontoise	(Examinateur)
M.	Pascal Simon	Professeur LPS, Université Paris-Sud	(Examinateur)
Mme.	Karyn Le Hur	Directeur de recherche CPHT, Ecole Polytechnique	(Directrice de thèse)
M.	Christophe Mora	Maître de Conférences LPA, ENS	(Directeur de thèse)

Remerciements

Après ces trois années de thèse, il y a bien des gens que je souhaite remercier de m'avoir accompagné, aidé, soutenu ou supporté tout au long des moments parfois difficiles qui l'ont parsemée.
Tout d'abord, je remercie les membres du jury d'avoir accepté de participer à mon jury de thèse. Je remercie Julia Meyer et Frank Pollmann d'avoir accepté d'être les rapporteurs de ce long manuscrit, Hubert Saleur d'avoir accepté la présidence de ce jury, et Nicolas Laflorencie, Philippe Lecheminant et Pascal Simon de jouer le rôle d'examinateurs.
Je remercie bien évidemment Christophe Mora et Karyn Le Hur, qui ont su me guider dans cette tâche compliquée qu'est une thèse. Merci pour leur patience, leur disponibilité permanente et pour les innombrables discussions que nous avons eu. Sans eux, cette thèse ne se serait sûrement jamais achevée. La complémentarité de leur enseignement m'a beaucoup apporté, permis de sortir (un peu) de mon point de vue très particulier et énormément appris.
Merci à Jean-Noël Fuchs, Philippe Lecheminant, William Witczak-Krempa d'avoir répondu à mes interrogations, parfois bêtes, souvent très techniques. Sans leur patience, je n'aurais pas pu résoudre certains des problèmes qui me taraudaient. Je témoigne aussi ma reconnaissance à Mazyar Mirrahimi, qui a encadré mon stage de Master 1, et qui m'a confirmé mon goût pour le souvent dur, parfois ingrat mais toujours passionnant métier de chercheur.
Merci aussi à Jens Bardarson, Ignacio Cirac, Karsten Flensberg, Ion Garate, Michael Knap, Martin Leijnse, Joseph Maciejko, Serguej Moroz, André-Marie Tremblay, Frank Pollmann, David Sénéchal, Norbert Schur et William Witczak-Krempa d'avoir eu le temps et la patience de me rencontrer et de discuter de mes projets. J'espère avoir l'occasion de travailler avec eux dans un futur proche.
Cette thèse a été aussi l'occasion de faire de nombreuses rencontres et de créer des amitiés durables, au Centre de Physique de Théorique de l'X comme au Laboratoire Pierre Aigrain. Merci à Silke Biermann d'avoir été ma tutrice, à Nicolas Régnault pour ses conseils, et aux deux équipes administratives pour leur aide précieuse dans toutes mes démarches. Je pense à tous les doctorants et post-doctorants qui ont partagé mon quotidien, et des fois mon bureau: Adrien, Arthur, Alex, Cécile, Corneliu, Danijela, Fan, l'autre Loïc, Matthieu, Maxime, Sarah, Tal, Udson. En particulier, je remercie Clémence pour tous les moments que nous avons passé à nous complaire dans cet art si français de la complainte et Kirill pour sa compagnie et son humour si russe.
J'ai toujours pu compter sur la présence de mes amis, les très vieux Toulousains qui ne le sont plus pour la plupart Benoit, Emmanuel, Pierre, Quentin et Victor, mais aussi ceux qui m'ont rejoint plus tard Amina, Aurélie, Félix, Louis, Lucille, Stanislas, Sylvain et Thomas. Il m'est impossible d'oublier les Faerixiens et consorts: Aurélie, Antoine, Cyprien, Guillaume, Godeffroy, Jean-Baptiste, Jeremy, Karlos, Pascal, Pierre-Alain et Simon. J'ai une pensée particulière pour Alvaro, Florian, Henri et Morgane qui ont réussi à me supporter dans la souffrance libératoire de nos crapahutages en Islande et en Corse. Merci aussi à tous mes amis boxeurs qui ont dû subir mon besoin de ventiler les frustrations des longues journées: Armelle, Ludovic, Lionel, Marion, Yves et tous les autres.
Je remercie enfin ma famille pour son soutien et sa confiance sans cesse renouvellée.

List of publications

Phase Diagram and Entanglement of two interacting topological Kitaev chains
L. Herviou, C. Mora and K. Le Hur
Phys. Rev. B 93, 165142 (2016)

Many-terminal Majorana island: from Topological to Multi-Channel Kondo Model
L. Herviou, K. Le Hur and C. Mora
Phys. Rev. B 94, 235102 (2016). Editors' Suggestion.

Bipartite charge fluctuations in one-dimensional $\mathbb{Z}_2$ superconductors and insulators
L. Herviou, C. Mora and K. Le Hur
Phys. Rev. B 96, 121113(R) (2017)

Driven dissipative dynamics and topology of quantum impurity systems
K. Le Hur, L. Henriet, L. Herviou, K. Plekhanov, A. Petrescu, T. Goren, M. Schiro, C. Mora and P. Orth
Invited review for Comptes Rendus Académie des Sciences on Quantum Simulators
arXiv ePrints: 1702.05135

Bipartite fluctuations and topology in one- and two-dimensional semi-metals
L. Herviou, K. Le Hur and C. Mora
In preparation, working title

Contents

Introduction **1**

1 A general introduction to topology in Condensed Matter **5**

1.1 Kitaev's wire . . . 6
1.1.1 Generalities . . . 6
1.1.2 Majorana fermions and edge states . . . 7
1.1.3 Bogoliubov formalism and bulk topology . . . 9
1.1.4 Quantum Ising model and locality . . . 11
1.2 General band theory for non-interacting fermions . . . 13
1.2.1 Single particle Hamiltonian in Fourier space . . . 13
1.2.2 Two-band Hamiltonians and general solutions . . . 14
1.3 Topological approach to band theory . . . 15
1.3.1 Introduction to topology . . . 15
1.3.2 Bulk hamiltonians and homotopy . . . 18
1.3.3 Symmetry and classification . . . 19
1.3.4 Relevant topological invariants for two-band Hamiltonians . . . 21
1.4 Bulk-edge correspondence and edge states . . . 27
1.4.1 D class for $d = 1$ . . . 28
1.4.2 BDI class for $d = 1$ . . . 29
1.4.3 D class for $d = 2$ . . . 29
1.5 Topical examples in 1D . . . 30
1.5.1 The Su-Schrieffer-Heeger model . . . 31
1.5.2 Longer-range Kitaev's wire . . . 31
1.5.3 Rashba spin-orbit superconductors . . . 35
1.6 Topical examples in 2D . . . 36
1.6.1 The $p + ip$ superconductor . . . 36
1.6.2 A very brief overview of graphene . . . 39
1.6.3 Haldane model for topological insulator . . . 40

2 Entanglement properties of normal and topological states **43**

2.1 Entanglement entropy . . . 44
2.1.1 Definition of the von Neumann Entanglement Entropy . . . 44
2.1.2 Entanglement entropy in many-body systems . . . 46
2.2 Entanglement spectrum and topological systems . . . 53
2.2.1 Definition of the entanglement spectrum . . . 53

2.2.2 Entanglement spectrum in topological systems 54
2.3 Bipartite fluctuations as a "weak" measure of entanglement 57
2.3.1 The problem of entanglement measure 57
2.3.2 General definition of bipartite fluctuations 59
2.3.3 Bipartite charge fluctuations in Luttinger Liquids 61
2.3.4 Beyond one dimension 63

3 Bipartite fluctuations in non-interacting topological systems 65
3.1 Bipartite fluctuations in 1D: generalities 68
3.1.1 Preliminaries on charge-conservation breaking 68
3.1.2 Bipartite fluctuations in arbitrary non-interacting systems 70
3.1.3 The Fejér Kernel: properties and consequences 72
3.2 One-dimensional BDI class 77
3.2.1 BDI Hamiltonian and fluctuations 77
3.2.2 Discontinuity of the derivative of the linear term 78
3.2.3 Logarithmic contributions and generalized fluctuations 79
3.2.4 Conformal origin of the logarithm 81
3.2.5 Structure factor of the BCF 82
3.2.6 Bipartite fluctuations in Kitaev's model and the SSH chain 84
3.2.7 Bipartite fluctuations in the extended Kitaev's model 87
3.2.8 Extension to finite length and finite temperature 88
3.2.9 A brief comparison with other charge-based measurements 92
3.2.10 Beyond the two-band paradigm 95
3.3 One-dimensional D class 96
3.3.1 Preliminaries 96
3.3.2 Cusp of the linear term 96
3.3.3 Logarithmic coefficients 96
3.3.4 An example: extended Kitaev model 97
3.4 Bipartite fluctuations in 2D Dirac materials 98
3.4.1 Geometric shape, Kernel functions and Sobolev spaces 99
3.4.2 Fluctuations for a single isotropic Dirac cone 102
3.4.3 Beyond the single isotropic Dirac cone 110

4 Beyond non-interacting systems: a complex interplay 115
4.1 Interactions and bipartite fluctuations 117
4.1.1 Interacting systems and numerical simulations 117
4.1.2 Bosonization at the critical point 118
4.1.3 Bipartite fluctuations and interactions 120
4.2 Model and simple limiting cases 123
4.2.1 Microscopic model 123
4.2.2 Phase diagram 124
4.2.3 The Hubbard model 125
4.3 Close to half-filling: bosonization and RG 127
4.3.1 Bosonization at half-filling 127
4.3.2 RG analysis 128

4.3.3 Characterization of the 4 Majorana phase . . . 130
4.3.4 Behavior of the large g phases . . . 132
4.3.5 Nature of the transitions . . . 134
4.4 The Double Critical Ising phase . . . 136
4.4.1 Mean-field precursor to the DCI . . . 136
4.4.2 Unraveling the ladder . . . 137
4.4.3 Large g model . . . 139
4.4.4 Numerical approach . . . 140

5 Transport in topological systems 145
5.1 Motivation and summary . . . 145
5.1.1 Motivation . . . 145
5.1.2 Summary of the main results . . . 149
5.2 Model and bosonization . . . 151
5.2.1 Model . . . 151
5.2.2 Tunelling term and number of Majoranas . . . 152
5.2.3 Bosonization and Majorana fermions . . . 155
5.3 Quantum Brownian Motion and Topological Kondo model . . . 155
5.3.1 Quantum Brownian Motion . . . 156
5.3.2 Far from charge degeneracy: the Topological Kondo limit . . . 157
5.4 Charge degeneracy point: an exact mapping to the multichannel Kondo Model . . . 161
5.5 Phase diagram at charge degeneracy . . . 163

Conclusion and perspectives 169

A Résumé en français 171

B Brief summary of abbreviations 191

C Brief summary on Hilbert-Sobolev spaces 193

D Details on microscopic computations 195
D.1 Brillouin Zone and reciprocal lattice . . . 195
D.2 Diagonalization and correlation functions of the Rashba nanowires . . . 196
D.3 Schrieffer-Wolff transformation in Kitaev's ladder . . . 198

E Luttinger liquids, bosonization and RG 201
E.1 Basics of Luttinger Liquids theory . . . 201
E.2 Bipartite charge fluctuations of a critical $c = m$ bosonic model . . . 202
E.3 RG analysis in bosonized theories . . . 204
E.3.1 Overview . . . 204
E.3.2 Derivation for the sine-Gordon model . . . 204
E.3.3 Beyond the simple sine-Gordon model . . . 206
E.3.4 Bosonization of the Kitaev-Hubbard model . . . 208

F Conformal Theory computations **211**
F.1 Bipartite charge fluctuations for a $c = \frac{1}{2}$ model 211
F.2 Bipartite charge fluctuations for a $c = 1$ boson 212

G Topological Kondo model **215**
G.1 RG flow 215
G.1.1 RG equations for the Topological Kondo model 215
G.1.2 RG equations for the M-CKM 217
G.2 Kubo approach to conductance 219
G.2.1 Kubo formula 219
G.2.2 Application for the strong coupling limit far from charge degeneracy 220

Introduction

Classifying the phases of matter is one of the main goals of physics. From trivial "real-life" examples such as evaporation or melting of water to the most abstract theoretical studies, the properties of these different states and of the transitions between them are of fundamental importance to understand our world. Condensed matter physics focuses on studying the wealth of phenomena that appear in liquids and solids, most of the time given by the collective behavior of the many atoms and electrons that compose them. This behavior is a truly many-body, or emergent, effect, where the properties of the macroscopic system cannot all be understood from the individual particles.

The historical paradigm to describe phases and phase transitions in this context, for both quantum and classical systems, was formulated by Ginzburg and Landau. Instead of starting from first principles with an unsolvable model, it relies on building effective simpler theories. The set of symmetries, *i.e.* the transformations that should leave the system invariant, and more precisely its energy, limits the possible terms that can appear. One can then define a local physical observable, the order parameter, whose value changes and becomes non-zero in the ground states (the lowest-energy states) or the thermal states at the phase transition, while some of the symmetries enforce that its mean must vanish. This phenomenon is called a spontaneous breaking of symmetry, as single states seem to violate the symmetries of the system. Of course, these are not directly broken but the level at which they are applied change. In the disordered phase, the symmetries are directly enforced on the states, and the order parameter is zero for all ground states, while in the ordered phase, they are now enforced on the space of states: the order parameter can take a non-zero value in some states, but will cancel on average. This usually also leads to a change in the degeneracy (number) of ground states. Maybe the most simple example is the following: take a real or complex quantity such as a spin polarization or a superconducting pairing ϕ, and a potential energy that only depends on its norm: $V(\phi) = r|\phi|^2 + |\phi|^4$. The system has some symmetries: V is invariant under the change $\phi \to -\phi$ if ϕ is real (resp. $\phi \to e^{i\theta}\phi$ if ϕ is complex). One talks about a $\mathbb{Z}_2$ symmetry (resp. $U(1)$), from their group representation. Ignoring all dynamics, to minimize the energy is to minimize V. If r is positive, the minimum of V is reached for $\phi = 0$, which is left invariant by the aforementioned transformations: it corresponds to a disordered phase. Conversely, if r is negative, the minimum is reached for $|\phi| = \frac{\sqrt{|r|}}{2}$ and is now two-times (resp. infinitely) degenerate. It corresponds to an ordered phase: the symmetries do not leave the states invariant but map ground states onto each other.

Landau's approach to phase transitions was tremendously successful in a wide variety of models and materials to explain many different phase transitions. Yet, between 1971 and

1973, Berezinskii [1, 2], Kosterlitz and Thouless [3, 4] introduced a new phase transition that could not be described by the breaking of a symmetry, in a two-dimensional classical magnet. Such a magnet can be described minimally by a plane lattice of ferromagnetic spins (carried by the atoms) that interact and tend to align with each other. At zero temperature, the spins are perfectly aligned, but when the temperature increases, excitations consisting in pairs of vortices and anti-vortices start to appear and form a dilute gas. At a finite critical temperature, a phase transition occurs while the well-known Mermin-Wagner theorem prevents any breaking of the relevant continuous symmetries. The pairs split, and isolated vortices appear. These works, that were awarded the Nobel Prize in 2016, shared with F. Haldane, are the first example of a topological phase transition and of a phase where topological defects (the vortices) play a fundamental role.
Perhaps even more well-known examples are the Integer and Fractional Quantum Hall Effects (I/FQHE), discovered in 1980[5] and 1982[6]. These phases arise when confining a gas of electrons in two dimensions at low temperature and in a strong orthogonal magnetic field. When applying a voltage on two sides of the plane, a perpendicular current is generated. When varying the intensity of the magnetic field, one finds perfect plateaus for the transverse Hall conductivity while the longitudinal conductivity vanishes. On each plateau, the conductivity is equal to the quantum of conductance $\frac{e^2}{h}$ times an integer (a rational for the FQHE) to an astonishing precision of 10^{-9}, far beyond what impurities and defects would normally allow. It is now used in metrology experiment for defining the hyperfine constant. The current is purely carried by the edges of the sample while the bulk of the system stays an insulator. No local physical observables can distinguish between it and an atomic insulator (where the electrons are simply localized on their individual atoms). Nonetheless, the quantization of the conductance was directly linked by Thouless *et al*[7] to the properties of the bulk electronic bands. The quantized term that appears in the conductance corresponds to a global topological invariant of the band structure (or of the many-body wave function[8]), that can be used to classify these phases (and cancels for the trivial atomic insulator). By definition, this invariant is largely independent of the microscopic details of the system, and highly resilient to the presence of defects and impurities, as observed experimentally. In the case of the IQHE, the topological invariant, called the Chern number, also corresponds to the number of gapless edge modes that carry the orthogonal current. The trivial atomic insulator does not have any edge mode. This underlying bulk-edge correspondence is at the core of the study of topological materials.
The discovery of these first topological insulators lead to a revolution in condensed matter studies. In a few decades, more and more different topological materials were discovered. From the realization that phases similar to the IQHE could be created even in the absence of strong magnetic fields[9] to the construction of topological superconductors[10], topology became ubiquitous in theoretical (and experimental) condensed matter physics. All non-interacting fermionic topological phases were classified according to the spatial dimension and their symmetries[11, 12]. The classification of interacting topological phases, on the other hand, is a much more complicated problem. The FQHE was the first example of such phases where the interactions lead to the emergence of new exotic quasi-particles. These excitations behave like fractions of electrons, called anyons. Their charge is a fraction of the electronic charge, and their exchange statistics are neither that of a boson or a fermion. This fractionalization leads to a robust degeneracy of the ground state, that

depends only on the genus of the system, and not on the details of its geometry and parameters.
In the last decade, the rise of quantum information, and especially the race towards quantum computers and simulators lead to additional interest in these fractionalized edge states or excitations. As a typical example, in the case of topological superconductors (even in non-interacting systems), zero-energy Majorana modes appear at the edges or as excitations in the core of vortices[10, 13]. The existence of Majorana fermions was first proposed by the physicist Ettore Majorana[14] in 1937 as a peculiar solution of the Dirac equation: particles who would be their own antiparticles, though high-energy physics has yet to discover them. The main obstacle preventing the realization of the fabled quantum computer is decoherence: the fact that the environment tends to couple to the quantum degrees of freedom. The quantum information is then dissipated in a macroscopic number of degrees of freedom, leaving the system in an effective classical state. The topological and fractional nature of the Majorana fermions and other anyonic excitations would strongly limit such couplings and in principle make them perfect candidates for quantum bits[15]: as no local observable can distinguish between states differing only by the presence or absence of such a quasi-particle, the environment cannot be strongly coupled to the system. Indeed, several schemes have been proposed to realize complete sets of quantum gates and memories, using superconducting wires with Majorana fermions at each extremities [16–19]. Direct and decisive experimental proof of the existence of these Majorana fermions remains, though, an essentially inconclusive problem.

In this thesis

This thesis is devoted to answer some of the questions that arise in this context. We will study many different aspects of these topological systems: criticality and the signs of topological phase transitions in generic one- and two-dimensional models, the effect of large interactions on topological superconductors, and electronic transport mediated by Majorana fermions.

This manuscript is organized as follows. Chapter 1 and 2 are introductory chapters on topology and entanglement in condensed matter physics. In Chapter 1, after a detailed description of the celebrated Kitaev's chain[13] that we will use as an example throughout this thesis, we proceed to a general introduction to topological systems. We essentially limit ourselves to non-interacting two-band fermionic systems, in order to keep a simple description in terms of homotopic equivalence classes. After presenting the classification of topological phases in terms of symmetries, the various topological invariants and an overview of the bulk-edge correspondence, we introduce the different topical examples of topological systems, in one and two dimensions, that we will use in the thesis. Chapter 2 is then devoted to the concept of entanglement, fundamental to quantum mechanics and strongly correlated materials. We present there the von Neumann entanglement entropy and the entanglement spectrum that will be useful to characterize gapless and topological phases. Finally, we introduce the concept of bipartite fluctuations through the example of the charge fluctuations in Luttinger Liquids. The bipartite fluctuations are meant to be a weak, experimentally accessible, measure of entanglement.

The rest of the thesis is then devoted to our own works. Chapter 3 presents an extension of the previous works on bipartite charge fluctuations to fluctuations of arbitrary fermionic bilinears in generic non-interacting symmetry protected topological systems, where the observed charge is not conserved. We focus on the standard critical points that describe topological phase transitions, and are able to derive exact properties on the correlation functions and the bipartite fluctuations that allow for a characterization of such models. We observe quantized, universal logarithmic terms in one and two dimensions, with, in the latter case, a dependency on the topological properties of the Dirac cones that appear. We also observe a new volume contribution that is linked to the quantum Fisher information[1], and is a marker of entanglement.
Methods used: exact solutions and integral forms, Hilbert-Sobolev (Fourier) spaces, exact diagonalization
The following Chapter 4 is concerned with the effects of interactions in such topological systems. The first part of the Chapter focuses on building a reliable description of the topological critical point for an interacting topological superconductor, and on the effect of the interactions on the previously studied bipartite fluctuations. Then, in a second step, we study the phase diagram of two Coulomb-coupled p-wave paired superconducting wires. We are interested in their behavior when the interactions are strong enough to break the topological protection: the interplay between unconventional superconductivity and interactions leads to the appearance of new exotic phases, characterized by orbital currents or uncommon gapless excitations.
Methods used: bosonization, renormalization group, exact diagonalization, MPS-based DMRG
Finally, Chapter 5 is dedicated to the study of the transport properties of a superconducting island in the presence of Majorana impurities. This device, introduced in Refs. [20, 21], is meant to be a building block for an eventual quantum computer[22]. The Majorana fermions affect the statistics of the charge carriers in this multichannel terminal, which leads to resilient fractionalized transport. We extend previous studies to the charge degenerate case, when the total number of fermions in the island can fluctuate, and map it to the well-known Multi-Channel Kondo model.
Methods used: bosonization, renormalization group
Conclusion and perspectives are contained in the final chapter.

[1]The Quantum Fisher Information, defined as the connected fluctuations of an observable for a pure state, measures the producibility of the wave function, that is to say how separable the state is in a space where the observable is local.

Chapter 1

A general introduction to topology in Condensed Matter

Contents

1.1 Kitaev's wire **6**
1.1.1 Generalities 6
1.1.2 Majorana fermions and edge states 7
1.1.3 Bogoliubov formalism and bulk topology 9
1.1.4 Quantum Ising model and locality 11
1.2 General band theory for non-interacting fermions **13**
1.2.1 Single particle Hamiltonian in Fourier space 13
1.2.2 Two-band Hamiltonians and general solutions 14
1.3 Topological approach to band theory **15**
1.3.1 Introduction to topology 15
1.3.2 Bulk hamiltonians and homotopy 18
1.3.3 Symmetry and classification 19
1.3.4 Relevant topological invariants for two-band Hamiltonians 21
1.4 Bulk-edge correspondence and edge states **27**
1.4.1 D class for $d = 1$ 28
1.4.2 BDI class for $d = 1$ 29
1.4.3 D class for $d = 2$ 29
1.5 Topical examples in 1D **30**
1.5.1 The Su-Schrieffer-Heeger model 31
1.5.2 Longer-range Kitaev's wire 31
1.5.3 Rashba spin-orbit superconductors 35
1.6 Topical examples in 2D **36**
1.6.1 The $p + ip$ superconductor 36
1.6.2 A very brief overview of graphene 39
1.6.3 Haldane model for topological insulator 40

The goal of this chapter is to provide a simple and concise introduction to different basic aspects of topology in condensed matter physics through a set of examples. This thesis essentially focuses on theoretical works at (or close to) zero temperature. Generically, a system in quantum mechanics can be described through its Hamiltonian, an operator or integral form that gives its energy. A quantum state is an eigenstate of this operator. While at finite temperature, the system will be described by a weighted sum of such eigenstates, at zero temperature, it is enough to focus on the ground state (the lowest-energy state) of the Hamiltonian, which can be degenerate. In this chapter, we will focus on the properties of these ground states, which can also be directly deduced from the properties of the Hamiltonian itself. We start by a brief presentation of Kitaev's wire, a paradigmatic example of topological superconductors that we will use as a reference model. We allude through this first example to some of the most important properties of topological systems. We then follow with the generic formalism we use to describe non-interacting systems, with a particular focus on two-band models. Then, the main part of this chapter is a description of topology in non-interacting systems, following the classification of Ref. [12, 23]. The bulk-edge correspondence, linking the topological properties of the Hamiltonian to the presence or absence of edge states is briefly addressed. We conclude with a description of the different models that will be relevant in this thesis. The last two Sections are meant to be skipped at first reading and refered to when needed.

1.1 Kitaev's wire

1.1.1 Generalities

The model was proposed in Ref. [13], and is probably one of the simplest examples of topological models, where the unusual properties associated to topology are directly visible. There has been several proposals and realizations of this model, for example by coupling a semiconducting nanowire to the bulk of two- or three-dimensional superconductors via a strong spin-orbit interaction and by applying a magnetic field to select one spin species in the wire[19, 23–33]. Other implementations have been discussed with ferromagnetic metallic chains [34, 35] and ultra-cold atoms [36, 37]. Majorana fermions can also occur as a result of purely intrinsic attractive interactions [38].
It consists in a chain of spinless fermions, where p-wave superconductivity has been introduced at the mean-field level. It corresponds to the following tight-binding model:

$$H_{\mathcal{K}} = -\mu \sum_j c_j^\dagger c_j - t \sum_j (c_j^\dagger c_{j+1} + c_{j+1}^\dagger c_j) + (\Delta c_j^\dagger c_{j+1}^\dagger + \Delta^* c_{j+1} c_j), \tag{1.1}$$

where t is a hopping term describing the hopping of electrons from one site to another, Δ is an a priori complex pairing term, μ is a chemical potential and $c_j^{(\dagger)}$ are fermionic annihilation (creation) operators at site j. They verify the standard anti-commutation rules:

$$\{c_j, c_{j'}\} = \{c_j^\dagger, c_{j'}^\dagger\} = 0 \text{ and } \{c_j, c_{j'}^\dagger\} = \delta_{j,j'}, \tag{1.2}$$

with δ the Kronecker symbol. We consider a chain of length L and the sum carries on all sites. We will fix the boundary conditions at a later time.

The pairing term, breaking charge conservation, represents the formation of Cooper pairs inside the wire, coming from an infinite reservoir of such pairs. If one neglects the fluctuations in the substrate and if the correlation length of the Cooper pairs is of the order of the lattice spacing, Eq. 1.1 is a possible approximation for superconductivity by proximity: by adding a normal semi-conducting wire on the surface of a macroscopic superconductor, one expects the tunnelling of Cooper pairs into the wire, and vice-versa.
Through a redefinition of the fermionic operator, the phase of the superconducting substrate can be absorbed. For $\Delta = |\Delta| e^{i\phi}$, the new operators $\tilde{c}$ are defined by:

$$\tilde{c}_j = e^{-i\frac{\phi}{2}} c_j. \tag{1.3}$$

Consequently, without loss of generality, we take in this thesis Δ positive and real. Nonetheless, it comes at the price of the loss of this gauge freedom. The broken $U(1)$ symmetry is equivalent to the broken charge conservation in this model.

1.1.2 Majorana fermions and edge states

Any fermion can be represented as a sum of two Majorana fermions. Those are real (not complex) fermions, that consequently act as their own anti-particle. They follow the Clifford algebra:

$$\{\gamma_j, \gamma_l\} = \delta_{j,l} \qquad \gamma_j = \gamma_j^\dagger \tag{1.4}$$

We define the Majorana operators corresponding to the real and imaginary part of the c operators:

$$\gamma_j^A = \frac{1}{\sqrt{2}}(c_j + c_j^\dagger) \qquad \gamma_j^B = \frac{i}{\sqrt{2}}(c_j^\dagger - c_j). \tag{1.5}$$

The Hamiltonian 1.1 can be straightforwardly rewritten in terms of these operators:

$$H_{\mathcal{K}} = -\mu \sum_j (i\gamma_j^A \gamma_j^B + \frac{1}{2}) + i \sum_j \left[(\Delta + t)\gamma_{j+1}^B \gamma_j^A + (\Delta - t)\gamma_{j+1}^A \gamma_j^B\right] \tag{1.6}$$

A simple understanding of the phase diagram can be obtained by looking at an open system at three different points. First let us consider $\mu \to -\infty$. In this case, the Hamiltonian is essentially equivalent to:

$$H_{\mathcal{K}} = -\mu \sum_j^L (i\gamma_j^A \gamma_j^B + 1) = -\mu \sum_{j=1}^L c_j^\dagger c_j \tag{1.7}$$

Obtaining the ground state is straightforward: all sites of the wire are empty. The system is therefore in the trivial state $|0\rangle_c$, defined by:

$$\forall j,\ c_j |0\rangle_c = 0 \tag{1.8}$$

A second, more interesting point is given by $\mu = 0$, $t = \Delta$. In this limit, one can define $L-1$ new fermionic operators d_j, by analogy with the previous case, that leads to a simple Hamiltonian:

$$d_j = \frac{1}{\sqrt{2}}(\gamma_{j+1}^B + i\gamma_j^A), \qquad H_{\mathcal{K}} = 2it \sum_{j=1}^{L-1} \gamma_{j+1}^B \gamma_j^A = 2t \sum_{j=1}^{L-1} d_j^\dagger d_j - \frac{1}{2} \tag{1.9}$$

The two Majorana operators γ_1^B and γ_L^A do not appear in the Hamiltonian, as represented in Figure 1.1. One can then define a non-local, boundary fermion $d_0 = \frac{1}{\sqrt{2}}(\gamma_1^B + i\gamma_L^A)$ that has strictly zero energy and commutes with the Hamiltonian. The ground states (and all other states) are consequently doubly degenerate and a basis of the low-energy subspace is given by $|0\rangle_d$ and $d_0^\dagger |0\rangle_d$.

This picture stays valid for $\mu \neq 0$: in the thermodynamic limit, the system is always two-fold degenerate, as long as $\Delta \neq 0$ and $|\mu| < 2t$ [13]. At each extremity of the wire an exponentially localized Majorana fermion $\tilde{\gamma}^{A/B}$ can be found:

$$\tilde{\gamma}^A = \frac{1}{\mathcal{N}} \sum_{j=1} e^{-mj} \gamma_{L+1-j}^A, \quad \tilde{\gamma}^B = \frac{1}{\mathcal{N}} \sum_{j=1} e^{-mj} \gamma_j^B, \tag{1.10}$$

such that $\{H, \tilde{\gamma}^{A/B}\} = 0$ in the thermodynamic limit. $\mathcal{N}$ is a normalization factor and m a parameter dependent inverse length ($m \to +\infty$ for $\mu = 0$, $t = \Delta$, and $m \to 0$ when $|\mu| \to 2t$). The anti-commutation with the Hamiltonian implies that that $\tilde{d}_0 = \frac{1}{\sqrt{2}}(\tilde{\gamma}^A + i\tilde{\gamma}^B)$ still does not appear in the Hamiltonian and has zero energy. When going to a finite system, there is generally a residual lifting of the degeneracy of order $e^{-\frac{aL}{\chi}}$, where χ is the correlation length and a the lattice spacing (taken to 1 in the rest of the thesis).

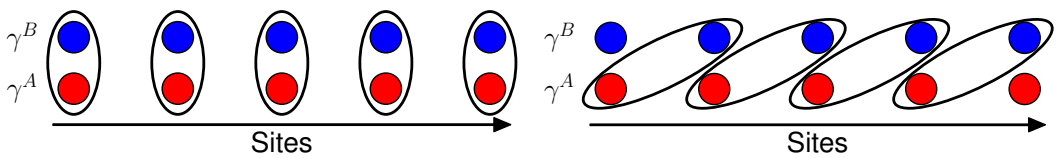

Figure 1.1: Schematic view of the Majorana couplings in Kitaev's chain. Each fermion is divided into two Majorana fermions γ_A (bottom) and γ_B(top). Ellipses represent the dominant couplings that build a new local fermion that is either empty or occupied. On the left, the trivial case when $\mu \gg t, \Delta$. The Majorana fermions pair on site, and the occupied fermions are the physical ones. On the right, the topological phase when $t = \Delta$, $\mu = 0$. A Majorana fermion couples with another on the neighbouring site, instead of one on site. Two of them are left uncoupled if the wire has open boundaries.

Finally, it is interesting to consider what happens precisely at the phase transition for $\mu = -2t$, $t = \Delta$. Then defining the Majorana operators α_j such that:

$$\alpha_{2j-1} = \gamma_j^B, \qquad \alpha_{2j} = \gamma_j^A, \tag{1.11}$$

the Hamiltonian can be rewritten as a simple chain of free Majorana fermions of length $2L$:

$$H_{\mathcal{K}} = 2it \sum_{j=1}^{2L-1} \alpha_j \alpha_{j+1} \tag{1.12}$$

The identification of the critical model is consequently straightforward: at the critical point, there is precisely one free Majorana mode, which corresponds to the universality class of the Ising chain. The system is then gapless. Figure 1.2 summarizes the phase diagram of the Kitaev wire.

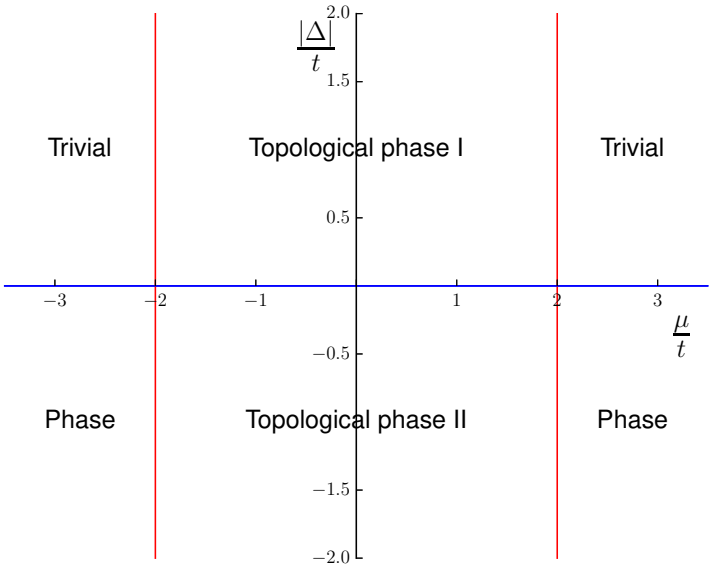

Figure 1.2: Phase diagram of Kitaev's wire. For $\mu > 2t$, $\Delta \neq 0$, the wire is in a trivial superconducting phase. For $\mu < 2t$, $\Delta \neq 0$, the system is in a topological phase, characterized by the presence of two Majorana edge states exponentially localized at the boundaries of the wire. In red are represented the transition lines $\mu = \pm 2t$. On these lines, the system is gapless and in the Ising universality class. Finally in blue, the line $\Delta = 0$ corresponds to a line of normal metal (free fermions), gapless for $|\mu| < 2t$.

1.1.3 Bogoliubov formalism and bulk topology

An alternative and convenient way to describe Kitaev's wire can be obtained using periodic boundary conditions (or by taking formally the thermodynamic limit). It also provides a simple way to define a topological invariant in this model. It follows the Bogoliubov-de Gennes formalism, further detailed in Section 1.2. It corresponds to the Bardeen-Cooper-Schrieffer [39] (BCS) approach to superconductivity.[1]
Due to translation invariance, the momentum k is a good quantum number. Consequently we directly work in momentum space with the following convention for the Fourier transform:

$$c_j = \frac{1}{\sqrt{L}} \sum_{k \in \mathcal{BZ}} c_k e^{ikj}, \qquad c_k = \frac{1}{\sqrt{L}} \sum_{j=1}^{L} c_j e^{-ikj}, \tag{1.13}$$

[1]BCS approach is a mean-field approach to superconductivity: Δ represents the mean pairing of two fermions, and is the BCS order parameter. To describe a proper superconductor in BCS theory, we would also need to check the autocoherence of the mean-field approximation. As Δ is imposed by a non-described external substrate, this step is not required here.

where $\mathcal{BZ}$ is the Brillouin Zone associated to the lattice (see Appendix D.1 for a proper definition). With periodic boundary conditions and for a finite lattice, $\mathcal{BZ} = \{\frac{2n\pi}{L}, n \in \mathbb{N}, 0 \leq n \leq L-1\}$, and in the continuum limit, $\mathcal{BZ} =]-\pi, \pi]$ (and the finite sums are replaced by integrals). c_k verifies the same anti-commutation rules as the original c_j operators. The Hamiltonian can be consequently rewritten in Fourier space as:

$$H_{\mathcal{K}} = \sum_{k \in \mathcal{BZ}} (-\mu - 2t\cos k) c_k^\dagger c_k + i\Delta \sin k (c_k^\dagger c_{-k}^\dagger - c_{-k} c_k) \tag{1.14}$$

$$= (-\mu - 2t) c_0^\dagger c_0 + (-\mu + 2t) c_\pi^\dagger c_\pi + \sum_{k \in \mathcal{BZ}, 0<k<\pi} \left(\Psi_k^\dagger h(k) \Psi_k - \mu - 2\cos k \right), \tag{1.15}$$

where

$$h(k) = \begin{pmatrix} -\mu - 2t\cos k & 2i\Delta \sin k \\ -2i\Delta \sin k & \mu + 2t\cos k \end{pmatrix}, \qquad \Psi_k^\dagger = \begin{pmatrix} c_k^\dagger, & c_{-k} \end{pmatrix}$$

The separation in momentum space is fundamental for describing the system in terms of bulk bands and finding a simple solution. It is due to the translation-invariance and the non-interacting nature of the system. Forgetting the modes $k = 0, \pi$, the Hamiltonian can be reinterpreted as a sum of commuting Hamiltonians (each one living in a 4-dimensional space and described by a 2×2 matrix), that can be diagonalized. Ψ_k is called a spinor. Introducing the Bogoliubov-De Gennes quasi-particles η_k, the mixing angle θ_k and the energy E_k defined by:

$$\cos\theta_k = \frac{-\mu - 2t\cos k}{E_k}, \qquad \sin\theta_k = \frac{2\Delta \sin k}{E_k}, \tag{1.16}$$

$$E_k = \sqrt{(-\mu - 2t\cos k)^2 + (2\Delta \sin k)^2}, \tag{1.17}$$

$$\eta_k = \cos\frac{\theta_k}{2} c_k + i \sin\frac{\theta_k}{2} c_{-k}^\dagger, \tag{1.18}$$

the Hamiltonian admits the simple representation (up to a constant contribution that we discard), including the modes 0 and π:

$$H_{\mathcal{K}} = \sum_{k \in \mathcal{BZ}} E_k \eta_k^\dagger \eta_k \tag{1.19}$$

Analysis of the results is fairly straightforward: the operators η_k describe the fermionic quasi-particles in Kitaev's chain. These excitations are a superposition of an electron and a hole and carry an energy E_k. E_k cancels either when $\Delta = 0$ and $|\mu| \leq 2t$, or for $\Delta \neq 0$ and $|\mu| = 2t$. Outside these lines, the system is gapped (all excitations have finite, non-zero energies) and the ground state is unique:

$$|0\rangle_\eta = (1 + \delta_{\mu > -2t}(c_0^\dagger - 1))(1 + \delta_{\mu > 2t}(c_\pi^\dagger - 1)) \prod_{k \in \mathcal{BZ}, 0<k<\pi} (\cos\frac{\theta_k}{2} - i \sin\frac{\theta_k}{2} c_k^\dagger c_{-k}^\dagger) |0\rangle_c \tag{1.20}$$

The closure of the gap at the aforementioned gapless lines marks phase transitions and corresponds to those obtained in Figure 1.2. Direct differentiation of the phases from the periodic ground state is not simple. At first sight, the only difference comes from the parity of the number of fermions. We introduce the fermionic parity operator:

$$P = \exp(i\pi \sum_{j=1}^{L} c_j^\dagger c_j) = \prod_{j=1}^{L}(1 - 2c_j^\dagger c_j) = \prod_{j=1}^{L} 2i\gamma_j^B \gamma_j^A. \tag{1.21}$$

Neglecting finite size-effects (such as the mode π not existing if L is odd, due to frustration), $\langle P \rangle = -1$ in the two topological phases and $\langle P \rangle = 1$ in the trivial phases. The parity here plays the role of an order parameter for the topological phase transition, yet, as it is not local, it is not a standard one a la Landau. In fact, no local observables can distinguish between the two phases: this will be a common and very important feature of topological models.
To entice the reader, we can nonetheless go further: let us informally define the winding number of θ_k by:

$$\nu = \oint_{k \to \theta_k} \frac{d\theta_k}{2\pi} = \int_{k \in \mathcal{BZ}} \frac{\partial \theta_k}{\partial k} \frac{dk}{2\pi} \tag{1.22}$$

The precise mathematical meaning of the first integral will be made explicit in Section 1.3.4. Physically, ν counts the number of times the path $\{\theta_k, k \in \mathcal{BZ}\}$ winds around the origin. Figure 1.3 provides a visual representation of ν for several values of the parameters $\{\mu, t, \Delta\}$. Inside the topological phases, $\nu = \pm 1$, while in the trivial phase, $\nu = 0$. The winding number is a topological property of the function θ, *i.e.* it is not affected by smooth deformation of the function, or small local perturbations applied to the Hamiltonian. As a consequence, the ground states are topologically distinct, and the topological phases can be differentiated directly from bulk properties.

1.1.4 Quantum Ising model and locality

One-dimensional spinless fermions can be easily mapped onto spin-$\frac{1}{2}$ operators through the Jordan-Wigner transform. For a wire, a possible choice for this transformation is:

$$\sigma_j^z = 2c_j^\dagger c_j - 1, \quad \sigma_j^x = (c_j^\dagger + c_j) e^{i\pi \sum_{k<j} c_k^\dagger c_k}, \quad \sigma_j^y = i(c_j^\dagger - c_j) e^{i\pi \sum_{k<j} c_k^\dagger c_k}. \tag{1.23}$$

The Jordan-Wigner cord $e^{i\pi \sum_{k<j} c_k^\dagger c_k} = (-1)^{j-1} \prod_{k<j} \sigma_k^z$ enforces the commutation relations on different sites:

$$[\sigma_j^x, \sigma_{j'}^y] = 2i\delta_{j,j'}\sigma_j^z \text{ and circular permutations.} \tag{1.24}$$

The transformation is a bijection, and can actually be generalized to any dimension. The advantage in one dimension is the cancellation of the cord, that considerably simplifies the treatment of the spin system.
Using this Jordan-Wigner transformation, Kitaev's chain with open boundary conditions

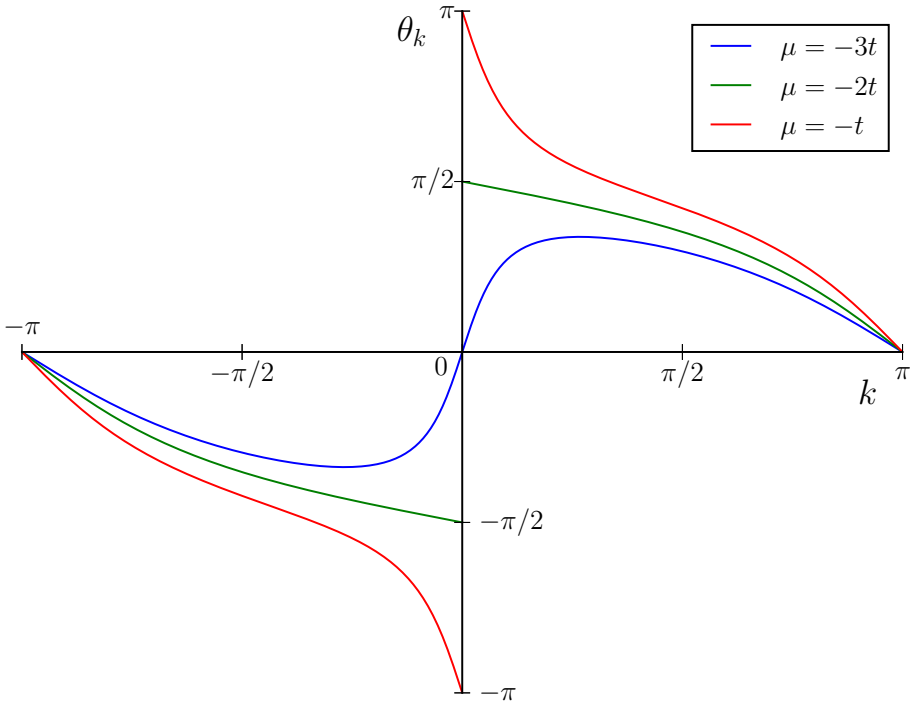

Figure 1.3: θ_k as a function of the momentum for different values of μ and $\Delta = 2t$ in Kitaev's wire. θ_k is an angle, and as such is defined on a torus, such that $\theta_k \equiv \theta_k + 2\pi$. In blue, $\mu = -3t$: the wire is in the trivial phase and θ_k does not wind around the Brillouin Zone. Conversely, for $\mu = -t$ (red), the curve winds -1 times around the BZ. Finally, the green curve describes precisely the QPT ($\mu = -2t$): θ is ill-defined at $k = 0$, leading to a discontinuity, characteristic of such a phase transition.

is actually equivalent to one of the most famous and well-know spin models, the Quantum Ising model in a transverse field[40]. Its Hamiltonian is given by:

$$H_{QIM} = -\frac{\mu}{2}\sum_j \sigma_j^z + \frac{t-\Delta}{2}\sum_j \sigma_j^x \sigma_{j+1}^x + \frac{t+\Delta}{2}\sum_j \sigma_j^y \sigma_{j+1}^y. \tag{1.25}$$

Its phase diagram is still given by Figure 1.2. The trivial phase corresponds to a paramagnetic phase polarized in the σ^z-direction. The two topological phases correspond to an anti-ferromagnet (for $\Delta > 0$) in the σ^y direction or in the σ^x direction for $\Delta < 0$. Note that ferromagnet and anti-ferromagnet are here equivalent through the gauge changes:

$$\sigma_j^z \to \sigma_j^z, \quad \sigma_j^x \to (-1)^j \sigma_j^x, \quad \sigma_j^y \to (-1)^j \sigma_j^y. \tag{1.26}$$

$$\sigma_j^z \to \sigma_j^z, \quad \sigma_j^x \to -\sigma_j^y, \quad \sigma_j^y \to \sigma_j^x. \tag{1.27}$$

This model follows the standard Landau paradigm for phase transitions. The order parameter for the two intermediate phases are simply σ_j^y for $\Delta > 0$ and σ_j^x for $\Delta < 0$. It is a local object, while the corresponding fermionic observable is not. The change in locality

is essential for the break down of topology: a non-local transformation has no reason to preserve the topological properties of a Hamiltonian. The two anti-ferromagnetic phases are not topologically protected. Indeed, while the ground state is two-fold degenerate, there are no edge states. For example, at $\mu = 0$ and $t = \Delta$, the two ground states are

$$|+\rangle = |\leftarrow_y\rangle_1 |\rightarrow_y\rangle_2 |\leftarrow_y\rangle_3 |\rightarrow_y\rangle_4 ..., \qquad |-\rangle = |\rightarrow_y\rangle_1 |\leftarrow_y\rangle_2 |\rightarrow_y\rangle_3 |\leftarrow_y\rangle_4 ... \tag{1.28}$$

The degeneracy is not protected: a small local perturbation such as σ_j^y will directly lift it.

1.2 General band theory for non-interacting fermions

This section contains the formalism we will use to describe both non-interacting superconductors and insulators. A particular attention is given to the two-band limit.

1.2.1 Single particle Hamiltonian in Fourier space

As a first step towards topology in quantum materials, we initially start from a non-interacting fermionic theory, without disorder. Actual physical realizations of course generically violate both these assumptions, but the topological nature of these systems means that a good part of the derived properties will remain true, at least for both weak interactions and weak disorder. More attention will be given to interacting systems in Chapter 4.

As we consider only non-interacting systems for now, Hamiltonians consist of a sum of quadratic fermionic terms. The most generic Hamiltonian for non-interacting fermions for a system $\mathcal{S}$ of dimension d can be written as:

$$H = \sum_{\vec{r},\vec{r}'\in\mathcal{S}^2,\sigma,\sigma'} \mathcal{H}_{\vec{r},\vec{r}',\sigma,\sigma'} c^\dagger_{\vec{r},\sigma} c_{\vec{r}',\sigma'} + \frac{i}{2}(\mathcal{A}_{\vec{r},\vec{r}',\sigma,\sigma'} c^\dagger_{\vec{r},\sigma} c^\dagger_{\vec{r}',\sigma'} - \mathcal{A}^*_{\vec{r},\vec{r}',\sigma,\sigma'} c_{\vec{r}',\sigma'} c_{\vec{r},\sigma}), \tag{1.29}$$

where $\mathcal{H}$ (resp $\mathcal{A}$) is an hermitian (resp. anti-hermitian) matrix of size $S \times S$ (S is the total number of sites), and $c^{(\dagger)}_{\vec{r},\sigma}$ are the fermionic annihilation (creation) operators on sites $\vec{r}$ and of species σ. The species can represent spin-polarization, but also different types of quasi-particles or dimerized sites. $\mathcal{H}$ includes standard hopping terms and chemical potential contributions, while $\mathcal{A}$ is an anomalous contribution that represents superconductivity at the mean-field level by electron pairing. We remind the reader that the fermionic operators follow the following algebra:

$$\{c_{\vec{r},\sigma}, c^\dagger_{\vec{r}',\sigma'}\} = \delta_{\vec{r},\vec{r}'}\delta_{\sigma,\sigma'} \qquad \{c_{\vec{r},\sigma}, c_{\vec{r}',\sigma'}\} = 0, \tag{1.30}$$

where δ is the Kronecker symbol (Dirac delta in a continuum limit). Due to the absence of disorder, the family of Hamiltonians we study is generically invariant by real-space translation in the thermodynamic limit or with periodic boundary conditions (PBC). It is consequently convenient to work in momentum space. Assuming for now perfect translation symmetry, we define the Fourier transform by:

$$c_{\vec{r},\sigma} = \frac{1}{\sqrt{S}} \sum_{\vec{k}\in\mathcal{BZ}} c_{\vec{k},\sigma} e^{i\vec{k}.\vec{r}}, \qquad c_{\vec{k},\sigma} = \frac{1}{\sqrt{S}} \sum_{\vec{r}\in\mathcal{S}} c_{\vec{r},\sigma} e^{-i\vec{k}.\vec{r}}, \tag{1.31}$$

where $\mathcal{BZ}$ is the Brillouin Zone associated to the lattice and we took the lattice spacing to be 1. The Brillouin Zone is simply the elementary cell of the reciprocal lattice (see Appendix D.1 for a proper definition). The unit-cell in real space comports as many fermions as the number of species[2]. The total Hamiltonian can then be rewritten as a sum over (a subset of) the Brillouin zone of small commuting Hamiltonians:

$$H = \sum_{\vec{k}\in\mathcal{BZ}} h(\vec{k}), \qquad [h(\vec{k}), h(\vec{q})] = 0 \tag{1.32}$$

Each Hamiltonian $h(\vec{k})$ can be treated separately and is a quadratic form of a small number of $c_{\vec{k},\sigma}$ operators. Solving the many-body Hamiltonian H reduces to solving a parametrized family of few-body Hamiltonians. In this thesis, we will encounter three different situations. For specific values of $\vec{k}$, $h(\vec{k})$ will only be a quadratic form of only one $c_{\vec{k},\sigma}$ operator, and is therefore trivially solved. Most of the time though, $h(\vec{k})$ will be a function of two such operators: this leads to what is called the two-band problem and is detailed in the following section. Finally, we also study a more complex and realistic model of topological superconductor, the Rashba nanowire, where $h(\vec{k})$ will be a function of four operators in Section 1.5.3 and 3.2.10.

1.2.2 Two-band Hamiltonians and general solutions

In this section, we give the general solution of two-band Hamiltonians. As mentioned in the previous part, they correspond to $h(\vec{k})$ being a quadratic form of two $c_{\vec{k},\sigma}$ operators. One can conveniently rewrite $h(\vec{k})$ in the following way:

$$h(\vec{k}) = \Psi^\dagger_{\vec{k}} \left(E_0(\vec{k})\mathbb{1} + \vec{n}(\vec{k}).\vec{\sigma} \right) \Psi_{\vec{k}}. \tag{1.33}$$

$\mathbb{1}$ is the 2×2 identity matrix and $\vec{\sigma} = (\sigma^x, \sigma^y, \sigma^z)$ the vector of Pauli matrices:

$$\sigma^x = \begin{pmatrix} 0 & 1 \\ 1 & 0 \end{pmatrix}, \ \sigma^y = \begin{pmatrix} 0 & -i \\ i & 0 \end{pmatrix}, \ \sigma^z = \begin{pmatrix} 1 & 0 \\ 0 & -1 \end{pmatrix}, \tag{1.34}$$

and $\vec{n} = (n_x, n_y, n_z)$. $\Psi_{\vec{k}}$ is a 2-fermion spinor. Depending whether we have a superconductor or an insulator, it will typically take the form

$$\Psi_{\vec{k}} = \begin{pmatrix} c_{\vec{k}} \\ c^\dagger_{-\vec{k}} \end{pmatrix} \quad \text{or} \quad \Psi_{\vec{k}} = \begin{pmatrix} c_{\vec{k},A} \\ c_{\vec{k},B} \end{pmatrix}, \tag{1.35}$$

where A and B mark two sub-lattices. This form of $h(\vec{k})$ is the most general Hamiltonian for a two-band problem. Due to the decomposition in terms of Pauli matrices, it can be simply diagonalized. We define:

$$E(k) = ||\vec{n}(\vec{k})||, \tag{1.36}$$

$$\theta_{\vec{k}} = \mathrm{Arg}(n_z(\vec{k}) + i\sqrt{n_x(\vec{k})^2 + n_y(\vec{k})^2}), \ \phi_{\vec{k}} = \mathrm{Arg}(n_x(\vec{k}) + in_y(\vec{k})), \tag{1.37}$$

[2]It is chosen in order to have the translation symmetry.

such that:

$$\vec{n}(\vec{k}).\vec{\sigma} = E(\vec{k}) \begin{pmatrix} \cos(\theta_{\vec{k}}) & e^{-i\phi_{\vec{k}}}\sin(\theta_{\vec{k}}) \\ e^{i\phi_{\vec{k}}}\sin(\theta_{\vec{k}}) & -\cos(\theta_{\vec{k}}) \end{pmatrix}. \tag{1.38}$$

θ and ϕ are simply the spherical coordinates of the vector $\vec{n}$. The latter matrix has ± 1 as eigenvalues and we define the diagonalizing matrix $P_{\vec{k}}$ and the Bogoliubov-de Gennes spinor $\Upsilon_{\vec{k}}$ by:

$$P_{\vec{k}} = \begin{pmatrix} \cos(\frac{\theta_{\vec{k}}}{2}) & e^{-i\phi_{\vec{k}}}\sin(\frac{\theta_{\vec{k}}}{2}) \\ -e^{i\phi_{\vec{k}}}\sin(\frac{\theta_{\vec{k}}}{2}) & \cos(\frac{\theta_{\vec{k}}}{2}) \end{pmatrix} \qquad \Upsilon_{\vec{k}} = P_{\vec{k}}\Psi_{\vec{k}}, \tag{1.39}$$

where we define $\Upsilon^{\dagger}_{\vec{k}} = \begin{pmatrix} \eta^{\dagger}_{\vec{k},+}, & \eta_{\vec{k},-} \end{pmatrix}$ (for superconducting spinors given in Eq. 1.35, $\eta_{\vec{k},-} = \eta^{\dagger}_{-\vec{k}}$). η are still fermionic operators. Up to some discarded constant, we obtain:

$$h(\vec{k}) = (E_0(k) + E(k))\eta^{\dagger}_{\vec{k},+}\eta_{\vec{k},+} + (E(\vec{k}) - E_0(\vec{k}))\eta^{\dagger}_{\vec{k},-}\eta_{\vec{k},-} \tag{1.40}$$

η are the annihilation operators for the effective quasi-particles. In BCS superconductors, the quasi-particles are particle-hole superposition, while in insulators they correspond to a superposition of fermions of both species. $E(\vec{k}) \pm E_0(\vec{k})$ are the two energy bands and each quasi-particle state is independently occupied or empty depending on the sign of its energy. The ground state of the total system is simply obtained from the product of the ground states of each $h(\vec{k})$

$$|GS\rangle = (\prod_{\vec{k} \text{ s.t. } E(\vec{k})\pm E_0(\vec{k})<0} \eta^{\dagger}_{\vec{k},\pm})\,|0\rangle_{\eta}\,, \tag{1.41}$$

where $|0\rangle_{\eta}$ is the state where all quasi-particle states are unoccupied, *i.e.* $\eta_{\vec{k},\pm}|0\rangle_{\eta} = 0$ for all $\vec{k} \in \mathcal{BZ}$. From now on, we take $E_0(\vec{k}) = 0$. It is the case in most of the systems we consider and considerably simplifies the discussions. Moreover, it does not affect the topological nature of each band. Everything mentioned in the following can be easily generalized to non-zero $E_0(\vec{k})$. In this limit, the ground state is simply $|0\rangle_{\eta}$.

1.3 Topological approach to band theory

Building from the example of Kitaev's wire and the general formalism introduced in the previous Section, we present the complete characterization of the non-interacting fermionic systems based on their symmetries[11, 12]. Focusing on the bulk properties of two-band systems, we then give different formulations for the topological invariants.

1.3.1 Introduction to topology

Before studying how one can define topological properties in condensed matter physics, it is a good idea to give an overview of the basic concepts behind topology. More precisely, we will be interested in the concept of homotopy, a specific form of topological equivalence for continuous functions. We start by specifying the proper definition, before concluding

with a few specific simple examples.
Let E and F be two spaces with a properly defined distance (called topological spaces). Let f and g be two continuous functions from E to F. An homotopy between f and g is a continuous function α defined by:

$$\begin{aligned}\alpha_{f,g}:\ & E\times[0,1]\to F\\ & (u,t)\to\alpha(u,t) \text{ such that } \alpha(u,0)=f(u) \text{ and } \alpha(u,1)=g(u)\ \forall u\in E\end{aligned} \tag{1.42}$$

Two functions are said to be homotopically equivalent if there exists such an homotopy mapping one onto the other. In other words, if f can be continuously deformed into g. Being homotopic is obviously an equivalence relation:

- f is homotopic to itself (in this case $\alpha_{f,f}(u,t)=f(u)\ \forall t$),
- the relation is symmetric ($\alpha_{g,f}(u,t)=\alpha_{f,g}(u,1-t)$)
- and it is transitive $\alpha_{f,h}(u,t)=\delta_{t\leq 0.5}\alpha_{f,g}(u,2t)+\delta_{t>0.5}\alpha_{g,h}(u,2t-1)$).

It is therefore possible to define equivalence classes of the mappings from E to F based on homotopies: these will be called topological classes. In general, we will call a function (topologically) trivial if it is in the equivalence class of the constant mapping $f_v(u)=v\ \forall u\in E$.
Finally, without entering into fine details, the so-called homotopy group $\Pi(E,F)$ will give the number and the structure of the equivalence classes with respect to a composition we detail in the following examples. Physically, this composition will be equivalent to putting the two physical systems described by f and g together. Two spaces that have the same homotopy groups are (homotopically) equivalent, and a space where all functions are trivial (e.g. $\mathbb{C}$) is also called trivial.

A concrete example: let us consider the one-dimensional torus $\mathbb{T}^1$. We represent it by $[0,2\pi[$, and identify 0 and 2π. The continuous functions from $\mathbb{T}^1$ to $F=\mathbb{C}\setminus\{D(0,1)\}$, where $D(0,1)$ is the disc of radius 1 are simply all oriented loops in F. Figure 1.4 represents examples of loops in distinct topological classes. Let us consider the loop $\mathcal{L}_1$ that circles one time around the origin (its equation is $\mathcal{L}_1(k)=2e^{ik}$). If we wanted to deform it onto $\mathcal{L}_2$ (of equation $\mathcal{L}_2(k)=2+0.5e^{ik}$), we would need to cross the forbidden disk $D(0,1)$: it is therefore impossible. Both loops are in different topological classes. Moreover, $\mathcal{L}_2(k)$ is topologically trivial: let $\alpha_{2,0}$ be defined by:

$$\alpha_{2,0}(k,t)=2+0.5(1-t)e^{ik} \tag{1.43}$$

$\alpha_{2,0}$ is obviously continuous, takes its values in F, and reduce $\mathcal{L}_2$ to a point. A similar analysis can be performed for $\mathcal{L}_3$ and $\mathcal{L}_4$: the former winds one time in the anti-radian direction, while the latter winds twice in the anti-radian direction around the center disk. These two loops are homotopically distinct from the previous ones: two functions are equivalent if they wind the same number of times around the forbidden disk, signed by their direction. This winding number is our first example of topological invariant: a number that characterizes the topological equivalence class of the loop. It is here a signed integer. The family $\mathcal{L}_1^n$,

$$\mathcal{L}_1^n(k)=2e^{ink} \text{ for } n\in\mathbb{Z} \tag{1.44}$$

gives an example of all equivalence classes, n corresponding to the associated topological invariant.

Finally, examples of composition are given for $\mathcal{L}_1 \otimes \mathcal{L}_2$ and $\mathcal{L}_1 \otimes \mathcal{L}_3$. The composition operation is not uniquely defined. As an example, let f and g be two loops. Let $\tilde{f}$ (resp. $\tilde{g}$) be a continuous deformation of f (resp. g) such that $\tilde{f}(0) = 2$ (resp $\tilde{g}(0) = 2$). Then we define the composition $h = f \otimes g$ by:

$$h(k) = \begin{cases} \tilde{f}(2k) & \text{if } k \leq \pi \\ \tilde{g}(2k - \pi) & \text{if } k > \pi \end{cases} \tag{1.45}$$

Composed loops have a topological invariant equal to the sum of the topological invariant of the original loops. This structure translates in $\Pi(\mathbb{T}^1, F) = \mathbb{Z}$.

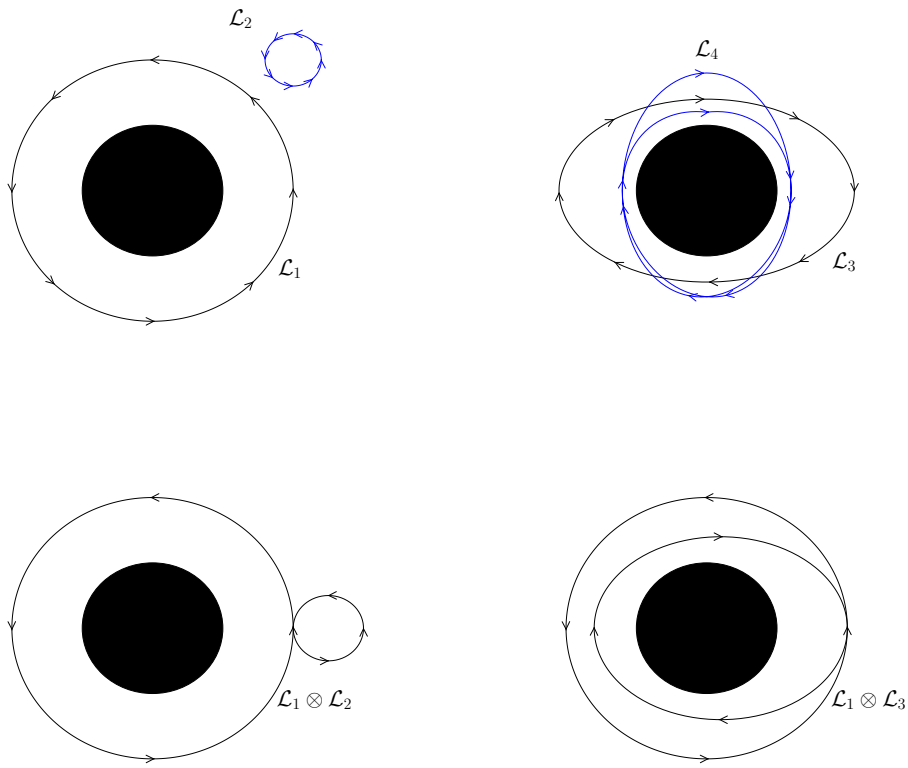

Figure 1.4: Elementary loops in $F = \mathbb{C} \setminus \{D(0,1)\}$. The black disk is the forbidden hole $D(0,1)$. Top left: $\mathcal{L}_1$ and $\mathcal{L}_2$ are two topologically distinct loops: $\mathcal{L}_2$ is trivial while $\mathcal{L}_1$ winds one time around the black disk in the radian direction. The associated topological invariant, counting the number of windings, are $\nu_1 = 0$ and $\nu_2 = 1$. Top right: $\mathcal{L}_3$ and $\mathcal{L}_4$ are also distinct. The number of turns must be counted with its sign: $\nu_3 = -1$ and $\nu_4 = -2$. Bottom left: the composition of $\mathcal{L}_1$ and $\mathcal{L}_2$ belongs to $\nu = \nu_1 + \nu_2 = 1 + 0 = 1$. Bottom right: the composition of $\mathcal{L}_1$ and $\mathcal{L}_3$ belongs to $\nu = \nu_1 + \nu_3 = 1 + (-1) = 0$.

All of these statements are also valid if we replace F by $\mathbb{R}^2 \setminus \{0\}$ or the 1-sphere $\mathbb{S}^1 = \mathbb{T}^1$ (the unit circle), though it is slightly less visual. The three spaces are homotopically equivalent.

1.3.2 Bulk hamiltonians and homotopy

As we are studying generic Hamiltonians, a natural question that arises is *under which conditions do two such Hamiltonians describe the same phase of matter and consequently are equivalent ?*
The Hamiltonian H can be reinterpreted as a mapping from the Brillouin Zone to the space of Hermitian matrices $h(\vec{k})$ of size $n \times n$ ($n = 2$ in the two-band limit), noted $\mathrm{Herm}(n)$. Taking the thermodynamic limit, or a continuous model, $\vec{k}$ is a continuous variable and the Brillouin Zone is a torus of dimension d (the physical dimension of the total system $\mathcal{S}$), noted $\mathbb{T}^d$.

$$\begin{aligned} h : \mathbb{T}^d &\to \mathrm{Herm}(n) \\ \vec{k} &\to h(\vec{k}) \end{aligned} \tag{1.46}$$

More generically, one can think of a class of model as a mapping from the parameter space $\mathcal{P}$ (for example a chemical potential, a hopping term etc...) to a mapping from $\mathbb{T}^d$ to $\mathrm{Herm}(n)$, or equivalently:

$$\begin{aligned} H : \mathcal{P} \times \mathbb{T}^d &\to \mathrm{Herm}(n) \\ (\{\mu, t, ...\}, \vec{k}) &\to h\{\mu, t, ...\}(\vec{k}), \end{aligned} \tag{1.47}$$

Two Hamiltonians, corresponding to two different values of the parameters, are equivalent if the functions h can be smoothly deformed into each other. They are then said to be topologically equivalent or more specifically homotopically equivalent, as defined in the previous part.
Let us use $n = 2$ as a test case, and take $E_0(\vec{k}) = 0$. An Hamiltonian is then entirely defined by the three functions $\vec{n}(k)$ introduced in Eq. 1.33, and consequently, h is strictly equivalent to:

$$\begin{aligned} h : \mathbb{T}^d &\to \mathbb{R}^3 \\ \vec{k} &\to \vec{n}(\vec{k}) \end{aligned} \tag{1.48}$$

As $\mathbb{R}^3$ is topologically trivial, all mappings h can be deformed onto each other and all Hamiltonians are equivalent. The reasoning can be extended to any n and the logical conclusion is that all phases of electrons are identical.
Obviously, this is wrong: the space of allowed transformations was too large and our definition of phases insufficient. As previously mentioned in the introduction to this thesis, we differentiate between gapped systems, that is to say phases where occupied and empty bands do not touch (are separated by a finite energy). The points in parameter space where bands touch, and consequently leave the system gapless, corresponds to possible quantum phase transitions (QPT). If such a transition occurs, the set of parameters is

called a quantum critical point (QCP). Again, going back to our $n = 2$ example, we enforce $E(\vec{k}) \neq 0$ for all $\vec{k}$ and all h. The mappings are now restricted to:

$$\begin{aligned} h : \mathbb{T}^d &\to \mathbb{R}^3 \setminus \{\vec{0}\} \\ \vec{k} &\to \vec{n}(\vec{k}) \end{aligned} \tag{1.49}$$

or more simply to:

$$\begin{aligned} \tilde{h} : \mathbb{T}^d &\to \mathbb{S}^2 \\ \vec{k} &\to \frac{\vec{n}(\vec{k})}{E(k)}, \end{aligned} \tag{1.50}$$

where $\mathbb{S}^2$ is the sphere of radius 1 in $\mathbb{R}^3$. Indeed, $\mathbb{S}^2$ and $\mathbb{R}^3 \setminus \{\vec{0}\}$ are homotopically equivalent[3]. The latter form should not come as a surprise: it is nothing but the reformulation of the two-band problem on the Bloch sphere. As $\mathbb{S}^2$ is not homotopically trivial, this leaves the possibility of different classes of Hamiltonians. In particular, for $d = 2$, we can point out that $\Pi(\mathbb{T}^2, \mathbb{S}^2) = \mathbb{Z}$. The phases of non-interacting electrons in dimension $d = 2$ are classified by an integer $n \in \mathbb{Z}$. As we will see in Section 1.3.4, this integer is the so-called Chern number.

1.3.3 Symmetry and classification

As we have just seen, restricting the possible transformations and the possible Hamiltonians changes the topological classification of our systems. It is consequently natural to check whether further restrictions can appear for physical reasons. The logical step for the physically savvy mathematicians is therefore to consider the impact of symmetries on the topological classification of fermions. We remind the reader that we define here symmetries in a very large sense: we call a transformation U acting on the Hamiltonian H a symmetry if it leaves H invariant. Since 1918, we know from Noether's theorem that symmetries impose conserved quantities, and consequently a set of quantum numbers that are conserved during a time evolution. This set of quantum numbers could (or should) a priori be respected in the smooth deformations we introduced. A complete classification in function of a set of discrete symmetries was indeed obtained[11, 12] and is summarized in Table 1.1.

We want to emphasize that the symmetries a priori do not necessarily change the space F, as restricting transformation to gapped systems did, but limit the authorized functions and therefore the continuous deformations. As an example, a symmetry can enforce the parity of a function (e.g. odd). That means that, at all steps t, the function $k \to \alpha_{f,g}(k, t)$, defined in Eq. 1.42 will have to stay odd, which may affect the homotopy group. Of course, it is sometimes more convenient to reformulate this restriction in terms of the final space F.

The three symmetries introduced in the classification are the Time-Reversal symmetry (TRS), the Particle-Hole symmetry (PHS) and the Chiral symmetry (CHS). The first

[3] In fact, $\mathbb{R}^{n+1} \setminus \{\vec{0}\}$ and $\mathbb{S}^n$ are always homotopically equivalent.

System	Cartan nomenclature	TRS	PHS	CHS	$d=1$	$d=2$	$d=3$
standard (Wygner-Dyson)	A (unitary)	0	0	0	-	$\mathbb{Z}$	-
	AI (orthogonal)	1	0	0	-	-	-
	AII (symplectic)	-1	0	0	-	$\mathbb{Z}_2$	$\mathbb{Z}_2$
chiral (sublattice)	AIII (chiral unitary)	0	0	1	$\mathbb{Z}$	-	$\mathbb{Z}$
	BDI (chiral orthogonal)	1	1	1	$\mathbb{Z}$	-	-
	CII (chiral symplectic)	-1	-1	1	$\mathbb{Z}$	-	$\mathbb{Z}_2$
Bogoliubov-de Gennes	D	0	1	0	$\mathbb{Z}_2$	$\mathbb{Z}$	-
	C	0	-1	0	-	$\mathbb{Z}$	-
	DIII	-1	1	1	$\mathbb{Z}_2$	$\mathbb{Z}_2$	$\mathbb{Z}$
	CI	1	-1	1	-	-	$\mathbb{Z}$

Table 1.1: Classification of gapped free (non-interacting) fermionic theories as a function of the Time-Reversal symmetry (TRS), the Particle-Hole symmetry (PHS) and the Chiral symmetry (CHS). The physical dimension is noted d. The first two columns label the different families, the next three columns precise the realization of the three symmetries. If 0, the system does not respect the symmetry. Otherwise, it represents the sign of the (projective) representation. The last three columns give the homotopy group from $\mathbb{T}^d$ to the relevant subset of Hermitian matrices. - notes the trivial group.

two symmetries are anti-unitary[4] while the latter is unitary. They are internal (on-site) symmetries, in the sense that they can be decomposed to act separately on each site. We will give here a physical interpretation of these symmetries, starting with TRS, in some simple cases.

In a time-reversal invariant system, the TRS, as the name implies, maps the evolution of a TRS preserving operator to its evolution in the past. Let $\hat{T}$ be a representation of the symmetry in the Hilbert space, that we take irreducible for simplicity's sake. For any TRS observable $\hat{O}$, it is equivalent to:

$$\hat{T}\hat{O}(t)\hat{T}^{-1} = \hat{T}e^{iHt}\hat{O}e^{-iHt}\hat{T}^{-1} = \hat{O}(-t) \quad \text{if } [\hat{T},\hat{O}] = 0, \tag{1.51}$$

and a natural definition for $\hat{T}$ for a quadratic fermionic Hamiltonian is:

$$\hat{T}c_{j,\sigma}\hat{T}^{-1} = \sum_j U_{\sigma,\sigma'}c_{j,\sigma}, \qquad \hat{T}i\hat{T}^{-1} = -i, \tag{1.52}$$

where U must be a unitary matrix to preserve the commutation relations. Naturally, TRS should square to 1, *i.e.* leave states invariant if we apply it twice. The gauge freedom of Quantum Mechanics ($|\psi\rangle$ and $e^{i\phi}|\psi\rangle$ describe the same state) means that we only require $U^*U = e^{i\phi}\mathbb{1}$, with ϕ an arbitrary complex phase. As U is unitary, it means that $U^* = e^{i\phi}U^\dagger$ and equivalently $U^T = e^{i\phi}U$. Multiplying the two leads to $e^{2i\phi} = 1$. An Hamiltonian can consequently belong to three symmetry classes: either it is not TRS, or

[4] A unitary matrix verifies $U_+U_+^\dagger = U_+^\dagger U_+ = \mathbb{1}$. An anti-unitary matrix U_- verifies $X^\dagger U_-^\dagger U_- Y = Y^\dagger X \ \forall X, Y$. One can always find a matrix U_+ such that $U_- = U_+\kappa$, κ being the complex conjugation.

it is TRS and $\hat{T}^2 = \mathbb{1}$ or it is TRS and $\hat{T}^2 = -\mathbb{1}$. It is represented in Table 1.1 by the symbols 0, 1 and -1 in the column TRS.
The PHS is very similar. Let us define $\hat{P}$ its representation in the Hilbert space (taken to be irreducible). It maps annihilation operators to corresponding creation operators:

$$\hat{P} c_j \hat{P}^{-1} = \sum_j U_{\sigma,\sigma'} c^\dagger_{j,\sigma'}, \qquad \hat{P} i \hat{P}^{-1} = -i, \tag{1.53}$$

where U is also a unitary matrix. It also consequently maps the sectors with M fermions c to the sectors with $S - M$ fermions. For the same reason as the TRS, it must square to $\pm\mathbb{1}$ and three different symmetry class appear for the PHS.
Finally, the CHS is a unitary transformation product of the TRS and the PHS. There can be situations where both the latter two are broken but where their product is preserved. Because it is a unitary transform, it will simply square to $\mathbb{1}$ if present, leading to the last separation into two symmetry class.
Taking the interdependencies between the symmetries into account leads to the 10-fold way of classifying non-interacting fermionic theories given in Table 1.1. Of course, the actual symmetries that will appear do not necessarily exactly match this physical interpretation. For example, Kitaev's wire has a particle-hole symmetry in the Bogoliubov-de Gennes formalism, but this does not translate into a true particle-hole symmetry for the original fermions due to the non-zero chemical potential.
For readers that are interested in more details on the derivation of the classification, we refer to the excellent review by Chiu, Teo, Schnyder and Ryu[41]. The next part focuses on the derivation of the topological invariant in the few cases that interest us, namely BDI and D, for $d = 1$, and the Chern number for $d = 2$.
In this thesis, we only discuss the so-called Symmetry Protected Topological (SPT) phases, by opposition to intrinsic and Symmetry Enriched Topological (SET) phases. The intrinsic topological phases do not require any symmetries to have non-trivial topological phases. They will present deconfined, fractionalized quasi-particles (anyons) in the bulk. The SET phases are a generalization that do require symmetries to present these deconfined quasi-particles. Conversely, the SPT we are interested in may only realize such exotic states at boundaries. The topological excitations, such as the Majorana fermions we have encountered, then only exist at boundaries (they are confined in the bulk of the system). In particular, we will not discuss the Fractional Quantum Hall effect.

1.3.4 Relevant topological invariants for two-band Hamiltonians

In this Section, we derive the topological invariant in the different classes of Hamiltonians we consider throughout the thesis. We essentially limit ourselves to two-band model, and refer the readers to Ref. [41] or [42].

Topological invariant for the BDI class in $d = 1$

We start with the BDI class, whose paradigmatic example is Kitaev's chain. In this class, the three aforementioned symmetries are realized and all square to 1. We will start from their representation in the simple case of Kitaev's chain before generalizing. The points

$k = 0$ and $k = \pi$ are special, as the two-band description breaks down. We can nonetheless safely ignore them in this discussion, and replace them by their limit $0^{\pm}$ or $\pi^{\pm}$ without difficulties, as long as the system is gapped.
The time-reversal symmetry for spinless fermions has a simple action:

$$\hat{T} c_j \hat{T}^{-1} = c_j, \qquad \hat{T} i \hat{T}^{-1} = -i, \tag{1.54}$$

leading to $\hat{T} = \kappa$, where κ is the complex conjugation. Eq. 1.1 is indeed invariant by TRS[5]. In Fourier space, it translates into $h(k) = h(-k)^*$.
Kitaev's chain has no particle-hole symmetry in the physical space, but the Bogoliubov-de Gennes formalism introduces an artificial PHS: one can rewrite Eq. 1.15 as:

$$H = \frac{1}{2} \sum_{k \in \mathcal{BZ}} \Psi_k^\dagger h(k) \Psi_k, \tag{1.55}$$

up to some constant factors. For Kitaev's chain, we have the equality:

$$\sigma^x \Psi_{-k} = (\Psi_k^\dagger)^T = \begin{pmatrix} c_k^\dagger \\ c_{-k} \end{pmatrix}, \tag{1.56}$$

where the transpose acts on $\Psi_k^\dagger$ seen as a 1×2 matrix of operators (and not on the c operators themselves). Applying the equality to Eq. 1.15 leads to

$$H = \frac{1}{2} \sum_{k \in \mathcal{BZ}} (\sigma^x \Psi_{-k})^T h(k) (\Psi_{-k}^\dagger \sigma^x)^T \tag{1.57}$$

$$= -\frac{1}{2} \sum_{k \in \mathcal{BZ}} \Psi_{-k}^\dagger \sigma^x h^*(k) \sigma^x \Psi_{-k}, \tag{1.58}$$

which translates into the equality $h(-k) = -\sigma^x h^*(k) \sigma^x$. We take this as the definition of the PHS.
Finally, the chiral symmetry is the composition of the two previous symmetries and translates into $h(k) = -\sigma^x h(k) \sigma^x$. For each quasi-particle of energy E, there must exist a corresponding quasi-particle of energy $-E$.
Now, we can start generalizing and extending the previous results to the whole BDI class. Let us assume that the three symmetries admit the previous representations. What can we say about $h(k)$?
First, we know that $h(k)$ is hermitian and consequently can be written as $h(k) = \vec{n}(k).\vec{\sigma}$. Then we can apply the two anti-unitary symmetries:

$$\text{TRS: } h(k) = h^*(-k) \quad \Rightarrow \begin{cases} n_x(k), n_z(k) & \text{are even in momentum space}^6 \\ n_y(k) & \text{is odd} \end{cases} \tag{1.59}$$

$$\text{PHS: } h(k) = -\sigma^x h^*(-k) \sigma^x \quad \Rightarrow \begin{cases} n_z(k) & \text{is even in momentum space} \\ n_x(k), n_y(k) & \text{are odd} \end{cases} \tag{1.60}$$

[5]This form of the TRS is only true for Δ real (*i.e.* in our chosen gauge). For a complex Δ, one can always find an alternative representation of TRS that will have similar properties.

The combination of the two symmetries consequently leaves $h(k) = n_z(k)\sigma^z + n_y(k)\sigma^y$, n_z being even and n_y odd. Enforcing that the gap does not cancel leaves us to study the homotopy group: $\pi(\mathbb{T}^1, \mathbb{R}^2 \setminus \{\vec{0}\}) = \pi(\mathbb{T}^1, \mathbb{T}^1\}) = \mathbb{Z}$. The latter result is actually true for all BDI hamiltonian: one can always find a basis where the two anti-unitary symmetries admit the previous representation and consequently h projects $\mathbb{T}^d$ on $\mathbb{T}^1$.
Finally the topological invariant is simple to describe for $d = 1$: it coincides with the one defined in Sec. 1.3.1. Two continuous mappings of the unit circle onto himself will be equivalent if they realize the same number of revolutions around the circle, as represented in Figure 1.4. The topological invariant is consequently this winding number ν that can be conveniently expressed in the following way.
Let $\theta_k = \mathrm{Arg}(n_z(k) + in_y(k))$[7]. θ_k is a periodic mapping of the (first) Brillouin Zone to the torus $[0, 2\pi[$, as θ_k and $\theta_k + 2\pi$ describes the exact same $h(k)$. It is consequently a representation of our Hamiltonian and its homotopic properties. Then the winding number ν is simply given by[43–45]:

$$\nu = \int\limits_{k\to\theta_k} d\theta \text{ where the integral carries on the loop defined by } \theta_k \tag{1.61}$$

$$= \int\limits_{k\in\mathcal{BZ}} \frac{\partial\theta_k}{\partial k} dk \quad \text{when } \theta_k \text{ is } \mathcal{C}^1 \text{ by part.} \tag{1.62}$$

Both expressions are equivalent, but can be difficult to evaluate. A more convenient discrete formulation can actually be obtained. To count the number of turns around the BZ, it is enough to look at a fixed value θ_0 (usually a multiple of $\pi/2$), and count the number of times it is attained, weighted by the direction of the curves (the sign of the slope). If the slope vanishes at one of the points, simply take another θ_0 (or use the second derivative). In practice, the curve rarely cross a well-chosen θ_0 more than twice.

$$\nu = \sum_{k_0\in\theta_k^{-1}(\theta_0)} \mathrm{sign}(\frac{\partial\theta_k}{\partial k}(k_0)) \quad \forall\theta_0 \qquad \begin{array}{c}\text{when } \theta_k \text{ is } \mathcal{C}^1 \text{ (can be relaxed)}\\ \text{and } \frac{\partial\theta_k}{\partial k}(k_0) \text{ does not cancel.}\end{array} \tag{1.63}$$

Similar winding numbers can be determined for higher-dimensional BDI Hamiltonians (or for other classes of problems) or for multi-bands problems.

Topological invariant for the D class in $d = 1$

The D class of Hamiltonians can be interpreted as members of the BDI class where a TRS-breaking term has been added. The topological invariant is no longer an element of $\mathbb{Z}$ but of $\mathbb{Z}_2$.
Let us first start with a concrete example to understand the reduction. Let us take two parallel Kitaev's wires both in the topological phase with the same parameters and open

[7] Note the slight difference with Eq. 1.37: ϕ_k can take only the values 0 or π, and the normalized $\vec{n}$ lives on a unit circle. Consequently, we use polar coordinates instead of spherical coordinates. We will often use this convention for BDI Hamiltonians

boundaries[8]. We note c_1 and c_2 the fermions operators of each wire. On each extremity of both wires lives a zero energy Majorana fermion. The ground state is consequently 4 times degenerate. Let $-2t < \mu < 0$ such that $\tilde{\gamma}^A_{1/2}$ and $\tilde{\gamma}^B_{1/2}$ are the four zero-energy Majorana fermions, following the notations of Eq. 1.10 (the additional index indicates the wire). We will show that there is no topological protection of the degeneracy of the ground state, i.e. that we can introduce small local terms in the Hamiltonian that lift the degeneracy in thermodynamic limit if we break the TRS. To do so, we compute the effect of the TRS on the Majorana fields:

$$\hat{T}\tilde{\gamma}^A_{1/2}\hat{T}^{-1} = \tilde{\gamma}^A_{1/2} \qquad \hat{T}\tilde{\gamma}^B_{1/2}\hat{T}^{-1} = -\tilde{\gamma}^B_{1/2} \tag{1.64}$$

Then we can classify typical two-body terms. Using perturbation theory, we can estimate the lifting of degeneracy induced by the inclusion of these terms in the Hamiltonian with amplitude ε much smaller than the gap $\Delta E = \min_k E_k$. We focus on the left-side extremity:

$$\begin{array}{lrl} \text{TRS-respecting:} & i\tilde{\gamma}^A_{1/2}\gamma^B_{1,1/2}, i\tilde{\gamma}^A_{1/2}\gamma^B_{2,1/2}... \rightarrow & \text{energy splitting } \mathcal{O}(\varepsilon(\frac{\varepsilon}{\Delta E})^L) \\ \text{TRS-breaking:} & i\tilde{\gamma}^A_1\tilde{\gamma}^A_2 \rightarrow & \text{energy splitting } \propto \varepsilon \end{array}$$

A similar reasoning can be applied to the right-side extremity. If we do not allow for TRS-breaking, the degeneracy cannot be lifted by arbitrarily small perturbations in the thermodynamic limit. The system stays in the BDI class and the topological invariant of the double Kitaev's chain is $\nu = 2$. The phase is not equivalent to the trivial one. On the other hand, if we allow for TRS-breaking, we jump to the D class and we can directly lift the degeneracy: a phase with $\nu = 2$ is equivalent to the trivial phase ($\nu = 0$). The proper topological invariant indeed lives in $\mathbb{Z}_2$.
Using the representation of the symmetries derived in the previous section, we can generalize our results. Classifying the phases in the D class is equivalent to compute a topological invariant for:

$$\begin{aligned} \tilde{h} : \mathbb{T}^1 &\rightarrow \mathbb{S}^2 \equiv \mathbb{R}^3 \setminus \{0\} \\ \vec{k} &\rightarrow \frac{\vec{n}}{E(k)} \end{aligned} \tag{1.65}$$

Without additional constraints from PHS, all such mapping are trivial. The PHS still enforces Eq. 1.60.: from it follows that $n_x(0/\pi) = n_y(0/\pi) = 0$ and consequently $\tilde{h}(0/\pi) = \pm(0, 0, 1)$. In other words, the symmetric momenta 0 and π are pinned to the z-axis of the Bloch sphere. The classification follows naturally. If $\tilde{h}(0) = \tilde{h}(\pi)$, the mapping is trivial: it can be reduced to a constant $\tilde{h}$ for all k: $\nu = 0$. The actual value has no consequence: by shifting continuously the representation of the PHS, one can inverse the poles. If $\tilde{h}(0) \neq \tilde{h}(\pi)$, $\tilde{h}$ cannot be reduced to a constant mapping: $\nu = 1$. This stays true even if we change the representation of the PHS as the PHS symmetric points must stay on the same diameter. Figure 1.5 represents the two classes of mapping. An integral

[8]Two wires can always be combined to create another one-dimensional system. One either defines a new unit-cell corresponding to the fusion of the ones of each wire, or just alternates between them and define longer range terms. Both points of view are equivalent.

representation of the topological invariant can also be given. A variant of the Berry phase can be used to characterize the path [42]:

$$\gamma = \oint_{\mathcal{BZ}} dk i \langle \vec{r}_k | \sigma^z \frac{d}{dk} | \vec{r}_k \rangle \tag{1.66}$$

$$= \oint_{\mathcal{BZ}} dk \frac{d\phi_k}{dk} \sin^2 \frac{\theta_k}{2} + f(k), \tag{1.67}$$

where $f(k)$ is a differential form whose integral vanishes. $|\vec{r}_k\rangle$ is the ground state of $\tilde{h}(k)$:

$$|\vec{r}_k\rangle = (-e^{-i\phi_k} \sin(\frac{\theta_k}{2}), \cos(\frac{\theta_k}{2})).$$

Care has to be given to the different definitions. The topological invariant is $\nu = \frac{1-e^{i\gamma}}{2}$. For multi-bands problems, the Berry phases of all occupied bands are summed to get the proper topological invariant.

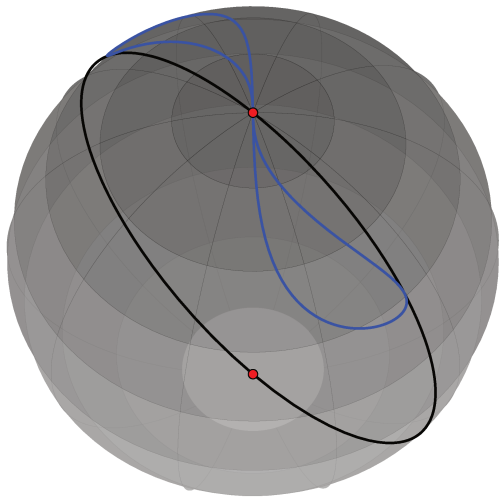

Figure 1.5: The two classes of mappings from $\mathbb{T}^1$ to $\mathbb{S}^2$ are represented in this Figure. The red points correspond to the PHS-fixed points $\pm\vec{e}_z$. In blue, a trivial loop that only crosses one of these points, in black an example of topological mapping (here taken from Kitaev's model).

Topological invariant for the D and A class in $d = 2$

Our last example of topological invariant is the first Chern number characterizing the A and D class of non-interacting models in dimension d. The A class is characterized by

an absence of discrete symmetries (and consequently $\vec{n}_k$ is arbitrary as long as it does not cancel), while the D class has the PHS squaring to 1. It was historically the first introduced, in the context of the Integer Quantum Hall effect[7].
We consider Hamiltonians in the D or A class, and still consider E_k to be 0. The Hamiltonian maps $\mathbb{T}^2 \equiv \mathbb{S}^2$ to $\mathbb{R}^3 \backslash \{\vec{0}\} \equiv \mathbb{S}^2$. Noting $\tilde{n}$ the normalized vector $\vec{n}$, a simple expression has been obtained for the topological invariant:

$$\nu = \frac{1}{4\pi} \int_{\mathcal{BZ}} d\vec{k}\tilde{n}.(\partial_{k_x}\tilde{n} \times \partial_{k_y}\tilde{n}) \tag{1.68}$$

ν is an integer, and classify the mappings. It corresponds to the number of times the initial torus (the $\mathcal{BZ}$) wraps around the sphere. As the integration can be quite technical for arbitrary functions, it is more convenient to identify the contributions that can give rise to non-zero Chern number. As $\mathbb{S}^2$ is a two-dimensional manifold, the texture of the vector $\tilde{n}$ can be always represented locally in a 2D plane, without affecting the topological properties. We pick a preferred direction for $\tilde{n}$, here z. Then we place ourselves at the momenta where $\tilde{n}$ is in this direction (if there is none, the mapping does not cover the whole sphere and is henceforth trivial). In Figure 1.6, we draw the (normalized) orthogonal component

$$\tilde{n}_\perp = \frac{1}{\tilde{n}_x^2 + \tilde{n}_y^2}(\tilde{n}_x, \tilde{n}_y)$$

in the neighborhood of such a momentum, noted $\vec{k}_0$, for the four basic contributions to the Chern number. As can be seen, this orthogonal component forms a vortex around $\vec{k}_0$. We define here a vortex by a configuration of $\tilde{n}_\perp$ with non-zero winding around $\vec{k}_0$, which is the center of the vortex. Defining $\tilde{\theta}_k = \mathrm{Arg}(\tilde{n}_x + i\tilde{n}_y)$, the winding number of the vortex can be computed using the formula 1.62 or 1.63 on an arbitrary small loop around k_0, oriented according the sign of $\tilde{n}_z(k_0)$. We call the winding number of such a vortex its topological charge.
From these considerations, a discrete formulation for the Chern number can be formulated[46, 47]:

$$\nu = \frac{1}{2} \sum_{k \in n_x^{-1}(0) \cap n_y^{-1}(0)} \mathrm{sign}((\partial_{k_x}\vec{n} \times \partial_{k_y}\vec{n}).\vec{e}_z)\ \mathrm{sign}(n_z). \tag{1.69}$$

It can be trivially generalized to any basis choice for $\vec{n}$. As usual, for multi-bands problem, the total Chern number can be extracted from the sum of the Chern numbers of all occupied bands.

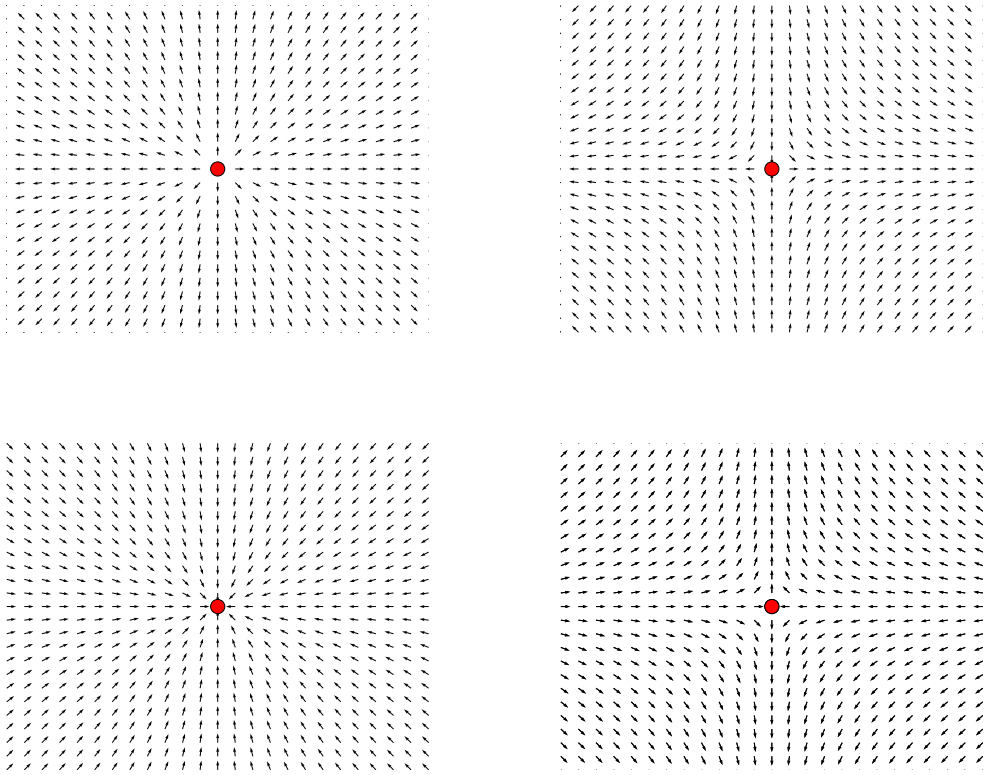

Figure 1.6: Examples of the 4 types of basic topological defects that can appear in h for $d = 2$. The normalized vector field corresponds to $\tilde{n}_\perp = (\tilde{n}_x, \tilde{n}_y)$ represented in a part of the Brillouin Zone. The vector $\tilde{n}_\perp$ cancels at the red point, that carries a topological charge $\text{sign}(n_z)$ on the left and $-\text{sign}(n_z)$ on the right. The total Chern number of the band can be obtained by summing the contributions of all such defects.

1.4 Bulk-edge correspondence and edge states

As we have just seen, Hamiltonians can be classified into topological families that cannot be deformed continuously into each other, depending on the symmetries of the system. An important question to address is the physical relevance of this classification, or, in other words, *are there any physical consequences to this classification ?*
One of the main features of these topological states is the presence of stable zero-energy bound states or free modes at boundaries, or point-like defects (dislocation of the lattice in $d = 2$ for example). Here stable means that weak perturbations have an effect exponentially small with the size of the considered systems. Going through a detailed proof of the bulk-edge correspondence goes far beyond the limit of this thesis, but we will give some phenomenological arguments allowing us to make a parallel between the topological invariant and the number of zero-energy modes. In particular, we show that out of the

number of zero modes we can build a quantity noted $\tilde{\nu}$ that shares a lot of properties with the topological invariant ν. The Atiyah-Singer index theorem[48] actually states that these quantities are identical.

1.4.1 D class for $d = 1$

First, we study the D class in $d = 1$. Let us consider the usual PHS. We take a generic Hamiltonian of the form:

$$H = \vec{\Psi}^\dagger \mathcal{H} \vec{\Psi}, \tag{1.70}$$

where Ψ is the vector of annihilation and destruction operators, $\Psi^\dagger = (c_1^\dagger, ..., c_L^\dagger, c_1, ..., c_L)$. By direct analogy with Eq. 1.60, an Hamiltonian invariant by PHS verifies $\{\hat{P}, \mathcal{H}\} = 0$ (with $\hat{P}$ the representation of the PHS and $\mathrm{Tr}(\mathcal{H}) = 0$). Applying this equality to any eigenstate $|\psi_\varepsilon\rangle$ of $\mathcal{H}$ of energy ε leads to:

$$\mathcal{H}\hat{P}\,|\psi_\varepsilon\rangle = -\varepsilon \hat{P}\,|\psi_\varepsilon\rangle\,. \tag{1.71}$$

The eigenvalues of $\mathcal{H}$ consequently comes in pairs at non-zero energies. Conversely, zero-energy eigenvalues can always be taken to be eigenvectors of $\hat{P}$ with eigenvalue 1 and there can be an odd number of zero-energy eigenvalues[9].
First consider an Hamiltonian with a single zero-energy mode, protected by a gap. No PHS respecting perturbation can change the energy of this mode: if it acquired a non-zero energy, the energy levels would no longer respect the paired structure. Now let us consider an Hamiltonian that has M zero-energy eigenstates. Due to the symmetry $\varepsilon \leftrightarrow -\varepsilon$, perturbations must leave the parity of M invariant. One can consequently separate the Hamiltonians invariant by PHS into two families characterized by:

$$\tilde{\nu} = M\ [2] \in \mathbb{Z}_2 \tag{1.72}$$

This separation is extremely similar to the homotopy group for the D class in $d = 1$. To apply non-trivially this argument to a concrete example such as Kitaev's wire, one needs to consider a semi-infinite geometry, with only one boundary. The zero-energy eigenvector of the Hamiltonian $\mathcal{H}$ then corresponds to the zero-energy Majorana at the edge of the superconductor. A convenient model to do so is the Jackiw-Rebbi model[49], a continuum version of Kitaev's chain, with:

$$H = \int dr \Psi_r^\dagger (i\Delta\sigma^y \partial_r + m(r)\sigma^z)\Psi_r, \tag{1.73}$$

where the mass $m(r)$ changes of sign at the boundary. It describes a domain-wall in a p-wave superconductor.

It turns out that the number of zero-energy modes at a boundary is indeed given by the bulk topological invariant. These zero-energy states must be localized close to the boundaries, as they should not affect the bulk description. Being localized, it is convenient

[9] As $\hat{P}$ is anti-unitary, if $|\psi\rangle$ is an eigenstate of $\hat{P}$ with eigenvalue -1, then $i\,|\psi\rangle$ verifies $\hat{P}i\,|\psi\rangle = -i(-\,|\psi\rangle) = i\,|\psi\rangle$, while representing the same quantum state.

to have a look at the possible realization of the PHS at the single cell level. For the usual two-band superconducting models such as Kitaev wire, the unit-cell only comports one fermion. The only non-trivial PHS objects that can be built out of a single fermion are Majorana fermions, which are indeed the localized zero-energy bound states. On the other hand, insulating models have two fermions by unit-cell,and one can build an equivalent complex fermion that will respect the "PHS": the edge states will be normal fermions. It is the case for the SSH model[50] detailed in Sec. 1.5.1.

1.4.2 BDI class for $d = 1$

In the BDI class, the system is also TRS and consequently CHS. As the TRS commutes with $\mathcal{H}$, the CHS anti-commutes with $\mathcal{H}$. Let $\hat{C}$ be the representation of CHS. $\hat{C}$ also sends eigenvectors of $\mathcal{H}$ with energy ε to eigenvectors with energy $-\varepsilon$. It commutes with the zero-energy sector of $\mathcal{H}$, which means they can be co-diagonalized. The eigenvalues ± 1 of $\hat{C}$ classify the zero-energy eigenvectors of $\mathcal{H}$[10]. Moreover, the trace of $\hat{C}$ is zero on each subspace $\mathrm{Span}(|\psi_\varepsilon\rangle, \hat{C}|\psi_\varepsilon\rangle)$, $\varepsilon > 0$. Let $M_\pm$ be the number of zero-energy states with $\hat{C}|\psi_0\rangle = \pm|\psi_0\rangle$. The trace of $\hat{C}$ on the total Hilbert space is simply $\tilde{\nu} = M_+ - M_-$. Any perturbation that leaves the system invariant by CHS also leaves its trace invariant as long as the bulk gap is not closed. $\tilde{\nu} \in \mathbb{Z}$ consequently classifies the Hamiltonians of the BDI class. Again, in $d = 1$, it turns out that $\tilde{\nu} = \nu$. The nature of the edge states is the same as in the D class. Non trivial applications should also be done in the semi-infinite geometries.

1.4.3 D class for $d = 2$

For this class of problem, we apply a more practical analysis: the topological invariant directly appears in a concrete observable when considering an open system (with a one-dimensional boundary), giving rise to the Integer Quantum Hall Effect.[7]
When studying electrons confined to 2 dimensions, at very low temperature and high magnetic field, the Hall resistivity $\rho_{x,y}$ (if we take the magnetic field to be in the vertical direction z, and apply a small electric field in an orthogonal direction, say x, the Hall resistivity is the response current in the y direction divided by this electric field: $\frac{dI_y}{dE_x}$) is not proportional to the magnetic field (as in the classical limit), but precisely quantized when bands are fully occupied. The longitudinal resistivity then vanishes. Using Kubo formula (linear response theory, see Appendix G.2), it is possible to show that:

$$\sigma_{x,y} = \frac{1}{\rho_{x,y}} = \frac{ie^2\hbar}{S}\sum_n \frac{\langle GS|\hat{v_x}|\psi_n\rangle\langle\psi_n|\hat{v_y}|GS\rangle - \langle GS|\hat{v_y}|\psi_n\rangle\langle\psi_n|\hat{v_x}|GS\rangle}{(E_0 - E_n)^2}, \tag{1.74}$$

where we note $|GS\rangle$ the ground state of the system, E_0 its energy, we sum over all excited states $|\psi_n\rangle$ of energy E_n, and $\hat{v}_{x/y}$ is the velocity operator in the x/y direction. Thouless, Kohmoto Nightingale and den Nijs [7] have shown that the Hall conductance can be expressed as an integral over the Brillouin Zone of the Berry curvature of the occupied bands. For our simple two-band models, where the lower-band is occupied, it can be

[10] The eigenvalues ± 1 of $\mathcal{C}$ are physical: $\hat{C}$ is unitary and therefore linear.

written has:

$$\sigma_{x,y} = \frac{e^2}{h} \int_{\mathcal{BZ}} \frac{(-i)d\vec{k}}{2\pi} (\partial_{k_x} \langle \vec{r_k} |)(\partial_{k_y} | \vec{r_k} \rangle) - (\partial_{k_y} \langle \vec{r_k} |)(\partial_{k_x} | \vec{r_k} \rangle) \tag{1.75}$$

$$= \frac{e^2}{h} \frac{1}{4\pi} \int_{\mathcal{BZ}} d\vec{k} \tilde{n}.(\partial_{k_x} \tilde{n} \times \partial_{k_y} \tilde{n}) \text{ for our two-band model} \tag{1.76}$$

$$= \nu \frac{e^2}{h}$$

For multiple bands, the conductivity can be simply expressed as:

$$\sigma_{x,y} = \frac{e^2}{h} \sum_{\text{all occupied bands } p} \nu_p, \tag{1.77}$$

where ν_p is the Chern number of the p band. It is thus a topological invariant, which explains its precise quantization in experiments. No perturbations can change its value as long as the bulk gap does not close. It also gives us an insight to the nature and number of edge modes for the D class. The bulk gap being large, no current is carried in the bulk of the insulator. On the other hand, $\sigma_{x,y}$ corresponds precisely to the conductance of $\sum_p \nu_p$ free fermionic chiral modes. It is quite natural to conclude from there that edges precisely carry $\sum_p \nu_p$ free fermionic chiral modes. The result can be formalized and generally proved for the topological insulators of class D[41]. This Chern number can also be seen by tweaking the boundary conditions of the many-body wave function, a formulation particularly useful in the interacting case[8].

1.5 Topical examples in 1D

In the following section, we will focus on giving a short overview of the different models of one-dimensional non-interacting fermions that we will use in the rest of the thesis. We invite the readers interested in the more general and abstract results of this thesis to directly pursue to the next chapter. We will refer to the listed models when needed. While we treat both superconductors and insulators with the same Bogoliubov framework, we separate them in this section. We first introduce the Shu-Schrieffer-Heeger model for dimerized fermions[50] as a simple reference model for topological insulators in Section 1.5.1. While it is mathematically quasi-equivalent to Kitaev's chain, we will precisely discuss some of the very important differences between the two. In a second time, we will present two models of topological superconductors. The first one (Section 1.5.2) is a variation of the Kitaev's wire with longer-range hopping and pairing terms[51]. It allows to explore the BDI and D classes in more details. Finally, the last model is the Rashba spin-orbit topological superconductor proposed by Ref. [23, 24] (Section 1.5.3). Contrarily to all previous models, it is not a two-band model but requires a more complex treatment. For some specific range of parameters, it can be projected onto Kitaev's wire. It has the physical advantage to be more realistic than Kitaev's wire.

1.5.1 The Su-Schrieffer-Heeger model

The Su-Schrieffer-Heeger (SSH) model[50] is a model introduced to describe the physics of polyacetylene, before the rise of topological materials. It consists in a chain of dimerized spinless fermions. For convenience, we define two species of fermions A and B that leave on the odd and even sites of the chain. The elementary cell is now composed of two fermions and the Hamiltonian can be written in the following form:

$$H_{SSH} = \sum_j -t_1(c^\dagger_{j,A}c_{j,B} + c^\dagger_{j,B}c_{j,A}) - t(c^\dagger_{j,B}c_{j+1,A} + c^\dagger_{j+1,A}c_{j,B}), \tag{1.78}$$

where we take t_1 and t to be positive. Defining the spinors $\Psi^\dagger_k$ as $(c^\dagger_{k,A}, c^\dagger_{k,B})$, the Hamiltonian in momentum space is given by:

$$H_{SSH} = \frac{1}{2}\sum_k \Psi^\dagger_k \left(-2(t_1 + t\cos(k))\sigma^x - 2t\sin(k)\sigma^y\right)\Psi_k \tag{1.79}$$

This Hamiltonian is identical to Kitaev's in Eq. 1.55, up to a rotation around the y-axis. Consequently, the phase diagram is still given by Fig 1.2, taking $\Delta = t$ and $\mu = 2t_1$, and the model belongs to the BDI class. There are nonetheless several differences between the two models, that are based on the definition of the spinor.
First, we no longer have $\Psi_k = \Psi^\dagger_{-k}$, i.e. the particle-hole symmetry that was intrinsic to the non-interacting superconductors is now a true symmetry, which must be preserved against disorder perturbations. Its representation is given by $\hat{P} = \sigma^z\kappa$, and it is trivially broken by any alternating chemical potential. The resilience of the SSH model to perturbations in a physical set-up is consequently very weak as disorder will easily break the PHS.
Secondly, the nature of the edge states changes. It can be trivially seen from analyzing the limit $t_1 \to 0$ which corresponds to the core of the topological phase. The Hamiltonian is now a sum of commuting terms:

$$-t(c^\dagger_{j,B}c_{j+1,A} + c^\dagger_{j+1,A}c_{j,B}),$$

that leads to the formation of dimers. Just as it is the case for Majorana fermions in Kitaev's model, two fermions do not appear in the Hamiltonian if we take an open chain: $c_{1,A}$ and $c_{L,B}$. These are the localized topologically protected edge states of the model. The change of nature is linked to the change in the unit-cell. While the number of electrons by unit-cell was 1 in Kitaev's model, it is 2 in the SSH model and the edge states correspond to half a unit cell in both cases (eigenvalues of the PHS). It implies in turn that the topological degeneracy of the ground state is 4 for the SSH model. For an equivalent Hamiltonian h, a topological insulator will have doubled edge-states compared to a topological superconductor.

1.5.2 Longer-range Kitaev's wire

In this part, we study an extension of Kitaev's model that presents longer-range hopping and pairing terms[51]. They present the advantage to realize more phases of the BDI class (with a topological invariant that can go beyond ± 1), and hence can host several

Majorana fermions at each boundary. The family of models is generically described by the following Hamiltonian:

$$H_K^G = -\mu \sum_j c_j^\dagger c_j + \sum_{l=1} \left(\sum_j -t_l (c_j^\dagger c_{j+l} + c_{j+l}^\dagger c_j) + \Delta_l (c_j^\dagger c_{j+l}^\dagger + c_{j+l} c_j) \right) \tag{1.80}$$

With Time-Reversal-Symmetry

In order for H_K^G to be invariant by TRS, there must exist a gauge where t_l and Δ_l are both reals for all l. In the following, we place ourselves in such a gauge. Following our Fourier convention, using PBC, the Hamiltonian can be rewritten in k-space as:

$$H_K^G = (-\mu - 2\sum_l t_l) c_0^\dagger c_0 + (-\mu + 2\sum_l (-1)^l t_l) c_\pi^\dagger c_\pi + \sum_{0<k<\pi} \Psi_k^\dagger \vec{n}_G(k).\vec{\sigma}\Psi_k,$$
$$\text{with } \Psi_k = \begin{pmatrix} c_k \\ c_{-k}^\dagger \end{pmatrix}, \ \vec{n}_G(k) = \left(0, -2\sum_l \Delta_l \sin kl, -\mu - 2\sum_l t_l \cos kl\right), \tag{1.81}$$

where we discarded unimportant constants. The energy spectrum is given by:

$$E_k^2 = (2\sum_l \Delta_l \sin kl)^2 + (-\mu - 2\sum_l t_l \cos kl)^2 \tag{1.82}$$

We focus on models that have finite-range, *i.e.* there exists l_m such that $(t_{l_m}, \Delta_{l_m}) \neq 0$ and $\forall l > l_m,\ (t_l, \Delta_l) = 0$. Finding the roots of E_k is then equivalent to finding the roots that lies on the unit circle of the polynomial (take $z = e^{ik}$):

$$z^{l_m}(\mu + \sum_{l=1}^{l_m} t_l (z^l + z^{-l}) + \Delta_l (z^l - z^{-l})), \tag{1.83}$$

which means that E_k can close at up to $2l_m$ different momenta, but also that the system can be gapped.
We can evaluate the maximum (absolute) value of the winding number of the ground state of H_G. Using the discrete formulation of the winding number in Eq. 1.63 with $\theta_0 = \frac{\pi}{2}$, assuming that the energy spectrum is gapped, the number of terms that appear in the sum is simply the number of zeros of $n_z(k)$ such that $n_y(k) > 0$, or equivalently half the number of roots lying on the unit circle of:

$$z^{l_m}(\mu + \sum_{l=1}^{l_m} t_l (z^l + z^{-l})). \tag{1.84}$$

This number is bounded by l_m. The absolute value of the winding number is therefore also bounded by l_m, implying that there can be up to l_m zero-energy Majorana fermions leaving at each extremity of the wire if we have open boundaries. As a general rule, two phases with winding numbers ν_1 and ν_2 will be separated by a gapless line where the gap closes $|\nu_1 - \nu_2|$ times. In the following, we present a few simple examples.

Pure models: first one can consider the simplest models where only one l has $(t_l, \Delta_l) \neq 0$. The system is then equivalent to l independent identical Kitaev's wires. The phase diagram is still given by Figure 1.2, where the topological phase now hosts l Majorana fermions at each extremity (and has a winding number $\pm l$). The gap closes at l different momenta on the vertical lines and $2l$ times on the metal line.

$t_1 - t_2$: A second more interesting example is given by taking $l_m = 2$. To simplify, we also assume $t_l = \Delta_l$. The phase diagram can be straightforwardly computed solving $E_k = 0$ and using the known limits of each phase to evaluate each winding number and is shown in Figure 1.7.

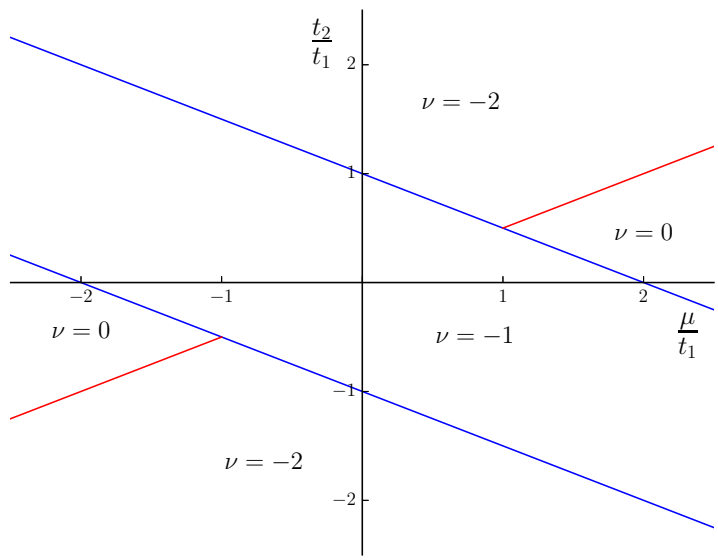

Figure 1.7: Phase diagram of the $t_1 - t_2$ model, assuming $\Delta_l = t_l$ and $t_1 > 0$. The blue and red lines mark the phase transitions between the different topological phases, of winding number ν. On the blue lines (of equation $2t_2 = -\mu \pm 2t_1$), the gap only closes either at $k = 0$ or at $k = \pi$, while it closes at two non-trivial momenta on the red lines(of equation $2t_2 = \mu$ for $|\mu| > t_1$). The intersections are special tricritical points where the dispersion relation stops to be linear at $k = 0$ or π.

$t_1 - t_3$: Our last example will be with $l_m = 3$, $t_l = \Delta_l$, $t_2 = 0$ and $t_1 > 0$. The richer phase diagram is explained in Figure 1.8 and will allow us to probe some additional phase transitions.

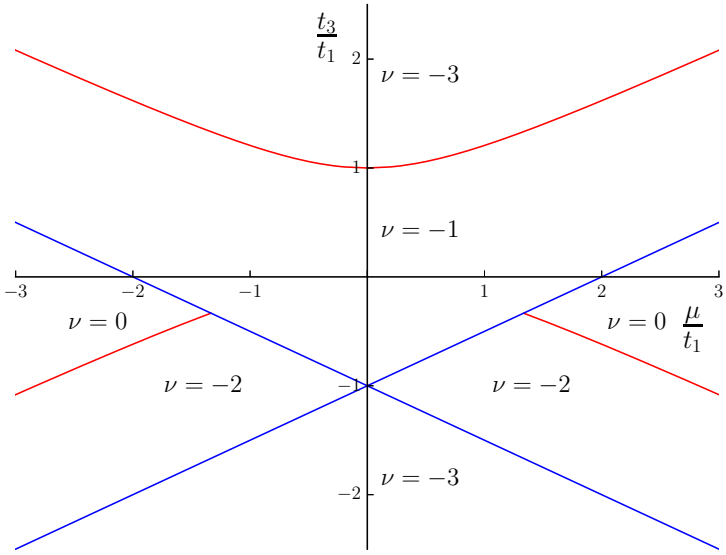

Figure 1.8: Phase diagram of the $t_1 - t_3$ model, assuming $\Delta_l = t_l$, $t_2 = 0$ and $t_1 > 0$. The blue and red lines mark the phase transitions between the different topological phases, of winding number ν. The gap closes only once on the two blue lines, of equations $\pm\mu = 2t_1 + 2t_2$. It closes at two different momenta on the red lines, of equations $\mu = \pm 2t_3\sqrt{1 - \frac{t_1}{t_3}}$ for $\frac{t_3}{t_1}$ in $]-\infty, -\frac{1}{3}] \cup [1, +\infty[$. Intersections are special tri-critical points.

Breaking Time-Reversal-Symmetry

Finally, one can break the time-reversal symmetry in this system, in order to get a model in the D class. Let us consider the simplest of such models, with $t_j = \Delta_j = 0$ for $j \geq 3$. We still consider $t_1 = \Delta_1$, and $t_2 = |\Delta_2|$, but we now have $\Delta_2 = it_2$ an imaginary number. For non-zero Δ_1, the phase of Δ_2 cannot be absorbed, and the system is not TRS. The Hamiltonian is given by:

$$H = \frac{1}{2} \sum_{k \in \mathcal{BZ}} \Psi_k^\dagger (-2t_2 \sin 2k, -2t_1 \sin k, -\mu - 2t_1 \cos k - 2t_2 \cos 2k) \Psi_k \tag{1.85}$$

For $t_1 \neq 0$, the phase diagram has a simple structure. The gap can close only at $k_0 = 0$ and $k = \pi$. For $\mu < -2t_1 - 2t_2$ and $\mu > 2t_1 - 2t_2$, the wire is in a trivial gapped state, while for $-2t_1 - 2t_2 < \mu < 2t_1 - 2t_2$ it is in a topological state (with one protected zero-energy Majorana edge state at each extremity if we take open boundary conditions).
Compared to the $t_1 = 0$ limit, the topological invariant now lives in $\mathbb{Z}_2$: there is up to one zero-energy, protected Majorana fermion at each extremity. Were we to start with $t_1 = 0 = \mu$, and consequently two Majorana fermions at each edge, an arbitrarily small t_1 would couple them together to form a normal fermion of finite energy.

1.5.3 Rashba spin-orbit superconductors

The Kitaev model for 1D topological superconductors is a toy model that needs to be replaced by a more realistic model for experimental realization. Among the many different proposals, we focus on the Rashba spin-orbit superconductor[23, 24]. A 1D semi-conducting wire is deposited on the surface of a 2D or 3D s-wave superconductor. A strong Rashba spin-orbit interaction is present in the wire and a strong magnetic field, orthogonal to both the wire and the superconducting substrate is applied. The model is in the BDI class and carries Majorana edge modes. Such a model has received a lot of attention from the experimental community as it requires only s-wave superconductors, and the realization of a one-dimensional semi-conducting wire[25–33]. The actual experimental discovery of Majorana fermions in such a set-up is still debated[52–59].
In this part, we introduce a lattice model for the semi-conducting wire, and present some of the main ideas behind its solution and its properties.
The system is described in real-space by the Hamiltonian:

$$H_{\mathcal{R}} = -\mu \sum_j c^\dagger_{j,\sigma} c_{j,\sigma} + \Delta(c^\dagger_{j,\uparrow} c^\dagger_{j,\downarrow} + c_{j,\downarrow} c_{j,\uparrow}) + \sum_{j,\alpha,\beta} -t(c^\dagger_{j,\sigma} c_{j+1,\sigma} + h.c.) + V c^\dagger_{j,\alpha} \sigma^z_{\alpha,\beta} c_{j,\beta} - \lambda(i c^\dagger_{j,\alpha} \sigma^y_{\alpha,\beta} c_{j+1,\beta} + h.c.) \quad (1.86)$$

where c are spin-$\frac{1}{2}$ fermionic annihilation operator ($c_\uparrow$ represent electrons spin-polarized in the direction of the external magnetic field), μ is a chemical potential and t a hopping term. The wire is taken to be in the x-direction. The magnetic field tends to align the electrons' spins in its direction through the Zeemann coupling V, while the Rashba spin-orbit coupling λ favors the y-direction. Finally, due to the proximity of the superconductor, Cooper pairs can tunnel from the substrate to the wire. This leads to superconducting correlations represented at the mean-field level by the s-wave pairing Δ, taken to be real. As it is a non-interacting problem, it can be exactly solved. To do so, we assume PBC and go to momentum space. Up to some unimportant constants, the Hamiltonian can be expressed as a sum of 4×4 matrices. As usual for superconductors, the points $k = 0$ and $k = \pi$ are special and will be ignored in this discussion. Introducing the Nambu 4-spinors $\Psi^\dagger_k = (c^\dagger_{k,\uparrow}, c^\dagger_{k,\downarrow}, c_{-k,\downarrow}, c_{-k,\uparrow})$, we obtain:

$$H_{\mathcal{R}} = \sum_k \Psi^\dagger_k h(k) \Psi_k \quad (1.87)$$

$$\text{with } h(k) = \begin{pmatrix} \varepsilon(k) + V & -i\varepsilon_2(k) & \Delta & 0 \\ i\varepsilon_2(k) & \varepsilon(k) - V & 0 & -\Delta \\ \Delta & 0 & -\varepsilon(k) + V & -i\varepsilon_2(k) \\ 0 & -\Delta & i\varepsilon_2(k) & -\varepsilon(k) - V \end{pmatrix}, \quad (1.88)$$

where $\varepsilon(k) = -\mu - 2t\cos k$ is the kinetic energy and $\varepsilon_2(k) = 2\lambda \sin k$ the contribution of the Rashba term. By squaring twice $h(k)$, the energy spectrum can be determined:

$$E^2_{k,\pm} = \Delta^2 + \varepsilon(k)^2 + \varepsilon_2^2(k) + V^2 \pm 2\sqrt{V^2\varepsilon(k)^2 + \varepsilon(k)^2\varepsilon_2(k)^2 + \Delta^2 V^2}. \quad (1.89)$$

The bands $\pm E_+$ are always gapped and separated from $\pm E_-$ as long as both Δ and V are non-vanishing. We consequently focus on the latter two bands. Closing of the gap is

equivalent to:

$$\Delta^2 + \varepsilon^2(k) = V^2 + \varepsilon_2^2(k) \tag{1.90}$$

The Hamiltonian is a member of the D class, and its topological invariant lives in $\mathbb{Z}_2$. For a non-trivial transition, we consequently require that the gap closes an odd number of times. Due to the symmetry $k \leftrightarrow -k$, it implies a gap closure at either $k = 0$ or $k = \pi$, leading to the simple condition:

$$V^2 = \Delta^2 + (\mu \pm 2t)^2 \tag{1.91}$$

The topological invariant can be computed[23, 24] using the Berry phase defined in Eq. 1.67. We sum over the two occupied bands:

$$\gamma = \sum_{\varepsilon=\pm} i \int_{k\in\mathcal{BZ}} \langle \vec{r}_{k,\varepsilon} | \frac{d}{dk} | \vec{r}_{k,\varepsilon} \rangle dk, \tag{1.92}$$

where $|\vec{r}_{k,\pm}\rangle$ is the (occupied) eigenstate of $h(k)$ corresponding to the eigenvalue $-E_{k,\pm}$. The band $+$ is always trivial, while the band $-$ can have a non-trivial Berry phase. The system is in a topological phase if:

$$V^2 > \Delta^2 + (\mu \pm 2t)^2 \tag{1.93}$$

Various correlations functions of the Rashba nanowire are computed in Appendix D.2. They will be used in Section 3.2.10.

1.6 Topical examples in 2D

Similarly to the previous section, we will now introduce a few models of non-interacting fermions that present topological phases or topological excitations for $d = 2$. In particular, we will focus on Dirac systems. These systems are characterized by a linear dispersion of the energy when the bulk becomes gapless, with the formation of the so-called Dirac cones at a finite number of momenta. These cones are very similar to the aforementioned vortices, and can carry a topological charge. Transition between two non-equivalent phases will necessitate the appearance of such cones, and the difference in Chern number of the two phases can usually be obtained from the winding number of the cones at the QCP.
We will start by a simple model for topological superconductors in $d = 2$, the $p + ip$ superconductor taken on a square lattice. It is the generalization to two dimensions of the Kitaev's wire, and as a member of the D class, presents topological phase transitions. We will then pursue with the staple model for Dirac metals: the graphene. While not a topological system per se, as it is gapless, it is a nice first step to understand the physics of the Dirac cone and a good stepping-stone to the last model: Haldane's topological insulator.

1.6.1 The $p + ip$ superconductor

The $p + ip$ superconductor[60] is a two-dimensional model of fermionic superconductors with unconventional superconductivity. For convenience, we limit ourselves to a regular

square lattice. Its tight-binding Hamiltonian is given by:

$$H_{p+ip} = -\mu \sum_{\vec{r}} c^\dagger_{\vec{r}} c_{\vec{r}} - t \sum_{<\vec{r},\vec{r'}>} (c^\dagger_{\vec{r}} c_{\vec{r'}} + c^\dagger_{\vec{r'}} c_{\vec{r}}) + \sum_{\vec{r}} -i\Delta_x (c^\dagger_{\vec{r}} c^\dagger_{\vec{r}+\vec{e}_x} - h.c.) + \Delta_y (c^\dagger_{\vec{r}} c^\dagger_{\vec{r}+\vec{e}_y} + h.c.), \tag{1.94}$$

where c are spinless fermionic annihilation operators, $< \vec{r}, \vec{r'} >$ represents the nearest-neighbor links and $\vec{e}_{x/y}$ the lattice-defining vectors. Δ_x and Δ_y are taken to be real and positive and represents mean-field, p-wave superconducting pairing. Experimental realization of such a model proves to be quite difficult and similarly to Kitaev's wire, requires complex heterostructures. The most promising is probably inducing superconductivity in a bulk 3D topological insulator. In that limit, its surface states will naturally realize a $p + ip$ superconductor by proximity[61]. The system is characterized by the presence of Majorana fermions at the core of vortex excitations in real space[15, 62, 63], and of free Majorana modes at the boundaries[10], as shown in Figure 1.10
The system can be straightforwardly diagonalized using our usual Bogoliubov approach. Defining the spinor $\Psi^\dagger_{\vec{k}} = (c^\dagger_{\vec{k}}, c_{-\vec{k}})$, the Hamiltonian can be easily rewritten as:

$$H_{p+ip} = \frac{1}{2} \sum_{\vec{k} \in \mathcal{BZ}} \Psi^\dagger_{\vec{k}} \vec{n}(\vec{k}).\vec{\sigma} \Psi_{\vec{k}},$$
$$\text{with } \vec{n}(\vec{k}) = (2\Delta_x \sin k_x, -2\Delta_y \sin k_y, -\mu - 2t\cos k_x - 2t \cos k_y) \tag{1.95}$$

While the TRS is broken, the PHS, intrinsic to the Bogoliubov formalism for superconductors, is still present (and has the same representation as in Kitaev's wire). H_{p+ip} is therefore in the D class, which for $d = 2$ has the Chern number as topological invariant. For $(\Delta_x, \Delta_y) \neq 0$, the bulk energy $||\vec{n}||^2$ cancels only for $\mu = \pm 4t$ and $\mu = 0$. Let us focus first on categorizing the different phases.
Use of the discrete formulation of the Chern number in Eq. 1.68, with the z-axis singularized, leads to:

$$\begin{aligned} \nu &= \frac{1}{2} \sum_{k_x=0/\pi, k_y=0/\pi} \text{sign}(-\cos k_x \cos k_y) \text{sign}(-\mu - 2t\cos k_x - 2t \cos k_y) \\ &= \frac{1}{2} \left(\text{sign}(\mu + 4t) + \text{sign}(\mu - 4t) - 2\text{sign}(\mu) \right) \\ &= \begin{cases} 1 & \text{for } -4t < \mu < 0 \\ -1 & \text{for } 0 < \mu < 4t \\ 0 & \text{for } |\mu| > 4t \end{cases} \end{aligned} \tag{1.96}$$

Similarly to Kitaev's wire, the phase diagram is independent of Δ_x and Δ_y as long as they are both different from 0.

At the phase transitions, the gap closes at either 1 or 2 precise momenta, which corresponds to PHS points. At $\mu = -4t$, Figure 1.9 represents the band spectrum: the gap closes at $\vec{k} = 0$ and the energy forms a cone around this point: this is the so-called Dirac cone. Linearization of $E_{\vec{k}}$ and $\vec{n}$ near $\vec{k} = 0$ leads to:

$$\delta\vec{n} = (2\Delta_x k_x, -2\Delta_y k_y, 0), \qquad \delta E_{\vec{k}} = 2\sqrt{\Delta_x^2 |k_x|^2 + \Delta_y^2 |k_y|^2} \tag{1.97}$$

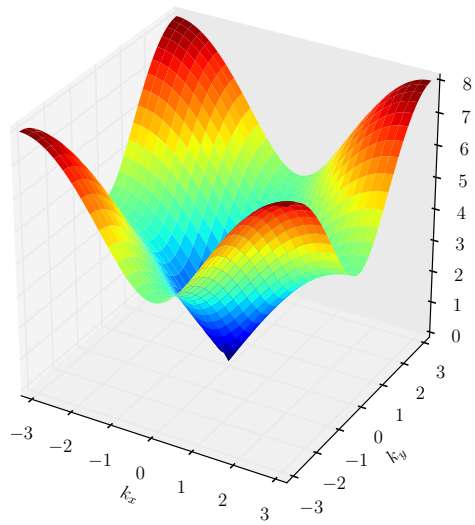

Figure 1.9: Energy spectrum for the $p+ip$ superconductor at $\mu = -4t$, for $\Delta_x = \Delta_y = t$. A Dirac cone appears at $k = 0$, characterized by a linear dispersion, and a non-trivial winding of the vector (n_x, n_y) around it. The configuration in this case corresponds to the one depicted in the top-right corner of Figure 1.6.

The dispersion is linear, and perfectly proportional to $||\vec{k}||$ in the limit $\Delta_x = \Delta_y$, which corresponds to restoring the rotation symmetry of the lattice. Near the transition, at $\vec{k} = 0$, $\vec{n} = (0, 0, -\mu - 4t)$, it is therefore natural to singularize the z direction and look at the spin texture in the plan Oxy. At $\mu = -4t$, the vector $\delta\vec{n}$ winds around the cone, as depicted in the top-right corner of Figure 1.6. It consequently forms a vortex and has a winding number -1. When $\mu < -4t$, $n_z(0)$ is positive, while when $0 > \mu > -4t$, it becomes negative. The orthogonal contribution is unchanged, and the local texture consequently go from a Chern number -1 to a Chern number 1. Taking into account the factor $\frac{1}{2}$, we recover that the Chern number of the band increase by 1. This analysis can be extended to any topological model where Dirac cones appear at the transitions: these cones are the natural points where the homotopic class of the Hamiltonian can change.
The same results extend to $\mu = 4t$.
At $\mu = 0$, the gap now closes twice at $\vec{k}_+ = (\pi, 0)$ and $\vec{k}_- = (0, \pi)$. Two Dirac cones carrying a charge $+1$ appear: the total topological charge is 2, consistent with the change in Chern number observed in Eq. 1.96 (the factor -1 again comes from the change of sign of n_z at the phase transition).

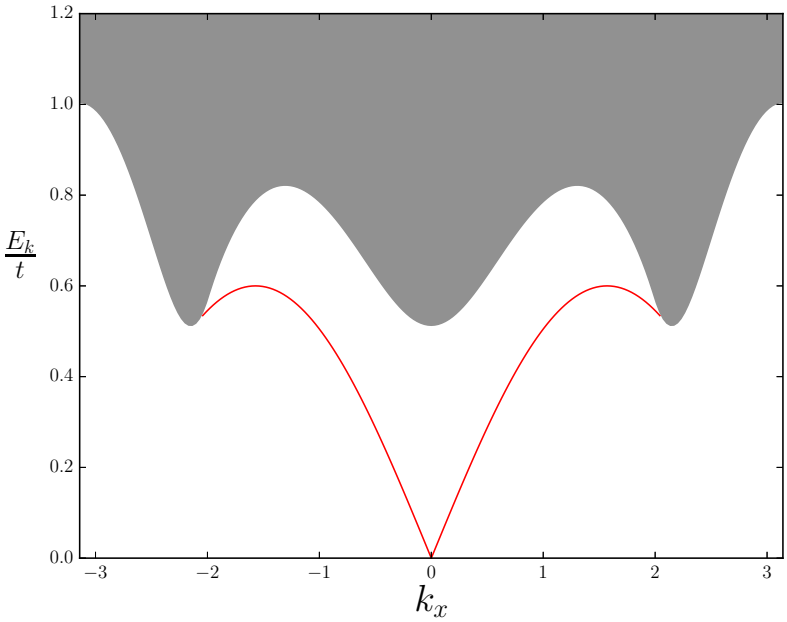

Figure 1.10: Energy spectrum for the $p + ip$ superconductor on a cylinder at $\mu = -t$, for $\Delta_x = \Delta_y = 0.3t$. The system is periodic in the x-direction (with an arbitrary length), and has open boundaries in the y-direction. The energy spectrum is obtained through exact diagonalization for 100 sites in the y-direction. The continuum of gapped energy states is represented in grey, while a gapless edge mode appears in red. This edge state is located on both edges of the cylinder. It corresponds to a free Majorana mode at each edge.

1.6.2 A very brief overview of graphene

As we have seen in the previous example, the physics of Dirac cones is indeed fundamental for two-dimensional non-interacting topological models, as these cones carries topological charge, and therefore allows for a change in the topological invariant at the phase transition. As such, it is a good idea to spend a few paragraphs on graphene, before attacking Haldane's constructions of a topological insulator.
The graphene is a purely two-dimensional layer of carbon atoms forming a honeycomb lattice, depicted in Figure 1.11. This metal was isolated for the first time in 2005[64] and attracted an enormous attention due to the presence of these Dirac cones: the physics of the Dirac cones is nothing but the physics of relativistic fermions. The honeycomb can be interpreted as a triangular lattice with two sites by unit-cell. An effective tight-binding model is then simply given by:

$$H_{\mathcal{G}} = -t \sum_{\vec{r}} (c^\dagger_{\vec{r},A} c_{\vec{r},B} + c^\dagger_{\vec{r},A} c_{\vec{r}+\vec{a}_1,B} + c^\dagger_{\vec{r},A} c_{\vec{r}+\vec{a}_2,B} + h.c.), \tag{1.98}$$

with the vectors $\vec{a}_1 = (1,0)$ and $\vec{a}_2 = (-\frac{1}{2}, -\frac{\sqrt{3}}{2})$. As the lattice is not square, care has to be given to the definition of the reciprocal lattice, and of the first Brillouin Zone, they are presented in Figure 1.11. Defining $\Psi^\dagger_{\vec{k}} = (c^\dagger_{\vec{k},A}, c^\dagger_{\vec{k},B})$, the band Hamiltonian is straightforwardly obtained:

$$H = \sum_{\vec{k}\in\mathcal{BZ}} \Psi^\dagger_{\vec{k}} \vec{n}.\vec{\sigma}\Psi_{\vec{k}}, \text{ with } n_z = 0, n_x + in_y = -t(1 + e^{-ik_x} + e^{i(\frac{k_x}{2}+\frac{\sqrt{3}}{2}k_y)}) \tag{1.99}$$

The energy of the quasi particles are $\pm E_k$, with

$$E^2_{\vec{k}} = t^2 \left((1 + \cos k_x + \cos(\frac{k_x}{2} + \frac{\sqrt{3}}{2}k_y))^2 + (\sin k_x - \sin(\frac{k_x}{2} + \frac{\sqrt{3}}{2}k_y))^2 \right),$$

and consequently closes at $K_\pm = \pm\frac{2\pi}{3}(1, \sqrt{3})$. The two Dirac cones have each non-zero vorticity (± 1) but opposite signs.

The graphene itself is not a topological insulator, as it is gapless and carries no topological charge. Yet it is a good starting point for building one. In order to do so, one should gap only one of the cones. The new material would therefore be at a critical point separating two topologically different phases, as it would have only one cone of non-zero vorticity. To do so requires breaking the TRS (which maps one cone onto the other), at least locally and is at the core of Haldane's model[9]. Note that it is not the only way to create a topological phase in the graphene. By adding a spin-orbit coupling, it is possible to realize the $\mathbb{Z}_2$ Quantum Spin Hall effect [65–67]. We will not discuss this phase in the thesis.

1.6.3 Haldane model for topological insulator

This model was proposed for the first time in 1988[9] as a microscopic model for the appearance of an Integer Quantum Hall Effect but with 0 net flux, that is to say a model where the magnetic field, while present, cancels in average at the level of the unit-cell. The starting point of this model is the aforementioned model of graphene, with a few added ingredients. First an alternating chemical potential, differentiating between the sites A and B is added, which gaps the system. A periodic magnetic field is added in order to break the TRS. The flux is chosen to be 0 on each hexagonal unit-cell. It has consequently no effect on either the chemical potential or the nearest-hopping terms. Therefore, a second-nearest neighbour hopping term is added: electrons on site A (resp. B) may hop directly to the nearest A (resp. B) sites. These acquire a non-trivial phase, as the shortest closed loops of second-hopping terms only enclose half the unit-cell (and break the local PHS). The corresponding matrix element acquires a non-trivial phase which explicitly breaks the TRS. Figure 1.12 sums up the construction of the model and specifies the signs of the phase of the hopping term. The microscopic Hamiltonian is simply given by (the

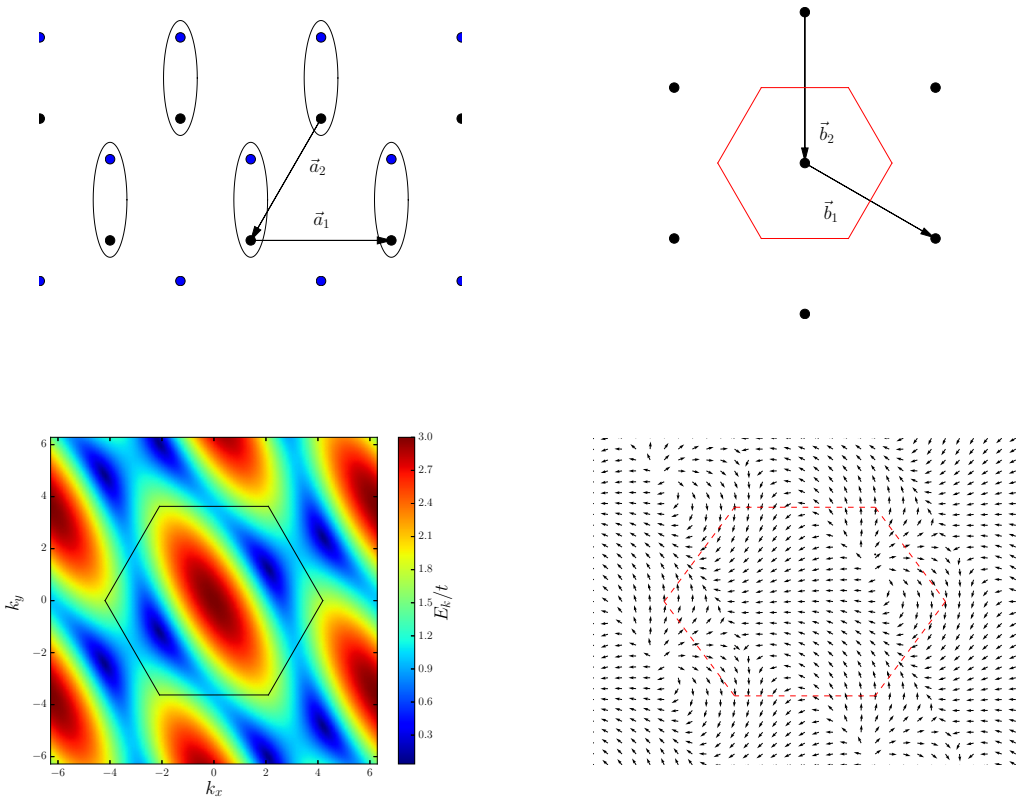

Figure 1.11: Properties of the graphene and the honeycomb lattice. Top left: honeycomb lattice and the underlying triangular lattice used in diagonalization. In black (resp. blue) the sites A (resp. B). The ellipses represent the sites for the triangular lattice, and $\vec{a}_1$ and $\vec{a}_2$ define the lattice. Top right: the reciprocal lattice associated. $\vec{b}_{1/2}$ are defined by $\vec{b}_i.\vec{a}_j = 2\pi\delta_{i,j}$. In red is represented the first Brillouin Zone. Bottom left: energy spectrum as a function of k_x and k_y. The Brillouin Zone is represented in black. The gap closes at $K_\pm = \pm\frac{2\pi}{3}(1, \frac{1}{\sqrt{3}})$ forming two Dirac cones. Bottom right: the normalized vectors (n_x, n_y) on the first Brillouin zone. The two Dirac cones have opposite topological charge.

summation on $\vec{r}$ is implied):

$$\begin{aligned} H_{\mathcal{H}} = &-\Delta\left(n_{A,\vec{r}} - n_{B,\vec{r}}\right) - t\left(c^\dagger_{\vec{r},A}c_{\vec{r},B} + c^\dagger_{\vec{r},A}c_{\vec{r}+\vec{a}_1,B} + c^\dagger_{\vec{r},A}c_{\vec{r}+\vec{a}_2,B} + h.c.\right) \\ &- t_2 \sum_{\sigma=A,B}\Big(e^{i\sigma\phi}\Big[c^\dagger_{\sigma,\vec{r}}c_{\sigma,\vec{r}-\vec{a}_1} + c^\dagger_{\sigma,\vec{r}+\vec{a}_1}c_{\sigma,\vec{r}} + c^\dagger_{\sigma,\vec{r}}c_{\sigma,\vec{r}-\vec{a}_2} + c^\dagger_{\sigma,\vec{r}+\vec{a}_2}c_{\sigma,\vec{r}} \\ &+ c^\dagger_{\sigma,\vec{r}}c_{\sigma,\vec{r}-\vec{a}_3} + c^\dagger_{\sigma,\vec{r}+\vec{a}_3}c_{\sigma,\vec{r}}\Big] + h.c.\Big), \end{aligned} \tag{1.100}$$

where we note $\vec{a}_3 = -\vec{a}_1 - \vec{a}_2$ and $e^{iA/B\phi} = e^{i\pm\phi}$. Δ is the alternating chemical potential, t_2 is the strength of the second-neighbour hopping, taken to be real, and ϕ is a third of the

flux enclosed by the black loop of Figure 1.12. The Hamiltonian is still non-interacting. With the spinor $\Psi_k^\dagger = (c_{k,A}^\dagger, c_{k,B}^\dagger)$, the Hamiltonian in momentum space is given by:

$$\vec{n}(\vec{k}) = (\mathrm{Re}(\mathcal{A}), \mathrm{Im}(\mathcal{A}), -\Delta + 4t_2 \sin(\phi)\mathrm{Im}(\mathcal{B})) \tag{1.101}$$

$$E_0(\vec{k}) = -4t_2 \cos(\phi)\mathrm{Im}(\mathcal{B}) \tag{1.102}$$

$$\mathcal{A} = -t(1 + e^{-ik_x} + e^{i(\frac{k_x}{2} + \frac{\sqrt{3}}{2}k_y)}) \tag{1.103}$$

$$\mathcal{B} = \sum_{j=1}^{3} e^{-i\vec{k}.\vec{a}_j} \tag{1.104}$$

E_0 can safely be ignored for the purpose of determining the topology of the bands. The gap vanishes when $\vec{n} = \vec{0}$. As long as $t \neq 0$, $\mathcal{A}$ cancels only at $K_\pm = \pm\frac{2\pi}{3}(1, \frac{1}{\sqrt{3}})$, which leads to the condition:

$$\Delta = \mp 6t_2\sqrt{3}\sin\phi \tag{1.105}$$

For a non-zero flux, the gap closes at only one of the two momenta. At this momentum, a Dirac cone still appears, and has a non-trivial winding number, implying a topological phase transition. Indeed, using Eq. 1.69 to determine the topological invariant, the phase diagram can be easily obtained, and is shown in Figure 1.12:

$$\nu = \frac{1}{2}(\mathrm{sign}(-\Delta - 6t_2\sqrt{3}\sin\phi) - \mathrm{sign}(-\Delta + 6t_2\sqrt{3}\sin\phi) \tag{1.106}$$

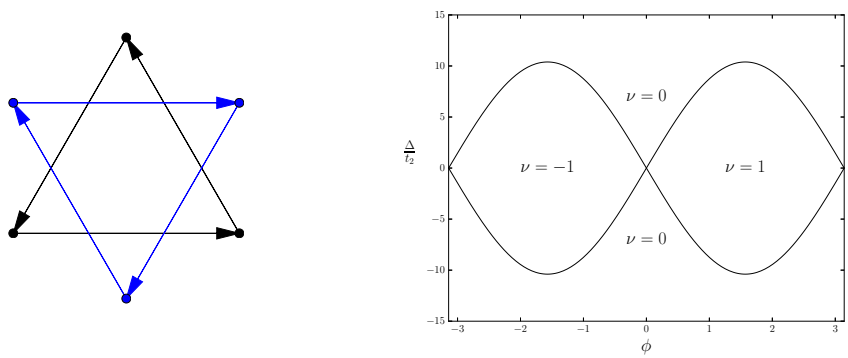

Figure 1.12: Left: structure of the second-nearest neighbour hopping in the Haldane model. Black arrows carry a phase ϕ while blue ones carry a phase $-\phi$. The total flux is zero. Right: phase diagram of the Haldane model for $t \neq 0$. As long as $\phi \neq 0, \pi$, the transition lines are characterized by only one closing of the gap at either K_+ or K_-.

Chapter 2

Entanglement properties of normal and topological states

Contents

2.1 Entanglement entropy 44
2.1.1 Definition of the von Neumann Entanglement Entropy 44
2.1.2 Entanglement entropy in many-body systems 46
2.2 Entanglement spectrum and topological systems 53
2.2.1 Definition of the entanglement spectrum 53
2.2.2 Entanglement spectrum in topological systems 54
2.3 Bipartite fluctuations as a "weak" measure of entanglement . 57
2.3.1 The problem of entanglement measure 57
2.3.2 General definition of bipartite fluctuations 59
2.3.3 Bipartite charge fluctuations in Luttinger Liquids 61
2.3.4 Beyond one dimension 63

Entanglement has, up to now, stayed away from our discussions on topological materials. Yet, these non-local correlations are the fundamental difference between quantum and classical systems, and at the core of the topological nature of the ground states. Historically, the study of entanglement was first reserved to quantum information and to attempts to understand the consequences of quantum mechanics as a physical theory. The first experiments, based on verifying the Bell's inequality, illustrating the Einstein-Podolsky-Rosen paradox, were meant to check the validity and completeness of quantum mechanics. Nonetheless, the rushing development of quantum computing and information during the last decades has yield an increasing amount of new insights on the properties of entanglement, even in many-body systems. The study of the structure of entanglement has proved to be invaluable to describe (topological) phase transitions at zero temperature and (topological) ground states. Indeed, for such systems, the traditional study of correlation functions usually fail to properly describe the changes the system undergoes. The standard quantum correlations are not sufficient to discriminate between different topological phases, while the study of entanglement, through for example the entanglement

entropy or the entanglement spectrum gives clear insights on the nature of the different phases.
This Chapter consists in an introduction to the notion of entanglement in quantum systems, and more precisely in many-body physics. Section 2.1 starts by introducing the von Neumann entanglement entropy and other basic entanglement measures. After describing its global properties through a set of examples, we give an overview of the main ideas behind the study of entanglement in many-body systems, with a focus on gapless models. Section 2.2 is dedicated to the entanglement spectrum. It is especially useful for characterizing topological states that possess edge states, as the measure of the entanglement spectrum is based on the creation of artificial edges. Finally, we present in Section 2.3 an introduction to the concept of bipartite fluctuations. These fluctuations can be used as a weak probe of entanglement, that has the added advantage to be experimentally measurable. We give a short presentation of previous works on this topic, that focused on normal Luttinger liquids and other charge-conserving models, before devoting the next Chapter to our extension to topological models.
To go beyond the short review proposed in this Chapter, we refer the reader to Ref. [68].

2.1 Entanglement entropy

2.1.1 Definition of the von Neumann Entanglement Entropy

Definition

At the core of quantum mechanics is the idea of non-local correlations. Such correlations correspond, in some sense, to shared information between the different parts of the system. While we may know perfectly a system $\mathcal{S}$, quantum correlations and superposition may prevent us from knowing the state of any subpart of the system. The amount of shared information can be measured, just as in the classical case, by an entropy function. We will focus on this thesis on the von Neumann entanglement entropy (vNEE), and we will limit ourselves to the bipartite case, where we measure the entanglement between two different subsystems.
Let us consider a closed system $\mathcal{S}$ at zero-temperature, which is quite naturally in a *pure* state $|\psi\rangle$. Let $\mathcal{A}$ be a physical subpart of this system, we note $\overline{\mathcal{A}}$ the rest of the system. The density matrix $\rho_{\mathcal{A}}$ entirely describes $\mathcal{A}$ and its correlations with $\overline{\mathcal{A}}$:

$$\rho_{\mathcal{A}} = \mathrm{Tr}_{\overline{\mathcal{A}}}(|\psi\rangle\langle\psi|). \tag{2.1}$$

$|\psi\rangle\langle\psi|$ is the projector on the state $|\psi\rangle$ in the Hilbert space that describes the total system $\mathcal{S}$, and the trace carries on all degrees of freedom (all sites for example) that do not belong to $\mathcal{A}$. The associated vNEE is:

$$\mathcal{S}_E(\mathcal{A}) = -\mathrm{Tr}_{\mathcal{A}}(\rho_{\mathcal{A}} \ln \rho_{\mathcal{A}}). \tag{2.2}$$

The logarithmic term is unique and properly defined as $\rho_{\mathcal{A}}$ can be diagonalized and has all its eigenvalues between 0 and 1. It is the direct quantum equivalent of the classical Shannon entropy.

0D limit: the case of two spins

Let us directly go through an example before discussing the general properties of the vNEE. Consider two $\frac{1}{2}$-spins labeled A and B. The subsystem we consider is simply $\mathcal{A} = A$. If the two spins are independent, the wave function of the total system (a vector of $\mathbb{C}^4$) can be written as:

$$|\psi\rangle = |\psi_A\rangle \otimes |\psi_B\rangle \,, \tag{2.3}$$

where $\left|\psi_{A/B}\right\rangle$ are two vectors of $\mathbb{C}^2$ that describe the state of each spin. The density matrix of A is simply $|\psi_A\rangle\langle\psi_A|$, and the corresponding vNEE is $\mathcal{S}_E(A) = 0$. Note that $\mathcal{S}_E(B) = 0$ too.
The two spins can also form a singlet:

$$|\psi\rangle = \frac{1}{\sqrt{2}}\left(|\uparrow_A\rangle|\downarrow_B\rangle - |\downarrow_A\rangle|\uparrow_B\rangle\right), \tag{2.4}$$

$$\rho_A = \frac{1}{2}\left(|\uparrow_A\rangle\langle\uparrow_A| + |\downarrow_A\rangle\langle\downarrow_A|\right) = \begin{pmatrix} \frac{1}{2} & 0 \\ 0 & \frac{1}{2} \end{pmatrix}, \tag{2.5}$$

and the entanglement entropy is then $\mathcal{S}_E(A) = \ln 2$ $(= \mathcal{S}_E(B))$. The two spins are maximally-entangled: there is a perfect correlation between the orientation they take (the two spins form a Bell pair), and consequently the vNEE is maximal. For an arbitrary state, the vNEE continuously goes from 0 to $\ln 2$.

Generic properties

A first important property of the vNEE is its symmetry, *i.e.*, whatever the subsystem chosen, $\mathcal{S}_E(\mathcal{A}) = \mathcal{S}_E(\overline{\mathcal{A}})$.
Mathematically, it can be easily seen from the Schimdt decomposition of a pure state. Indeed, linear algebra assures that, if $\mathcal{H}_\mathcal{A}$ is the Hilbert space describing the (sub)system $\mathcal{A}$, such that $\mathcal{H}_\mathcal{S} = \mathcal{H}_\mathcal{A} \otimes \mathcal{H}_{\overline{\mathcal{A}}}$, then the wave function $|\psi\rangle$ can be written as:

$$|\psi\rangle = \sum_{m=1}^{M} \sqrt{\lambda_m}\, |e_m\rangle \otimes |\overline{e}_m\rangle \,, \quad \sum_{m=1}^{M} \lambda_m = 1 \tag{2.6}$$

where M is the so-called bond dimension, smaller than $\min(\dim\mathcal{H}_\mathcal{A}, \dim\mathcal{H}_{\overline{\mathcal{A}}})$, λ_m is a set of real numbers in $]0,1]$ and $|e_m\rangle$ (resp. $|\overline{e}_m\rangle$) a family of orthonormal vectors of $\mathcal{H}_\mathcal{A}$ (resp. $\mathcal{H}_{\overline{\mathcal{A}}}$). The equality of the vNEEs follows from this decomposition, as

$$\rho_\mathcal{A} = \sum_{m=1}^{M} \lambda_m |e_m\rangle\langle e_m| \,, \quad \rho_{\overline{\mathcal{A}}} = \sum_{m=1}^{M} \lambda_m |\overline{e}_m\rangle\langle\overline{e}_m| \tag{2.7}$$

$$\text{and } \mathcal{S}_E(\mathcal{A}) = \mathcal{S}_E(\overline{\mathcal{A}}) = -\sum_{m=1}^{M} \lambda_m \ln \lambda_m \tag{2.8}$$

As $\mathcal{S}(\mathcal{A}) = \mathcal{S}(\overline{\mathcal{A}})$, the entropy cannot depend on the volume of $\mathcal{A}$, but should be related to its boundaries, common to $\mathcal{A}$ and $\overline{\mathcal{A}}$. This phenomenological argument (another example

of the bulk-edge correspondence or holographic principle) can be made rigorous in some special limits of condensed matter systems, but also in quantum gravity. The holographic principle states that the physics of some systems is encoded in its boundaries (probably the most famous examples are the black hole and the AdS-CFT equivalence[69]).

It is also important to mention an additional set of properties that the vNEE verifies. Similarly to the Shannon entropy, it is actually uniquely specified by the following set of properties:

- $\mathcal{S}_E$ must be continuous (with respect to a continuous change in $\mathcal{A}$ or in $\rho_{\mathcal{A}}$).
- It is invariant under local unitary transformations.
- It must be additive for independent subsystems: if $\mathcal{A} = \mathcal{A}_1 \otimes \mathcal{A}_2$ such that $\rho_{\mathcal{A}} = \rho_{\mathcal{A}_1} \otimes \rho_{\mathcal{A}_2}$, then $\mathcal{S}_E(\mathcal{A}) = \mathcal{S}_E(\mathcal{A}_1) + \mathcal{S}_E(\mathcal{A}_2)$. It must be sub-additive in the general case: $\mathcal{S}_E(\mathcal{A}) \leq \mathcal{S}_E(\mathcal{A}_1) + \mathcal{S}_E(\mathcal{A}_2)$.

The vNEE can also be extended to non-pure states, and in particular it can be defined at non-zero temperature for thermal states. Cross-over from $T = 0$ to large temperature can be derived easily in the family of models that we will study (conformal models).

Though it is the most fundamental, the vNEE is not the only entropy-like function. If we relax the sub-additivity assumption, it is possible to define other functions that will have similar properties (but order differently the entangled states). Typical examples are the Renyi entropies defined by:

$$\mathcal{S}_{\mathcal{R},n}(\mathcal{A}) = \frac{1}{1-n}\mathrm{Tr}(\rho_{\mathcal{A}}^n) = \frac{1}{1-n}\sum_{m=1}^{M}\lambda_m^n \text{ with } \mathcal{S}_E = \lim_{n\to 1}\mathcal{S}_{\mathcal{R},n}. \tag{2.9}$$

These entropies measure different properties of the reduced density matrix $\rho_{\mathcal{A}}$. Studying all the Renyi entropies is equivalent to studying our next object of focus, the entanglement spectrum.

Finally, we introduce the mutual information $I_{\mathcal{S}_E}$ of two disjointed regions $\mathcal{A}$ and $\mathcal{B}$.

$$I_{\mathcal{S}_E} = \mathcal{S}_E(\mathcal{A}) + \mathcal{S}_E(\mathcal{B}) - \mathcal{S}_E(\mathcal{A}\cup\mathcal{B}) \tag{2.10}$$

The mutual information can be straightforwardly extended to any entropy-like function by analogy with Eq. 2.10. It usually has the advantage of being free from artificial divergences that can appear in continuum theories, at the price of generally requiring the computation of the multipartite entanglement entropy. In the case of the vNEE, it is additionally positive and monotonically increasing (if $\mathcal{B}\subset\mathcal{C}$, $I_{\mathcal{S}_E}(\mathcal{A},\mathcal{B}) \leq I_{\mathcal{S}_E}(\mathcal{A},\mathcal{C})$). It is only exactly known for free, non-interacting fermions in one dimension[70]. It has been shown that it is not only a function of the central charge, but also of more microscopic details of the theory, such as the Luttinger parameter of Luttinger Liquids[71, 72].

2.1.2 Entanglement entropy in many-body systems

The entanglement entropy reveals many properties of the many-body ground states. In this Section, we expose some of the main ideas on how to use entanglement entropy to

characterize phases and critical theories. We are essentially interested in gapless phases, where anomalous logarithmic terms appear, that can be used to classify the different phases. After a first general discussion, we focus on one and two-dimensional models.

Dependence on the boundaries

As we previously mentioned, the entanglement entropy of a subsystem $\mathcal{A}$ with the rest of the system essentially scales with the length of its boundaries. We first derive some phenomenological physical arguments on the different scalings that can appear for different many-body systems.

Let us first consider the case of gapped systems, *i.e.* systems where the excited states have a finite energy in the thermodynamic limit. The energy gap ΔE, difference of energy between the ground state and the first excited states naturally defines a length scale $\chi \propto \Delta E^{-1}$ that will govern the behavior of the system. In particular, one expects an exponential decrease in the correlations, with a characteristic length proportional to χ. Now let us consider d-dimensional region $\mathcal{A}$ of characteristic length $l_{\mathcal{A}}$ such as represented in Figure 2.1. Then, the vNEE can be seen as a re-summation of the correlations between $\mathcal{A}$ and $\overline{\mathcal{A}}$: given the exponential decrease in these, its long range behavior should scale at best as:

$$\int_{\partial\mathcal{A}} d\vec{r}_{\parallel} \int dr_{\perp} e^{-\frac{\alpha r_{\perp}}{\chi}} \approx |\partial\mathcal{A}| f(\chi) = \mathcal{O}(l_{\mathcal{A}}^{d-1} f(\chi)), \tag{2.11}$$

where $\partial\mathcal{A}$ is the boundary of $\mathcal{A}$, $\vec{r}_{\perp}$ the local normal vector to the boundary, α some numerical constant and f a non-universal function. This indeed corresponds to a dominant scaling exactly proportional to the boundaries between $\mathcal{A}$ and the rest of the system. For gapped systems, this *area*-law (by opposition to a volume-law where the entropy would scale as $l_{\mathcal{A}}^{d}$) has been rigorously proven for both fermions and bosons[73, 74]. It is important to stress the importance of this result: if we take a random state of the Hilbert space $\mathcal{H}_{\mathcal{A}}$, for $\dim\mathcal{H}_{\mathcal{A}} \ll \mathcal{H}_{\overline{\mathcal{A}}}$, the vNEE should scale as $\ln \dim \mathcal{H}_{\mathcal{A}} \propto \mathcal{V}_{\mathcal{A}}$, the volume of $\mathcal{A}$[75]. Typical ground states of gapped Hamiltonian are very different from random states.

For gapless systems, the analysis is more complex. As the gap vanishes, the correlation length χ diverges. Typically, two-points correlation functions may scale now as power laws of the distance between the two points. For free non-interacting fermions, it has been shown that the leading contributions to the entanglement entropy scales as [76–80]:

$$S_E(\mathcal{A}) = \alpha l_{\mathcal{A}}^{d-1} \ln l_{\mathcal{A}} + \mathcal{O}(l_{\mathcal{A}}^{d-1}), \tag{2.12}$$

with

$$\alpha = \frac{1}{(2\pi)^{d-1}} \frac{1}{12} \int_{\partial\Gamma} d\vec{k} \int_{\partial\mathcal{A}} d\vec{r} |\vec{n}_{\partial\Gamma}(\vec{k}).\vec{n}_{\partial\mathcal{A}}(\vec{r})|, \tag{2.13}$$

$\partial\Gamma$ is the Fermi surface, *i.e.* the surface in momentum space defined by $E_{\vec{k}} = 0$ ($E_{\vec{k}}$ is the energy of the quasi-particle at momentum $\vec{k}$). It is supposed to be a $(d-1)$-dimensional manifold and $\vec{n}_{\partial\Gamma}(\vec{k})$ is the normal vector to the Fermi Surface at the point $\vec{k}$. $\partial\mathcal{A}$ is the boundary of the region $\mathcal{A}$, taken to be of volume 1. $\vec{n}_{\partial\mathcal{A}}$ is its normal vector. We will develop on this formula in the next two paragraphs. For now, it suffices to say that the area-law is broken by this additional logarithmic factor. The appearance of a dominant

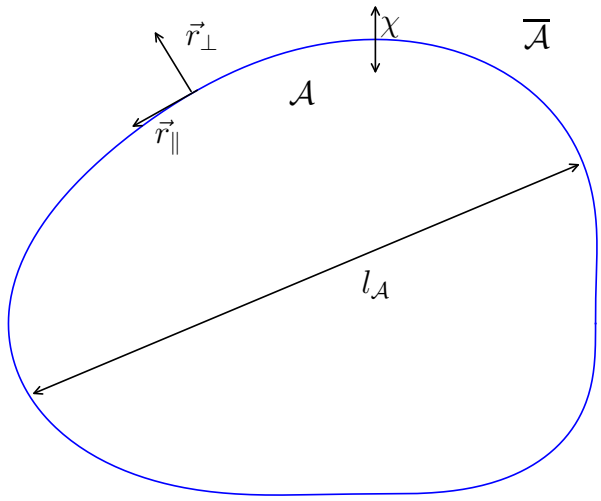

Figure 2.1: The subregion $\mathcal{A}$ is entangled with the rest of the system on a length scale χ. $l_\mathcal{A}$ is a characteristic length of $\mathcal{A}$, $\vec{r}_\parallel$ and $\vec{r}_\perp$ are the tangent and normal vectors to the contour of $\mathcal{A}$.

logarithmic factor will in fact be taken as a marker of gaplessness.
Finally, we conclude by mentioning that additional sub-leading contributions may also appear when $\mathcal{A}$ has sharp corners and when the dimension of the Fermi surface is smaller than $d-1$. This is in particular the case for the Dirac metals that will be the subject of Sections 2.1.2 and 3.4.

Gapless systems in one dimension

We start by considering the one-dimensional limit of Eq. 2.13. Let us consider the vNEE of a segment of length $l_\mathcal{A}$ in the middle of an infinite wire. Its boundaries are two zero-dimensional points. Correspondingly, we assumed that the Fermi surface consists in a set of M points. Then, the formula significantly simplifies to:

$$S_E(\mathcal{A}) = \frac{M}{6} \ln l_\mathcal{A} + \mathcal{O}(1), \tag{2.14}$$

Let us consider perfectly free, non-superconducting fermions, described by the tight-binding Hamiltonian:

$$-\mu \sum_j c_j^\dagger c_{j+1} - t \sum_j (c_j^\dagger c_{j+1} + c_{j+1}^\dagger c_j) = \sum_k (-\mu - 2t\cos k) c_k^\dagger c_k \tag{2.15}$$

The energy of each quasi particle is $E_k = -\mu - 2t\cos k$, and consequently cancels at exactly two points for $|\mu| < 2t$. The limit $|\mu| > 2t$ corresponds to a fully empty or occupied wire, and is therefore not really interesting. Eq. 2.14 leads to $\alpha = \frac{1}{3}$.

On the other hand, in Kitaev's wire (described in Section 1.1), on the lines $\mu = \pm 2t, \Delta \neq 0$, the gap closes only at either $k = 0$ or $k = \pi$. The coefficient in front of the logarithmic term is now $\alpha = \frac{1}{6}$. Given that their vNEEs differ, these two gapless models are not equivalent, in other words, they are not in the same universality class.

In fact, the classification through the vNEE of one-dimensional gapless systems is much more generic. Many critical physical systems are described by a conformal field theory (CFT)[81][1]. One-dimensional critical points can be described entirely by these CFTs. In particular, the vNEE of a region of size $l_{\mathcal{A}}$ for an infinite system with PBC scales as:

$$S_E(\mathcal{A}) = \frac{c}{3} \ln l_{\mathcal{A}} + \mathcal{O}(1), \tag{2.16}$$

where c is the central charge of the corresponding CFT[70, 82–84]. It essentially labels the type of low-energy critical models and defines its universality class. This central charge does not depend on the microscopic details of the theory, but only on its low-energy behavior. A change in the central charge means that a phase transition occurred. This also includes the interacting fermionic theories that we will study in Chapter 3. The two families that interest us in this thesis are the Ising universality class and the free bosons. The former corresponds to the Quantum Ising model in a transverse field or the Kitaev's chain at the critical point, where $c = \frac{1}{2}$ and there is one free Majorana mode. The latter corresponds to normal free electrons, or alternatively to Luttinger liquids or a free scalar boson (described in Appendix E), where $c = 1$ and there is one free complex fermionic mode.

Slightly away from the gapless point, the length $l_{\mathcal{A}}$ is cut-off by the correlation length χ, that is to say that the entropy saturates at:

$$\frac{c}{3} \ln \chi + \mathcal{O}(1) \tag{2.17}$$

The conformal invariance also allows us to address the two important questions of finite temperature and finite size, which are essentially the same due to the conformal invariance. The finite temperature plays the role of a finite length in imaginary time. In these cases, the logarithm is replaced by the universal terms[70]:

$$\ln\left(\frac{L}{\pi}\sin(\frac{l\pi}{L})\right) \text{ for finite size and } \ln\left(\frac{v\beta}{\pi}\sinh(\frac{l\pi}{v\beta})\right) \text{ for finite temperature,} \tag{2.18}$$

with v the effective celerity, β the inverse temperature and L the total length of the system. With the latter form, we recover the linear dependence in the size of the system at infinite temperature, as is physically expected[2].

When juxtaposing several independent critical models, their central charge simply sums. Therefore, two $c = \frac{1}{2}$ systems are equivalent to a $c = 1$ model. Indeed, the two

[1] Conformal field theories are field theories where the set of conformal symmetries has been enforced. These symmetries in particular relate the real space behavior of the fields to their behavior in imaginary or real time[81].

[2] At infinite temperature, each eigenstate of the Hamiltonian is equally weighted. Each degree of freedom being in a perfect superposition, the total entropy $S_E(\mathcal{S})$ of the system is proportional to its size S. It is also true on all subregions.

$c = \frac{1}{2}$ models are described at low energy by two free Majorana chains, leading to the Hamiltonian:

$$it \sum_j \gamma_j^1 \gamma_{j+1}^1 + \gamma_j^2 \gamma_{j+1}^2, \tag{2.19}$$

where $\gamma^{1/2}$ are Majorana fermions and the upper index marks the wire. Now, defining the fermions

$$c_{2j} = \frac{(-1)^j}{\sqrt{2}}(\gamma_{2j}^1 + i\gamma_{2j}^2), \quad c_{2j+1} = \frac{(-1)^j}{\sqrt{2}}(-\gamma_{2j+1}^2 + i\gamma_{2j+1}^1), \tag{2.20}$$

the Hamiltonian can be rewritten as:

$$t \sum_j \left(c_j^\dagger c_{j+1} + c_{j+1}^\dagger c_j \right), \tag{2.21}$$

which indeed describes a free complex fermion at half-filling.

Finally, when considering open systems, such that $\mathcal{A}$ is at one of the boundaries, the coefficient in front of the logarithm is divided by 2 and the dominant contribution to the fluctuations is:

$$\frac{c}{6} \ln l_{\mathcal{A}} \tag{2.22}$$

Two-dimensional systems and Dirac metals

The second family of gapless models studied in this thesis are the Dirac metals. These systems, whose paradigmatic example is the Graphene described in Section 1.6.2, are 2-dimensional gapless systems where the gap only closes at a finite number of momenta, with a linear dispersion. The contribution given by Eq. 2.13 actually vanishes and the dominant term is now of order $l_{\mathcal{A}}$. A simple way to verify this affirmation is to consider a continuous model of two-dimensional free electrons of spectrum:

$$E_{\vec{k}} = v_F |\vec{k}| - \mu \tag{2.23}$$

with μ a chemical potential that regulates the number of quasi-particles, and v_F the Fermi velocity. For $\mu > 0$, the Fermi surface is the circle of radius $\frac{\mu}{v_F}$. When $\mu = 0$, the system is still gapless, but the Fermi surface reduces to a point (we have a Dirac cone). Finally, for $\mu < 0$, the system is fully gapped. Let $\mathcal{A}$ be a disk of radius R. The coefficient α can be trivially computed for $\mu > 0$ using Equation 2.13

$$\alpha = \frac{1}{3\sqrt{\pi}} \frac{\mu}{v_F},$$

α vanishes when $\mu \to 0$. This is symptomatic of $(d-2)$-dimensional Fermi surfaces. Note also that α is clearly not universal for two-dimensional systems: the previous model stays in the same universality class for $\mu > 0$, and yet the coefficient continuously varies.

This problem of universality is general for more than one-dimensional problems. Isolating terms that will be universal (that characterize the low-energy theory) is complex. In

two-dimensions for point-like Fermi surface, it has been shown that universal sub-leading logarithmic contribution can still appear in the vNEE:

$$S_E = Cl_{\mathcal{A}} - \alpha \ln l_{\mathcal{A}} + \mathcal{O}(1) \tag{2.24}$$

where C is a non-universal term and α only depends on the geometric form of $\mathcal{A}$ and the low-energy theory[79, 85–87]. α is non-zero only if $\mathcal{A}$ has sharp corners, and it depends on the value of the corners' angles. For example, for a square subsystem, $\alpha = 4a(\frac{\pi}{2})$ while for a part of a circle of angle ψ, $\alpha = a(\psi) + 2a(\frac{\pi}{2})$, with a the universal contribution of a single corner (the corner function). As the vNEE is symmetric under $\mathcal{A} \leftrightarrow \overline{\mathcal{A}}$, it verifies $a(\psi) = a(2\pi - \psi)$. We subsequently take ψ in $[0, \pi]$. It has been conjectured[88, 89] then shown[90–92] that the central charge c_T associated with the stress tensor of the CFT[93] is given by:

$$c_T = \frac{24}{\pi^2} \lim_{\psi \to \pi} \frac{a(\psi)}{(\pi - \psi)^2} \tag{2.25}$$

Note however that the central charge is not enough to characterize two-dimensional low-energy theories: $c_T = \frac{3}{16\pi^2}$ for both the complex boson and the complex fermions with a Dirac cone for example (called Dirac fermions in the following). In the limit $\psi \to 0$, $a(\psi)$ diverges as:

$$a(\psi \to 0) \approx \frac{\kappa}{\psi}, \tag{2.26}$$

where κ is a universal constant characterizing the CFT. The divergence can be understood from the following argument[94]: when reducing the corner to a line, $\mathcal{A}$ becomes of zero surface, and the entropy must vanish. The dominant coefficient must vanish, which means it must be canceled by the sub-leading logarithmic term. This in turn formally requires a divergence of the logarithmic contribution. This constant κ appears in the universal entanglement in systems with periodic boundary conditions.

The determination of the exact corner function for generic CFTs is still an open problem[94], except in a few specific cases. In the rest of this Section, we will focus on two models: the Dirac fermions and the so-called Extensive Mutual Information model (EMIm), and start with the latter.

The EMIm is a family of models of free fermions, not defined by their Hamiltonian, but purely by their conformal invariance and by the extensivity of their mutual information. It has been useful in analyzing the vNEE of CFTs in higher dimensions[3] as it allows for a geometric computation of the entropy[79, 95]. As the name indicates, the mutual information of the vNEE is extensive, that is to say:

$$I_{\mathcal{S}_E}(\mathcal{A}, \mathcal{B}) + I_{\mathcal{S}_E}(\mathcal{A}, \mathcal{C}) = I_{\mathcal{S}_E}(\mathcal{A}, \mathcal{B} \cup \mathcal{C}) \text{ for } \mathcal{A}, \mathcal{B} \text{ and } \mathcal{C} \text{ disjointed regions.} \tag{2.27}$$

Free complex fermions in one dimension verify this extensivity condition, but not in higher dimensions. Several more complex models have been proposed to be in this family, such

[3] In a general fashion, to keep things simple, when we speak of d-dimensional CFT, d is the dimension in real space of the studied system. In the literature, it is referred as $d+1$-dimensional CFTs: the imaginary time is taken into account at the same level as the physical distance.

as some black hole models. In any case, no more information is needed to compute the form of the entropy and the corner function that will arise:

$$a_{\text{EMIm}}(\psi) = \frac{\pi^2 c_T}{8}\left(1 + (\pi - \psi)\cot\psi\right), \ \kappa_{\text{EMIm}} = \frac{\pi^3 c_T}{8} \approx 3.876 c_T \tag{2.28}$$

For 2-dimensional Dirac fermions, no exact form is known for the corner function. It has been nonetheless thoroughly studied and differs from the EMIm's. We refer the reader to Ref. [94] for a review. In particular,

$$\frac{\kappa_{\text{Dirac}}}{c_T} \approx 3.800. \tag{2.29}$$

As a general rule, the difference between the corner functions of Dirac fermions and of an EMIm with the same central charge remains extremely small for $\theta > \frac{\pi}{2}$, and diverges when $\theta \to 0$.

Topological entropy

Finally, it is impossible to talk about entanglement entropy in topological systems without mentioning the topological entropy that appear in intrinsically topological models. Though it will not be of direct use in this thesis, we present in this section a brief overview of the concept.

Discovered in 2006 by Refs. [96, 97], the topological entropy is the constant term that appears in the vNEE in two-dimensional topologically ordered (intrinsic) system, noted γ:

$$\mathcal{S}_E(\mathcal{A}) = Cl_{\mathcal{A}} - \gamma + o(1). \tag{2.30}$$

As the system is gapped, no logarithmic contribution appears at the dominant or sub-leading order. This constant γ depends on the type of anyonic quasi-particle excitations that can appear in the bulk:

$$\gamma = \frac{1}{2}\ln\sum_{\alpha} d_\alpha^2, \tag{2.31}$$

where d_α is the so-called quantum dimensions of the anyonic sectors. For Abelian anyons, $d_\alpha = 1$, for non-Abelian anyons, $d_\alpha > 1$. It can be used to partially identify a given phase. As an example, in Kitaev's toric code[98], $\gamma = \ln 2$[99], while in a $\frac{1}{q}$-Laughlin state[100] with odd q, $\gamma = \frac{1}{2}\ln q$.

While theoretically interesting, the topological entropy is actually difficult to extract numerically, as it requires careful scaling analysis and/or precise re-summations of the contribution of different zones[101]. It also does not uniquely determine the topological order in the state: this is why the study of the entanglement spectrum presented in the next Section is of crucial importance.

2.2 Entanglement spectrum and topological systems

2.2.1 Definition of the entanglement spectrum

Definition

First introduced in Ref. [102] to study the Fractional Quantum Hall effect, the entanglement spectrum (ES) has become a common tool for studying topological systems. It is nothing but an extension of the entanglement entropy and of the study of the reduced density matrix of a system. Instead of computing the entropy, the ES reinterprets the density matrix $\rho_{\mathcal{A}}$ as a thermal Hamiltonian:

$$\rho_{\mathcal{A}} = \frac{1}{Z} e^{-\beta^* H_{\mathcal{A}}}, \tag{2.32}$$

where β^* is an effective temperature taken to be 1[4], and $H_{\mathcal{A}}$ is the so-called entanglement Hamiltonian. This reformulation is possible because the reduced density matrix stays definite positive. The ES is the set of eigenvalues $\varepsilon_m = -\ln \lambda_m$ of $H_{\mathcal{A}}$, where λ_m have been defined in Eq. 2.6. All ε_m are positive, given that $\lambda_m < 1$. The vNEE can be evidently rewritten as a sum over the ES, that therefore offers much more information. Computation of the ES is mathematically strictly equivalent to computation of all the Renyi entropies[5].

A core idea proposed in Ref. [102] is the classification of the different energies in terms of their local quantum numbers. Let $\hat{O}$ be an operator than can be decomposed as $\hat{O} = \hat{O}_{\mathcal{A}} + \hat{O}_{\overline{\mathcal{A}}}$. Then basic matrix algebra leads to:

$$\mathrm{Tr}_{\overline{\mathcal{A}}}([\hat{O}, \rho]) = \mathrm{Tr}_{\overline{\mathcal{A}}}([\hat{O}_{\mathcal{A}}, \rho]) + \mathrm{Tr}_{\overline{\mathcal{A}}}([\hat{O}_{\overline{\mathcal{A}}}, \rho]) = \mathrm{Tr}_{\overline{\mathcal{A}}}([\hat{O}_{\mathcal{A}}, \rho]) = [\hat{O}_{\mathcal{A}}, \rho_{\mathcal{A}}] \tag{2.33}$$

If $\hat{O}$ commutes with the Hamiltonian, and hence defines a proper quantum number, then $\hat{O}_{\mathcal{A}}$ commutes with $\rho_{\mathcal{A}}$, and the two can be co-diagonalized. The different entanglement energies are therefore associated to different local quantum numbers associated to $\hat{O}_{\mathcal{A}}$.

The ES has many variants, with different properties, depending on the chosen cut $\mathcal{A}$. Up to know, we chose a separation of the Hilbert space in terms of physical space, but any criterion can be used. We note in particular the possibility of choosing the so-called particle cut, where we integrate out a certain number of particles of the system[104], orbital cuts where orbitals are removed on each site[105], or cuts in momentum space[106] to study critical phases. In the rest of this section, we will nonetheless focus on the real-space cut, that has the most direct application for the one-dimensional systems we study.

The case of two spins

Let us illustrate the properties of the ES by going back to the two-spins example. If A and B are in the singlet state

$$|\psi\rangle = \frac{1}{\sqrt{2}}(|\uparrow_A\rangle |\downarrow_B\rangle - |\downarrow_A\rangle |\uparrow_B\rangle), \tag{2.34}$$

[4]The choice of effective temperature has no importance for the computation of the entanglement spectrum though it can be relevant for ensuring continuity of thermodynamics quantities[103].

[5]Basic polynomial analysis for finite systems

the reduced density matrix of the spin A (or B) is given by:

$$\rho_A = \begin{pmatrix} \frac{1}{2} & 0 \\ 0 & \frac{1}{2} \end{pmatrix}, \tag{2.35}$$

and its entanglement spectrum is $\{\ln 2, \ln 2\}$.

If they are in a product state,

$$|\psi\rangle = |\psi_A\rangle |\psi_B\rangle , \tag{2.36}$$

and the ES is formally $\{0, +\infty\}$. The infinite values correspond to never occupied states of the entanglement Hamiltonian, which are conveniently dropped in the following: we are only interested in non-zero eigenvalues of $\rho_{\mathcal{A}}$.

A first difference appears between entangled and non-entangled states directly in the ES: for non-entangled states, whatever the dimension of the Hilbert space of $\mathcal{A}$, the entanglement spectrum is $\{0\}$, while entangled states lead to the appearance of multiple levels. Maximally entangled states will simply have $D = \min(\text{ dim } \mathcal{A}, \text{ dim } \overline{\mathcal{A}})$ degenerate entanglement states with entanglement energy $\ln D$. Counting the number of low-energy quasi-degenerate eigenvalues and measuring the gap with eventual higher excited energies is therefore fundamental to describe the entanglement of the studied state.

2.2.2 Entanglement spectrum in topological systems

Generalities in $d > 1$.

The main idea behind the study of the entanglement spectrum is that it is somehow related to the boundary physics of the original Hamiltonian. Take a topological system in a topological phase (gapped), with periodic boundary conditions (no edge states). Tracing out the rest of the system creates artificial boundaries for the region $\mathcal{A}$. For 2 and 3 dimensional models, it was conjectured in Ref. [102], and later proved in a variety of models by Ref. [107, 108] that the entanglement spectrum coincides with the spectrum of gapless edge states that would appear in an open system with the same geometry as $\mathcal{A}$. In particular, one can identify CFT theories through their tower of states, and consequently identify the topological order of the system. Much more could be said on the properties of the entanglement spectrum in $d > 1$, but we will focus on $d = 1$ in the rest of the section.

Kitaev's chain and the quantum Ising model

Let us first illustrate the main properties of the entanglement spectrum in one dimensional systems through the example of Kitaev's chain. We consider the Hamiltonian introduced in Eq. 1.1 and place ourselves at the two simple limits $P_1 = (t = \Delta = 0, \mu < 0)$ and $P_2 = (t = \Delta > 0, \mu = 0)$. We consider an open wire of length L, and the region $\mathcal{A}$ corresponds to the first $L_{\mathcal{A}} > 1$ sites.

At the point P_1, the system is deep in the trivial phase, its Hamiltonian can be rewritten

as

$$H = |\mu| \sum_{j=1}^{L} c_j^\dagger c_j, \tag{2.37}$$

and the ground state of the system is non-degenerate and given by $|0\rangle_c$. Tracing out $\overline{\mathcal{A}}$ is straightforward, the density matrix of $\mathcal{A}$ is simply given by

$$\rho_{\mathcal{A}} = \left|\tilde{0}\right\rangle_c \left\langle\tilde{0}\right|_c, \tag{2.38}$$

where the state $\left|\tilde{0}\right\rangle_c$ is the state of $\mathcal{A}$ that cancel c_j for $1 \leq j \leq L_{\mathcal{A}}$. The entanglement spectrum is therefore trivial and given by: $\{0\}$, whatever the length of $\mathcal{A}$.

Conversely, at the point P_2, the system is deep in the topological phase. Its Hamiltonian has been rewritten as:

$$H_{\mathcal{K}} = 2t \sum_{j=1}^{L-1} d_j^\dagger d_j \text{ with } d_j = \frac{1}{\sqrt{2}}(\gamma_{j+1}^B + i\gamma_j^A). \tag{2.39}$$

The ground state of the Hamiltonian is two times degenerate: the fermion $d_0 = \frac{1}{\sqrt{2}}(\gamma_1^B + i\gamma_L^A)$ does not appear in the previous expression and consequently has zero energy. The two ground states are $|0\rangle_d$ and $d_0^\dagger |0\rangle_d$, eigenvalues of the total fermionic parity operator. Following Li and Haldane reasoning, we select one of the two as they are eigenvalues of a symmetry of the global system[109]:

$$|\text{even/odd}\rangle = \frac{1}{2^{\frac{L}{2}}} \prod_{j=1,\text{even/odd}}^{L} (1 + c_j^\dagger) |0\rangle_c, \tag{2.40}$$

where the even/odd index marks that we keep terms with an even/odd number of creation operators. The convention for the operator products is the following:

$$\prod_{j=1}^{L}(1 + c_j^\dagger) = (1 + c_L^\dagger)(1 + c_{L-1}^\dagger)...(1 + c_1^\dagger) \tag{2.41}$$

We consider the odd ground state that we rewrite as:

$$|\text{odd}\rangle = \frac{1}{2^{\frac{L}{2}}} \prod_{j=1,\text{even}}^{L_{\mathcal{A}}} (1 + c_j^\dagger) \prod_{j=1+L_{\mathcal{A}},\text{odd}}^{L} (1 + c_j^\dagger) |0\rangle_c + \frac{1}{2^{\frac{L}{2}}} \prod_{j=1,\text{odd}}^{L_{\mathcal{A}}} (1 + c_j^\dagger) \prod_{j=1+L_{\mathcal{A}},\text{even}}^{L} (1 + c_j^\dagger) |0\rangle_c. \tag{2.42}$$

We artificially create a boundary by writing the system as a sum of tensor products. As each term has different fermionic parity in $\overline{\mathcal{A}}$, they are necessary orthogonal and the

density matrix is:

$$\rho_{\mathcal{A}} = \frac{1}{2^{L_{\mathcal{A}}}} \prod_{j=1,\text{even}}^{L_{\mathcal{A}}} (1+c_j^\dagger) \left|0\right\rangle_c \left\langle 0\right|_c \prod_{j=L_{\mathcal{A}},\text{even}}^{1} (1+c_j) + \frac{1}{2^{L_{\mathcal{A}}}} \prod_{j=1,\text{odd}}^{L_{\mathcal{A}}} (1+c_j^\dagger) \left|0\right\rangle_c \left\langle 0\right|_c \prod_{j=L_{\mathcal{A}},\text{odd}}^{1} (1+c_j) \quad (2.43)$$

The ES is $\{\ln 2, \ln 2\}$ and consequently perfectly degenerate. Out of the possible $2^{L_{\mathcal{A}}}$ entanglement energies, only two are non-zero. We obtain the same result when considering the even ground state. When leaving the point $\mathcal{P}_2$, new high energy entanglement energies appear but the spectrum stay exactly twice degenerate as long as the system is in the topological phase. This degeneracy is a direct consequence of the presence of Majorana edge states.

Yet, the picture is not complete: if we had computed the entanglement spectrum for either $|\pm\rangle = \frac{1}{\sqrt{2}}(|\text{even}\rangle \pm |\text{odd}\rangle)$, we would have obtained $\{0\}$. Imposing the symmetry is therefore of crucial importance. For Kitaev's wire, a convenient way to choose a valid GS is to consider periodic boundary conditions. At $\mathcal{P}_2$, the ground state is actually still given by $|\text{odd}\rangle$, and consequently the ES is still twice degenerate, with one eigenvalue in each parity sector. The structure of the entanglement Hamiltonian exactly matches the boundary Hamiltonian.

It is worth considering the Quantum Ising model before concluding. Kitaev's chain with open boundaries at the point $\mathcal{P}_2$ is equivalent to the spin-$\frac{1}{2}$ quantum Ising model given by:

$$H = -\sum_j \sigma_j^x \sigma_{j+1}^x \quad (2.44)$$

The two ground states of the system are obviously $|L\rangle = \bigotimes_j |\leftarrow\rangle_j$ and $|R\rangle = \bigotimes_j |\rightarrow\rangle_j$, whether we have periodic or open boundary conditions. The difference in degeneracy between the Quantum Ising model and Kitaev's model arises from the non-locality of the Jordan-Wigner transformation. Periodic boundary conditions on Kitaev's chain is not equivalent to periodic boundary conditions on the Quantum Ising model (in fact, one of the parity sector will be periodic, the other one anti-periodic).
If we choose the eigenstates $|L\rangle \pm |R\rangle$ of the fermionic parity , equivalent here to $\prod_j \sigma_j^z$, the ES is exactly twice degenerate, with one eigenstate in each parity sector. If we prefer the "physical" ground states $|L\rangle$ and $|R\rangle$ that maximize the broken symmetry and are classical states, the ES is trivial. Choosing the proper basis for the computation of the ES is therefore crucial.[6]

[6]Taking the prescription $\rho = \frac{1}{n}\sum_{j=1}^{n} |\psi_j\rangle\langle\psi_j|$, with $|\psi_j\rangle$ an orthogonal basis of the degenerate low-energy space, does not really solve the problem. In the case of the Ising model, the entanglement spectrum is then always twice degenerate. For Kitaev's wire with OBC, the entanglement spectrum would be the same.

Entanglement spectrum in topological systems

Let us summarize our previous discussion. The entanglement Hamiltonian is strongly reminiscent of the boundary Hamiltonian in Kitaev's chain, and we recover the same structure with an exactly degenerate ES whether we consider the unique periodic ground state, or one of the two ground states with open boundaries that are eigenvalues of the fermionic parity. The exact degeneracy of the ES is therefore a tempting symptom for the detection of topological phases.
Yet, the example of the Quantum Ising model should be a good warning: studying only the degeneracy of the ES is not enough. For systems where we can find a local order parameter and that are well described by a theory a la Landau, *i.e.* where a symmetry is broken, it is (retrospectively obviously) more physical to work in a basis where we saturate the symmetry breaking, instead of a basis where we artificially make it survive.
As a general rule, the entanglement spectrum can give us strong indications that we are in the topological phase only after a careful treatment and analysis of the low-energy sector. The degeneracy (in the thermodynamic limit) of the ground states must be checked. The number of edge states will generally given by the ratio degeneracy of the ES divided by the degeneracy of the periodic system. In particular, for Kitaev's chain the two-fold degeneracy corresponds to the degeneracy of the open system and marks the presence of Majorana edge states, while for the Su-Schrieffer-Heeger model, the ES would be four times degenerate in the topological phase.

For a proper derivation of the properties of the entanglement spectrum in topological system for non-degenerate ground states, we refer the reader to Ref. [110], that gives a clear and detailed discussion on the relation between the topological phases and their entanglement spectrum. Our previous example-based discussion will be enough to follow the rest of this thesis.

2.3 Bipartite fluctuations as a "weak" measure of entanglement

In this section, we give a definition and an overview of the main properties of the bipartite (charge) fluctuations (B(C)F), and of some of the works where it has been successfully applied. We focus on systems where the total charge or spin polarization, whose fluctuations we are measuring, are conserved, through the example of Luttinger Liquids. In this limit, the BF share some properties with the vNEE and other entanglement probes, and can be used to partially characterize phases and phase transitions.

2.3.1 The problem of entanglement measure

While the vNEE and the ES are important theoretical tools, these quantities are challenging to experimentally measure in a generic interacting fermionic system, despite some recent proposals and experimental efforts[111]. Several schemes[112–114] have been proposed to measure the Renyi entropies or the entanglement spectrum, and we give a brief overview of the common idea behind them.

First, let us briefly explain how to measure the vNEE or the entanglement spectrum in a non-interacting system[115]. The Hamiltonian of such a system is a bilinear of fermionic operators. All correlation functions are entirely determined by the two-fermion correlators on different sites, due to Wick's theorem. We remind the reader the form of Wick's theorem for an arbitrary fermionic operator a, and for an eigenstate with fixed fermionic parity (in particular the ground state):

$$\langle a_{i_1}...a_{i_{2n}}\rangle = \frac{1}{n!}\sum_{\sigma\in\mathbb{S}'_{2n}}(-1)^{P(\sigma)}\langle a_{\sigma(i_1)}a_{\sigma(i_2)}\rangle...\langle a_{\sigma(i_{2n-1})}a_{\sigma(i_{2n})}\rangle, \tag{2.45}$$

where $\mathbb{S}'_{2n}$ is the space of the permutations of $(1,...,2n)$ such that $\sigma(i_{2k+1}) < \sigma(i_{2k+2})$ for all k and $P(\sigma)$ the signature of the permutation σ. A simple example is:

$$\langle c_1^\dagger c_2 c_3^\dagger c_4\rangle = \langle c_1^\dagger c_2\rangle\langle c_3^\dagger c_4\rangle - \langle c_1^\dagger c_3^\dagger\rangle\langle c_2 c_4\rangle + \langle c_1^\dagger c_4\rangle\langle c_2 c_3^\dagger\rangle \tag{2.46}$$

In systems where the charge is conserved, the Wick's theorem accepts the simpler representation, for states that are eigenstates of the fermionic number operator:

$$\langle c_{i_1}^\dagger...c_{i_n}^\dagger c_{j_1}...c_{j_n}\rangle = (-1)^{n-1}\sum_{\sigma\in\mathbb{S}_n}(-1)^{P(\sigma)}\langle c_{i_1}^\dagger c_{j_{\sigma(1)}}\rangle...\langle c_{i_n}^\dagger c_{j_{\sigma(n)}}\rangle, \tag{2.47}$$

where $\mathbb{S}_n$ is the space of the permutations of $(1,...,n)$. Both versions are also valid for thermal averages.
Conversely, the entanglement Hamiltonian can be shown to still be a fermionic bilinear, given that all correlation functions inside the region $\mathcal{A}$ are still determined by the two-fermion correlators of sites included in region $\mathcal{A}$. If the system is described by the density matrix

$$\rho_{\mathcal{A}} = e^{-\sum_{i,j}\mathcal{H}_{i,j}c_i^\dagger c_j},$$

then the correlation functions are:

$$\langle c_i^\dagger c_j\rangle = (1+e^{\mathcal{H}})^{-1}_{i,j}, \text{ or conversely } \mathcal{H} = \ln(\mathcal{C}-1), \tag{2.48}$$

with $\mathcal{C}$ the matrix of correlations in $\mathcal{A}$, $\mathcal{C}_{i,j} = \langle c_i^\dagger c_j\rangle$. The entanglement spectrum (and therefore the vNEE) is directly obtained from a measurement of the correlations, and similarly for the entropy.

For interacting systems, it is in practice much more difficult to measure the entanglement as Wick's theorem no longer applies. In principle, the entanglement Hamiltonian is also interacting (and therefore not quadratic).
Several proposals have recently been made in different set-ups, and essentially rely on a similar trick. To measure either Renyi entropies, or the entanglement spectrum, several "copies" (in the sense of identical systems) of the studied system are brought together. Propositions then rely on the existence of a swap operator S that exchange the wave functions of the systems. In this short presentation, we focus on the case of the second Renyi entropy $\mathcal{S}_{\mathcal{R},2}$ and the entanglement spectrum that both requires only two copies of the system. Let the two systems be in the identical state $|\psi\rangle = \sum_n \lambda_n |L_n\rangle_{\mathcal{A}_j}\otimes|R_n\rangle_{\overline{\mathcal{A}_j}}$,

where the cut is taken at the boundary of the region $\mathcal{A}_j$ in each wire j. Assume the swap operator acts only on the part $\overline{\mathcal{A}}$. With the swap, the system goes from the state:

$$|0\rangle = \left(\sum_n \lambda_n |L_n\rangle_{\mathcal{A}_1} \otimes |R_n\rangle_{\overline{\mathcal{A}_1}}\right) \otimes \left(\sum_n \lambda_n |L_n\rangle_{\mathcal{A}_2} \otimes |R_n\rangle_{\overline{\mathcal{A}_2}}\right) \tag{2.49}$$

to

$$|0'\rangle = \left(\sum_n \lambda_n |L_n\rangle_{\mathcal{A}_1} \otimes |R_n\rangle_{\overline{\mathcal{A}_2}}\right) \otimes \left(\sum_n \lambda_n |L_n\rangle_{\mathcal{A}_2} \otimes |R_n\rangle_{\overline{\mathcal{A}_1}}\right), \tag{2.50}$$

and the overlap between the two is then $\langle 0'|0\rangle = \sum_n \lambda_n^4 = e^{-\mathcal{S}_{\mathcal{R},2}}$. To measure this overlap, interferometry of an auxiliary ancilla that conditions the swap is enough.
To perform the measure of the entanglement spectrum, instead of applying directly a conditioned pulse operator S, one needs to apply sequentially small pulses such that the system evolves as $e^{i\varepsilon S}\rho_{\mathcal{A}_1} \otimes \rho_{\mathcal{A}_2} e^{-i\varepsilon S}$, where S now applies on $\mathcal{A}_j$. After n such operations, the first system is approximately in the state

$$e^{-in\varepsilon\rho_{\mathcal{A}_2}} \rho_{\mathcal{A}_1} e^{in\varepsilon\rho_{\mathcal{A}_2}}$$

The first system consequently undergoes a time evolution equivalent to the density matrix of the second system. Using again an auxiliary ancilla to apply a conditioned swap allows a measure of interference patterns on the polarization of a single qubit, given by:

$$\sum_m \lambda^m \cos(2t_n\lambda_m), \tag{2.51}$$

where $t_n = n\varepsilon$ and λ_m are the eigenvalues of $\rho = \rho_{\mathcal{A}_1} = \rho_{\mathcal{A}_2}$. Fourier analysis of the signal gives the different eigenvalues, their degeneracy and consequently, the entire ES.

For more than a simple overview of these two experimental proposals, we refer the reader to the original papers[113, 114]. Our message here is simple: these proposals rely on creating complex interference patterns between identical systems. While such a precision may be in principle attained in very controlled set-ups such as cavity or circuit quantum Electrodynamics, or in cold atoms experiments with a reasonably small number of atoms, the study of traditional condensed matter systems, with their impurities and disorder, seems out of reach.

2.3.2 General definition of bipartite fluctuations

Measurement of the vNEE or the entanglement spectrum are therefore challenging, in particular for condensed matter systems. As these quantities are properties of the reduced density matrix, it is natural to wonder whether it is possible to acquire similar informations by looking directly at local observables[116]. In particular, Ref. [117] proposed to look at the BCF in charge conserving fermionic systems. Let us define a general formalism for bipartite fluctuations[118–120]. For a region $\mathcal{A}$, we consider an operator $\hat{O}$ that can be written as $\hat{O} = \hat{O}_{\mathcal{A}} \otimes \mathbb{1} + \mathbb{1} \otimes \hat{O}_{\overline{\mathcal{A}}}$. Generally, we will consider operators that as a sum of local commuting operators acting on a unit-cell:

$$\hat{O}_{\mathcal{A}} = \sum_{\vec{r}\in\mathcal{A}} \hat{O}_{\vec{r}}, \tag{2.52}$$

where $\hat{O}_{\vec{r}}$ the operator for site $\vec{r}$. We define the bipartite fluctuations of $\hat{O}$ on $\mathcal{A}$, $\mathcal{F}_{\hat{O}}(\mathcal{A})$ by:

$$\mathcal{F}_{\hat{O}}(\mathcal{A}) = \langle \hat{O}_{\mathcal{A}}^2 \rangle - \langle \hat{O}_{\mathcal{A}} \rangle^2 = \langle (\hat{O}_{\mathcal{A}} - \langle \hat{O}_{\mathcal{A}} \rangle)^2 \rangle \tag{2.53}$$

$$= \mathrm{Tr}(\hat{O}_{\mathcal{A}}^2 \rho) - \mathrm{Tr}(\hat{O}_{\mathcal{A}} \rho)^2 = \mathrm{Tr}(\hat{O}_{\mathcal{A}}^2 \rho_{\mathcal{A}}) - \mathrm{Tr}(\hat{O}_{\mathcal{A}} \rho_{\mathcal{A}})^2 \tag{2.54}$$

$$= \sum_{\vec{r},\vec{r}' \in \mathcal{A}} \langle \hat{O}_{\vec{r}} \hat{O}_{\vec{r}'} \rangle - \langle \hat{O}_{\vec{r}} \rangle \langle \hat{O}_{\vec{r}'} \rangle, \tag{2.55}$$

where the average is usually taken in the ground state, but can be extended to any thermal states. By analogy with usual diagrammatic expansion, we call $\langle \hat{O}_{\vec{r}} \hat{O}_{\vec{r}'} \rangle - \langle \hat{O}_{\vec{r}} \rangle \langle \hat{O}_{\vec{r}'} \rangle$ the connected average that we note $\langle \hat{O}_{\vec{r}} \hat{O}_{\vec{r}'} \rangle_c$ (and similarly for $\langle \hat{O}_{\mathcal{A}}^2 \rangle_c$).
As defined above, the fluctuations are always positive. They correspond to the variance of the operator $\hat{O}$ in the ground state (or thermal ensemble), that is to say the second order cumulants of $\hat{O}$. They can be generalized to any order by:

$$(-i\partial_\lambda)^n \ln \langle e^{i\lambda \hat{O}_{\mathcal{A}}} \rangle |_{\lambda=0} \tag{2.56}$$

Let us focus on the zero-temperature limit where the system is taken in its ground state, that we take as an eigenstate of $\hat{O}$. It is a consequence of the commutation of $\hat{O}$ with the Hamiltonian. Then, the fluctuations verify the following set of entropy-like properties:

- The fluctuations cancel for a product state $|\psi\rangle_{\mathcal{A}} \otimes |\psi\rangle_{\overline{\mathcal{A}}}$. As the total state is an eigenstate of $\hat{O}$, the product state structure requires that both $|\psi\rangle_{\mathcal{A}}$ and $|\psi\rangle_{\overline{\mathcal{A}}}$ are eigenstates of $\hat{O}_{\mathcal{A}}$ and $\hat{O}_{\overline{\mathcal{A}}}$. Indeed:

$$\langle \hat{O}^2 \rangle_c = \mathcal{F}_{\hat{O}}(\mathcal{A}) + \mathcal{F}_{\hat{O}}(\overline{\mathcal{A}}) + 2\langle \hat{O}_{\mathcal{A}} \hat{O}_{\overline{\mathcal{A}}} \rangle - 2\langle \hat{O}_{\mathcal{A}} \rangle \langle \hat{O}_{\overline{\mathcal{A}}} \rangle$$
$$0 = \mathcal{F}_{\hat{O}}(\mathcal{A}) + \mathcal{F}_{\hat{O}}(\overline{\mathcal{A}}),$$

  which are each positive. The converse is of course false: states that cancel the fluctuations (and even all cumulants) are not necessarily product states. A good example is the state $\frac{1}{\sqrt{2}}(|01\rangle_{\mathcal{A}} \otimes |10\rangle_{\overline{\mathcal{A}}} + |10\rangle_{\mathcal{A}} \otimes |01\rangle_{\overline{\mathcal{A}}})$ for $\hat{O}$ that counts the number of 1. Cumulants at all order cancel, but the vNEE is $\ln 2$. Yet, local conservation of $\hat{O}$ will be rare, and even usually unphysical. The reciprocal statement $\mathcal{F}(\mathcal{A})_{\hat{O}} = 0 \Rightarrow$ ($\mathcal{A}$ and $\overline{\mathcal{A}}$ form a product state) is therefore empirically true.

- The fluctuations are in fact symmetric for pure states: $\mathcal{F}_{\hat{O}}(\mathcal{A}) = \mathcal{F}_{\hat{O}}(\overline{\mathcal{A}})$.

$$\langle (\hat{O}_{\mathcal{A}}^2 \rangle_c - \langle (\hat{O}_{\overline{\mathcal{A}}}^2 \rangle_c = \langle (\hat{O} - \langle \hat{O} \rangle)(\hat{O}_{\mathcal{A}} - \hat{O}_{\overline{\mathcal{A}}} - \langle \hat{O}_{\mathcal{A}} - \hat{O}_{\overline{\mathcal{A}}} \rangle) \rangle = 0 \tag{2.57}$$

  This symmetry is a direct consequence that the fluctuations arise at the boundaries between $\mathcal{A}$ and the rest of the system.

- Fluctuations admit a weak form of sub-additivity: $\mathcal{F}_{\hat{O}}(\mathcal{A}) + \mathcal{F}_{\hat{O}}(\mathcal{B}) \geq \mathcal{F}_{\hat{O}}(\mathcal{A} \cup \mathcal{B}) = 0$, if $\hat{O}$ is conserved in $\mathcal{A} \cup \mathcal{B}$. It simply comes from $\mathcal{F} \geq 0$.

2.3.3 Bipartite charge fluctuations in Luttinger Liquids

Instead of a complete overview of the physical systems previously studied with the help of bipartite fluctuations, we will focus on the seminal example of the Luttinger liquids (LL) in one dimension. We note nonetheless that bipartite fluctuations were also used in very different contexts, such as the superradiant transition[121] or in relation with Many-Body Localization and disordered systems[122–125]. A brief overview of LL formalism is kept in Appendix E. We here study the properties of the charge or spin fluctuations in such a system. We only discuss systems where the total charge is conserved.

Bipartite charge fluctuations

It was initially proposed to take $\hat{O}$ to be either the fermionic charge or equivalently the spin polarization. This choice follows quite naturally from both theoretical and practical reasons.

First, for simple non-interacting systems, the vNEE and all Renyi entropies can be expressed as a sum over the charge cumulants, as was shown in Ref. [126]. As an example, we give the formula for the vNEE:

$$\mathcal{S}_E = \lim_{M\to+\infty} \sum_{n=1}^{M+1} \alpha_n(M) C_n = \sum_{n=1}^{+\infty} 2\zeta(2n) C_{2n}, \tag{2.58}$$

where C_n is the nth charge cumulant, ζ is the Riemann zeta function and α is defined by:

$$\alpha_n(M) = \begin{cases} 2 \sum\limits_{k=n-1}^{M} \frac{S_1(k,n-1)}{k!k} & \text{for n even} \\ 0 & \text{for n odd} \end{cases}, \tag{2.59}$$

where S_1 are the unsigned Stirling number of the first kind. The two sums are formally equivalent, but the first one has more convenient convergence properties. Derivation of this formula is quite technical and we invite the interested reader to consult Ref. [126].

Secondly, the charge and the spin polarization are usually convenient objects to measure in any kind of systems. A few proposals have been made to implement the measure. For cavity or circuit QED, or in cold atoms, one can directly probe the two-point correlation functions, in particular of the charge, or even directly the charge of a region[127, 128], and from there rebuild the fluctuations[7]. For the more interesting case of condensed matter systems (the real superconductors and insulators), probing the local charge through grids or electronic microscopes would be enough.

Fluctuations and entanglement in Luttinger Liquids

Let us consider the simpler case of Luttinger liquids[129–131] (LL) described in Appendix E. Luttinger liquids are a way of representing one-dimensional fermionic theories in terms of their bosonic density- and spin-waves. Mapping fermionic theories to bosonic ones

[7] In practice, it is even enough to extract the long-range behavior of these correlations to get the different properties and coefficients.

allows for a convenient perturbative treatment of interactions, but also a convenient way to compute entropy and BF. LL form a CFT with central charge $c = 1$ (which corresponds to the central charge of the non-interacting fermions). Its entanglement entropy for a single mode is therefore given by:

$$\mathcal{S}_E(\mathcal{A}) = \frac{1}{3} \ln l_{\mathcal{A}} + \mathcal{O}(1), \tag{2.60}$$

where $O(1)$ represents a non-universal constant, and other sub-leading terms. The considered one-dimensional system has been taken to be infinite and $\mathcal{A}$ far from its edges.

The computation of the fluctuations is actually straightforward in a Luttinger Liquid. The charge operator corresponds in the continuum limit to the density operator:

$$\rho(x) = \rho_0 - \frac{1}{\pi} \partial_x \phi(x), \tag{2.61}$$

where ρ_0 is the mean density. The total charge in $\mathcal{A}$ is straightforwardly expressed as:

$$\hat{Q}_{\mathcal{A}} - \langle \hat{Q}_{\mathcal{A}} \rangle = -\frac{1}{\pi} (\phi(l_{\mathcal{A}}) - \phi(0)) \tag{2.62}$$

Using expressions given in Appendix E leads to a simple form for the fluctuations:

$$\mathcal{F}_{\hat{Q}}(\mathcal{A}) = \frac{K}{\pi^2} \ln l_{\mathcal{A}} + \mathcal{O}(1). \tag{2.63}$$

The derivation can be alternatively obtained directly from CFT computations (Appendix F.2), which allows to simply recover that the fluctuations admit the same finite size and finite temperature form as the entanglement entropy. For the purpose of numerical simulations, in particular for open boundary conditions, these finite-size corrections are crucial (Friedel oscillations)[70, 117, 132]. About a hundred sites are required to get a precise value of either the charge central or K.

Interestingly enough, the ratio $\mathcal{S}_E / \mathcal{F}_{\hat{Q}}(\mathcal{A})$ for free fermions is, for $l_{\mathcal{A}} \gg 1$, given by $\frac{\pi^2}{3}$, which is exactly the limit of $\alpha_2(M)$ for $M \to +\infty$ in Eq. 2.59. It has been shown in Ref. [133] that such a ratio holds in any dimension and for all Renyi entropies for non-interacting fermion gases in the thermodynamic limit[8]

$$\frac{S_{\mathcal{R},\alpha}(\mathcal{A})}{\mathcal{F}_{\hat{Q}}(\mathcal{A})} = \frac{(1 + \alpha^{-1})\pi^2}{6} + o(1) \tag{2.64}$$

For non-interacting free fermions, in systems where the charge is conserved, measuring the vNEE or the BCF is essentially equivalent. We will see in the next section an alternative derivation of $\mathcal{F}$ for free fermions.

For interacting systems described by Luttinger liquids, the relation is still fairly straightforward. The additional factor K that appears nonetheless means a loss of universality. Two LL with different Luttinger parameters belong to the same universality class, as they

[8] The ratio is also valid for other inhomogeneous fermionic systems in one dimension[134]

are both described by a $c = 1$ bosonic CFT, yet the coefficients of the logarithmic term in the fluctuations differ. It is nonetheless not a pure negative point: the BCF give a very convenient way to measure the Luttinger parameter in LL (for example in numerical simulations), without any free parameters. The BCF have been used with a lot of success to characterize LL at phase transitions[135–139].

A final interesting property is the link between the coefficient of the fluctuations and the compressibility of the charge. We define the compressibility by:

$$\chi = \frac{\partial}{\partial \mu} \langle \rho \rangle, \tag{2.65}$$

with $\langle \rho \rangle$ the average value of the charge density taken in its thermal average. Noting $\mathbf{b}_{\hat{Q}}$ the logarithmic coefficient of the charge fluctuations, the compressibility theorem[126, 140] states that:

$$\mathbf{b}_{\hat{Q}} = \frac{v\chi}{\pi} \text{ with } v \text{ the celerity.} \tag{2.66}$$

In terms of standard thermodynamics, $\overline{\mathcal{A}}$ acts as a reservoir at equilibrium with $\mathcal{A}$, treated in the grand canonical ensemble. This result is only valid if the total charge is conserved, i.e. the equality does not stand in the systems studied in Chapter 3[140].

2.3.4 Beyond one dimension

The study of the BCF in generic two dimensional models is still quite an open question. For non-interacting systems, the methods used in Ref. [126] are still valid, but the required computations are much more involved. As soon as we go to interacting systems, except for a few exactly solvable models, numerics are required to compute both the vNEE or the BCF.

On the other hand, the BCF offer a convenient tool to probe the edge states that appear in some topological models. A paradigmatic example is the case of the Integer Quantum Hall effect[141]. It has also been shown that for free fermions, the BCF follow the same dominant scaling laws as the vNEE[142]. They were also used in various spin models.[139, 143].

Chapter 3

Bipartite fluctuations in non-interacting topological systems

Contents

3.1 Bipartite fluctuations in 1D: generalities 68

3.1.1 Preliminaries on charge-conservation breaking 68

3.1.2 Bipartite fluctuations in arbitrary non-interacting systems 70

3.1.3 The Fejér Kernel: properties and consequences 72

3.2 One-dimensional BDI class 77

3.2.1 BDI Hamiltonian and fluctuations 77

3.2.2 Discontinuity of the derivative of the linear term 78

3.2.3 Logarithmic contributions and generalized fluctuations 79

3.2.4 Conformal origin of the logarithm 81

3.2.5 Structure factor of the BCF 82

3.2.6 Bipartite fluctuations in Kitaev's model and the SSH chain . . . 84

3.2.7 Bipartite fluctuations in the extended Kitaev's model 87

3.2.8 Extension to finite length and finite temperature 88

3.2.9 A brief comparison with other charge-based measurements 92

3.2.10 Beyond the two-band paradigm 95

3.3 One-dimensional D class 96

3.3.1 Preliminaries 96

3.3.2 Cusp of the linear term 96

3.3.3 Logarithmic coefficients 96

3.3.4 An example: extended Kitaev model 97

3.4 Bipartite fluctuations in 2D Dirac materials 98

3.4.1 Geometric shape, Kernel functions and Sobolev spaces 99

3.4.2 Fluctuations for a single isotropic Dirac cone 102

3.4.3 Beyond the single isotropic Dirac cone 110

This Chapter is dedicated to our own work on bipartite fluctuations in non-interacting topological systems. More specifically, we focus on bipartite fluctuations at and near the usual critical phases that appear in such systems, as bipartite fluctuations bring more informations for gapless phases. Finding such critical phases is not a guarantee of topological phase transition, as it is always possible to build convoluted models where they appear without change in the topology of the system, but it is still a strong signature of these transitions. Additionally, some gapless systems are themselves topologically protected[41] (for example, the DIII class in $d = 2$): the BCF are then a perfect tool for their study.

In this Chapter, we focus on one- and two-dimensional critical systems that are typical of topological phase transitions. We consider fluctuations of local fermionic bilinears such as the charge, or the different pseudo-spin polarizations. We start in Section 3.1 by an overview of the mathematical properties of the fluctuations of such systems in one dimension. Using Wick's theorem, one can conveniently express fluctuations as a simple scalar product of the Green functions modulated by a kernel function, the so-called Fejér Kernel. This function has very interesting properties that allow us to determine the general form of the fluctuations for non-interacting systems:

$$\mathcal{F}_{\hat{O}}(\mathcal{A}) = i_{\hat{O}} l_{\mathcal{A}} + \mathbf{b}_{\hat{O}} \ln l_{\mathcal{A}} + O(1), \tag{3.1}$$

with $\hat{O}$ the considered operator, and $l_{\mathcal{A}}$ the length of the subsystem $\mathcal{A}$. We also prove that $i_{\hat{O}}$ is linked to the Quantum Fisher Information density[144] (QFID). The QFID, introduced in quantum metrology and information, gives bounds on the reproducibility of the quantum systems. For the superconductors and two-band insulators that we study here, we derive strong bounds on this coefficient:

$$i_{\hat{O}} \leq \frac{q_e}{2} \text{ with } q_e \text{ the charge per unit-cell.} \tag{3.2}$$

The logarithmic term itself can only appear if the system is gapless and is directly related to the amplitude of the correlation functions and to the symmetries at the gap-closing momenta.

In Section 3.2 we apply the previously derived formalism to the BDI family of topological models. Focusing on our two-band models, we compute the fluctuations for the complete family of local fermionic bilinears. We show that at phase transitions, the linear coefficient has characteristic cusps that make it particularly convenient to detect the gapless QPTs. The discontinuity of the derivative can be linked to the speed of the different components of the Hamiltonian. At simple phase transitions, where the gap closes at only one momentum, we show that the particle-hole (PHS) and time-reversal (TRS) symmetries enforce that the logarithmic coefficient of the charge fluctuations is universal and given by:

$$\mathbf{b}_{\hat{Q}} = -\frac{q_e}{2\pi^2}. \tag{3.3}$$

The negative sign proves that these fluctuations cannot be described in terms of density fluctuations of a Luttinger Liquid. For superconductors, $q_e = 1$, and $|\mathbf{b}_{\hat{Q}}|$ is half of what

it would be for free fermions. This factor of two is directly analogous to the one appearing in the central charge.
When considering more complex phase transitions, with several points at which the gap closes, we lose universality of the coefficient, thought the cusp in the linear term generally survives. To recover the exact nature of the QPT, we introduce the structure factor of the bipartite fluctuations:

$$\mathcal{SF}_{\hat{O}}(\mathcal{A},\psi) = \langle|\sum_{j\in\mathcal{A}} e^{i\psi j}\hat{O}_j|^2\rangle - |\langle\sum_{j\in\mathcal{A}} e^{i\psi j}\hat{O}_j\rangle|^2 \tag{3.4}$$

This quantity allows us to recover the exact number of gap-closing points and their properties. Finally, we also address finite-temperature and finite-size corrections. The latter is especially important in numerical simulations of topological superconductors, as proper care has to be taken of the special 0- and π-modes. We find the exact corrections for Kitaev's model, and check the numerical convergence of fluctuations in Matrix Product States simulations. We also take the time to treat, as an example of results beyond the two-band paradigm, the Rashba-nanowire model for topological superconductor introduced in Section 1.5.3. We find that a proper choice of the charge leads to the same results as in Kitaev's simpler model.

Section 3.3 is devoted to the study of the bipartite fluctuations in D class Hamiltonians. We find that most of the previously derived properties are still valid: cusp at the phase transitions, quantized logarithmic coefficients...

Finally, we study in Section 3.4 typical models of two-dimensional gapless fermions. More exactly, we focus on models presenting Dirac cones, that are characteristic of transitions in two-dimensional topological models. We focus on charge fluctuations in two-band models. We first show, using the 2D analogue of Fejér Kernel, that the fluctuations scale as:

$$i_{\hat{O}}A_{\mathcal{A}} + c_{\hat{O}}R_{\mathcal{A}} + \mathbf{b}_{\hat{O}}\ln l_{\mathcal{A}} + O(1), \tag{3.5}$$

with $A_{\mathcal{A}}$ the area of the considered subregion and $R_{\mathcal{A}}$ and $l_{\mathcal{A}}$ two characteristic lengths ($R_{\mathcal{A}}$ is usually the perimeter). We then prove that the area coefficient is still given by the QFID associated to the charge. It does not present cusps at QPTs, but a logarithmic divergence of its second derivative. We can extend this result to higher dimensions: for a point-like Fermi surface and a linear energy dispersion, we expect discontinuity of the dth derivative in odd dimensions and its logarithmic divergence in even dimensions.
We then focus on the logarithmic term for a single isotropic Dirac cone. $\mathbf{b}$ can be non-zero only if the system is gapless and depends on the winding number m of the Dirac cone. We also show that, just as for the vNEE, it appears if there are corners in the subsystem $\mathcal{A}$. Each corner gives independently a contribution of

$$\frac{q_e m^2}{32\pi^2}(1+(\pi-\psi)\cot\psi)\ln l_{\mathcal{A}}, \text{ with } \psi \text{ the angle of the corner.} \tag{3.6}$$

The function $\psi \to 1+(\pi-\psi)\cot\psi$ is called a corner function. It does not correspond to the corner function that appears in the entropy of Dirac fermions in two dimensions, but

to the one that appears in the Extensive Mutual Information model. This result, initially computed on a square lattice, is actually lattice-invariant. Note also the positive sign of the logarithmic term, which is opposite to the one appearing in the vNEE of the relevant systems.

We then generalize these results to more complex situations. First, we look at potentially anisotropic Dirac cones. We show that anisotropies in momentum space translate into anisotropy in real space: fluctuations become dependent on the direction of $\mathcal{A}$, and the corner function is deformed. Then we conclude by looking at critical points with several Dirac cones. We show that the structure factor of the fluctuations allows us to distinguish between a trivial phase such as the graphene, where two cones with opposite winding number, and the $\mu = 0$ gapless phase of the $p + ip$ superconductor where the two cones have the same winding number.

Most of the results in this Chapter were derived directly for tight-binding Hamiltonians, using symmetries to minimize the importance of the microscopic details of the considered models. We could have a similar approach using directly Conformal Field Theory reasoning directly in terms of Operator Product Expansions and operator dimensions. Our choice of not going through such a derivation follows from the simple observation that, for experiments, the way observables map on the conformal fields is just as important as the behavior of the conformal fields at low energy. Treating directly physical observables therefore bypass this problem, and the mapping from observables to conformal fields is straightforward from the quantized coefficients. We also want to point out that the discussion and quantification of the fluctuations can also be expressed in terms of quantification of the dominant terms in the correlation functions. As a simple example, universality of the logarithmic coefficient in one dimension for the charge fluctuations in topological superconductors means that:

$$\langle n_j n_{j'} \rangle_c = -\frac{\mathbf{b}_{\hat{Q}}}{2} \frac{1}{(j-j')^2} + o(\frac{1}{(j-j')^2}). \tag{3.7}$$

This Chapter is based on Ref. [145] and other works in preparation.

3.1 Bipartite fluctuations in 1D: generalities

3.1.1 Preliminaries on charge-conservation breaking

Before attacking the proper study of bipartite fluctuations in topological systems and at the topological phase transitions, it is worth spending some time considering the general properties of the BF when the considered observable $\hat{O}$ is *not* a global conserved quantity. Indeed, in Kitaev's model, only the parity of the total charge is conserved. For other topological systems, such as the SSH model, we will be interested in the pseudo-spin polarization, which is also not conserved.

Before studying many-body examples, we can have a look at the similarities with the vNEE that were obtained in Section 2.3.2. All of these properties break down when

considering an observable $\hat{O}$ that is not conserved. Let us go through an example of each violation. We take $\hat{O}$ to count the number of 1 in all the following examples.

- The state $\frac{1}{2}\left(|0\rangle_{\mathcal{A}} + |1\rangle_{\mathcal{A}}\right) \otimes \left(|0\rangle_{\overline{\mathcal{A}}} + |1\rangle_{\overline{\mathcal{A}}}\right)$ verifies $\mathcal{F}_{\hat{O}}(\mathcal{A}) = \frac{1}{4} \neq 0$ while it is a product state.
- The state $\frac{1}{\sqrt{2}}|0\rangle_{\mathcal{A}} \otimes \left(|0\rangle_{\overline{\mathcal{A}}} + |1\rangle_{\overline{\mathcal{A}}}\right)$ obviously violates the symmetry between $\mathcal{A}$ and $\overline{\mathcal{A}}$.
- The state $\frac{1}{\sqrt{2}}\left(|0\rangle_{\mathcal{A}} \otimes |0\rangle_{\overline{\mathcal{A}}} + |1\rangle_{\mathcal{A}} \otimes |1\rangle_{\overline{\mathcal{A}}}\right)$ breaks the weak sub-additivity.

The consequences for many-body systems are far-reaching: in systems where $\hat{O}$ is not a conserved number, the absence of symmetries implies that the BF do not follow boundary laws (or even logarithmic corrections to the boundary laws). Indeed, this is what we observe in the rest of the Section. The bipartite charge fluctuations generally scale at least linearly with the size of the considered region $\mathcal{A}$.

On the other hand, we can define another object, the mutual fluctuations that still directly measure the entanglement of the subsystems. By analogy, the mutual fluctuations for disjointed regions $\mathcal{A}$ and $\mathcal{B}$ are defined by:

$$\mathcal{I}_{\hat{O}}(\mathcal{A},\mathcal{B}) = \mathcal{F}_{\hat{O}}(\mathcal{A}\cup\mathcal{B}) - \mathcal{F}_{\hat{O}}(\mathcal{A}) - \mathcal{F}_{\hat{O}}(\mathcal{B}) \tag{3.8}$$

$$= 2\sum_{j\in A, j'\in\mathcal{B}} \langle \hat{O}_{\mathcal{A}}\hat{O}_{\mathcal{B}}\rangle_c \tag{3.9}$$

The mutual fluctuations still verify ($\mathcal{I}_{\hat{O}}(\mathcal{A},\mathcal{B}) = 0$ for all product states). It also follows from their definition that they are extensive:

$$\mathcal{I}_{\hat{O}}(\mathcal{A},\mathcal{B}) + \mathcal{I}_{\hat{O}}(\mathcal{A},\mathcal{C}) = \mathcal{I}_{\hat{O}}(\mathcal{A},\mathcal{B}\cup\mathcal{C}) \text{ with } \mathcal{A},\ \mathcal{B} \text{ and } \mathcal{C} \text{ disjointed.} \tag{3.10}$$

It has the added advantage to remove the volume terms, and therefore the logarithmic contribution is directly visible. We nonetheless keep the focus on the BCF as the dominant scaling term carries information on the phase transition, and as the generic computation of $\mathcal{I}$ requires the more complex computation of multipartite fluctuations. They also give a very interesting bound on the mutual entropy[74]:

$$\mathcal{I}(\mathcal{A},\mathcal{B}) \geq \frac{1}{8}\frac{\mathcal{I}_{\hat{O}}(\mathcal{A},\mathcal{B})^2}{||\hat{O}_{\mathcal{A}}||^2||\hat{O}_{\mathcal{B}}||^2} \tag{3.11}$$

This bound is actually far from exhaustion in the models we consider in this Chapter: while it will generally guarantee a non-trivial algebraic decay of the mutual entropy, it is not a precise measurement of the exponent. We generally find that mutual charge fluctuations and mutual information have the same scaling laws. An improvement on the latter formula in this context would be interesting, as an experimental signature of the long range entanglement in the critical phases. From a numerical point of view, it will also be interesting to measure $\mathcal{I}(\mathcal{A},\overline{\mathcal{A}})$, as it will be dominated by the logarithmic terms we are interested in.

3.1.2 Bipartite fluctuations in arbitrary non-interacting systems

In this section, we introduce the general formalism for computing the bipartite fluctuations in non-interacting systems. We propose the generic derivation first for the fluctuations in typical insulating systems, then for superconductors, and we limit ourselves here to two-band models. The bipartite fluctuations are computed directly in the bulk: the goal is to probe the bulk properties and in particular at phase transitions. Analysis of the results in different seminal models will follow in the next part. The reader not interested in the technical discussions can directly refer to Table 3.2 and Eq. 3.17 for the general expressions of the bipartite fluctuations.

BF in insulators

Let us start with an insulating model with two fermions by unit-cell, noted A and B. We assume a form of translation symmetry such that the bulk Hamiltonian can be rewritten as:

$$H = \frac{1}{2}\sum_{k\in\mathcal{BZ}} \Psi_k^\dagger \vec{n}.\vec{\sigma}\Psi_k, \text{ with } \vec{n} = (n_x(k), n_y(k), n_z(k)) \text{ and } \Psi_k^\dagger = \begin{pmatrix} c_{k,A}^\dagger, & c_{k,B}^\dagger \end{pmatrix}. \quad (3.12)$$

The total charge $n_{j,A} + n_{j,B}$ is locally conserved, and the ground state is always in the sector $n_{j,A} + n_{j,B} = 1$. Fluctuations of the total charge are consequently always zero. Perturbations that lift this symmetry break the PHS.

Instead, it is more interesting to look at the pseudo-spin polarization operators. Excluding the total charge, a complete basis for these terms is given by:

$$\frac{q_e}{2}\Psi_j^\dagger \vec{\sigma}\Psi_j = (c_{j,A}^\dagger c_{j,b} + h.c., ic_{j,B}^\dagger c_{j,A} + h.c., n_{j,A} - n_{j,B}), \quad (3.13)$$

where q_e is the charge per unit cell ($q_e = 2$). The interest of this notation will be apparent when comparing superconductors and insulators.

Computing the fluctuations is straightforward, thanks to Wick's theorem and charge conservation. Let $\hat{O}_{j,\alpha,\beta} = c_{j,\alpha}^\dagger c_{j,\beta}$, with α and β indexing a sub-lattice. To compute the general bipartite fluctuations, we need to compute:

$$\begin{aligned}
\sum_{m,n=1}^{l_\mathcal{A}} \langle \hat{O}_{m,\alpha,\beta}\hat{O}_{n,\alpha',\beta'}\rangle_c &= \sum_{m,n=1}^{l_\mathcal{A}} \langle c_{m,\alpha}^\dagger c_{m,\beta} c_{n,\alpha'}^\dagger c_{n,\beta'}\rangle_c \\
&= \sum_{m,n=1}^{l_\mathcal{A}} \frac{1}{L^2}\sum_{k,k',q,q'} e^{i(k'-k)m} e^{i(q'-q)n} \langle c_{k,\alpha}^\dagger c_{k',\beta} c_{q,\alpha'}^\dagger c_{q',\beta'}\rangle_c \\
&= \frac{1}{L^2}\sum_{k,k',q,q'} \frac{1-e^{i(k'-k)l_\mathcal{A}}}{1-e^{i(k'-k)}} \frac{1-e^{i(q'-q)l_\mathcal{A}}}{1-e^{i(q'-q)}} \delta_{k,q'}\delta_{k',q} \langle c_{k,\alpha}^\dagger c_{k,\beta'}\rangle\langle c_{q,\beta} c_{q,\alpha'}^\dagger\rangle \\
&= \frac{1}{L^2}\sum_{k,q} \frac{\sin^2\frac{k-q}{2}l_\mathcal{A}}{\sin^2\frac{k-q}{2}} \langle c_{k,\alpha}^\dagger c_{k,\beta'}\rangle\langle c_{q,\beta} c_{q,\alpha'}^\dagger\rangle
\end{aligned}$$

$\mathcal{G}_{A,A}(k)$	$\cos^2(\frac{\theta_k}{2})$	$\mathcal{G}_{B,B}(k)$	$\sin^2(\frac{\theta_k}{2})$
$\mathcal{G}_{A,B}(k)$	$\frac{1}{2}\sin(\theta_k)e^{-i\phi_k}$	$\mathcal{G}_{B,A}(k)$	$\frac{1}{2}\sin(\theta_k)e^{i\phi_k}$

Table 3.1: Green functions for an arbitrary non-interacting two-band insulator at half-filling.

$$\sum_{m,n=1}^{l_{\mathcal{A}}} \langle \hat{O}_{m,\alpha,\beta}\hat{O}_{n,\alpha',\beta'}\rangle_c = \frac{l_{\mathcal{A}}}{L^2}\sum_{k,q\in\mathcal{BZ}} f_F(k-q,l_{\mathcal{A}})\mathcal{G}_{\beta,\alpha'}(k)(\delta_{\alpha,\beta'}-\mathcal{G}_{\beta',\alpha}(q)) \tag{3.14}$$

$$= l_{\mathcal{A}}\iint_{k,q\in\mathcal{BZ}} \frac{dkdq}{4\pi^2} f_F(k-q,l_{\mathcal{A}})\mathcal{G}_{\beta,\alpha'}(k)(\delta_{\alpha,\beta'}-\mathcal{G}_{\beta',\alpha}(q)), \tag{3.15}$$

where f_F is the Fejér Kernel, and $\mathcal{G}_{\alpha,\beta}(k) = \langle c_{k,\alpha}c^\dagger_{k,\beta}\rangle$ is the fermionic Green functions. An overview of the properties of the Fejér Kernel is given in the following Section. No other contributions appear due to the total charge conservation (anomalous Green functions vanish) and the cancellation of the connected contributions. Eq. 3.14 and 3.15 are the basic blocks upon which we will build the fluctuations. The continuous version is valid in the thermodynamic limit, and except when we will consider the finite-size effects, it is the most convenient.

Taking our usual conventions to compute the Green functions

$$\phi_k = \mathrm{Arg}(n_x + in_y) \text{ and } \theta_k = \mathrm{Arg}(n_z + i\sqrt{n_x^2+n_y^2}), \tag{3.16}$$

we obtain an integral form for arbitrary bipartite fluctuations. The Green functions are listed in Table 3.1 and the integral forms are given in Table 3.2. As a general rule, these integrals are elliptic and not analytically computable. Depending on what is the most convenient and explicit, we will indifferently use the notations $\mathcal{F}_{\hat{O}}$ for the bipartite fluctuations of the operator $\hat{O}$ or $\mathcal{F}_{\alpha\beta}$, $\alpha,\beta = X/Y/Z$ for

$$\langle \hat{O}^\alpha_{\mathcal{A}}\hat{O}^\beta_{\mathcal{A}}\rangle_c, \text{ with } \hat{O}^\alpha_j = \frac{q_e}{2}\Psi^\dagger_j\sigma^\alpha\Psi_j$$

As an example, the bipartite fluctuations of the pseudo-spin density $n_{j,A} - n_{j,B}$ are:

$$\mathcal{F}_{ZZ}(\mathcal{A}) = \frac{l_{\mathcal{A}}q_e}{4}\iint_{k,q\in\mathcal{BZ}} \frac{dkdq}{4\pi^2} f_F(k-q,l_{\mathcal{A}})\left(1-\cos\theta_k\cos\theta_q+\cos(\phi_k-\phi_q)\sin\theta_k\sin\theta_q\right). \tag{3.17}$$

BF in superconductors

For superconductors, the derivations are essentially similar. We consider an Hamiltonian of the form:

$$H = \frac{1}{2}\sum_{k\in\mathcal{BZ}} \Psi^\dagger_k\vec{n}.\vec{\sigma}\Psi_k, \text{ with } \vec{n} = (n_x(k),n_y(k),n_z(k)) \text{ and } \Psi^\dagger_k = \begin{pmatrix} c^\dagger_k, & c_{-k}\end{pmatrix}. \tag{3.18}$$

Term $\alpha\beta$	Integral form $g_{\alpha\beta}$
ZZ	$1-\cos\theta_k\cos\theta_q+\cos(\phi_k-\phi_q)\sin\theta_k\sin\theta_q$
XX	$1+\cos\theta_k\cos\theta_q-\cos(\phi_k+\phi_q)\sin\theta_k\sin\theta_q$
YY	$1+\cos\theta_k\cos\theta_q+\cos(\phi_k+\phi_q)\sin\theta_k\sin\theta_q$
XZ	$-4\cos\phi_q\sin\theta_q\cos\theta_k$
YZ	$-4\sin\phi_q\sin\theta_q\cos\theta_k$
XY	$-2\sin(\phi_k+\phi_q)\sin\theta_k\sin\theta_q$

Table 3.2: Expressions for the bipartite fluctuations for an arbitrary polarization for the topological insulators. We take the following convention: if $\hat{O}_{\vec{m}} = \frac{q_e}{2}\Psi_j^\dagger \vec{m}.\vec{\sigma}\Psi_j$, avec $\vec{m} = (m_x, m_y, m_z) \in \mathbb{R}^3$, then the associated fluctuations are given by: $\mathcal{F}_{\hat{O}_{\vec{m}}}(\mathcal{A}) = \frac{q_e l_{\mathcal{A}}}{4} \sum_{\alpha\leq\beta=x,y,z} m_\alpha m_\beta \iint_{k,q\in\mathcal{BZ}} \frac{dkdq}{4\pi^2} f_F(k-q, l_{\mathcal{A}}) g_{\alpha\beta}(k,q)$.

$\Psi_j^\dagger \sigma^{x/y}\Psi_j$ now vanishes for all sites j, so we only consider the charge fluctuations. The charge operator is $\hat{Q}_j = n_j - \frac{1}{2} = \frac{q_e}{2}\Psi_j^\dagger\sigma^z\Psi_j$, with q_e the charge by unit cell ($q_e = 1$). The additional constant gives no contribution to the fluctuations. Wick's theorem now leads to:

$$\mathcal{F}_{\hat{Q}}(\mathcal{A}) = \frac{l_{\mathcal{A}}}{L^2} \sum_{k,q\in\mathcal{BZ}} f_F(k-q, l_{\mathcal{A}}) \left(\mathcal{G}(k)(1-\mathcal{G}(q)) - \mathcal{D}(k)\mathcal{D}^*(-q)\right) \tag{3.19}$$

where $\mathcal{G}(k) = \langle c_k c_k^\dagger\rangle$ is the normal Green function and $\mathcal{D}(k) = \langle c_k^\dagger c_{-k}^\dagger\rangle$ the anomalous one. Using the standard conventions, the final expression for the charge fluctuations exactly matches Eq. 3.17.

3.1.3 The Fejér Kernel: properties and consequences

This section is dedicated to the Fejér Kernel as its appearance is fundamental to the analytical solvability of the BF in non-interacting models.

Main properties of the Fejér Kernel

It is a recurring function in interference problems that has a few very convenient and powerful properties. As a remarkable example, it appeared in Ref. [78] in the computation of bounds for the vNEE, that were used to check the violation of the area law for two-dimensional free fermions with a one-dimensional Fermi surface. We give in this section the main properties of the Kernel, with a focus on what makes it computable and remarkable. First, it has a fairly simple expression in terms of Fourier coefficients:

$$f_F(k,l) = \frac{\sin^2(\frac{kl}{2})}{l\sin^2(\frac{k}{2})} = \sum_{j=-l}^{l}(1-\frac{|j|}{l})e^{i(jk)}. \tag{3.20}$$

Secondly, it is a uniform approximation of the Dirac delta for convolutions such that

$$f_F(k,l) \to 2\pi\delta(k) \text{ when } l \to +\infty. \tag{3.21}$$

$$\int_{-\pi}^{\pi} \frac{dk}{2\pi} f_F(k-q,l)g(k) \to g(q) \text{ when } l \to +\infty \text{ and } g \text{ continuous in } q. \tag{3.22}$$

Scaling laws

Let us explore the consequences of these properties for the forms we have derived. All bipartite fluctuations can be expressed as a sum of terms of the form

$$\frac{l_{\mathcal{A}} q_e}{4} \iint_{k,q\in BZ} \frac{dkdq}{4\pi^2} f_F(k-q,l_{\mathcal{A}})f(k)g(q), \tag{3.23}$$

that we note $\langle\langle f,g\rangle\rangle$. We limit ourselves to f and g continuous by part (which will be verified in the considered systems). When $l_{\mathcal{A}}$ is much larger than 1, Eq. 3.21 translates into:

$$\langle\langle f,g\rangle\rangle = \frac{l_{\mathcal{A}} q_e}{4} \int_{k\in\mathcal{BZ}} \frac{dk}{2\pi} f(k)g(k) + o(l_{\mathcal{A}}). \tag{3.24}$$

For all the considered non-interacting systems, the fluctuations consequently cannot scale faster than linearly, even though they are initially a quadratic object. Intuitively, each pair of sites in momentum space contributes independently. The linear coefficient has a simple analytical form and will be analyzed in various models, close to the phase transitions. It necessarily vanishes when charge conservation is recovered.

By analogy with the LLs and the vNEE, we are interested in logarithmic contributions that may appear. These contributions may now be sub-leading, but fortunately, Eq. 3.20 allows us to avoid any perturbative computations.

$$\langle\langle f,g\rangle\rangle = \frac{q_e}{4} \sum_{j=-l_{\mathcal{A}}}^{l_{\mathcal{A}}} (l_{\mathcal{A}} - |j|)\mathcal{FT}\{f\}(j)\mathcal{FT}\{g\}(-j) \tag{3.25}$$

$$= \frac{q_e l_{\mathcal{A}}}{4} \sum_{j=-l_{\mathcal{A}}}^{l_{\mathcal{A}}} \mathcal{FT}\{f\}(j)\mathcal{FT}\{g\}(-j) - \frac{q_e}{4} \sum_{j=-l_{\mathcal{A}}}^{l_{\mathcal{A}}} |j|\mathcal{FT}\{f\}(j)\mathcal{FT}\{g\}(-j) \tag{3.26}$$

where $\mathcal{FT}\{f\}$ (resp. $\mathcal{FT}\{g\}$) is the Fourier transform of f (resp. g).

From there, basic Fourier and series analysis prove to be especially useful. A function f that is periodic and continuous by part (here we take that it can be discontinuous only at a finite number of points) verifies:

$$\mathcal{FT}\{f\}(j) = \mathcal{O}(\frac{1}{j}), \tag{3.27}$$

while a function that is continuous and of derivative continuous by part verifies

$$\mathcal{FT}\{f\}(j) = \mathcal{O}(\frac{1}{j^2}). \tag{3.28}$$

This well-known property can be of course extended to any order. Using these bounds on the convergence of the Fourier transform, it is possible to determine when a sub-leading logarithmic term can arise. Analysis of the second term is straightforward: a logarithmic term may appear only if $\mathcal{FT}\{f\}(j)\mathcal{FT}\{g\}(-j) = \mathcal{O}(j^{-2})$, that is to say if both are only continuous by part. Analysis of the first term is slightly more complex: a logarithmic contribution appears only if a scaling term $\ln l_{\mathcal{A}}/l_{\mathcal{A}}$ appears. As f and g are at least continuous by part, we only need to evaluate the convergence speed of $\sum_j \frac{1}{j^2}$. Given that:

$$\sum_{j>l} \frac{1}{j^2} < \int_l^{+\infty} \frac{dx}{x^2} = \frac{1}{l}, \tag{3.29}$$

no logarithmic term can appear from the first summation. To summarize, we have proven that logarithmic contributions to the bipartite fluctuations can only appear only when f and g are both discontinuous. When considering the previously obtained expressions for the BF, it means that **a logarithmic term can only appear at a gapless point**, even though linear contributions appear both for gapped and gapless phases. Sub-leading logarithmic terms will consequently be fundamental to characterize the phase transitions. Additionally, we have proven that the fluctuations in non-interacting one-dimensional systems are always of the form:

$$\mathcal{F}_{\hat{O}}(\mathcal{A}) = i_{\hat{O}} l_{\mathcal{A}} + \mathbf{b}_{\hat{O}} \ln l_{\mathcal{A}} + \mathcal{O}(1) \tag{3.30}$$

This result can be reinterpreted in terms of correlation functions:

$$\langle \hat{O}_j \hat{O}_{j'} \rangle_c = -\frac{\mathbf{b}_{\hat{O}}}{2|j-j'|^2} + o(\frac{1}{|j-j'|^2}) \tag{3.31}$$

but also for the global mutual fluctuations:

$$\mathcal{I}(\mathcal{A},\mathcal{B}) = \mathbf{b}_{\hat{O}} \ln \frac{l_{\mathcal{A}} + l_{\mathcal{B}}}{l_{\mathcal{A}} l_{\mathcal{B}}} \text{ for } \mathcal{A} \text{ and } \mathcal{B} \text{ connected.} \tag{3.32}$$

Interpretation of the linear coefficient

Given the previously obtained scaling laws, we can present a systematic physical interpretation of the coefficient of the linear term. Indeed, for any observable $\hat{O}$ whose fluctuations take the form of Eq. 3.23, we have obtained:

$$\lim_{l_{\mathcal{A}} \to +\infty} \frac{F_{\hat{O}}(\mathcal{A})}{l_{\mathcal{A}}} = i_{\hat{O}}. \tag{3.33}$$

This, combined with the integral form for $i_{\hat{O}}$, implies that

$$i_{\hat{O}} = \lim_{L \to +\infty} \frac{1}{L} \sum_{m,n \in \mathcal{S}} \langle \hat{O}_m \hat{O}_n \rangle - \langle \hat{O}_m \rangle \langle \hat{O}_n \rangle, \tag{3.34}$$

that is to say that the linear coefficient coincides with the density of fluctuations in the total system in the thermodynamic limit. Measurement of the bipartite fluctuations consequently allows us to measure a global property with a good precision (outside gapless points, the convergence is fast in $\frac{1}{l_{\mathcal{A}}}$).

Remarkably, $i_{\hat{O}}$ coincides at $T = 0$ and for pure states with the Quantum Fisher Information density[144] (QFID) associated to $\hat{O}$. The Quantum Fisher Information has been used to characterize several transitions[127, 146–149] or study quenches in the quantum Ising model[150]. We invite the reader to read Refs. [151, 152] for a complete review on the Quantum Fisher Information, and its relation with entanglement. Note that, for the convention used in this review, the QFID corresponds to $4i_{\hat{O}}$ for Ref. [152]. The QFID gives a bound, from Cramér-Rao identity, on the precision of measurements. If one performs a small rotation of amplitude θ such that $|\Psi\rangle \to e^{-i\theta\hat{O}}|\Psi\rangle$, then the precision with which one can identify θ is given by:

$$(\Delta\theta)^2 \geq \frac{1}{4Li_{\hat{O}}}, \tag{3.35}$$

and for any operator $\hat{M}$,

$$\frac{i_{\hat{M}}}{|\partial_\theta\langle\hat{M}\rangle|^2} \geq \frac{1}{4Li_{\hat{O}}}. \tag{3.36}$$

Finally, the Quantum Fisher Information also gives information on the entanglement of the system, and more precisely a bound on the producibility of the ground state in real or momentum space[153, 154]. We define a state $|\Psi\rangle$ to be r-producible in momentum space if:

$$|\Psi\rangle = \bigotimes_{m=1}^{N/r} |\psi_m\rangle\,, \text{ with } |\psi_m\rangle = f(c^\dagger_{k_{m,1}}, ..., c^\dagger_{k_{m,r}})\,|0\rangle\,, \tag{3.37}$$

or in other words, if $|\Psi\rangle$ is the tensor product of states involving r fermions. Note that here N is the total number of fermionic operator (and not sites). Then, for any observable that can be written $\hat{O} = \sum_{k\in\mathcal{BZ}} \hat{O}_k$, one has the bound:

$$\langle\hat{O}^2\rangle_c = \sum_{m=1}^{N/r}\langle(\sum_{j=1}^{r}\hat{O}_{k_{m_j}})^2\rangle \leq \frac{L}{r}\times\frac{r^2}{4}(O_{\max}-O_{\min})^2, \tag{3.38}$$

where $O_{\max/\min}$ is the largest/smallest eigenvalue of $\hat{O}_k$. The definition in real space is identical up to the basis change. One can apply this bound for our superconductors and insulators. We limit ourselves to charge and pseudo-spin density fluctuations, but the bounds will be valid for any polarization. For superconductors, N is the actual number of sites L, while $\hat{O} = \hat{Q} = \sum_k c^\dagger_k c_k$ such that $O_{\max} - O_{\min} = 1$, leading to:

$$i_{\hat{Q}} \leq \frac{r}{4}. \tag{3.39}$$

For insulators, we need to slightly adapt our conventions to take into account the two fermions by unit-cell properly, and obtain the bound

$$i_{\hat{O}} \leq \frac{r}{2}. \tag{3.40}$$

The two-band non-interacting systems such as the ones studied in this Chapter are always 2-producible, which lead to the universal bound

$$i_{\hat{O}} \leq \frac{q_e}{2}. \tag{3.41}$$

Additionally, if $i_{\hat{O}} > \frac{q_e}{4}$, the linear term proves that the ground state is not 1-producible in real or momentum space, that is to say a simple tensor product of one-fermion wave functions.

Determination of logarithmic coefficients

Knowing that the logarithmic sub-leading term appears only for discontinuous functions f and g, we can systematically determine the coefficients of the logarithmic contributions.

First, let us assume that f (resp. g) is discontinuous only at the point $k = k_f$ (resp. k_g). We note δf (resp. δg) the amplitude of the discontinuity. We introduce the test function h defined by:

$$h(k) = \frac{k}{\pi} \text{ for } k \in]-\pi, \pi] \text{ and periodic.} \tag{3.42}$$

Its Fourier transform is straightforward to obtain: $\tilde{h}(j) = \delta_{j\neq 0}\frac{i(-1)^j}{\pi j}$. Then we can rewrite $f(k)$ as $f_c(k) + \frac{\delta f}{2}h(k - \pi - k_f)$, where f_c is a continuous function, and similarly for g. The logarithmic contribution can then only arise from:

$$-\frac{q_e}{4}\sum_{j=-l_{\mathcal{A}}}^{l_{\mathcal{A}}} |j| e^{-ij(k_f+\pi)}\tilde{h}(j)e^{ij(k_g+\pi)}\tilde{h}(-j) = -\frac{q_e \delta f \delta g}{8\pi^2}\sum_{j=1}^{l_{\mathcal{A}}}\frac{\cos((k_f - k_g)j)}{j} \tag{3.43}$$

Then, a logarithmic term appears only when $k_f = k_g$, and then its coefficient is given by:

$$\mathbf{b}_{fg} = -\frac{q_e \delta f \delta g}{8\pi^2} \tag{3.44}$$

It depends only in the amplitude of the discontinuities of the functions f and g, in a very simple way. This result allows us to compute the exact coefficient in any system without having to treat integrals. It can also be expanded to more complex situations. Assume now that f (resp. g) is discontinuous n_f (resp. n_g times) at the points $k_{f,j}$ (resp. $k_{g,j}$) with amplitude δf_j (resp. δg_j). A similar approach introducing n_f and n_g test functions leads to a logarithmic contribution of weight:

$$\mathbf{b}_{fg} = -\frac{q_e}{8\pi^2}\sum_{j=1}^{n_f}\sum_{j'=1}^{n_g}\delta f_j \delta g_{j'} \delta_{k_{f,j}=k_{g,j'}\ [2\pi]} \tag{3.45}$$

With these last two formula, we end this section on the kernel properties, and will now look at the physical consequences in different classes of problem.

3.2 One-dimensional BDI class

In this Section, we focus on the bipartite fluctuations in one-dimensional systems that belong to the BDI class. The PHS and TRS symmetries limit the possible behavior of the BF, and lead to a set of universal signatures of the phase transitions. After exposition of the properties for arbitrary Hamiltonians, we conclude with the examples of the (extended) Kitaev's chain and the SSH model. We also briefly treat the finite-temperature and finite-size limits, relevant for both experiments and numerical simulations.

3.2.1 BDI Hamiltonian and fluctuations

From Chapter I, we know that Hamiltonians in the BDI class can be expressed as:

$$H = \Psi_k^\dagger(0, \Delta_k, \varepsilon_k).\vec{\sigma}\Psi_k, \tag{3.46}$$

where Ψ_k is a fermionic spinor, ε_k an effective kinetic energy and Δ_k an effective pairing or cross-hopping term. ε_k is even in momentum space while Δ_k is odd. Before addressing the BF, we introduce an additional mathematical assumption on the functions ε_k and Δ_k. We assume that these functions can always be Taylor-Lagrange expanded at a non-zero order. It is not a strong assumption as in most cases, for translation-invariant systems, these functions are in fact analytical and $\mathcal{C}^\infty$. In turn, it means that dispersion relations for Δ_k and ε_k are always of the form $(k - k_0)^n$, with $n \in \mathbb{N}$, and cannot be, for example, $|k - k_0|$. All models previously introduced verify these assumptions.

Following the conventions of Section 3.1.2 (even for superconductors), we define

$$\phi_k = \frac{\pi}{2}\text{sign}(\Delta_k) \text{ and } \theta_k = \text{Arg}(\varepsilon_k + i|\Delta_k|)$$

ϕ_k is also odd while θ_k is even. Though ϕ_k is always discontinuous with this definition, a logarithmic contribution only appears at the phase transition. The discontinuity is regularized by $\sin(\theta_k)$ in all other cases. The linear terms can be obtained for all polarizations:

$$i_{ZZ} = \frac{q_e}{2} \int\limits_{k\in\mathcal{BZ}} \frac{dk}{2\pi} \sin^2\theta_k \tag{3.47}$$

$$i_{XX} = \frac{q_e}{2} \tag{3.48}$$

$$i_{YY} = \frac{q_e}{2} \int\limits_{k\in\mathcal{BZ}} \frac{dk}{2\pi} \cos^2\theta_k \tag{3.49}$$

$$i_{XY} = i_{XZ} = i_{YZ} = 0 \tag{3.50}$$

We find that the bounds derived in Eq.3.41 are indeed verified for all models. Only i_{ZZ} can be measured in superconductors. i_{XX} also shows that the ground state cannot be a pure local product state, as it is expected. Though the coefficients depend on the angle θ_k, there is no direct dependency on the winding number or any simple link with the topological properties of the ground state. A good way to realize this fact is to consider the following test functions:

$$\theta_k^n = nk \text{ for } n \in \mathbb{N}^* \text{ and } \theta_k^0 = \frac{\pi}{4},$$

which all verify $\int\limits_{k\in\mathcal{BZ}} \frac{dk}{2\pi}\sin^2\theta_k^n = \frac{1}{2}$.

By analogy with the vNEE, we are therefore interested in computing the BF at, or close to, a phase transition.

3.2.2 Discontinuity of the derivative of the linear term

In this section, we focus on the linear coefficient. For now, assume that the gap closes only at one momentum k_0. We can then show that a cusp will appear in both i_{ZZ} and i_{XX}. This cusp is an extremely visible marker of the phase transition. Let us give a proof of this result.

The PHS enforces either $k_0 = 0$ or $k_0 = \pi$. Moreover, ε_k must be even and Δ_k odd at these two points. Close to k_0, except for very specific models or at special multicritical points, $\varepsilon_k \approx \frac{1}{m_\varepsilon}(k-k_0)^2$, while $\Delta_k^0 \approx v_\Delta(k-k_0)$, with m_ε and v_Δ non-zero. Slightly away from the transition, Δ_k must still vanish due to parity. The only way to gap the system through an arbitrarily small continuous deformation is therefore to introduce a small effective chemical potential $\delta\mu$ such that $\varepsilon_k \approx \delta\mu + v_e(k-k_0)^2$.[1] Finally, to describe different topological phases, we require that $\delta\mu$ is positive in one of the two phases but negative in the other[2]. It ensures that the winding number, defined in Section 1.4.2 is different on each side of the QPT. Indeed, as the gap closes only at k_0, the small perturbation does not affect the number of times where θ_k cancels, except in the vicinity of k_0. On the other hand, $\theta_{k_0}(\delta\mu = 0^+) = 0$ while $\theta_{k_0}(\delta\mu = 0^-) = \pi$. The discrete formulation of the winding number given in Eq. 1.63 allows us to conclude.

Let us prove the result for i_{ZZ}. The rest will directly follow from $i_{XX} = \frac{q_e}{2} - i_{ZZ}$. We define $DI(x) = \partial_{\delta\mu} i_{ZZ}|_{\delta\mu=x}$. We compute the difference between the derivative on two sides of the transition. Let $x > 0$ and $\Delta DI(x) = \frac{1}{q_e}(DI(x) - DI(-x))$. Let us define $\delta\varepsilon_k = \varepsilon_k - x$, and x is sufficiently small such that $\delta\varepsilon_k$ only vanishes at k_0.

$$\begin{aligned}\Delta DI(x) &= \int\limits_{\mathcal{BZ}} \frac{dk}{2\pi}\Delta_k^2\left(\frac{x+\delta\varepsilon_k}{((x+\delta\varepsilon_k)^2+\Delta_k^2)^2} - \frac{-x+\delta\varepsilon_k}{((-x+\delta\varepsilon_k)^2+\Delta_k^2)^2}\right)\\ &= x\int\limits_{\mathcal{BZ}} (R_k(x)+A_k(x))\frac{dk}{2\pi},\end{aligned} \tag{3.51}$$

where

$$\begin{aligned}R_k(x) &= -4\frac{\delta\varepsilon_k^2\Delta_k^2((-x+\delta\varepsilon_k)^2+(x+\delta\varepsilon_k)^2+2\Delta_k^2)}{((-x+\delta\varepsilon_k)^2+\Delta_k^2)^2((x+\delta\varepsilon_k)^2+\Delta_k^2)^2}\\ A_k(x) &= \Delta_k^2\left(\frac{1}{((x+\delta\varepsilon_k)^2+\Delta_k^2)^2} + \frac{1}{((-x+\delta\varepsilon_k)^2+\Delta_k^2)^2}\right)\end{aligned}$$

$R_k(x)$ is regular in k_0 when $x = 0$ ($\lim\limits_{k\to k_0}|R_k(0)| < \infty$) and consequently $|\int\limits_{\mathcal{BZ}} \frac{dk}{2\pi}R_k(x)| < \infty$ when $x \to 0$. Conversely, $A_k(k_0) \approx \frac{2}{v_\Delta^2(k-k_0)^2}$ when $(k-k_0)^2 \ll 1$. One can then show

[1] For completeness, the "velocities" v_e and v_Δ may also slightly vary near the phase transition. As it does not affect the result of our computation, we drop the dependency.

[2] If $\delta\mu$ has the same sign in both phases, as long as $\partial_{\delta\mu} i_{ZZ}$ is not zero when $\delta\mu \neq 0$, there is evidently a cusp when crossing the "phase transition".

that $\int_{\mathcal{BZ}} \frac{dk}{2\pi} A_k(x)$ diverges as $\frac{1}{2|v_\Delta|x}$ and then:

$$\lim_{x\to 0} \Delta DI(x) = \lim_{x\to 0} x \int_{\mathcal{BZ}} \frac{dk}{2\pi} A_k(x) = \frac{1}{2|v_\Delta|} \tag{3.52}$$

The derivative is indeed discontinuous at a phase transition where the winding number of θ_k changes.

Another relevant case is $\varepsilon_k \propto (k-k_0)^2$ and $\Delta_k \propto (k-k_0)^3$. In this case, the cusp vanishes (in practice, the second derivative is logarithmically divergent). It is nonetheless a special case that usually corresponds to tricritical points.

More complex phase transitions with the gap closing at several momenta can also occur. When the transition is driven by an effective chemical potential, the previous computation stands, with (quasi-)independent contributions of each gap-closing momenta. For middle of band transitions where both ε_k and Δ_k are linear at the gap closing momentum k_F, ($\varepsilon_k \approx v_\varepsilon(k-k_F)$, $\Delta_k \approx v_\Delta(k-k_F)$, the contribution to the discontinuity arising from k_F is:

$$\lim_{x\to 0} \Delta DI(x) = \frac{|v_\Delta|(v_\Delta^2 - v_\varepsilon^2)}{2(v_\Delta^2 + v_\varepsilon^2)^2} \tag{3.53}$$

Another form of transition is possible, corresponding to the normal line in Kitaev's model. Δ_k vanishes at the phase transition, while the kinetic energy goes to zero at two momenta $\pm k_F$[3]. This time, v_Δ play the role of the small varying parameter. We take $DI(x) = \partial_{v_\Delta} i_{ZZ}|_{v_\Delta = x}$ and follow the same procedure. ε_k is a priori linear close to $\pm k_F$: $\varepsilon_k = v_\varepsilon(k-k_F)$ for $k \approx k_F$ and $\varepsilon_k = -v_\varepsilon(k+k_F)$ for for $k \approx -k_F$, leading to:

$$\lim_{x\to 0^+} \Delta DI(x) = \frac{\partial_{v_\Delta}\Delta_{k_F}}{\Delta_{k_F}} \frac{|\Delta_{k_F}|}{|v_\varepsilon|} = \lim_{v_\Delta \to 0^+} \frac{|\Delta_{k_F}|}{v_\Delta |v_\varepsilon|} \tag{3.54}$$

3.2.3 Logarithmic contributions and generalized fluctuations

First, assume that the gap closes only at one momentum $k_0 = 0$ or $k_0 = \pi$, with a quadratic kinetic energy. Then, due to the parities of the functions θ_k and ϕ_k imposed by the symmetries of the BDI class, we straightforwardly obtain the logarithmic coefficients. For a linear Δ_k (and in fact as long as $\frac{\varepsilon_k}{\Delta_k} \to 0$ when $k \to k_0$),

$$\mathbf{b}_{ZZ} = -\frac{q_e}{2\pi^2}, \quad \mathbf{b}_{XX} = -\frac{q_e}{2\pi^2}, \quad \mathbf{b}_{YY} = \frac{q_e}{2\pi^2}, \tag{3.55}$$

$$\mathbf{b}_{XY} = \mathbf{b}_{XZ} = \mathbf{b}_{YZ} = 0, \tag{3.56}$$

where $\mathbf{b}_{\alpha\beta}$ is the logarithmic coefficient (following conventions of Section 3.1.2).

The logarithmic contributions take the value

$$\mathbf{b}_{ZZ} = \frac{q_e}{2\pi^2}, \quad \mathbf{b}_{XX} = -\frac{q_e}{2\pi^2}, \quad \mathbf{b}_{YY} = -\frac{q_e}{2\pi^2}, \quad \mathbf{b}_{XY} = \mathbf{b}_{XZ} = \mathbf{b}_{YZ} = 0. \tag{3.57}$$

[3]We take $0 < k_F < \pi$ as we are not interested in the special tri-critical points in general. In Kitaev's model, they correspond to a fully empty or occupied wire.

when Δ_k cancels faster than ε_k. It corresponds generally to tri-critical/special points, as Δ_k needs to be at least cubic. For a normal model of free fermions with one fermion per unit cell, and a gap closing at two different momenta $\pm k_F$, following the convention for superconductors, the logarithmic coefficients are:

$$\mathbf{b}_{ZZ} = \frac{1}{\pi^2}, \quad \mathbf{b}_{XX} = -\frac{1}{\pi^2}, \quad \mathbf{b}_{YY} = -\frac{1}{\pi^2}, \quad \mathbf{b}_{XY} = \mathbf{b}_{XZ} = \mathbf{b}_{YZ} = 0, \tag{3.58}$$

which corresponds to the coefficients obtained for a non-interacting Luttinger Liquid in Eq. 2.63. Note that these coefficients are universal: they do not depend on any microscopic details of our theory.

There are consequently two signs of the exotic nature of the critical points: the fact that $|\mathbf{b}_{ZZ}|$ is twice as small as in Luttinger Liquids for superconductors, and its change of sign.
This factor of two is also seen in the central charge: for superconductors, the critical model has central charge $\frac{1}{2}$ and corresponds to a free Majorana field (or equivalently the critical Ising model), instead of 1 for free normal fermions. The reduction in the number of degrees of freedom therefore also manifests in the charge fluctuations at the phase transition. To obtain such an amplitude in an interacting Luttinger Liquid would require a LL parameter $K = \frac{1}{2}$ and therefore strong interactions. Note that we recover (in absolute value) that for the charge fluctuations:

$$\frac{\mathcal{S}_E}{|\mathbf{b}_{\hat{Q}}|} = \frac{\pi^2}{3} + o(1) \tag{3.59}$$

The extension of the formula of Ref.[133] is consequently valid for the vNEE of these critical models (and also for the Renyi entropies).

For insulators, we find the same amplitude for the logarithmic coefficient as in LLs. This was to be expected, the central charge at the QPTs in such models is also $c = 1$.
On the other hand, for both superconductors and insulators we find the negative sign. One can show that it is impossible to for charge fluctuations of a Luttinger Liquid to give rise to such a negative logairhtmic coefficient[155]. In fact, this stays true if considering an arbitrary number of LLs: one cannot explain such a term as the superposition of any number of bosonic densities[4]. The complete demonstration, quite long and technical, is in Appendix E.2. For the topological superconductors, one can also recover the exact value of the logarithmic term directly from CFT arguments[155]. The demonstration is in Section 3.2.4.

When the gap closes at several momenta, universality is initially lost. Let us focus on the BCF i_{ZZ}. Assume that the gap closes at n momenta noted $(k_j)_{1\leq j\leq n}$. The parity constraints on θ_k and ϕ_k only limit the values of the functions at 0 or π. Following 3.45,

[4] As we will see in Chapter 3, it is nonetheless possible to build an equivalent LL, at least for a topological insulator or two superconductors, though the chosen basis and the equivalent charge are quite different. Eq. 3.55 tells us that we should try to use the Y polarization as our LL charge.

the general coefficient of logarithmic contributions is given by:

$$\mathbf{b}_{ZZ} = q_e \sum_{j=1}^{n} \frac{(\cos\theta_{k_j^+} - \cos\theta_{k_j^-})^2 - (\sin\phi_{k_j^+}\sin\theta_{k_j^+} - \sin\phi_{k_j^-}\sin\theta_{k_j^-})^2}{8\pi^2} \tag{3.60}$$

Its absolute value is bounded by $\frac{q_e n}{2\pi^2}$, as expected, but there are no additional constraints. Identifying the critical model simply by looking at this coefficient is not possible. It is interesting to note that both our previous topological example and normal free fermions saturate the inequality. To recover universality, we introduce the structure factor of the BF in Section 3.2.5.

3.2.4 Conformal origin of the logarithm

We show that one can obtain this logarithmic term directly from the underlying conformal field theory. We give here the main arguments, and details on the computation are kept in Appendix F.1. To get the proper value for an observable, one also needs to take into account the way the model maps onto the low-energy Hamiltonian. To do so, we consider a Kitaev wire and place ourselves at $t = \Delta$ for simplicity.
The continuous version of the Hamiltonian can be written as:

$$H_K = \int dx \frac{iv}{2} \left(\gamma_L \partial_x \gamma_L - \gamma_R \partial_x \gamma_R\right) - im\gamma_L\gamma_R, \tag{3.61}$$

where $\gamma_{L/R}$ are Majorana fields, $v = 2ta$ the velocity of the Majorana fields and $m = a(\mu + 2t)$ a mass term. a is the lattice spacing. At $m = 0$ (the critical point), one can identify the Hamiltonian with the conformal action, and $\gamma_{L/R}$ corresponds to the holomorphic and anti-holomorphic components of the fields.
Then, we can rewrite the density operator as:

$$\rho(x) = i\gamma_L(x)\gamma_R(x), \tag{3.62}$$

such that the fluctuations are given by:

$$F_A(l) = -\iint_{[0,l]^2} dxdy \langle \gamma_L(x)\gamma_R(x)\gamma_L(y)\gamma_R(y)\rangle_c \tag{3.63}$$

Using the Operator Product Expansion (OPE)[81, 130] for the Majorana field directly yields the result:

$$\begin{aligned} F_A(l) &= \iint_{[0,l]^2} dxdy \frac{1}{4\pi^2}\frac{1}{|x-y|^2} \\ &\approx -\frac{1}{2\pi^2\varepsilon^2}\log l + \alpha l + \beta. \end{aligned} \tag{3.64}$$

α and β are a priori non-universal constants that arise from the integration, and are linked to the cut-off of our theory. We recover the minus sign and the value of the coefficient we predicted in microscopic computations. A comparison with the CFT computations for the bosonic field is made in Appendix F.2.

3.2.5 Structure factor of the BCF

Universality can be restored by looking at a generalization of the fluctuations: their structure factor (SF). The SF is defined for a one-dimensional lattice model by:

$$\mathcal{SF}_{\hat{O}}(\mathcal{A},\psi) = \langle|\sum_{j\in\mathcal{A}} e^{i\psi j}\hat{O}_j|^2\rangle - |\langle\sum_{j\in\mathcal{A}} e^{i\psi j}\hat{O}_j\rangle|^2 = \langle|\mathcal{FT}_{\mathcal{A}}\{\hat{O}\}(\psi)|^2\rangle - |\langle\mathcal{FT}_{\mathcal{A}}\{\hat{O}\}(\psi)\rangle|^2, \tag{3.65}$$

where $\mathcal{FT}_{\mathcal{A}}\{\hat{O}\}$ is the Fourier transform of the charge in the region $\mathcal{A}$. The integral form for the BCF is:

$$\mathcal{SF}_{\hat{O}}(\mathcal{A},\psi) = \frac{l_{\mathcal{A}}q_e}{4}\iint \frac{dkdq}{4\pi^2} f_F(k-q-\psi, l_{\mathcal{A}})\,(1-\cos\theta_k\cos\theta_q + \cos(\phi_k-\phi_q)\sin\theta_k\sin\theta_q) \tag{3.66}$$

$$= \frac{l_{\mathcal{A}}q_e}{4}\iint \frac{dkdq}{4\pi^2} f_F(k-q, l_{\mathcal{A}})\,(1-\cos\theta_k\cos\theta_{q+\psi} + \cos(\phi_k-\phi_{q+\psi})\sin\theta_k\sin\theta_{q+\psi}) \tag{3.67}$$

It is identical to the expression of $\mathcal{F}_{\hat{O}}(\mathcal{A})$ up to the additional phase ψ in the Fejér Kernel, or equivalently a translation of ψ of one of the momenta k or q. The additional phase changes both the behaviour of the linear and the logarithmic term.

Let us first address the logarithmic coefficients. The shift induces oscillations in the Fourier transforms. For finite-size systems, they suppress the logarithmic terms as soon as ψ is of order $\frac{\pi}{L}$, and in the thermodynamic limit, the logarithmic contribution instantaneously vanishes. Indeed, following the notations of Section 3.1.3, the logarithmic contributions arise from:

$$-\frac{q_e}{4}\sum_{j=-l_{\mathcal{A}}}^{l_{\mathcal{A}}} |j| e^{-ij(\psi+k_f+\pi)}\tilde{h}(j)e^{ij(k_g+\pi)}\tilde{h}(-j) = -\frac{q_e\delta f\delta g}{8\pi^2}\sum_{j=1}^{l_{\mathcal{A}}}\frac{\cos((k_f-k_g+\psi)j)}{j}, \tag{3.68}$$

and hence the logarithmic contributions are given by:

$$q_e\sum_{j,j'=1}^{n}\frac{(\cos\theta_{k_j^+}-\cos\theta_{k_j^-})(\cos\theta_{k_{j'}^+}-\cos\theta_{k_{j'}^-})}{8\pi^2}\delta_{k_j-k_{j'}=\psi}$$
$$-\frac{(\sin\phi_{k_j^+}\sin\theta_{k_j^+}-\sin\phi_{k_j^-}\sin\theta_{k_j^-})(\sin\phi_{k_{j'}^+}\sin\theta_{k_{j'}^+}-\sin\phi_{k_{j'}^-}\sin\theta_{k_{j'}^-})}{8\pi^2}\delta_{k_j-k_{j'}=\psi} \tag{3.69}$$

Logarithmic terms may appear whenever ψ corresponds to the difference between two gap-closing momenta. In particular, given the symmetries of the BDI class, if the gap closes at $k_j \neq 0,\pi$, it also closes to $-k_j$. At $\psi = 2k_j$ (assuming no other combination $k_j - k_{j'}$ sums to ψ), a logarithmic term appears, of coefficient:

$$-\frac{q_e}{4\pi^2}\left(1-\cos(\theta_{k_j^+}-\mathrm{sign}(\Delta_{k_j^+}\Delta_{k_j^-})\theta_{k_j^-})\right) \tag{3.70}$$

	$\varepsilon_{k_j^+} = \varepsilon_{k_j^-}$		$\varepsilon_{k_j^+} = -\varepsilon_{k_j^-}$	
	$\Delta_{k_j^+} = \Delta_{k_j^-}$	$\Delta_{k_j^+} = -\Delta_{k_j^-}$	$\Delta_{k_j^+} = \Delta_{k_j^-}$	$\Delta_{k_j^+} = -\Delta_{k_j^-}$
$\psi = 0$	0	$-\frac{q_e}{2\pi^2}\sin^2\theta_{k_j^+}$	$\frac{q_e}{2\pi^2}\cos^2\theta_{k_j^+}$	$\frac{q_e}{2\pi^2}\cos 2\theta_{k_j^+}$
$\psi = 2k_j$	0	$-\frac{q_e}{2\pi^2}\sin^2\theta_{k_j^+}$	$-\frac{q_e}{2\pi^2}\cos^2\theta_{k_j^+}$	$-\frac{q_e}{2\pi^2}$

Table 3.3: Coefficients of the logarithmic contributions arising from the discontinuities at $\pm k_j$ in the structure factor $\mathcal{SF}_{\hat{Q}}(\mathcal{A}, \psi)$. The line $\psi = 0$ corresponds to the coefficient of the contribution k_j only, while $\psi = 2k_j$ takes into account the cross-terms arising from $\pm k_j$.

Assuming either a "bottom of band" transition such that ε_k is quadratic close to k_j while Δ_k is linear (or vice versa), or that both Δ_k and ε_k are linear at k_j as it is expected in the middle of a band, the expression simplifies into:

$$-\frac{q_e}{2\pi^2}, \tag{3.71}$$

and no longer depends on the microscopic parameters. Except at some fine-tuning points, these assumptions are generally verified at a topological QPT. Table 3.3 summarizes for reference all possible logarithmic contributions in the structure factor depending on the local parity of ε_k and Δ_k near k_j.

Let us briefly comment on its effect on the linear term. The expression of the coefficient is obviously affected by the presence of ψ, and is given for the BCF as an example:

$$i_{ZZ}(\psi) = \frac{q_e}{4}\int \frac{dk}{2\pi}\left(1 - \cos\theta_k \cos\theta_{k+\phi} + \cos(\phi_k - \phi_{k+\phi})\sin\theta_k \sin\theta_{k+\phi}\right) \tag{3.72}$$

As a general rule, $i_{\hat{O}}(\psi)$ is much more difficult to analytically compute (as it is an elliptical form). Discontinuities of $\partial_\psi i_{\hat{O}}(\psi)$ also occur at $\psi = k_j - k_{j'}$, and easily mark the points requiring more careful analysis. We present a short proof for the BCF.

$$\partial_\psi i_{ZZ}(\psi) = q_e \sum_{j=1}^{n} \frac{\sin\phi_{k_j-\psi}\sin\theta_{k_j-\psi}(\sin\phi_{k_j^+}\sin\theta_{k_j^+} - \sin\phi_{k_j^-}\sin\theta_{k_j^-})}{8\pi} - \frac{\cos\theta_{k_j-\psi}(\cos\theta_{k_j^+} - \cos\theta_{k_j^-})}{8\pi} + R(\psi), \tag{3.73}$$

where R is a continuous function. Then, we note $\Delta I(\psi_0, \delta\psi) = \partial_\psi i_{ZZ}(\psi_0 + \delta\psi) - \partial_\psi i_{ZZ}(\psi_0 - \delta\psi)$, and discard R which does not contribute in the limit $\delta\psi \to 0$. It can be expressed as:

$$q_e \sum_{j=1}^{n} \frac{(\sin\phi_{k_j-\psi_0-\delta\psi}\sin\theta_{k_j-\psi_0-\delta\psi} - \sin\phi_{k_j-\psi_0+\delta\psi}\sin\theta_{k_j-\psi_0+\delta\psi})}{8\pi} \times (\sin\phi_{k_j^+}\sin\theta_{k_j^+} - \sin\phi_{k_j^-}\sin\theta_{k_j^-}) - \frac{(\cos\theta_{k_j-\psi_0-\delta\psi} - \cos\theta_{k_j-\psi_0+\delta\psi})(\cos\theta_{k_j^+} - \cos\theta_{k_j^-})}{8\pi} \tag{3.74}$$

It will take non-zero values only if the gap also closes at $k_j - \psi_0$. In particular, for $\psi_0 = 2k_j$, the discontinuity arising from the term j is:

$$-q_e \frac{(\sin\phi_{k_j^+}\sin\theta_{k_j^+} - \sin\phi_{k_j^-}\sin\theta_{k_j^-})^2 + (\cos\theta_{k_j^+} - \cos\theta_{k_j^-})^2}{8\pi} = -\frac{q_e}{2\pi} \tag{3.75}$$

with the same assumptions as in Eq. 3.71.

3.2.6 Bipartite fluctuations in Kitaev's model and the SSH chain

In this section, we give examples of our previous results in the Kitaev's model and the SSH chain.

Kitaev's model

We use expressions obtained in Section 3.1.2, with $\phi_k = 0$ and $\theta_k = \mathrm{Arg}(-\mu - 2t\cos k + 2i\Delta\sin k)$ for Kitaev's model. The charge correlator corresponds to the physical electronic charge:

$$\hat{Q} = \frac{q_e}{2}\Psi_j^\dagger \sigma^z \Psi_j = c_j^\dagger c_j - \frac{1}{2}, \tag{3.76}$$

The charge fluctuations take the form:

$$\mathcal{F}_{\hat{Q}}(\mathcal{A}) = \frac{l_\mathcal{A}}{4} \iint\limits_{k,q\in\mathcal{BZ}} \frac{dkdq}{4\pi^2} f_F(k-q, l_\mathcal{A})\left(1 - \cos\theta_k\cos\theta_q + \sin\theta_k\sin\theta_q\right). \tag{3.77}$$

The linear coefficient is therefore given by:

$$i_{\hat{Q}} = \frac{1}{4}\int\limits_{k\in\mathcal{BZ}} \frac{dk}{2\pi}\left(1 - \cos^2\theta_k + \sin^2\theta_k\right) = \frac{1}{2}\int\limits_{k\in\mathcal{BZ}} \frac{dk}{2\pi}\sin^2\theta_k \tag{3.78}$$

An exact analytical expression can be obtained for $i_{\hat{Q}}$ [155]:

$$i_{\hat{Q}} = \begin{cases} \frac{|\Delta|}{2(|\Delta|+|t|)} & \text{if } |\mu| \leq 2t \\ \frac{2\Delta^2}{|\mu|+\sqrt{\mu^2+4\Delta^2-4t^2}}\frac{1}{\sqrt{\mu^2+4\Delta^2-4t^2}} & \text{if } |\mu| > 2t \end{cases} \tag{3.79}$$

In particular, the linear coefficient does not depend on μ in the topological phase[149, 155]. It is an interesting feature of Kitaev's model, and a strong experimental signature but it is not universal to topological models. It can also be used to measure the strength of the pairing term. Figure 3.1 gives a visual representation of the linear term. In particular, the cusp is here present at all phase transitions.

The logarithmic contribution itself may only appear on the lines $\Delta = 0$ or $\mu = \pm 2t$. Let us start with the line of normal metal. On this line, the linear coefficient itself vanishes, as the charge is conserved. For $|\mu| \geq 2t$, the wire is either totally occupied or empty, and the system is actually gapped: the logarithmic term is zero, and in fact the fluctuations themselves cancel. For $|\mu| < 2t$, this model of free fermions is gapless and the gap closes at the two momenta $\pm k_f = \pm\arccos\frac{-\mu}{2t}$. The function $\sin(\theta_k)$ is continuous (and uniformly

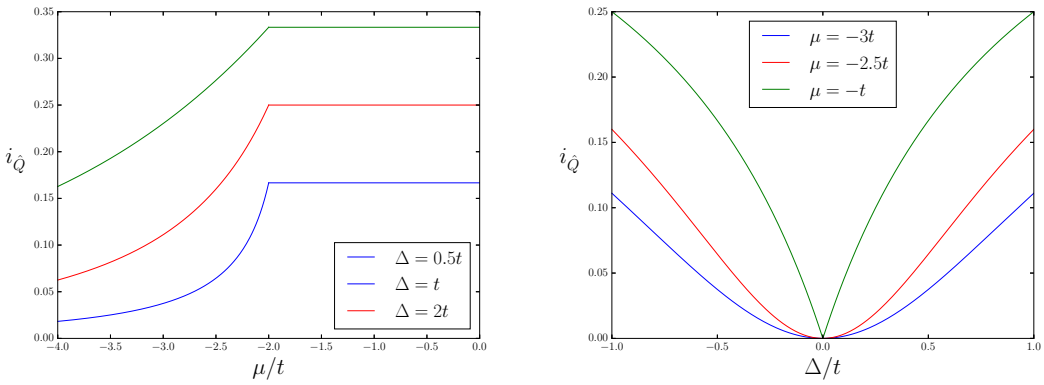

Figure 3.1: Left: linear coefficient of the bipartite charge fluctuations in Kitaev's model for several values of the pairing term Δ as a function of the chemical potential μ. The cusp marks the phase transition at $\mu = -2t$. The linear term is constant inside the topological phase for Kitaev's model. Right: linear coefficient of the bipartite charge fluctuations in Kitaev's model for several values of μ as a function of Δ. A transition occurs at $\Delta = 0$ only for $|\mu| < 2t$. The cusp disappears when $|\mu| > 2t$.

zero) while $\cos(\theta_k)$ is discontinuous with amplitude ∓ 2 at $\pm k_f$. The logarithmic coefficient is then given by

$$\frac{1}{\pi^2}. \tag{3.80}$$

We recover the coefficient in non-interacting LLs.

Now we can focus on the topological transition. By symmetry, we will consider only what happens at $\mu = -2t$. The gap closes only at $k = 0$, and the sinus is discontinuous with amplitude -2 while the cosine term is continuous. Hence, the logarithmic coefficient is given by:

$$\mathbf{b}_{ZZ} = -\frac{1}{2\pi^2}. \tag{3.81}$$

SSH chain

The different observables for the SSH model correspond to the pseudo-spin polarizations

$$\frac{q_e}{2}\Psi_j^\dagger \sigma^z \Psi_j = c_{j,A}^\dagger c_{j,A} - c_{j,B}^\dagger c_{j,B}, \quad \frac{q_e}{2}\Psi_j^\dagger \sigma^x \Psi_j = c_{j,A}^\dagger c_{j,B} + c_{j,B}^\dagger c_{j,A},$$
$$\frac{q_e}{2}\Psi_j^\dagger \sigma^y \Psi_j = i c_{j,B}^\dagger c_{j,A} - i c_{j,A}^\dagger c_{j,B}. \tag{3.82}$$

Note this does not correspond to the previous convention for the bipartite fluctuations, but a rotated basis. The conventional "charge" fluctuations corresponds to the σ^x polarization. To recover our previous notations, one would need to rotate the fermionic spinors such that:

$$\sigma^x \to \sigma^z, \quad \sigma^y \to -\sigma^y, \quad \sigma^z \to -\sigma^x. \tag{3.83}$$

Term $\alpha\beta$	Linear contributions	**b** at $t_1 = \pm t$	**b** at $t_2 = 0$
ZZ	1	$-\frac{1}{\pi^2}$	$-\frac{2}{\pi^2}$
XX	$\begin{cases} \frac{\lvert t_2\rvert}{(\lvert t_2\rvert+\lvert t\rvert)} & \text{if } \lvert t_1\rvert \leq t \\ \frac{t_2^2}{\lvert t_1\rvert+\sqrt{t_1^2+t_2^2-t^2}}\frac{1}{\sqrt{t_1^2+t_2^2-t^2}} & \text{if } \lvert t_1\rvert > t \end{cases}$	$-\frac{1}{\pi^2}$	$\frac{2}{\pi^2}$
YY	$\begin{cases} \frac{\lvert t\rvert}{(\lvert t_2\rvert+\lvert t\rvert)} & \text{if } \lvert t_1\rvert \leq t \\ 1-\frac{t_2^2}{\lvert t_1\rvert+\sqrt{t_1^2+t_2^2-t^2}}\frac{1}{\sqrt{t_1^2+t_2^2-t^2}} & \text{if } \lvert t_1\rvert > t \end{cases}$	$\frac{1}{\pi^2}$	$-\frac{2}{\pi^2}$
XZ	0	None	None
YZ	0	None	None
XY	0	None	None

Table 3.4: Linear and logarithmic coefficients appearing in the bipartite fluctuations for the SSH model following the convention of Section 3.1.2. The second column gives the linear coefficient, for the different polarizations. The third column gives the coefficient of the logarithmic sub-leading term appearing at the topological phase transition, for $t_1 = \pm t$. The last column corresponds to the same coefficient but on the line $t_2 = 0$ and for $|t_1| < t$. For $|t_1| > t$, they all cancel.

We choose in this Section not to proceed with this rotation and instead give the expression for the fluctuations in the initial basis for simplicity's sake. In the SSH model, $\phi_k = \mathrm{Arg}(-2(t_1 + t\cos k) - 2it_2 \sin k)$ and $\theta_k = \frac{\pi}{2}$. In the basic model introduced in Section 1.5.1, $t_2 = t$, but we slightly extend it in this section for completeness. Following the notations obtained in Section 3.1.2, Table 3.4 summarizes the linear and logarithmic terms appearing in the BF depending on the chosen observable. Taking into account the spin-rotation, the XX line corresponds to the BCF in Kitaev's chain: we recover the same properties and structure, up to a factor $q_e = 2$.

Ising model

Similar computations could be done directly in the Quantum Ising model in a transverse field, introduced in Section 1.1.4. Bipartite polarization fluctuations have the same definition:

$$\mathcal{F}_{\sigma^\alpha}(\mathcal{A}) = \sum_{j,j'\in\mathcal{A}} \langle \sigma_j^\alpha \sigma_{j'}^\alpha \rangle_c \tag{3.84}$$

For $\alpha = z$, these fluctuations exactly correspond to the BCF of the Kitaev model (or half the XX fluctuations in the SSH model), and consequently, due to the Jordan-Wigner transformation, have the exact same expression.

Nonetheless, it is interesting to notice that the Jordan-Wigner string does not vanish for $\alpha = x$ and $\alpha = y$., and consequently fluctuations do not match those of the SSH model. In particular, for the Quantum Ising model at the critical point

$$-\sum_j \sigma_j^z - \sum_j \sigma_j^x \sigma_{j+1}^x,$$

following McCoy[156] and Pfeuty[157] computations, the main correlation functions are given by:

$$\langle \sigma_j^x \sigma_{j+r}^x \rangle = \frac{1}{4}(\frac{2}{\pi})^r 2^{2r(r-1)} \frac{e^{\sum_{j=1}^{r-1} 4j \ln r-j}}{e^{\sum_{j=1}^{2r-1} j \ln 2r-j}} \approx \frac{1}{4} e^{\frac{1}{4}} 2^{\frac{1}{12}} A^{-3} n^{-\frac{1}{4}} (1 - \frac{1}{64n^2} + o(n^{-2})), \quad (3.85)$$

$$\langle \sigma_j^y \sigma_{j+r}^y \rangle = -\frac{1}{4r^2-1} \langle \sigma_j^x \sigma_{j+r}^x \rangle \approx -\frac{1}{16} e^{\frac{1}{4}} 2^{\frac{1}{12}} A^{-3} n^{-\frac{9}{4}} (1 + \frac{15}{64n^2} + o(n^{-2})), \quad (3.86)$$

$$\langle \sigma^x \rangle = \langle \sigma^y \rangle = 0, \quad (3.87)$$

with $A \approx 1.2824$. From there, long range integrations leads to:

$$\mathcal{F}_{\sigma^x}(\mathcal{A}) \approx \frac{4}{21} e^{\frac{1}{4}} 2^{\frac{1}{12}} A^{-3} l_{\mathcal{A}}^{\frac{7}{4}} \quad (3.88)$$

$\mathcal{F}_{\sigma^x}(\mathcal{A})$ is no longer linear in the size of $l_{\mathcal{A}}$. It implies that in the spin-basis, the ground state is no longer producible, but a pure macroscopically entangled, quantum state. This is a direct consequence of the non-local nature of the Jordan Wigner transform.

3.2.7 Bipartite fluctuations in the extended Kitaev's model

The extended Kitaev's model allows us to probe more complex phase transitions where the topological number jumps by more than one, while Δ_k does not vanish uniformly. It is therefore a perfect model to consider the structure factor of the bipartite fluctuations. We consider here the $t_1 - t_3$ model where phases with up to 3 Majorana fermions can appear, and take $t_1 = \Delta_1$ and $t_3 = \Delta_3$ to simplify the discussion. Section 1.5.2 presents a study of the phase diagram of the model. We define

$$\varepsilon_k = -\mu - 2t_1 \cos k - 2t_3 \cos 3k, \qquad \Delta_k = -2t_1 \sin k - 2t_3 \sin 3k \quad (3.89)$$

As it is a superconducting model, we only consider the BCF.

$\underline{t_1 = 0}$

For $t_1 = 0$, the phase diagram is the same as Kitaev's, with transitions at $\mu \pm 2t_3$. The two topological phases have winding number ± 3, and at the phase transitions, the gap closes at the three different momenta. For $\mu = -2t_3$, these are $0, \pm\frac{2\pi}{3}$. Computation of the linear term is straightforward: a simple change of variables show that they are equal to those in Kitaev's model.

Computation of the logarithmic term is just as simple: ε_k is quadratic at each gap closing momenta and therefore

$$\mathbf{b}_{ZZ} = -\frac{3}{2\pi^2} \quad (3.90)$$

For completeness, we can compute the structure factor of the BCF anyway. Due to the simple structure of ε_k and Δ_k, the structure factor is periodic in ψ of period $\frac{2\pi}{3}$, with discontinuities of the derivative of $i_{ZZ}(\psi)$ of amplitude $-\frac{3}{2\pi}$ and logarithmic contributions of coefficient $-\frac{3}{2\pi^2}$ at $\psi = 0, \pm\frac{2\pi}{3}$.

$\underline{t_1 \neq 0}$

For $t_1 \neq 0$, the phase diagram is more complex and given in Section 1.5.2. On any gapless

line between phases with winding number differing by 1, there is a discontinuity of the derivative of i_{ZZ} and $\mathbf{b}_{ZZ} = -\frac{1}{2\pi^2}$. On transition lines between phases with winding number differing by 2, the gap closes at two momenta $\pm k_f$ and $\mathbf{b}_{ZZ}$ is not universal. Figure 3.2 represents the variation of the linear term across several phase transitions. The universality of $\mathbf{b}_{ZZ}$ can be recovered using the structure factor of the BCF, as shown in Figure 3.3.

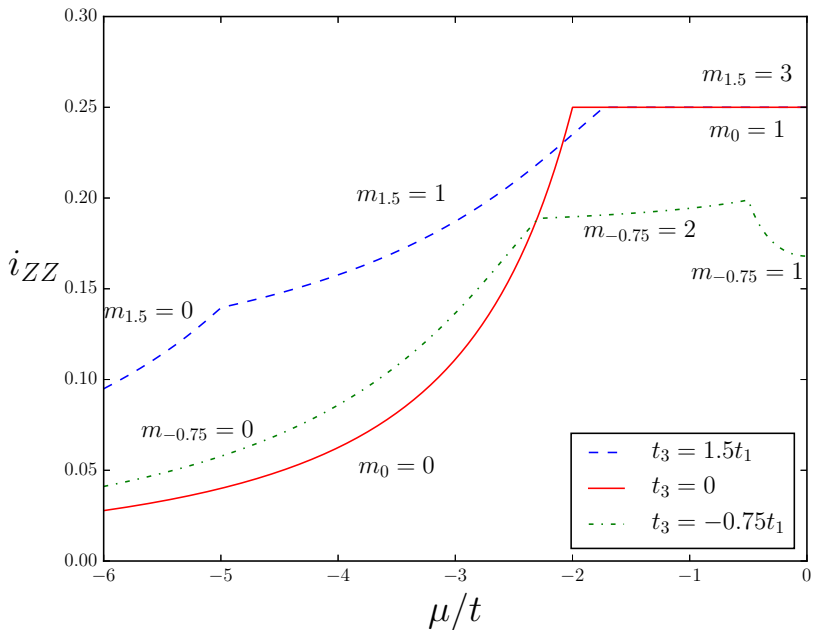

Figure 3.2: Linear contribution i_{ZZ} to the bipartite fluctuations in the $t_1 - t_3$ Extended Kitaev model as a function of the chemical potential for several values of $\frac{t_3}{t_1}$ with $\Delta_l = t_l$. Cusps in the linear term mark each phase transition. m is the winding number associated to each phase, corresponding to the number of protected Majorana fermions.

3.2.8 Extension to finite length and finite temperature

Just as was done for the vNEE, it is worth spending some time determining the finite-length and finite-temperature corrections that appear in the BF. The latter is mostly relevant for physical experiments, while the former is relevant for experiments but also for numerical simulations. We start by considering the finite-temperature limit.

Finite temperature

At $T > 0$, each quasi-particle state (corresponding to $\eta_k^\dagger |0\rangle_\eta$ in Bogoliubov formalism) is populated with probability $f_D(E_k, \beta)$, where E_k is the corresponding eigenenergy, $\beta = \frac{1}{T}$

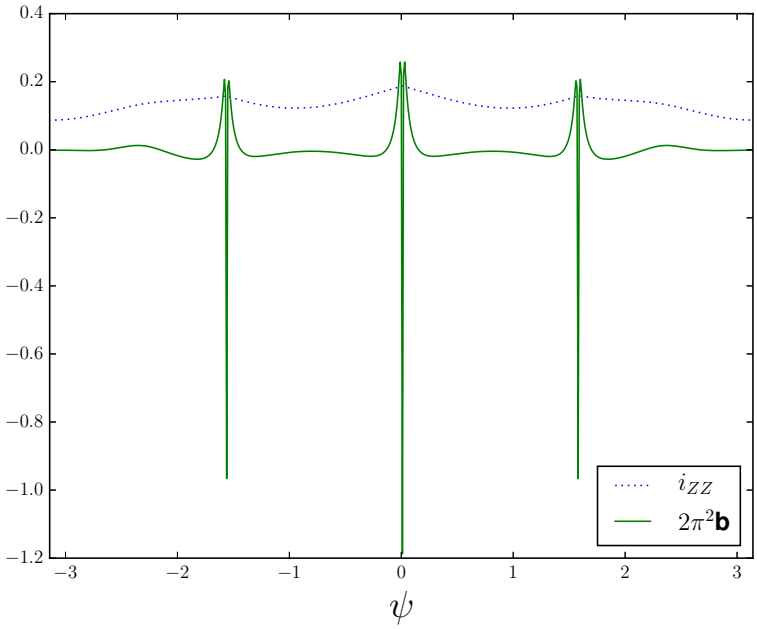

Figure 3.3: Example of linear and logarithmic contributions to the structure factor obtained from a numerical fit, as a function of ψ, in the extended Kitaev model[51] for $t_3 = -t_1$, $\mu = 2\sqrt{2}t$ (on the critical line between $m = 0$ and $m = 2$). We consider a subsystem of up to $l = 1000$ sites. The gap closes linearly at momenta $k_F = \pm 2\arctan(1+\sqrt{2})$. The logarithmic coefficient is bounded by $\frac{1}{\pi^2}$ but does not saturate ($\mathbf{b}(0) \approx -\frac{0.6}{\pi^2}$). To recover the band structure, we vary ϕ. Logarithmic contributions first vanish then reappear as two sharp peaks at $\pm 2k_F$, and saturate at the universal value $-\frac{1}{2\pi^2}$. The change in the sign of $\mathbf{b}$ close to $\psi = 0$, and $\psi = \pm 2k_j$ is an artifact of the fit. We also measure discontinuities of $i_{ZZ}(\phi)$ at $\pm 2k_F$.

the inverse temperature[5] and f_D the Fermi-Dirac distribution:

$$f_D(E, \beta) = \frac{1}{1 + e^{\beta E}} \tag{3.91}$$

As Wick's theorem still applies at finite temperature, the computations are similar and we only give the final substitution rules:

$$\cos\theta_k \to \cos\theta_k \tanh\frac{\beta E_k}{2} \tag{3.92}$$

$$\sin\theta_k \to \sin\theta_k \tanh\frac{\beta E_k}{2} \tag{3.93}$$

[5]We take the Boltzmann constant $k_B = 1$. To restore the proper dependencies, replace T by $k_B T$

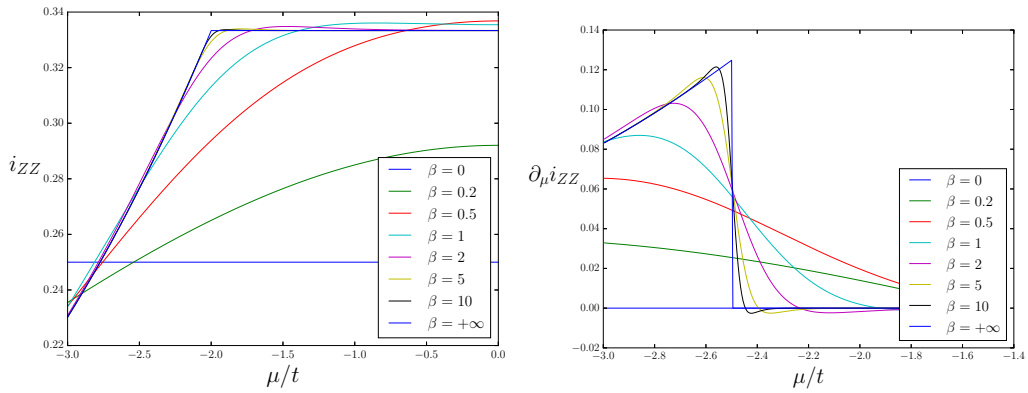

Figure 3.4: Evolution in temperature of the linear term of the BCF in Kitaev's wire for $\Delta = 2t$. Left: evolution of the linear term as function of the chemical potential for different values of the temperature. Right: derivative of the linear term as a function of μ. Fluctuations due to temperature smoothen the discontinuity at the phase transition.

We then focus as an example on the BCF. In the thermodynamic limit, the term linear with the size of the system is still given by:

$$i_{ZZ}(\beta) = \frac{q_e}{4} - \frac{q_e}{4} \int\limits_{k \in \mathcal{BZ}} \frac{dk}{2\pi} \cos 2\theta_k \tanh^2 \frac{\beta E_k}{2} \tag{3.94}$$

In the infinite temperature limit, we recover that the linear term is equal to $\frac{q_e}{4}$, which is exactly the fluctuations of independent, on-site fermions, with correction in β^2, while at low-temperature ($\beta^{-1} \ll \min_k E_k$), the first corrections are exponentially decreasing in β. Figure 3.4 and 3.5 summarizes the different behaviors of the linear term in Kitaev's wire for $\Delta = 2t$. In particular, temperature-induced fluctuations smoothen out the cusp at the phase transition.

At the critical point, a logarithmic term still appears in the fluctuations. Conformal field theory gives the exact dependency of the logarithmic term: β acts as a cut-off length[70] such that the fluctuations are given by:

$$i_{\hat{O}}(\beta) l + \mathbf{b}_{\hat{O}} \ln \left(\frac{v\beta}{\pi} \sinh \frac{\pi l_{\mathcal{A}}}{v\beta} \right), \tag{3.95}$$

where v is the effective velocity. At high temperature $\beta \ll t$, the logarithm transforms in a term linear with the temperature.

Finite length

In order to proceed to accurate estimations of the different coefficients in numerical simulations, in particular for interacting systems where the size of the system is a strong constraint, one needs to carefully compute the corrections to the BF. They have two origins: the first one is the discretization of the integrals into finite sums, and the second one

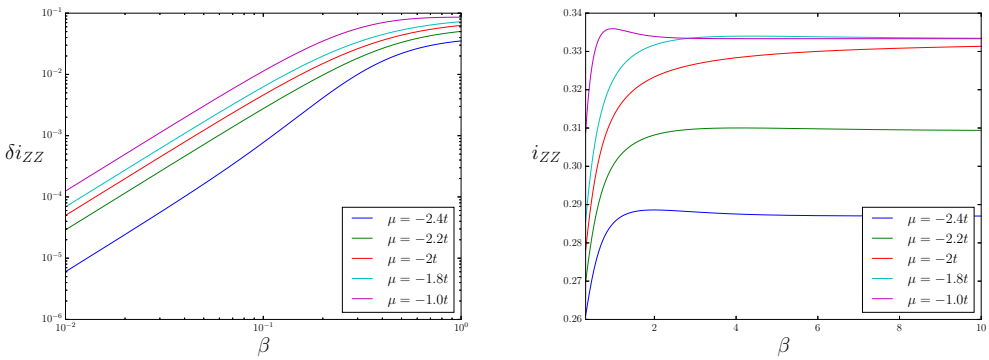

Figure 3.5: Evolution in temperature of the linear term of the BCF for several values of μ in Kitaev's wire for $\Delta = 2t$. At high temperature, $\delta i_{ZZ}(\beta) = i_{ZZ}(\beta) - i_{ZZ}(0)$ is quadratic in β while at low temperature, it converges exponentially to the zero temperature limit.

is the presence of the 0 and π modes that are not always taken properly into account in the computations.

We focus as an example on the charge fluctuations in a Kitaev's wire with L sites and compute the finite-size density-density correlator at the critical point $\mu = -2t$:

$$\langle c_j^\dagger c_j c_{j+r}^\dagger c_{j+r}\rangle_c = \frac{1}{L^2}\sum_{k,q\in\mathcal{BZ}^2} e^{i(q-k)r}(-\langle c_k^\dagger c_{-k}^\dagger\rangle\langle c_q c_{-q}\rangle + \langle c_k^\dagger c_k\rangle\langle c_q c_q^\dagger\rangle) \tag{3.96}$$

$\langle c_k^\dagger c_{-k}^\dagger\rangle$ cancels for $k = 0, \pi$. On the other hand, for $k \neq 0, \pi$, $\langle c_k^\dagger c_{-k}^\dagger\rangle = i\sin\theta_k$. As $\sin\theta_{0\pm} = \pm 1$, for continuity and Riemann sum convergence, we fix $\sin\theta_0 = 1$. $k = \pi$ requires no correction since $\sin\theta_\pi = 0$. The first correlator can therefore be rewritten as:

$$\langle c_k^\dagger c_{-k}^\dagger\rangle = \frac{i}{2}(\sin\theta_k - \delta_{k,0}) \text{ with } \delta \text{ the Kronecker symbol} \tag{3.97}$$

Similarly, $\langle c_k^\dagger c_k\rangle = \frac{1-\cos\theta_k}{2} \to \frac{1}{2}$ when $k \to 0$. On the other hand, the ground states can be classified by their parity, and verifies $n_0 = 0(1)$ for the even (odd) ground state. One then need to replace the correlator by:

$$\frac{1-\cos\theta_k - \varepsilon\delta_{k,0}}{2} \text{ with } \varepsilon \text{ the parity of the ground state} \tag{3.98}$$

The density-density correlator can then be expressed as:

$$\begin{aligned}\langle c_j^\dagger c_j c_{j+r}^\dagger c_{j+r}\rangle_c = \frac{1}{4L^2}\sum_{k,q\in\mathcal{BZ}^2} e^{i(q-k)r}&((\sin\theta_k - \delta_{k,0})(\sin\theta_q - \delta_{q,0}) \\ &+ (1-\cos\theta_k - \varepsilon\delta_{k,0})(1+\cos\theta_q + \varepsilon\delta_{q,0})) \qquad (3.99)\\ = \frac{1}{4}&(\delta_{r,0} + \mathcal{FT}\{\sin\theta_k\}_L(r)|^2 - |\mathcal{FT}\{\cos\theta_k\}_L(r)|^2 \\ &- \frac{2\varepsilon}{L}\mathcal{FT}\{\cos\theta_k\}_L(r) - \frac{2}{L^2}, \qquad (3.100)\end{aligned}$$

where $\mathcal{FT}\{f\}_L$ is the discrete Fourier transform of f with L terms. We can classify the different terms: the first three leads to the discrete version of our previous integrals. The main effect of discretization is a smoothening of the cusp at the transition, and the well-known change in the logarithmic coefficient (from CFT [81])

$$\ln l_{\mathcal{A}} \to \ln\left(\frac{L}{\pi}\sin\frac{l_{\mathcal{A}}\pi}{L}\right), \tag{3.101}$$

that arises from:

$$\frac{1}{r^2} \to \frac{1}{(\frac{L}{\pi}\sin(\pi\frac{r}{L}))^2} \text{ in the Fourier transforms.} \tag{3.102}$$

The fourth term $-\frac{2\varepsilon}{L}\mathcal{FT}\{\cos\theta_k\}_L(r)$ leads to a small non-universal shift of order $\frac{1}{L}$ of the logarithmic coefficient, as $\mathcal{FT}\{\cos\theta_k\}_L(r) = O(\frac{1}{r^2})$ when $L \to +\infty$, and the linear term, that can be easily compensated by taking the average contribution of the even and odd ground states.
Finally, the constant term $-\frac{1}{2L^2}$ is the most bothering one. It is a consequence of the infinite range of the zero mode, and the absence of pairing at this momenta. It leads to a very small quadratic term in the fluctuations, that must be taken care of before a proper analysis can be realized. Fortunately, it is parameter-independent and can be easily removed by numerical analysis of the long range behavior of the density-density correlator.

To summarize, the proper form of the fluctuations for a finite system (once the constant term has been taken care of) is:

$$(i_{\hat{Q}} + O(\frac{1}{L}))l + (\mathbf{b}_{\hat{Q}} + \frac{a\varepsilon}{L} + O(\frac{1}{L^2}))\ln\left(\frac{L}{\pi}\sin\frac{l_{\mathcal{A}}\pi}{L}\right) + O(1) \tag{3.103}$$

An example is given in Figure 3.6 for Matrix Product States (MPS) simulations[158, 159] as a benchmark for the precision of our numerics. More details on MPS simulations are kept in Chapter 4.

3.2.9 A brief comparison with other charge-based measurements

Before concluding this Section, let us compare very briefly our results with other probes of quantum criticality for topological superconductors. We are especially interested in charge-based measurements. Most of those focus on direct detection of the Majorana fermions, notably with the help of small energy splitting of the Majorana fermions[160–165], but also on the phase transitions. We will be more interested in the latter. Let us first start by looking at the charge susceptibility.
The charge susceptibility is a conventional, experimentally accessible, observable that measures how the charge in the wire varies after a slight change in the chemical potential:

$$\chi_{\hat{N}} = \frac{1}{L}\partial_\mu\langle\hat{N}\rangle, \text{ with } \hat{N} \text{ the total charge operator of the system.} \tag{3.104}$$

The average is taken in the ground state at $T = 0$ and in a thermal state at $T > 0$. Let us assume an Hamiltonian of the form

$$H = H_0 - \mu\hat{N}$$

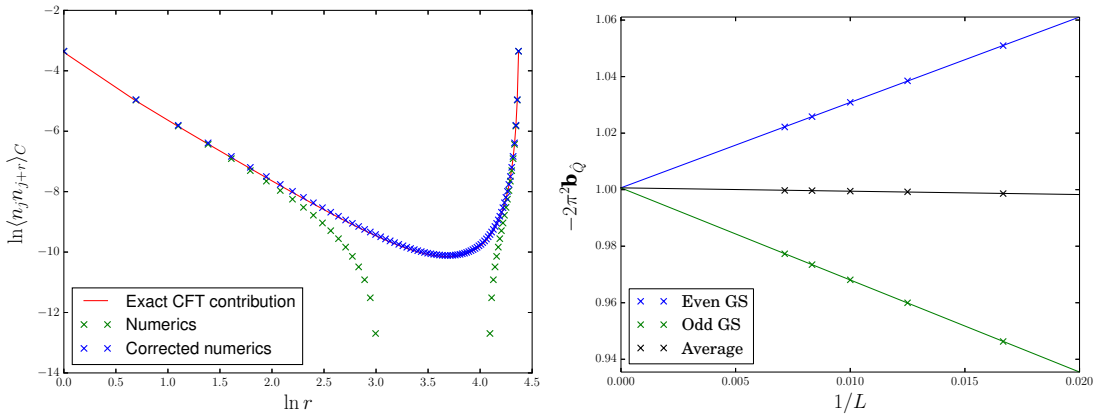

Figure 3.6: Left: finite-size correlation functions obtained from MPS simulations[158, 159] for a 80-site periodic Kitaev wire at the critical point ($\mu = -2t$ and $\Delta = t$). In red, correlation functions obtained from the discrete form integrals. In green, the numerical correlation function before the constant corrections. In blue, the correlation function after the correction. Right: logarithmic coefficient extracted from the correlation functions as a function of the total size of the system. Corrections in L^{-1} have opposite signs in each ground state and therefore can be easily compensated. Numerics leads to $-2\pi^2\mathbf{b}_{\hat{Q}} = 1.0006$.

Then, one can show that the susceptibility and the charge fluctuations are linked if the total charge is conserved[140]. It simply comes from:

$$\chi_{\hat{N}} = \frac{1}{L}\partial_\mu \frac{1}{Z}\mathrm{Tr}(\hat{N}e^{-\beta(H_0-\mu\hat{N})}) = \frac{\beta}{L}\beta\frac{\mathrm{Tr}(\hat{N}^2 e^{-\beta(H_0-\mu\hat{N})})}{Z} - \frac{\beta}{L}\left(\frac{\mathrm{Tr}(\hat{N}e^{-\beta(H_0-\mu\hat{N})}}{Z}\right)^2, \qquad \chi_{\hat{N}} = \frac{\beta}{L}\langle\hat{N}^2\rangle_c \tag{3.105}$$

where $Z = \mathrm{Tr}(e^{-\beta H})$ the normalization of the thermal density matrix. The equality will also essentially stands for partial susceptibilities in the thermodynamic limit.
On the other hand, in the system we considered, the total charge is not conserved, which means that H_0 and $\hat{N}$ do not commute. Then, we have

$$\chi_{\hat{N}} = \frac{\beta}{L}\frac{\mathrm{Tr}(\sum_{n=0}^{+\infty}\frac{1}{n!}\sum_{j=0}^{n-1}\hat{N}(-\beta H)^j\hat{N}(-\beta H)^{n-1-j})}{Z} - \frac{\beta}{L}\left(\frac{\mathrm{Tr}(\hat{N}e^{-\beta(H_0-\mu\hat{N})}}{Z}\right)^2, \tag{3.106}$$

which should not match the charge fluctuations. The exact microscopic computation can be done in Kitaev's model. Starting from:

$$\frac{\langle\hat{N}\rangle}{L} = \frac{q_e}{2} - \frac{q_e}{2}\int_{k\in\mathcal{BZ}}\frac{dk}{2\pi}\cos\theta_k\tanh(\frac{\beta E_k}{2}),$$

one trivially obtains:

$$\chi_{\hat{N}} = \frac{q_e}{2} \int\limits_{k\in\mathcal{BZ}} \frac{dk}{2\pi} \frac{\sin^2\theta_k}{E_k} \tanh(\frac{\beta E_k}{2}) + \frac{\beta q_e}{4} \int\limits_{k\in\mathcal{BZ}} \frac{dk}{2\pi} \cos^2\theta_k (1 - \tanh^2(\frac{\beta E_k}{2})). \quad (3.107)$$

This does not match Eq. 3.94, the finite temperature form of our linear term. For the gapped phases, at low temperature (T much smaller than the gap), the dominant contribution is the first integral, with an additional factor $\frac{1}{E_k}$ compared to our linear term. At high temperature, at first order in β, the susceptibility converges to the same value $\frac{\beta}{4}$ and one recovers the standard fluctuation theorem. For gapless phases, one must be careful in the ordering of the limits $\beta \to 0/+\infty$ and $L \to +\infty$. Taking first $L \to +\infty$, we obtain similar results. Finally, one can compute the dominant term of the susceptibility at zero temperature and show that it diverges logarithmically as a function of $||\mu| - 2t|$[166]:

$$\chi_{\hat{N}} \approx \frac{q_e}{2\pi v_F} \log(1 + \frac{v_F}{m}),$$

with $E_k \approx v_f|k| + m$. For these $\mathbb{Z}_2$ models, the charge fluctuations are not equivalent to the charge susceptibility.

Several proposals were made for measuring the phase transition and the appearance of the Majorana fermions through charge properties. Refs. [160, 163] proposed to couple a topological superconductor with a superconducting cavity. The photons of the cavity couple with the fermionic density, such that one can measure the electronic susceptibility through a measurement of the transmission coefficient of the cavity. In practice, one can measure:

$$\Pi(t) = -\frac{i}{L}\langle[\hat{N}(t), \hat{N}(0)]\rangle, \quad (3.108)$$

where t marks the time dependence of the operators. The presence of the commutator dramatically changes the behavior of Π compared to the fluctuations. In frequency space, it transforms into:

$$\Pi(\omega) = -\sum_{\varepsilon=\pm 1} \int\limits_{k>0} \frac{dk}{\pi} \sin^2(\theta_k) \frac{\varepsilon}{\omega + 2\varepsilon E_k + i0^+} \quad (3.109)$$

In the limit $\omega \to 0$, one indeed recovers the charge susceptibility we previously computed, and therefore a divergence of the real part of $\Pi(\omega)$ at the phase transition (in practice, the finite frequency at the critical point cut the divergence and split the peak). The imaginary part of the susceptibility, corresponding to the dissipative strength of the cavity, is given by:

$$\Pi''(\omega > 0) = -\frac{\sin^2\theta_k}{2\partial_k E_k}\Big|_{k=E_k^{-1}(\frac{w}{2})}. \quad (3.110)$$

The imaginary part is non-zero only inside the superconducting band, and it is therefore easy to probe the transition by looking at low frequencies. Additionally, the maximum converges towards $|\mu| = 2t$ when $\omega \to 0$. The peak close to the phase transition is (partially) due to saturation of $\sin^2\theta_{0^+}$ to 1 at the phase transition, while it goes to 0 normally (and at non-topological transition). This measure is therefore similar in spirit to the measure of the quantified $\mathbf{b}$ (the discontinuity being imposed by the symmetries, measuring a non-zero value of $\sin^2\theta_{0^+}$ is equivalent to measuring a discontinuity), though the obtained value is non-universal as one only measures at a finite frequency in principle.

3.2.10 Beyond the two-band paradigm

Studying the D class Hamiltonian gives the opportunity to check the behaviour of the fluctuations in more realistic and complex systems. In particular, we can study the fluctuations in the Rashba nanowires[23, 24] model introduced in Section 1.5.3. This model is no longer a two-band but a four-band superconducting model, which is still analytical. Exact computations of the BCF (up to close formed integrals) are possible, if lengthy. The different steps of the computation are presented in Appendix D.2, and we only summarize here the main arguments and results.
Due to the four-bands, there is a much larger variety of local correlators that one can study. We focus on the charge correlators to keep things simple. Four contributions can be singularized: $N_\uparrow$, $N_\downarrow$ and $N_\pm = N_\uparrow \pm N_\downarrow$. Bipartite fluctuations of these four operators can be computed and follow the same scaling rules: a dominant linear term, and a logarithmic sub-dominant contribution appearing at the critical points. The different linear terms are presented in Figure 3.7 across one of the topological transitions. The logarithmic coefficient $\mathbf{b}_{N_-}$ is quantized and given by $-\frac{1}{2\pi^2}$ as expected.

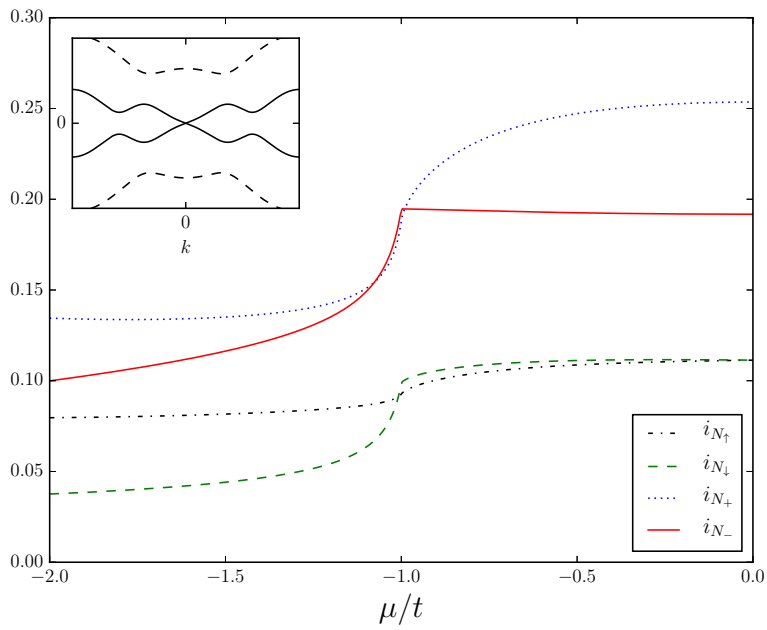

Figure 3.7: Linear coefficient for the four BCF in the Rashba nanowire model, for $\Delta = t$ and $V = \sqrt{2}$. At the topological phase transition at $\mu = -t$, the gap closes at $k = 0$. The system is in a trivial phase for $\mu < -t$. As can be seen, the behaviour of the relative density is similar to the one of the density in Kitaev's model. Indeed, we recover a quantified logarithmic coefficient for these fluctuations. In inset, the energy bands at the critical point $\mu = -t$.

3.3 One-dimensional D class

3.3.1 Preliminaries

Most of what we derived for BDI Hamiltonian also applies for Hamiltonians in the D class, due to our unusual definition of ϕ_k and θ_k. Generalization is therefore straightforward. Hamiltonians in the D class are given by:

$$H = \frac{1}{2}\sum_k \Psi_k^\dagger(\Delta_k^x, \Delta_k^y, \varepsilon_k).\vec{\sigma}\Psi_k, \tag{3.111}$$

where Ψ_k is a fermionic spinor, ε_k an effective kinetic energy and $\Delta_k^{x/y}$ are effective pairing or cross-hopping terms. ε_k is still even in momentum space while $\Delta_k^{x/y}$ are odd. We assume similar analytical structure of ε_k and $\Delta_k^{x/y}$ than in the previous Section. Following the conventions of Section 3.1.2, we define

$$\phi_k = \mathrm{Arg}(\Delta_k^x + i\Delta_k^y) \text{ and } \theta_k = \mathrm{Arg}(\varepsilon_k + i|\Delta_k^x + i\Delta_k^y|)$$

θ_k is even while $\phi_{-k} = \pi + \phi_k$ The linear terms can be obtained for all polarizations:

$$i_{ZZ} = \frac{q_e}{2}\int_{k\in\mathcal{BZ}} \frac{dk}{2\pi}\sin^2\theta_k \tag{3.112}$$

$$i_{XX} = \frac{q_e}{4}\int_{k\in\mathcal{BZ}} \frac{dk}{2\pi}(1+\cos^2\theta_k - \cos 2\phi_k \sin^2\theta_k) \tag{3.113}$$

$$i_{YY} = \frac{q_e}{4}\int_{k\in\mathcal{BZ}} \frac{dk}{2\pi}(1+\cos^2\theta_k + \cos 2\phi_k \sin^2\theta_k) \tag{3.114}$$

$$i_{XY} = -\frac{q_e}{2}\int_{k\in\mathcal{BZ}} \frac{dk}{2\pi}\sin 2\phi_k \sin^2\theta_k \tag{3.115}$$

$$i_{XZ} = i_{YZ} = 0 \tag{3.116}$$

$$\tag{3.117}$$

Previously derived bounds are still valid.

3.3.2 Cusp of the linear term

At phase transitions, one still expects cusps of the different linear terms. Proofs are mostly still valid as long as both Δ_k^x and Δ_k^y are linear close to the gap closing momenta (which is expected due to PHS).

3.3.3 Logarithmic coefficients

At phase transitions, both ϕ_k and θ_k may be discontinuous. Let us first focus on transitions where the gap closes at one momentum k_0 (0 or π due to PHS). Then $\phi_{k_0^+} = \pi + \phi_{k_0^-}$,

while $\theta_{k_0^\pm} = \pi/2$ as long as either Δ^x or Δ^y is linear (generic case). Then, we obtain:

$$\mathbf{b}_{ZZ} = -\frac{q_e}{2\pi^2},\ \mathbf{b}_{XX} = -\frac{q_e}{2\pi^2}\cos(2\phi_{k_0^+}),\ \mathbf{b}_{YY} = \frac{q_e}{2\pi^2}\cos(2\phi_{k_0^+}) \tag{3.118}$$

$$\mathbf{b}_{XY} = \frac{q_e}{\pi^2}\sin 2\phi_{k_0^+},\ \mathbf{b}_{XZ} = \mathbf{b}_{YZ} = 0 \tag{3.119}$$

Only the coefficient of the BCF does not depend on the microscopic details of the theory and is therefore universal. Measuring the other correlations nonetheless measures the velocity of the Δ terms. If $\Delta_k^{x/y} \approx v_{x/y}(k-k_0)$, then,

$$\cos(2\phi_{k_0^+}) = \frac{v_x^2 - v_y^2}{v_x^2 + v_y^2} \text{ and } \sin(2\phi_{k_0^+}) = \frac{2v_x v_y}{v_x^2 + v_y^2} \tag{3.120}$$

These correspond to topological phase transitions. Measuring the different fluctuations allows us to recover the ratio of v_x and v_y.
Other transitions may occur, with the gap closing in the middle of the band an even number of times. Both ε_k and $\Delta_k^{x/y}$ are generally linear, and just as in the BDI class, there is no longer universality of the logarithmic term that arises. For a gap closing at k_F, $\theta_{k_F^+} = \pi - \theta_{k_F^-}$ and $\phi_{k_F^+} = \pi + \phi_{k_F^-}$. Taking into account both $\pm k_F$, logarithmic contributions are:

$$\mathbf{b}_{ZZ} = \frac{q_e}{\pi^2}\cos 2\theta_{k_F^+} \tag{3.121}$$

$$\mathbf{b}_{XX} = -\frac{q_e}{\pi^2}(\cos^2\theta_{k_F^+} - \cos 2\phi_{k_F^+}\sin^2\theta_{k_F^+}) \tag{3.122}$$

$$\mathbf{b}_{YY} = -\frac{q_e}{\pi^2}(\cos^2\theta_{k_F^+} + \cos 2\phi_{k_F^+}\sin^2\theta_{k_F^+}) \tag{3.123}$$

$$\mathbf{b}_{XY} = \frac{2q_e}{\pi^2}\sin 2\phi_{k_F^+}\sin^2\theta_{k_F^+} \tag{3.124}$$

As before, universality is recovered by looking at the structure factor of the BCF.

3.3.4 An example: extended Kitaev model

As a short illustration, we consider the $t_1 - t_2$ extended Kitaev model, with $t_1 = \Delta_1 \geq 0$, $t_2 = |\Delta_2| \geq 0$, $\Delta_2 = i|\Delta_2|$. The TRS is explicitly broken and the model is indeed in the D class, as explained in Section 1.5.2. The topological invariant now leaves in $\mathbb{Z}_2$.
The Hamiltonian is given by:

$$H = \frac{1}{2}\sum_{k\in\mathcal{BZ}} \Psi_k^\dagger(-2t_2\sin 2k, -2t_1\sin k, -\mu - 2t_1\cos k - 2t_2\cos 2k)\Psi_k, \tag{3.125}$$

and we recall the phase diagram: as long as $t_1 \neq 0$, for $\mu < -2t_1 - 2t_2$ and $\mu > 2t_1 - 2t_2$, the wire is in a trivial gapped state, while for $-2t_1 - 2t_2 < \mu < 2t_1 - 2t_2$ it is in a topological state (with one protected zero-energy Majorana edge state).
Figure 3.8 gives an example of the linear coefficient to the bipartite fluctuations for $t_2 = 0.5t_1$. Cusps are still present at each phase transitions. The logarithmic coefficient $\mathbf{b}_{ZZ}$ is still given by $-\frac{1}{2\pi^2}$ at the QPTs.

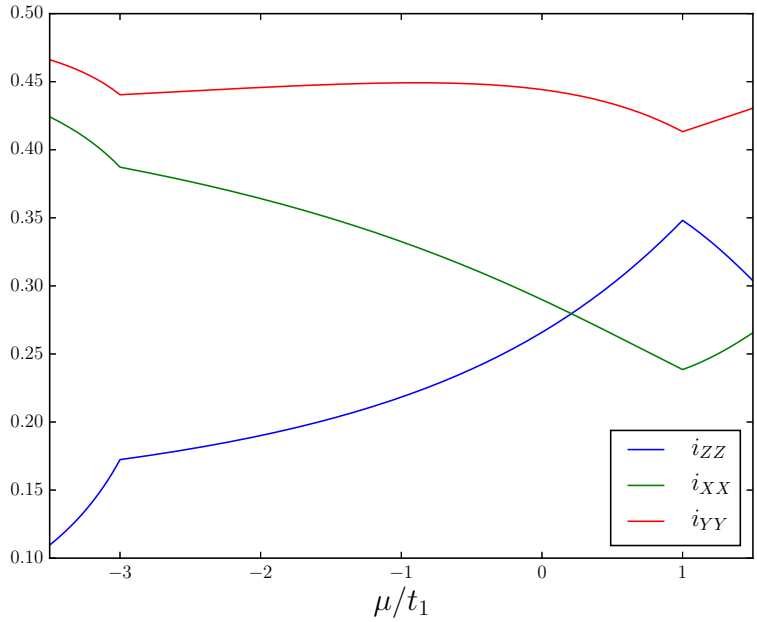

Figure 3.8: Linear coefficients to the fluctuations for the extended Kitaev model with complex Δ_2. We take $t_2 = |\Delta_2| = 0.5t_1$. Though only i_{ZZ} admits a proper representation for superconductors, we also compute i_{XX} and i_{YY} by analogy with an equivalent insulator model. At each phase transition, cusps are still present. The logarithmic coefficient $\mathbf{b}_{ZZ}$ is still quantized at the QPTs.

3.4 Bipartite fluctuations in 2D Dirac materials

As we have seen in the previous Section, bipartite fluctuations are a very useful tool to characterize the critical points of topological superconductors and insulators in one dimension. It is therefore natural to consider extensions to the corresponding 2D models. These models, such as the $p+ip$ superconductor, usually present Dirac cones at the phase transitions. In this Section, we study the behavior of the bipartite fluctuations for Dirac metals in two dimensions, considering only two-band models:

$$H_{2D} = \frac{q_e}{2} \sum_{\vec{k} \in \mathcal{BZ}} \Psi^\dagger_{\vec{k}} (\Delta^x_{\vec{k}}, \Delta^y_{\vec{k}}, \varepsilon_{\vec{k}}).\vec{\sigma} \Psi_{\vec{k}}, \tag{3.126}$$

where $\Psi_{\vec{k}}$ are the usual spinors (either superconducting or insulating) and $\varepsilon_{\vec{k}}$ and $\Delta^{x/y}_{\vec{k}}$ functions we will specify. By convention, $\varepsilon_{\vec{k}}$ is the kinetic energy.
To simplify the discussion, we will only consider charge fluctuations, but the results can be extended to any of the previously considered correlators. We note $\hat{Q}_j = \frac{q_e}{2} \Psi^\dagger_j \sigma^z \Psi_j$ the local charge operator, and $\hat{Q} = \sum_{j \in \mathcal{S}} \hat{Q}_j$.

3.4.1 Geometric shape, Kernel functions and Sobolev spaces

Before working on specific models, it is worth working on the generic kernel functions that appear in two dimensions. We have an additional freedom in the choice of our subsystem $\mathcal{A}$. We still limit ourselves to regular, connected domains that are compatible with the lattice geometries (we don't consider partial covering with holes), but we don't have to exactly respect the symmetry of the lattice.

To simplify notations, we assume a superconducting model with spinor $\Psi^\dagger_{\vec{k}} = (c^\dagger_{\vec{k}}, c_{-\vec{k}})$ in this Section. Computation of the bipartite charge fluctuations are then straightforward:

$$\mathcal{F}_{ZZ}(\mathcal{A}) = \frac{1}{S} \sum_{\vec{k},\vec{q}\in\mathcal{BZ}} \sum_{\vec{r}_1,\vec{r}_2\in\mathcal{A}} e^{i(\vec{k}-\vec{q}).(\vec{r}_1-\vec{r}_2)} \left(\mathcal{G}(\vec{k})(1-\mathcal{G}(\vec{q})) - \mathcal{D}(\vec{k})\mathcal{D}^*(-\vec{q})\right),$$

where S is the total surface of the domain, $\mathcal{G}$ ($\mathcal{D}$) the normal (anomalous) Green functions previously defined. The Kernel function that appears is then:

$$\mathcal{K}(\vec{k},\mathcal{A}) = \sum_{\vec{r}_1,\vec{r}_2\in\mathcal{A}} e^{i\vec{k}.(\vec{r}_1-\vec{r}_2)} \tag{3.127}$$

A first example: square lattice

Let us start with the simple case of a square lattice such as in the basic $p+ip$ model introduced in Section 1.6.1. Figure 3.9 presents three possible choices of $\mathcal{A}$. We consider the first case of a rectangular shape. One can factorize the Kernel such that:

$$\mathcal{K}(\vec{k},\mathcal{A}_{\text{sq}}) = \sum_{r_{x,1},r_{x,2}=1}^{l_x} e^{ik_x(r_{x,1}-r_{x,2})} \sum_{r_{y,1},r_{y,2}=1}^{l_y} e^{ik_y(r_{y,1}-r_{y,2})} = l_x l_y f_F(k_x,l_x) f_F(k_y,l_y), \tag{3.128}$$

where we have taken the lattice spacing to be 1 in any direction. The Kernel function is in this case simply the product of two Fejér Kernel in the canonic direction.

This result can be extended to any parallelogram defined by the vectors $\vec{a}$ and $\vec{b}$. If we consider geometries such as the second example in Figure where $\mathcal{A}$ is purely defined by $\{\vec{r} = n_a\vec{a} + n_b\vec{b}, 0 \le n_a < l_a, 0 \le n_b < l_b\}$, then, using a similar decomposition leads to a kernel of the form:

$$\mathcal{K}(\vec{k},\mathcal{A}_{\text{par}}) = l_a l_b f_F(\vec{k}.\vec{a},l_a) f_F(\vec{k}.\vec{b},l_b) \tag{3.129}$$

Finally, the third example is more complex. Exactly computing the lattice kernel leads to the appearance of additional terms to take into account the different sublattices. In the given example, we obtain:

$$\mathcal{K}(\vec{k},\mathcal{A}_{\text{par}}) = l_a l_b (2 + 2\cos\vec{\delta}.\vec{k}) f_F(\vec{k}.\vec{a},l_a) f_F(\vec{k}.\vec{b},l_b). \tag{3.130}$$

The additional factor appears due to the finite-size of the lattice. While it will be of importance for finite-size numerics and evaluations, it is in practice non-universal. In the following, when computing contributions from a lattice-based Hamiltonian, we will limit ourselves to the first and second examples.

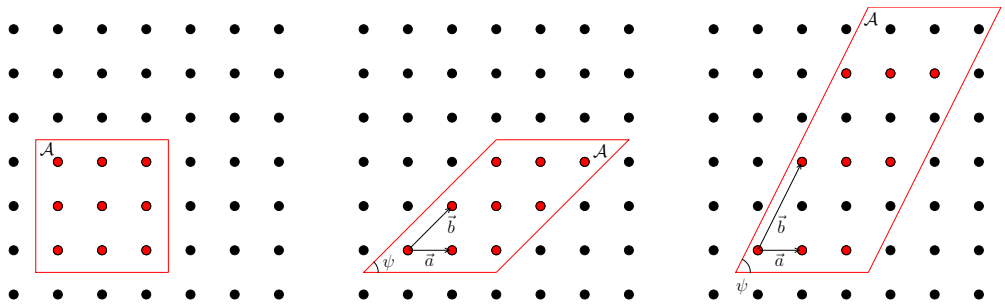

Figure 3.9: Schematics of the different possibilities for the sub-system $\mathcal{A}$. Left: $\mathcal{A}$ is simply a square sub-region of the lattice. It respects the symmetries of the model. Middle: we can also choose a parallelogram generated by the vectors $\vec{a}$ and $\vec{b}$. The area of the unit-cell they generate is one, and therefore the parallelogram is a complete cover of the lattice. We note ψ the angle between $\vec{a}$ and $\vec{b}$. Right: another possible choice for $\vec{a}$ and $\vec{b}$. The parallelogram is still well defined, but as $A_{\vec{a},\vec{b}} = 2$, all sites in $\mathcal{A}$ are not an integer linear combination of $\vec{a}$ and $\vec{b}$ (only those in red). There are corrections to the Kernel due to the finite lattice that induces a shift between the red and black sub-lattice of $\mathcal{A}$.

Beyond the square lattice

All of the previous reasoning are not significantly affected by the form of the lattice, due to the effective form we consider when the lattice and $\mathcal{A}$ do not simply match. The form of the lattice therefore only affects the global expression of the bipartite fluctuations. Taking the thermodynamic limit for an infinite system, we obtain:

$$\mathcal{F}_{ZZ}(\mathcal{A}) = \iiiint \frac{d\vec{k}d\vec{q}}{A_{\mathcal{BZ}^2}} \mathcal{K}(\vec{k}-\vec{q},\mathcal{A}) \left(\mathcal{G}(\vec{k})(1-\mathcal{G}(\vec{q})) - \mathcal{D}(\vec{k})\mathcal{D}^*(-\vec{q})\right), \tag{3.131}$$

A useful way of computing the low-energy contributions to the theory is to directly go to a continuous theory. In practice, it is more convenient and less complicated to keep the original form of $\mathcal{K}$ in this limit.

Scaling analysis

The scaling analysis in two dimensions is more complex than in one dimension. The dominant term is nonetheless still straightforward to obtain. Using the original definition of the Kernel in Eq. 3.127 or any of the subsequent lattice form, it converges to the Dirac distribution when $\mathcal{A}$ tends to cover the whole system, such that the leading coefficient is simply given by:

$$A_{\mathcal{A}} \iint_{\vec{k}\in\mathcal{BZ}} \frac{d\vec{k}}{A_{\mathcal{BZ}}} \mathcal{G}(\vec{k})(1-\mathcal{G}(\vec{k})) - \mathcal{D}(\vec{k})\mathcal{D}^*(veck), \tag{3.132}$$

where $A_{\mathcal{A}}$ is the area of $\mathcal{A}$. We still denote the coefficient i_{ZZ} as it has the same expression as the linear coefficient in one dimension:

$$i_{ZZ} = \frac{1}{S}\langle \hat{Q}^2 \rangle_c, \text{ with } \hat{Q} = \frac{q_e}{2}\sum_{\vec{r}\in\mathcal{S}} \Psi_j^\dagger \sigma^z \Psi_j \tag{3.133}$$

Discussion of the sub-dominant terms is best done using the example of the square lattice and using the Kernel form given in Eq. 3.128. Let us consider two arbitrary functions f and g and compute the "fluctuations":

$$\begin{aligned}
\langle\langle f, g\rangle\rangle &= \iiiint_{\vec{k},\vec{q}\in\mathcal{BZ}} \frac{d\vec{k}d\vec{q}}{A_{\mathcal{BZ}}^2}\mathcal{K}(\vec{k}-\vec{q})f(\vec{k})g(\vec{q}) \\
&= \sum_{n_x=-l_x}^{l_x}\sum_{n_y=-l_y}^{l_y}(l_x-|n_x|)(l_y-|n_y|)\mathcal{FT}\{f\}(n_x,n_y)\mathcal{FT}\{g\}(-n_x,-n_y) \qquad (3.134)\\
&= l_x l_y \sum_{n_x,n_y}\mathcal{FT}\{f\}(n_x,n_y)\mathcal{FT}\{g\}(-n_x,-n_y) \\
&\quad + l_x \sum_{n_x,n_y}|n_y|\mathcal{FT}\{f\}(n_x,n_y)\mathcal{FT}\{g\}(-n_x,-n_y) \\
&\quad + l_y \sum_{n_x,n_y}|n_x|\mathcal{FT}\{f\}(n_x,n_y)\mathcal{FT}\{g\}(-n_x,-n_y) \\
&\quad + \sum_{n_x,n_y}|n_x||n_y|\mathcal{FT}\{f\}(n_x,n_y)\mathcal{FT}\{g\}(-n_x,-n_y) \qquad (3.135)
\end{aligned}$$

The analogy with the one-dimensional case is direct. We consider diagonal terms $\langle\langle f, f\rangle\rangle$ for ease of notations. For gapped phases, the Green functions decrease exponentially and all four sums in Eq. 3.135 therefore converge, and we trivially obtain:

$$\langle\langle f, f\rangle\rangle = i_f l_x l_y + c_x l_x + c_y l_y + \mathcal{O}(1) = i_f A_{\mathcal{A}} + c_f R_{\mathcal{A}} + \mathcal{O}(1), \tag{3.136}$$

where $R_{\mathcal{A}}$ is a characteristic length of the region $\mathcal{A}$ (usually the perimeter). Contribution to c_f can arise both from finite-sum corrections to the first sum, and directly from the second and third summation. It is therefore non-universal.

For gapless Hamiltonians, singularities can appear in the different Green functions for the gap-closing momenta. Let us define the Fermi surface as the manifold $\delta\Gamma = \{\vec{k} \in \mathcal{BZ}, E_{\vec{k}} = 0\}$, where $E_{\vec{k}}$ is the energy of the quasi-particle with momentum $\vec{k}$. Depending on its dimensions and the order of singularities, $\mathcal{FT}\{f\}(\hat{n})$ will converge at different speed, and therefore the scaling laws will change.

For $\delta\Gamma$ of dimension 1 (free fermions for example), Green functions will usually exhibit discontinuities on the one-dimensional manifold. We will therefore have $|\mathcal{FT}\{f\}(\vec{n})|^2 = O(||\vec{n}||^{\frac{3}{2}})$. This in turn leads to sub-dominant scaling terms such that:

$$\langle\langle f, f\rangle\rangle = i_f A_{\mathcal{A}} + b_f l_{\mathcal{A}} \ln l_{\mathcal{A}} + \mathcal{O}(l_{\mathcal{A}}), \tag{3.137}$$

which have been observed for free fermions[136]. This $l \ln l$ scaling term is also found in the entanglement entropy for such models as was explained in Chapter 2[76–79].

For the models we are interested in, $\delta\Gamma$ consists only in a finite number of points. There will only be point-like singularities, that are not always removable. Then the Green functions will behave such that to $|\mathcal{FT}\{f\}(\vec{n})||^2 = O(||\vec{n}|^2)$. Then the fourth sum may give rise to logarithmic discontinuities[6] such that the scaling laws will be:

$$\langle\langle f, f\rangle\rangle = i_f A_{\mathcal{A}} + c_f R_{\mathcal{A}} + \mathbf{b}_f \ln l_{\mathcal{A}} + \mathcal{O}(1), \tag{3.138}$$

In both cases, the scaling laws are, except for the eventual dominant area term, identical to the scaling laws of the vNEE in such systems. By analogy, we will be most interested by the logarithmic coefficient $\mathbf{b}_f$. We will also look at the dominant scaling term.

All this discussion can be reformulated in more mathematical terms with the Hilbert-Sobolev spaces. We have rephrased the discussion in Appendix C for the more mathematically inclined readers. A complete categorization of the singularities that appear in the correlation functions, as a function of the different types of Fermi surface and in this language would be an interesting pursuit, if possible.

3.4.2 Fluctuations for a single isotropic Dirac cone

We start our study by the example of a gapless phase with a single Dirac cone through the example of the $p+ip$ superconductor. The basic two-band Hamiltonian is given by:

$$H_{2D} = \frac{q_e}{2} \sum_{\vec{k}\in\mathcal{BZ}} \Psi^\dagger_{\vec{k}}(\Delta^x_{\vec{k}}, \Delta^y_{\vec{k}}, \varepsilon_{\vec{k}}).\vec{\sigma}\Psi_{\vec{k}},$$

This model is in the D class: if there is only one Dirac cone, due to the PHS, it can only be at one of the four symmetric momenta $(0/\pi, 0/\pi)$ and is partially protected. We will consider a gap potentially closing at $\vec{k} = (0,0)$ in the following (corresponding to the $\mu = -4t$ for $p+ip$). Indeed, close to these points, the PHS guarantees that both Δ^x and Δ^y are odd, while $\varepsilon_{\vec{k}}$ is even. Except at multi-critical points, we can expect

$$\varepsilon_{\vec{k}} \approx v_x k_x^2 + v_y k_y^2 + v_{xy} k_x k_y,\ \Delta^{x/y}_{\vec{k}} = \Delta^{x/y}_x k_x + \Delta^{x/y}_y k_y.$$

This dispersion relation enforces the continuity and regularity of $\theta_{\vec{k}}$ in $\vec{k} = 0$ (and $\theta_{\vec{0}} = \frac{\pi}{2}$), while $\phi_{\vec{k}}$ can be singular. For the $p+ip$ superconductor, we have:

$$\phi_{\vec{k}} = \mathrm{Arg}(\Delta_x k_x + i\Delta_y k_y) \tag{3.139}$$

In this Section, we will mostly focus on the isotropic case $\Delta^x_x = \Delta^y_y = \Delta > 0$, $v_x = v_y > 0$ and $\Delta^y_x = \Delta^x_y = v_{xy} = 0$, which leads to the simple expression $\phi_{\vec{k}} \approx \mathrm{Arg}(k_x + ik_y)$ close to $\vec{0}$. $\phi_{\vec{k}}$ has a non-resolvable singularity in $\vec{0}$, corresponding to the vortex texture of the Dirac cone.
Finally, we recall the expression of the bipartite charge fluctuations for such a system:

$$\mathcal{F}_{ZZ}(\mathcal{A}) = \frac{q_e}{4} \iiiint \frac{d\vec{k}d\vec{q}}{A_{\mathcal{BZ}^2}} \mathcal{K}(\vec{k}-\vec{q}, \mathcal{A}) \left(1 - \cos\theta_{\vec{k}}\cos\theta_{\vec{q}} + e^{i(\phi_{\vec{k}}-\phi_{\vec{q}})}\sin\theta_{\vec{k}}\sin\theta_{\vec{q}}\right), \tag{3.140}$$

We start by considering the case of the square lattice and then proceed to an extension to any lattice as a conclusion.

[6] For completeness, we point out that logarithmic terms could appear from the finite-sum corrections of the first three sums. In practice, it is not the case for Dirac fermions.

Area law

Let us start with the computation of the area coefficient. Whether at the critical point or in one of the two gapped phases, the linear coefficient has the simple expression:

$$i_{ZZ} = \frac{1}{S}\langle \hat{Q}^2 \rangle_c = \frac{q_e}{2} \iint\limits_{k\in\mathcal{BZ}} \frac{d\vec{k}}{A_{\mathcal{BZ}}} \sin^2\theta_{\vec{k}} \tag{3.141}$$

i_{ZZ} still corresponds to the Quantum Fisher information associated to the charge $\hat{Q}$. It is therefore bounded for non-interacting systems by $\frac{q_e}{2}$. The exact computation is more difficult even in the simpler case of the $p+ip$ superconductor, and Figure 3.10 presents numerical computations of the area coefficient close to the phase transition. By opposition to what was obtained in one dimension, there is no cusp at the phase transition: the derivative of i_{ZZ} is continuous and its only the second-derivative that has a weak logarithmic divergence. The transition is therefore of higher order and the QFID is less efficient in detecting the QCP. This should not come as a surprise: as the Fermi surface is still reduced to a point while the physical dimension has increased, singularities in the thermodynamic quantities must be of higher order. Similar results were observed for the compressibility and other quantities linked to the thermodynamic potential[167].

Let us present a short proof of this result. We focus on transitions driven by a chemical potential μ. Close to $\vec{k} = \vec{0}$, due to the isotropy, we can approximate the low-energy contribution to i_{ZZ} to be

$$i_{ZZ} = \frac{q_e}{2}\int\limits_0^\Lambda k\frac{dk}{2\pi}\frac{\Delta^2 k^2}{\delta\mu^2+\Delta^2k^2} = -\frac{q_e}{16\pi}\delta\mu^2\ln\delta\mu + f(\Lambda), \tag{3.142}$$

where Λ is a momentum cut-off to regularize the integral and isolate the $\vec{k}=0$ contribution, and $\delta\mu$ the effective chemical potential such that the QPT occurs at $\delta\mu = 0$. The second derivative of i_{ZZ} indeed presents a logarithmic divergence. Note that this proof can be generalized to any dimension. If we didn't use it in one dimension, it is because it is less well-controlled in odd dimensions. As a general result, we obtain that for a point-like isotropic closing of the gap in physical dimension d, the dth derivative of the QFID is discontinuous if d is odd, while it diverges logarithmically for even d .

Logarithmic coefficient for rectangular $\mathcal{A}$

As a first step, we can compute the logarithmic contributions that appear when considering a rectangular subsystem $\mathcal{A}$. By analogy with the entropy, we expect a non-zero coefficient as $\mathcal{A}$ has corners. As θ_k is perfectly regular even for a gapless point, logarithmic contributions in Eq. 3.140 can only arise from:

$$\frac{q_e}{4}\iiiint \frac{d\vec{k}d\vec{q}}{A_{\mathcal{BZ}^2}}\mathcal{K}(\vec{k}-\vec{q},\mathcal{A})e^{i(\phi_{\vec{k}}-\phi_{\vec{q}})}\sin\theta_{\vec{k}}\sin\theta_{\vec{q}}.$$

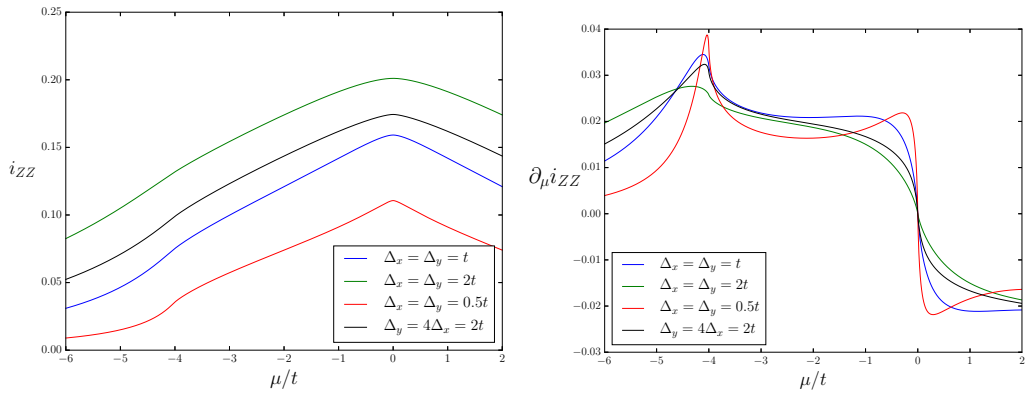

Figure 3.10: QFID (left) and its derivative (right) for the $p + ip$ superconductor as a function of μ/t for several choices of Δ_x and Δ_y. Phase transitions occurs at $\mu = -4t$ and $\mu = 0$. Each time, there is a logarithmic divergence of the second derivative, which marks quite clearly the phase transition.

We pose $f(\vec{k}) = e^{i\phi_{\vec{k}}} \sin\theta_{\vec{k}}$, and as in one dimension we introduce the test function $h(\vec{k})$ such that $f - h$ is regular. For the previously defined isotropic Dirac cone, we can define

$$h(\vec{k}) = \begin{cases} \frac{k_x+ik_y}{\sqrt{k_x^2+k_y^2}}(1 - \sqrt{k_x^2 + k_y^2}) = \frac{z}{|z|}(1 - |z|) \text{ if } |z| < 1 \\ 0 \text{ else.} \end{cases} \tag{3.143}$$

$(1 - |z|)$ play the role of a regularizing smooth cut-off. We directly generalize the test function to the family $h_{m,j}(z) = \frac{z^m}{|z|^m}(1 - |z|^j)$ that describes and regularizes isotropic Dirac cones of any topological charge m[7]. j checks that the dominant logarithmic term is not affected by the introduced cut-off. Note that for D class Hamiltonians, the PHS impose odd m. Let us define the vector $\vec{n} = (n_x, n_y) = (n = \sqrt{n_x^2 + n_y^2}, \theta_{\vec{n}})$ and compute

[7]The name Dirac cone for a winding number $|m| > 1$ may be a bit abusive. The more natural way to get such a model is to have $\Delta_k^x + i\Delta_k^y = (k_x + ik_y)^m$ for $m > 0$, and the complex conjugate otherwise. As long as ε_k vanishes faster than $||\vec{k}||^m$, our computation of the logarithmic coefficient stands. Obviously, the cone is parabolic (or of higher degree), and not linear. On the other hand, mathematically we can always take $\Delta_k^x + i\Delta_k^y = \frac{(k_x+ik_y)^m}{|k_x+ik_y|^{m-1}}$ and formally get a linear dispersion of the energy, especially for m odd where the denominator is a simple polynomial.

the exact Fourier transform:

$$\begin{aligned}\mathcal{FT}\{h_{m,j}\}(\vec{n}) &= \iint\limits_{[-\pi,\pi]^2} \frac{d\vec{k}}{4\pi^2} h_{m,j}(\vec{k}) e^{-i\vec{n}.\vec{r}} = \frac{1}{4\pi^2} \int\limits_0^1 k(1-k^j)dk \int\limits_{-\pi}^{\pi} d\theta e^{im\theta} e^{-ink\cos(\theta-\theta_{\vec{n}})} \\ &= \frac{e^{im(\theta_{\vec{n}}-\frac{\pi}{2})}}{2\pi} \int\limits_0^1 k(1-k^j) J_m(kn)dk \\ &= \frac{e^{im(\theta_{\vec{n}}-\frac{\pi}{2})}}{\pi 2^{m+2}} n^m \Big(\Gamma(1+\frac{m}{2}) {}_1\tilde{F}_2(1+\frac{m}{2}, 2+\frac{m}{2}, 1+m, -\frac{n^2}{4}) \\ &\qquad - \Gamma(1+\frac{j}{2}+\frac{m}{2}) {}_1\tilde{F}_2(1+\frac{j}{2}+\frac{m}{2}, 2+\frac{j}{2}+\frac{m}{2}, 1+m, -\frac{n^2}{4}) \Big)\end{aligned} \tag{3.144}$$

where J_m is the Bessel function of the first kind, and ${}_1\tilde{F}_2$ is the Hypergeometric PFQ Regularized function. The large n behavior can be obtained after an asymptotic expansion of the ${}_1\tilde{F}_2$ function:

$$\mathcal{FT}\{h_{m,j}\}(\vec{n}) = \frac{m e^{im(\theta_{\vec{n}}-\frac{\pi}{2})}}{2\pi} \frac{1}{n_x^2+n_y^2} + \mathcal{O}(n^{-5/2}) \text{ for all } j \tag{3.145}$$

The supplementary term oscillates regularly. We then evaluate the four sums:

$$l_x l_y \sum_{n_x>l_x, n_y>l_y} \frac{1}{(n_x^2+n_y^2)^2} \approx \frac{l_x^2(\frac{\pi}{2}-\arctan(\frac{l_x}{l_y})) + l_y^2(\frac{\pi}{2}-\arctan(\frac{l_y}{l_x})) - 2l_x l_y}{4 l_x l_y} \approx \mathcal{O}(1) \tag{3.146}$$

$$l_x \sum_{n_x>l_x, n_y>l_y} \frac{n_y}{(n_x^2+n_y^2)^2} \approx \frac{l_x}{2l_y}(\frac{\pi}{2} - \arctan(\frac{l_x}{l_y})) \approx \mathcal{O}(1) \tag{3.147}$$

$$\sum_{n_x<l_x, n_y<l_y} \frac{n_x n_y}{(n_x^2+n_y^2)^2} \approx \frac{1}{4} \ln\left(\frac{l_x^2 l_y^2}{l_x^2+l_y^2}\right), \tag{3.148}$$

and indeed obtain that only the last sum is divergent, and it diverges logarithmically. The logarithmic term appearing in the BCF in a 2D Dirac metal with a single cone for a square lattice and a rectangular subsystem is therefore:

$$\frac{q_e m^2}{8\pi^2} \ln \frac{l_x l_y}{\sqrt{l_x^2+l_y^2}} \tag{3.149}$$

For isotropic cones, measure of the fluctuations directly gives the winding number of the cone, up to a sign. The charge correlation functions scale as:

$$\langle \hat{Q}_{\vec{r}} \hat{Q}_{\vec{r'}} \rangle_c = q_e \frac{m^2}{16\pi^2} \frac{1}{|\vec{r}-\vec{r'}|^4} + o(\frac{1}{|\vec{r}-\vec{r'}|^4}) \tag{3.150}$$

Corner functions

By analogy with the vNEE, we expect that the coefficient of the logarithmic term is actually a function of the corners of $\mathcal{A}$. Let $a_{\hat{Q}}$ be this corner function. In the previous section, we computed the coefficient appearing for a square region $\mathcal{A}$, therefore given by $4a(\frac{\pi}{2})$. We here derive the exact corner function by considering successively a parallelogram, then a quadrant, to obtain

$$a(\psi) = 1 + (\pi - \psi)\cot\psi. \tag{3.151}$$

The corner function of the BCF is equal to the corner function that appear in the entropy in the EMIm, but not to the one of Dirac fermions. Finally, we can compute the ratio between the logarithmic coefficient of the vNEE and the one of the fluctuations. In the limit $\psi \to 0$, one obtains:

$$\frac{\mathbf{b}_{vNEE}}{\mathbf{b}_{\hat{Q}}} = -\frac{3}{4}\pi^2, \tag{3.152}$$

which differs from the result for Fermi gases in Eq. 2.64. Note that we recover, as in one dimension, that the coefficients have opposite signs.

Logarithmic coefficient for a parallelogram

A first step towards computing the corner functions that appear in the BCF, and to verify that they are non-trivial, is to compute the fluctuations on a parallelogram. We take $\mathcal{A}$ to be defined by

$$\vec{r} \in \mathcal{A} \Leftrightarrow \vec{r} = n_a\vec{a} + n_b\vec{b},\ 0 \leq n_a < l_a,\ 0 \leq n_b < l_b$$

If the area of the unit-cell parallelogram generated by $\vec{a}$ and $\vec{b}$ is equal to the area of the lattice unit-cell, it is a proper sub-cover of the lattice (it has no hole). We will proceed nonetheless to a generic computation, as we will be able to simply get rid of the finite-lattice contributions. We note ψ the angle between the two vectors. The coefficient of the logarithmic term should therefore be given by $\tilde{a}(\psi) = 2a(\psi) + 2a(\pi - \psi)$.
Using the definition of the Kernel, fluctuations require the computations of

$$\langle\langle f, g\rangle\rangle = \sum_{n_a=-l_a}^{l_a}\sum_{n_b=-l_b}^{l_b}(l_a - |n_a|)(l_b - |n_b|)\mathcal{FT}\{f\}(n_a, n_b)\mathcal{FT}\{g\}(-n_a, -n_b) \tag{3.153}$$

$$\text{with } \mathcal{FT}\{f\}(n_a, n_b) = \iint_{\vec{k}\in\mathcal{BZ}} \frac{d\vec{k}}{A_{\mathcal{BZ}}} f(\vec{k}) e^{-i\vec{k}.(n_a\vec{a}+n_b\vec{b})}. \tag{3.154}$$

In other words, going from a square to a parallelogram corresponds to a change of basis for the Fourier transform. Note that as $\mathcal{A}$ is a sub-lattice of the total lattice, $f(\vec{k})$ has the proper periodicity. We can proceed as usual and compute the change in the main Fourier contribution. The square norm of $(n_a\vec{a} + n_b\vec{b})$ is simply $(n_a^2||\vec{a}||^2 + n_b^2||\vec{b}||^2 + 2n_an_b\vec{a}.\vec{b})$. Noting $\theta_{\vec{n}}$ its polar angle, computations lead to

$$\mathcal{FT}\{h_{m,j}\}(n_a, n_b) = \frac{me^{im(\theta_{\vec{n}}-\frac{\pi}{2})}}{2\pi}\frac{1}{n_a^2|\vec{a}|^2 + n_b^2|\vec{b}|^2 + 2n_an_b\vec{a}.\vec{b}} + ... \tag{3.155}$$

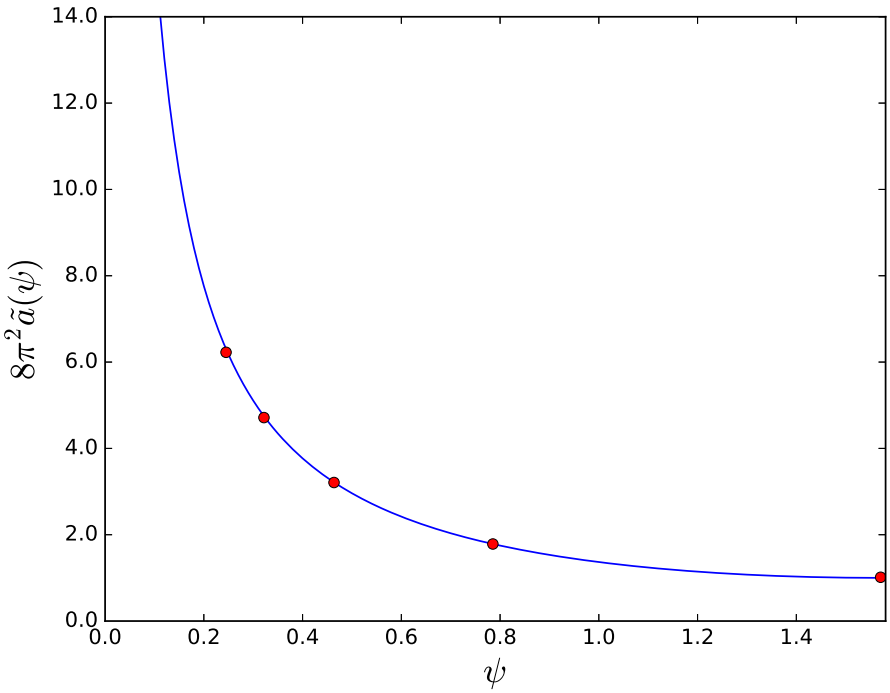

Figure 3.11: Normalized corner function appearing for a parallelogram $\tilde{a}$. The red points correspond to finite-size simulations of the $p+ip$ superconductor at $\mu = -4t$ and $\Delta_x = \Delta_y$. The simulations were realized for subsystems of up to $200\frac{\tan\psi}{1+\tan\psi} \times 200\frac{\tan\psi}{1+\tan\psi}$ sites for a quasi-infinite square lattice (around 500 million sites).

We then only need to evaluate the four sums. We define $\vec{a}.\vec{b} = ||\vec{a}||||\vec{b}||\cos\psi$, and take ψ in $]0,\pi[$. The first two still give constant contributions while the last one gives:

$$\frac{1}{|\vec{a}|^2|\vec{b}|^2}\left(\frac{1}{\sin^2\psi} + \frac{\cot\psi}{\sin^2\psi}(\frac{\pi}{2}-\psi)\right)\ln\left(\frac{l_a^2 l_b^2}{\sqrt{(l_a^2+l_b^2+2\cos\psi l_a l_b)(l_a^2+l_b^2-2\cos\psi l_a l_b)}}\right)$$
$$= \frac{1+(\frac{\pi}{2}-\psi)\cot\psi}{A^2_{\vec{a},\vec{b}}}\ln\left(\frac{l_a^2 l_b^2}{\sqrt{(l_a^2+l_b^2+2\cos\psi l_a l_b)(l_a^2+l_b^2-2\cos\psi l_a l_b)}}\right), \quad (3.156)$$

where $A_{\vec{a},\vec{b}}$ is the area of the unit-cell parallelogram. Getting the continuous limit contribution (and getting rid of any finite-lattice effect) is therefore as simple as fixing $A_{\vec{a},\vec{b}} = 1$. The logarithmic contribution for a parallelogram is:

$$\frac{q_e m^2\tilde{a}(\psi)}{64\pi^2}\ln\left(\frac{l_a^2 l_b^2}{\sqrt{(l_a^2+l_b^2+2\cos\psi l_a l_b)(l_a^2+l_b^2-2\cos\psi l_a l_b)}}\right) \quad (3.157)$$

with

$$\tilde{a}(\psi) = 4 + 4(\frac{\pi}{2}-\psi)\cot\psi$$

$\tilde{a}(\psi)$ does not match the expression one would obtain for the vNEE for Dirac fermions on $\mathcal{A}$, but corresponds to the one obtained in the Extensive Mutual Information model. It is represented in Figure 3.11.

Single corner function

To get the contribution of a single corner, we compute the BCF in the continuous limit on $\mathcal{A}(\psi)$ defined in Figure 3.12 as a quadrant of the disk of radius R, and of angle ψ. The obtained logarithmic contribution is the sum of $a(\psi) + 2a(\frac{\pi}{2})$. Substraction of $\tilde{a}$ gives the proper corner function. Computation of the BCF requires the evaluation of:

$$\langle\langle f, f\rangle\rangle = \frac{q_e}{4} \sum_{\vec{r},\vec{r}'\in\mathcal{R}^2} \frac{1}{S^2} \sum_{\vec{k},\vec{q}\in\mathcal{BZ}^2} e^{i\vec{k}.(\vec{r}-\vec{r}')} e^{-i\vec{q}.(\vec{r}-\vec{r}')} f(\vec{k})\overline{f}(\vec{q}) \tag{3.158}$$

$$= \frac{q_e}{4} \sum_{\vec{r},\vec{r}'\in\mathcal{R}^2} |\mathcal{FT}\{f\}(\vec{r}-\vec{r}')|^2, \tag{3.159}$$

where $\mathcal{R}$ is the observed zone. We use the ansatz

$$\mathcal{FT}\{f\}(\vec{r}) = \frac{m}{2\pi} \frac{1}{(e^2 + |\vec{r}|^2)}, \tag{3.160}$$

where e is a cut-off length that does not affect the vortex in $\vec{k} = 0$. The ansatz has the proper long-range behavior for a vortex of winding number m. The fluctuations scale as:

$$\langle\langle f, f\rangle\rangle = i_f \frac{\psi}{2} R^2 + c_f R + (a(\psi) + 2a(\frac{\pi}{2})) \ln R + \mathcal{O}(1) \tag{3.161}$$

Instead of directly computing the integral, we evaluate $\partial_R \partial_\psi \langle\langle f, f\rangle\rangle \approx i_f R + \frac{1}{R}\partial_\psi a(\psi)$. Lengthy computations lead to

$$\partial_R \partial_\psi \langle\langle f, f\rangle\rangle = \frac{1}{4\pi^2} \int_0^R \int_0^\psi dr d\theta \frac{rR}{(e^2 + R^2 + r^2 - 2rR\cos(\theta - \psi))^2} \tag{3.162}$$

$$= \frac{R^2}{16\pi^2 e^2} \times (\frac{\psi}{R} - \frac{2e}{R\sqrt{e^2 + 4R^2}} \arctan(\sqrt{1 + 4\frac{R^2}{e^2}} \tan \psi/2)$$
$$+ \frac{2\sqrt{2}\sin(\psi)}{\sqrt{2e^2 + R^2 - R^2\cos(2\psi)}} \left(\arctan \frac{\sqrt{2}R\cos\psi}{\sqrt{2e^2 + R^2 - R^2\cos(2\psi)}} \right.$$
$$\left. + \arctan \frac{\sqrt{2}R(1 - \cos\psi)}{\sqrt{2e^2 + R^2 - R^2\cos(2\psi)}} \right)) \tag{3.163}$$

Extraction of either the cut-off independent contribution, or of the $\frac{1}{R}$ coefficient in the $R \to +\infty$ limit allows us to identify the derivative of the corner function. The pre-factor of the $\frac{1}{R}$ coefficient is:

$$\frac{1}{32\pi^2}\partial_\psi a(\psi) = \frac{1}{32\pi^2}(-\cot\psi + (\pi - \psi\cot^2\psi)) \tag{3.164}$$

$$\text{leading to } a(\psi) = (\pi - \psi)\cot\psi + Cst \tag{3.165}$$

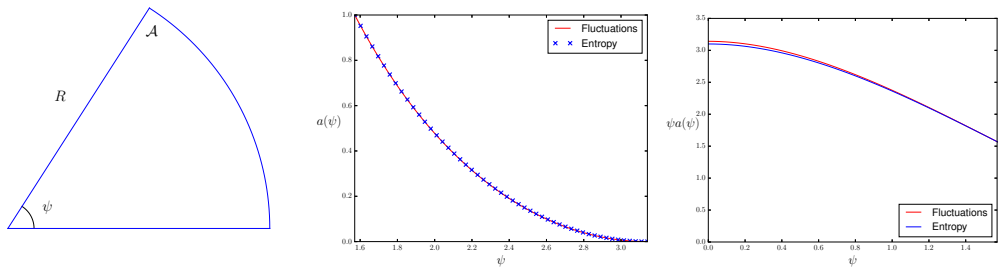

Figure 3.12: Left: form of the subsytem $\mathcal{A}$ used to determine the single-corner contribution. Middle: corner function of the fluctuations and of the entropy for Dirac fermions. We have normalized the latter such that $a(\frac{\psi}{2}) = 1$. Right: $\psi \times a(\psi)$ for the fluctuations and entropy of Dirac fermions with the same normalization. It is only at very small angle that there is a significant difference.

Finally, either using $a(\frac{\pi}{2}) = 1$ or by performing a numerical regression, one obtains the exact corner function for the BCF:

$$a(\psi) = 1 + (\pi - \psi)\cot\psi \tag{3.166}$$

which corresponds to the corner function that arises in the vNEE of the Extensive Mutual Information model in two dimensions. The contribution to the BCF of a corner ψ is therefore:

$$\frac{q_e m^2 a(\psi)}{32\pi^2}\ln R = \frac{q_e m^2 (1 + (\pi - \psi)\cot\psi)}{32\pi^2}\ln R, \tag{3.167}$$

where R will be a characteristic length of the considered subsystem $\mathcal{A}$. For a smooth boundary, there are no logarithmic contributions.

Extensivity and corner functions

The fact that the corner functions of the BCF and of the vNEE of the EMIm are identical is an interesting property. We postulate that this equality is the simple consequence of the extensivity of the BCF and the underlying CFT. Indeed, the mutual fluctuations we introduced in Section 3.1.1 are always extensive.

Comparison with the vNEE

For Fermi gases, a universal ratio exists between the dominant coefficient of the charge fluctuations and the vNEE (and all Renyi entropies). We can check that this ratio is no longer valid for the sub-dominant conformal logarithmic terms. First, as the corner functions differ, it is a priori impossible to get a constant ratio. There are, though, several limits one could consider (namely $\psi \to 0, \frac{\pi}{2}, \pi$). Using the values given in Ref. [88, 94], the different ratio are presented in Table 3.5. These ratios differ from Eq. 2.64, and the dependency in the degree of the Renyi entropy is also different.

where $\mathbf{b}_{2/3/4}$ is the logarithmic coefficient of the second/third/fourth Renyi entropies, and we have taken $|m| = 1$.

ψ	$\alpha = 1$	$\alpha = 2$	$\alpha = 3$	$\alpha = 4$
0	7.26	4.75	4.09	3.79
$\frac{\pi}{2}$	7.36	4.73	4.05	3.74
π	$\frac{3}{4}\pi^2$	$\frac{3}{2}\pi$	$\frac{20}{9\sqrt{3}}\pi$	$\frac{1+6\sqrt{2}}{8}\pi$

Table 3.5: Ratio between logarithmic contributions in the von Neumann ($\alpha = 1$) and the first Renyi entropies and the bipartite fluctuations $-\frac{\mathbf{b}_{\mathcal{S}_{\mathcal{R},\alpha}}(\psi)}{\mathbf{b}_{\hat{Q}}}$ for a single Dirac cone with winding number ± 1, for the three angles 0, $\frac{\pi}{2}$ and π. No simple relation of the form given in Eq. 2.64 emerges at any of these angles.

Generalization to any lattice

The generalization to any lattice is straightforward once the discrete-lattice effects have been eliminated.
The QFID is not affected as we kept the normalization in function of the Brillouin Zone area. Singularities at the QPT are renormalized by the factor $\frac{4\pi^2}{A_{\mathcal{BZ}}}$ as the low-energy behavior is not affected by the shape of the Brillouin Zone.
The logarithmic contribution is not affected. First, each of the Fourier coefficient is renormalized by $\frac{4\pi^2}{\mathcal{A}_{\mathcal{BZ}}}$. In a second time, the area of a unit-cell of the real-space lattice also changes. Taking both effects into account, the logarithmic coefficient is given by:

$$\frac{q_e m^2 a(\psi)}{32\pi^2} \times \left(\frac{4\pi^2}{A_{\mathcal{BZ}}}\right)^2 \times \frac{1}{A^2_{\vec{a},\vec{b}}}, \tag{3.168}$$

where $\vec{a}$ and $\vec{b}$ are vectors generating the lattice. As $A_{\mathcal{BZ}} A_{\vec{a},\vec{b}} = 4\pi^2$, the logarithmic contribution is lattice-independent:

$$\frac{q_e m^2 a(\psi)}{32\pi^2} \tag{3.169}$$

3.4.3 Beyond the single isotropic Dirac cone

In this section, we extend the results beyond the isotropic Dirac cone. To simplify notations, we will only consider models based on a square lattice in computations, but all results are straightforwardly extended to any lattice.

Anisotropies and topological invariant

The first natural extension is to consider an anisotropic Dirac cone. In the $p + ip$ superconductor for example, there is no reason to restrict ourselves to $\Delta^x = \Delta^y$. While it enforces an additional rotational symmetry, it does not change the phase diagram and the topological classification of the phases. One can actually treat the general case given by:

$$\Delta^x_{\vec{k}} \approx \Delta^x_x k_x + \Delta^x_y k_y, \ \Delta^y_{\vec{k}} \approx \Delta^y_x k_x + \Delta^y_y k_y \tag{3.170}$$

close to the Dirac cone. We still consider a quadratic $\varepsilon_{\vec{k}}$. Let us define the transformation:

$$R = \begin{pmatrix} \Delta_x^x & \Delta_y^x \\ \Delta_x^y & \Delta_y^y \end{pmatrix}, \qquad R^{-1} = \frac{1}{J}\begin{pmatrix} \Delta_y^y & -\Delta_y^x \\ -\Delta_x^y & \Delta_x^x \end{pmatrix} \text{ and } J = \det(R) = \Delta_x^x\Delta_y^y - \Delta_y^x\Delta_x^y$$

The winding number of the Dirac cone is $\mathrm{sign}(J)$. When it cancels, the winding is indeed 0 and there are no logarithmic contributions. The logarithmic contribution to the BCF is captured by the test function:

$$h_R(\vec{k}) = \frac{\Delta_x^x k_x + \Delta_y^x k_y + i(\Delta_x^y k_x + \Delta_y^y k_y)}{|\Delta_x^x k_x + \Delta_y^x k_y + i(\Delta_x^y k_x + \Delta_y^y k_y)|}\tilde{h}_R(\vec{k}), \tag{3.171}$$

where $\tilde{h}_R$ is a smooth, arbitrary cut-off function with $\tilde{h}_R(0) = 1$. We then compute the Fourier transform of h_R.

$$\begin{aligned}\mathcal{FT}\{h_R\}(\vec{n}) &= \iint_{\vec{k}\in\mathcal{BZ}} \frac{d\vec{k}}{A_{\mathcal{BZ}}} h(\vec{k}) e^{-i\vec{k}.\vec{n}} \\ &= \frac{1}{|J|}\iint_{\vec{k}'\in R(\mathcal{BZ})} \frac{d\vec{k}'}{A_{\mathcal{BZ}}} \frac{k'_x + ik'_y}{|k'_x + ik'_y|}\tilde{h}_R(R^{-1}(\vec{k}')) e^{-i\vec{k}'.{}^tR^{-1}\vec{n}}\end{aligned}$$

R is a smooth transformation, so we can take $\tilde{h}$ such that $\tilde{h}_R(R^{-1}(\vec{k}')) = 1 - |\vec{k}'|$ and we recover:

$$\mathcal{FT}\{h_R\}(\vec{n}) \approx \frac{e^{i(\theta_{{}^tR^{-1}\vec{n}} - \frac{\pi}{2})}}{2\pi|J|}\frac{1}{|{}^tR^{-1}\vec{n}|^2} + ... \tag{3.172}$$

If R is an orthogonal transformation, the logarithmic coefficient is consequently not affected by the transformation ($|J| = 1$ and $|{}^tR^{-1}\vec{n}|^2 = |\vec{n}|^2$). It is expected: such a transformation is equivalent to a simple change of basis in the Pauli matrices basis, and should not affect the charge fluctuations.

More general transformations deform the corner functions as they locally change the metric and angles. Moreover, as anisotropies appear, the corner function becomes also function of the direction of the region $\mathcal{A}$. The most convenient form to recover the coefficient is:

$$\begin{aligned}\sum_{\vec{r}_1,\vec{r}_2\in\mathcal{A}} \iint_{\vec{k}\in\mathcal{BZ}} \frac{d\vec{k}}{A_{BZ}} e^{i\vec{k}.(\vec{r}_1-\vec{r}_2)} h_R(\vec{k}) &= \sum_{\vec{r}_1,\vec{r}_2\in\mathcal{A}} \iint_{\vec{k}\in R(\mathcal{BZ})} \frac{d\vec{k}}{|J|A_{BZ}} e^{i\vec{k}.{}^tR^{-1}(\vec{r}_1-\vec{r}_2)} h_R(R^{-1}\vec{k}) \\ &= \sum_{\vec{r}_1,\vec{r}_2\in{}^tR^{-1}(\mathcal{A})} \iint_{\vec{k}\in R(\mathcal{BZ})} \frac{d\vec{k}}{|J|A_{BZ}} e^{i\vec{k}.(\vec{r}_1-\vec{r}_2)} h_R(R^{-1}\vec{k})\end{aligned}$$

One directly sees that deformations of the cone are equivalent to deformations of the region $\mathcal{A}$. Note that the transformation R cannot make new angles appear: the contribution still arise from the original angles, but is renormalized. We give two examples.

- Pure anisotropic dilatation: $\Delta_y^x = \Delta_x^y = 0$ and $\Delta_y^y = \alpha\Delta_x^x$, $\alpha > 0$. Let us consider $\mathcal{A}$ a parallelogram define by $\vec{a} = |a|(\cos\theta, \sin\theta)$ and $\vec{b} = |b|(\cos(\theta+\psi), \sin(\theta+\psi))$, with

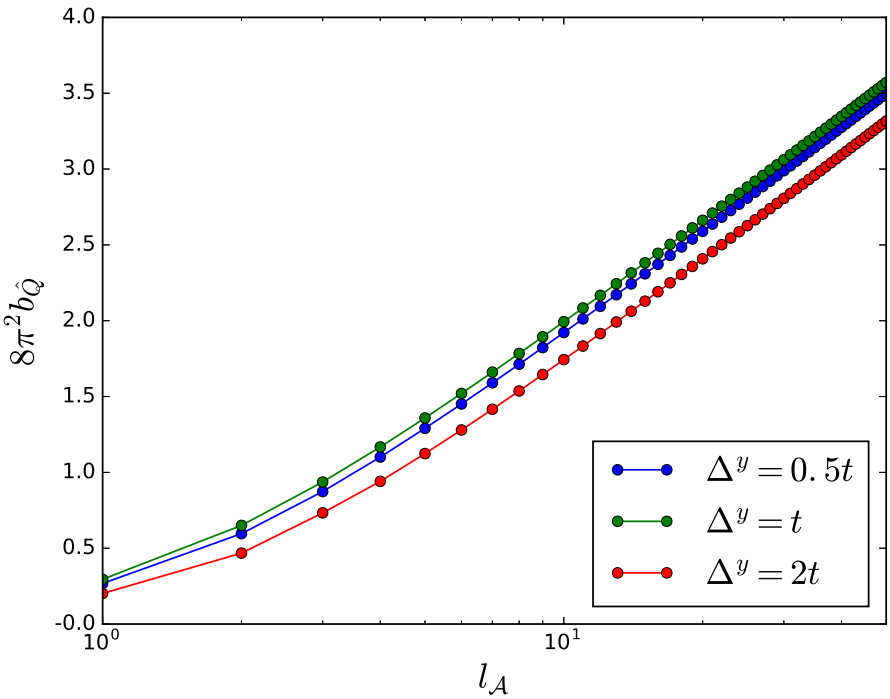

Figure 3.13: Fourth contribution (source of the logarithmic term) in the $p+ip$ superconductor for several values of Δ^y and $\Delta^x = t$ at the critical point $\mu = -4t$. The long range behavior is independent of the anisotropy when considering an aligned square sub-system $\mathcal{A}$. $l_{\mathcal{A}}$ is here the length of the side of $\mathcal{A}$. We recover the predicted coefficient.

ψ in $[0, \frac{\pi}{2}]$. Then the angle between ${}^tR^{-1}\vec{a}$ and ${}^tR^{-1}\vec{b}$ is still in the first quadrant and given by:

$$\tilde{\psi}(\psi, \theta) = \arcsin \frac{\alpha \sin \psi}{\sqrt{(1 + (\alpha^2 - 1)\sin^2\theta)(1 + (\alpha^2 - 1)\sin^2(\theta + \psi))}} \tag{3.173}$$

and the associated corner function is simply $a_\alpha(\psi, \theta) = a(\tilde{\psi})$ with a the corner function for the isotropic cone. Its coefficient is invariant. ψ in $[\frac{\pi}{2}, \pi]$ is obtained by symmetry. In particular, for $\vec{a} = \vec{e}_x$ and $\vec{b} = \vec{e}_y$, the logarithmic coefficient is not affected, as shown in Figure 3.13.

- Pure deformation: $R = \begin{pmatrix} 1 & \sin\alpha \\ 0 & \cos\alpha \end{pmatrix}$. Lengthy computations lead to a renormalization of ψ in $[0, \frac{\pi}{2}]$

$$\tilde{\psi}(\psi, \theta) = \arcsin \frac{\sin \psi \cos \alpha}{\sqrt{(1 - \sin\alpha \sin 2\theta)(1 - \sin\alpha \sin(2\theta + 2\psi))}} \tag{3.174}$$

and similarly the associated corner function is $a_\alpha(\psi, \theta) = a(\tilde{\psi})$, while the prefactor is not affected.

Note that in both cases we explicitly break the invariance by rotation in real space.

Multiple cones and structure factors

Another natural extension is what happens when there are several Dirac cones, with potentially different winding numbers. The first example is of course Graphene (see Section 1.6.2), but such a QCP also occurs at $\mu = 0$ in the $p + ip$ superconductor, with Dirac cones opening at momenta $(0, \pi)$ and $(\pi, 0)$. There is an important difference between the two cases. For Graphene, the two cones have opposite winding number (which is why they can be at the non-PHS-protected momenta $K_\pm$), while the two cones have the same topological charge in $p + ip$. This has strong consequences: Graphene naively describes a trivial QCP if we add a small chemical potential[8] while $\mu = 0$ is a topological phase transition for the $p + ip$, with a Chern number changing by 2.
Therefore, we are interested in computing the logarithmic contributions to the BCF for several cones, and in particular in distinguishing whether we have the same winding numbers. We will limit ourselves to the case of two Dirac cones, but results can be straightforwardly extended to any number. Let $K_\pm$ be the gap closing momenta, and $m_\pm$ the two winding numbers. We assume that both cones are isotropic[9] and compute fluctuations on a square subsystem $\mathcal{A}$. The corner functions being universal, they are not affected by the presence of multiple cones and are a simple global factor that we ignore. Finally, we assume that $\varepsilon_{\vec{k}}$ is still quadratic at $\vec{K}_\pm$.

Logarithmic coefficient of the BCF
Correlation functions now have two singularites at $K_\pm$. As $\varepsilon_{\vec{k}}$ is still quadratic in $\vec{K}_\pm$, the amplitude of each singularity is still 1. For isotropic simple cones, the proper test function that capture the long range scaling of the Fourier transform is:

$$h_{m_+,m_-,j}(\vec{k}) = h_{m_+,j}(\vec{k} - \vec{K}_+) + h_{m_-,j}(\vec{k} - \vec{K}_-) \tag{3.175}$$

$$\mathcal{FT}\{h_{m_+,m_-,j}\} = (m_+ e^{im_+(\theta_{\vec{n}} - \frac{\pi}{2})} e^{-i\vec{n}.\vec{K}_+} + m_- e^{im_-(\theta_{\vec{n}} - \frac{\pi}{2})} e^{-i\vec{n}.\vec{K}_-}) \frac{1}{2\pi} \frac{1}{||\vec{n}||^2} + \mathcal{O}(||\vec{n}||^{-\frac{5}{2}}) \tag{3.176}$$

We straightforwardly obtain:

$$|\mathcal{FT}\{h_{m_+,m_-,j}\}|^2 \approx \frac{m_+^2 + m_-^2 + 2m_+m_- \cos(\vec{n}.(\vec{K}_+ - \vec{K}_-) + (m_+ - m_-)(\theta_{\vec{n}} - \frac{\pi}{2}))}{4\pi^2 ||\vec{n}||^4} \tag{3.177}$$

Summing the oscillating terms on fixed $||\vec{n}||$ contour gives a term proportional to the Bessel function $J_{m_+-m_-}(|n||\vec{K}_+ - \vec{K}_-|)$ and therefore gives no contribution to the logarithmic term. The logarithmic coefficient is then:

$$\mathbf{b}_h = \frac{m_+^2 + m_-^2}{8\pi^2} \tag{3.178}$$

[8] Graphene can be obviously gapped to form a topological model, as can be seen in Haldane model in Section 1.6.3, but it requires something more complex than a simple chemical potential

[9] all results can be generalized to arbitrary cones

This straighforwardly generalize to multiple cones m_j:

$$\mathbf{b}_h = \frac{1}{8\pi^2}\sum_j m_j^2, \tag{3.179}$$

which means that one cannot always identify the number of cones and their winding numbers. The case of two cones with the same (in absolute value) winding number has nonetheless a unique signature.

Structure factor

To go beyond this first result, we again introduce the structure factor of the BCF. In two dimensions, these correspond to the observable:

$$\mathcal{SF}_{\hat{O}}(\vec{\phi},\mathcal{A}) = \langle|\sum_{\vec{r}\in\mathcal{A}} e^{i\vec{\phi}.\vec{r}}\hat{O}_{\vec{r}}|^2\rangle - |\langle\sum_{\vec{r}\in\mathcal{A}} e^{i\vec{\phi}.\vec{r}}\hat{O}_{\vec{r}}\rangle|^2 \tag{3.180}$$

Just as in one dimension, it corresponds to shifting by $\vec{\phi}$ one of the Green functions that appear in the computation. For the charge fluctuations, we obtain:

$$\mathcal{SF}_{\hat{O}}(\vec{\phi},\mathcal{A}) = \frac{q_e}{4}\iiiint \frac{d\vec{k}d\vec{q}}{A_{\mathcal{BZ}^2}}\mathcal{K}(\vec{k}-\vec{q},\mathcal{A})\left(1-\cos\theta_{\vec{k}+\vec{\phi}}\cos\theta_{\vec{q}} + e^{i(\phi_{\vec{k}+\vec{\phi}}-\phi_{\vec{q}})}\sin\theta_{\vec{k}+\vec{\phi}}\sin\theta_{\vec{q}}\right) \tag{3.181}$$

This in turn shift the phase of one of the Fourier transforms. Using the same test function to capture the singularity at $k=\vec{0}$, the logarithmic term may only arise from:

$$\sum_{|n_x|<l_x,|n_y|<l_y} |n_x n_y||\mathcal{FT}\{h_{m_+,m_-,j}\}(\vec{n})|^2\cos\vec{n}.\vec{\phi} \tag{3.182}$$

This time, it is the non-oscillating terms of $|\mathcal{FT}\{h_{m_+,m_-,j}\}|^2$ that are cancelled by the additional phase term. For $\vec{\phi}=\pm(\vec{K}_+-\vec{K}_-)$, logarithmic contributions may arise from the cross-product m_+m_-. The coefficient can be obtained from the series:

$$\frac{q_e}{16\pi^2}\sum_{|n_x|<l_x,|n_y|<l_y} |n_x n_y|\frac{m_+m_-\cos((m_+-m_-)(\theta_{\vec{n}}-\frac{\pi}{2}))}{||\vec{n}||^4} \tag{3.183}$$

If $m_+\neq m_-$, integration on a contour leads to a non constant term, that will depend on the direction of the corner as well as its angle, and vanishes when m_+-m_- is odd. On the other hand, if $m_+=m_-$, we recover a standard logarithmic contribution:

$$\mathbf{b}_h = \frac{q_e m_+ m_-}{8\pi^2} \tag{3.184}$$

and therefore we can distinguish between the Graphene and the $\mu=0$ $p+ip$ gapless phases.

Chapter 4

Beyond non-interacting systems: a complex interplay

Contents

4.1 Interactions and bipartite fluctuations 117
4.1.1 Interacting systems and numerical simulations 117
4.1.2 Bosonization at the critical point 118
4.1.3 Bipartite fluctuations and interactions 120
4.2 Model and simple limiting cases 123
4.2.1 Microscopic model 123
4.2.2 Phase diagram 124
4.2.3 The Hubbard model 125
4.3 Close to half-filling: bosonization and RG 127
4.3.1 Bosonization at half-filling 127
4.3.2 RG analysis 128
4.3.3 Characterization of the 4 Majorana phase 130
4.3.4 Behavior of the large g phases 132
4.3.5 Nature of the transitions 134
4.4 The Double Critical Ising phase 136
4.4.1 Mean-field precursor to the DCI 136
4.4.2 Unraveling the ladder 137
4.4.3 Large g model 139
4.4.4 Numerical approach 140

Up to now, we have only considered non-interacting systems. In this Chapter, we will focus on adding interactions to topological systems. The interplay between interactions and topology is extremely rich and complex as is illustrated in the Fractional Quantum Hall Effect (FQHE). The FQHE is the direct analog of the IQHE, with quantized current carried by edges, but the conductivity takes precise rational values instead of integers. This effect, experimentally discovered in [6] with a theoretical interpretation proposed in

[100], has since received a tremendous amount of attention. Indeed, the non-integer nature of the conductance is a symptom of the existence of anyons carrying a fractional charge. These quasi-particles do not verify the bosonic commutation or fermionic anticommutation relations, but more complex exchange rules.
Another non-trivial consequence of adding interactions is the reduction of the homotopy groups of the different Hamiltonians classes, and consequently the reduction in the topological invariant. Perhaps the most famous example of such is Fidkowski and Kitaev's $\mathbb{Z}_8$ reduction[110, 168, 169]. While the different classes of Hamiltonians are still well-defined in interactions, it has been shown that the topological invariant of the BDI class is no longer an element of $\mathbb{Z}$ but of $\mathbb{Z}_8$, just as it reduces to $\mathbb{Z}_2$ when breaking the TRS. Let us illustrate briefly the physical meaning of this reduction. If we take $n < 8$ Kitaev's wires in their topological phase with open boundary conditions, it is not possible to gap the $2n$ zero-energy Majorana edge modes by adding arbitrarily small interactions that both preserve TRS and PHS: the $2n$ Majorana fermions are still protected by the symmetries. On the other hand, if we take 8 Kitaev wires, it is possible to build interacting terms that give a finite energy to all zero-energy modes, which are therefore no longer protected.
While the FQHE tells us that interesting new physics can happen at large interactions, the $\mathbb{Z}_8$ classification limits the possible behaviors of our systems when the interactions are smaller than the gap of the system. In the following, we will focus on an intermediate point of view: starting from a topological system which is protected by the $\mathbb{Z}_8$ classification, we will be interested in what happens when interactions are large enough that the topological gap is broken, and in particular in the exotic (non-topological) phases that may arise from there.

In Section 4.1, we present, as an introduction, methods to treat the interacting versions of Kitaev's wires. In particular, we present a bosonization scheme that allows to describe the critical $c = \frac{1}{2}$ point in terms of a Luttinger Liquid. We then use this representation to compute the effects of interactions in a generic interacting model. We prove analytically and numerically that the logarithmic term survives in presence of interactions for topological superconductors, but that its coefficient is renormalized.

The rest of the Chapter is devoted to the study of another interacting model that we introduced in Ref. [155]. It is based on two Kitaev's wires, coupled by a density-density interaction, taken as a minimal implementation of the Coulomb interaction. Section 4.2 introduces the model and its Hamiltonian. After an extended discussion about the physical aspects of the model, we propose an overview of its phase diagram in Figure 4.3. Due to the preserved symmetries, the topological phase survives up to large interactions. At weak chemical potential and large coupling, we find two Mott phases that present unusual orbital currents. Section 4.3 presents a complete study of these two phases, along the derivation of their existence. At large chemical potential, the system becomes polarized. Finally, at an intermediate regime, where interactions and chemical potential are comparable, a new gapless phase opens. This phase, called Double Critical Ising, is studied in Section 4.4, and is an extension of the two $c = \frac{1}{2}$ points.

This Chapter is largely based on Ref. [155], with some additional new results.

4.1 Interactions and bipartite fluctuations

In this Section, we present some of the tools and transformation that we use to treat interacting systems. We present a brief overview of the numerical methods at hand, then discuss a bosonization scheme more adapted to the study of the critical points in topological superconductors. We finally use these tools to study bipartite fluctuations in interacting Kitaev's chains.

4.1.1 Interacting systems and numerical simulations

Except for special integrable models, most interacting systems cannot be exactly solved, and one has to rely on perturbative (semi-)analytical methods such as the renormalization group, or to proceed to strong approximations. As these methods are not always well-controlled and usually valid only in either very weak or large interactions, it is convenient to also use numerical computations to check their validity.
Nonetheless, naive numerical simulations of interacting systems through exact diagonalization are extremely time-consuming. Due to the interactions, one can no longer simply diagonalize the correlation matrix, but needs to diagonalize the full $2^L \times 2^L$ Hamiltonian. Taking into account the symmetries of the system, the sparsity of the matrix, and focusing only on the ground state and the first few excited states reduce slightly the complexity, but it generally stays exponential with the size of the system, which limits us, as a rule of thumb, to less than 40 fermions. For a ladder, it means that we can barely reach $L = 20$, and therefore the long-range properties of the system can be complex to extract.
Fortunately, in one-dimension, another method can be used: the density matrix renormalization group (DMRG), and in particular its variant based on matrix product states (MPS). We do not give a description of DMRG and MPS representations of many-body states in this thesis and will only point out the main physical ideas behind this method. We refer the readers to Ref. [170–172] for an introduction to, and review of the domain.

One dimensional ground-states are characterized by a weak scaling of the bipartite vNEE.
For gapped phases, the entanglement entropy saturates to a constant (proportional to the logarithm of the correlation length) when increasing the side of the considered subsystems. Very few eigenstates of the density matrix of any subsystem have a significant weight. Instead of trying to describe exactly the ground state of the system, the idea is then to approximate it by throwing out the low-entropy states.

For gapless systems, we have seen that the entropy scales logarithmically in the ground state, which means that the number of relevant entanglement eigenstates grows linearly with the size of the subsystem. Reaching a good approximation of the ground state should therefore scale only polynomially with the size of the system. Though one cannot reach the same precision as in a gapped phase, careful scaling analysis of the MPS results still allows for very reliable results.

In this Chapter, and in the rest of the thesis, we use the ALPS library[158, 159] for all our MPS computations (while any exact diagonalization simulations were done with our

own codes).

4.1.2 Bosonization at the critical point

In this part, we briefly present a method of bosonization we used in Ref. [155] to describe the critical point of an interacting Kitaev's wire, inspired by Ref. [173].

Bosonization is one of the most powerful analytical tools at hand to study interacting one-dimensional fermionic models. Complex fermionic theories (approximately) map to more conventional bosonic systems that can be perturbatively solved[130, 131]. In the case of the Kitaev's model, we are in particular interested in a description of the $c = \frac{1}{2}$ critical point and what it becomes when plugging in interactions. Describing such a critical model with bosonic fields seems difficult: simple bosonic models usually have integer central charge. To solve this problem, instead of studying one single Kitaev's wire, we study two of them, that we leave uncoupled. The critical model having $c = 2 \times \frac{1}{2}$ should be describable by a free boson.
Nonetheless, as we have seen in Chapter 3, the sign of the logarithmic contribution to the charge fluctuations is negative in Kitaev's wire, while it is positive for Luttinger Liquids. One therefore has to change the fermionic basis before standard bosonization. One can get an intuition of the right change in basis by looking at the sign of $\mathbf{b}_{YY}$ in a general BDI insulator: it is positive and therefore a good choice for our bosonic density. Going from the insulators to the superconductors is non-trivial, but works.

We start at the critical point $\mu = -2t$ of Kitaev's chain and take $\Delta = t$ for convenience. We rewrite the two independent fermionic wires to form two Majorana chains as discussed in Sec. 1.1 (see Eq. 1.12). With the additional index σ specifying the wires, the Hamiltonian is

$$-2it \sum_{j,\sigma} \alpha_{j-1,\sigma}\alpha_{j,\sigma}. \tag{4.1}$$

We then recombine them to form a single fermionic chain with a doubled number of lattice sites. The new fermions operators, depicted in Figure 4.1, are:

$$d_{2j} = \frac{(-1)^j}{\sqrt{2}}(\alpha_{2j-1,1} + i\alpha_{2j-1,2}) \tag{4.2a}$$

$$d_{2j+1} = \frac{(-1)^{j+1}}{\sqrt{2}}(\alpha_{2j,2} - i\alpha_{2j,1}). \tag{4.2b}$$

and we obtain the following final Hamiltonian:

$$H = -2t \sum_j (d_j^\dagger d_{j+1} + d_{j+1}^\dagger d_j). \tag{4.3}$$

The boundary conditions in this basis will depend on those of the initial model. For OBC in the original model, it will also have OBC in this effective model. For PBC, it will either have PBC if L is even or anti-periodic boundary conditions (APBC) if L is odd. In the following, we consider L to be even, but the conclusions will remain unaffected by this choice.

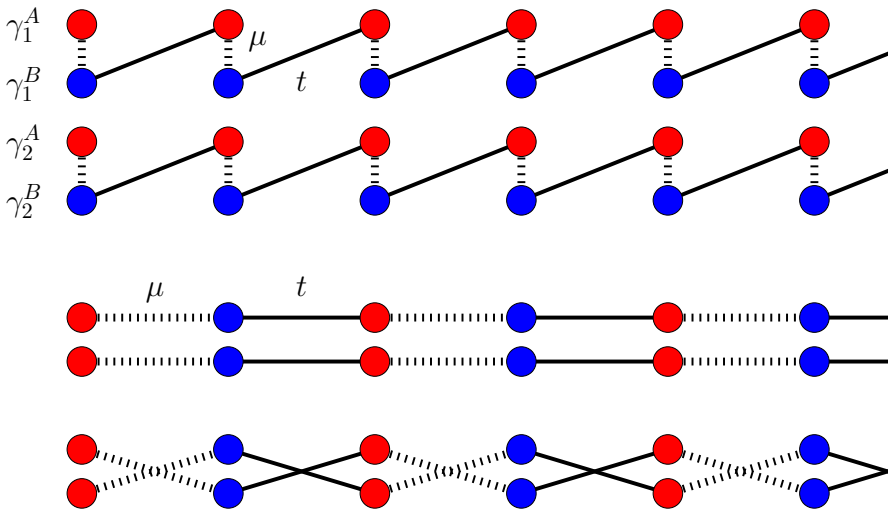

Figure 4.1: Unravelling scheme to obtain the model far from half-filling. The initial fermions are split into two Majoranas. Each fermionic wire is then reorganized into a Majorana wire with an alternating hopping term. Finally, recombination of the Majorana wires into new fermions composed of a Majorana of each wire.

We use an Abelian bosonization approach to get an equivalent model and separate each fermion field into its left- and right-moving part (see Appendix E for an overview on the bosonization methods):

$$d_j = e^{ik_F j} d_{1,j} + e^{-ik_F j} d_{-1,j}, \qquad d_{r,j} = \frac{U_r}{\sqrt{2\pi\alpha}} e^{-i(r\phi_j - \theta_j)}. \tag{4.4}$$

which leads to:

$$H = \frac{v_F}{2\pi}\left(\frac{1}{K}(\partial_x\phi)^2 + K(\partial_x\theta)^2\right) \tag{4.5}$$

with $v_F = 4t$ and $K = 1$. v_F is the Fermi speed of the fermions d, and K the Luttinger parameter. As the d fermions are non-interacting, it is fixed to 1. For reference, we also compute the density of the d operators:

$$d_2^\dagger j d_{2j} + d_{2j+1}^\dagger d_{2j+1} = i\left(c_{j,1}^\dagger c_{j,2} - c_{j,2}^\dagger c_{j,1}\right). \tag{4.6}$$

Our intuition was indeed valid: the conserved fermionic number of the d fermions is indeed the σ^y pseudo-spin contribution. It marks a "hidden" $U(1)$ symmetry that appear when considering the two chains. Finally, let us emphasize that making the change of basis *before* bosonization is crucial to obtain such a simple form. We will come back to these two results in Section 4.2.3 and 4.4.2.

Finally, one can check the validity of our approach by computing, for example, the bipartite charge fluctuations. As the density operator has a somewhat complex expression in terms of the d fermions, it is more convenient to consider the fluctuations of $n_{j,\pm} = n_{j,1} \pm n_{j,2}$. Due to the symmetry between the two wires, and as they are uncoupled,

$$\mathcal{F}_{n_+}(\mathcal{A}) = \mathcal{F}_{n_-}(\mathcal{A}) = \mathcal{F}_{n_1}(\mathcal{A}) + \mathcal{F}_{n_2}(\mathcal{A}) = 2\mathcal{F}_{n_1}(\mathcal{A}) = 2\mathcal{F}_{n_2}(\mathcal{A}). \tag{4.7}$$

In bosonized form, keeping only non-oscillating and the more relevant terms and with the convention $U_R^\dagger U_L = -i$ we obtain:

$$n_{j,+} = \frac{1}{2\pi}\left((\partial_x\phi)^2 + (\partial_x\theta)^2\right) + \frac{1}{\pi\alpha}\cos 2\phi \tag{4.8}$$

$$n_{j,-} = -\frac{1}{2\pi\alpha}\cos 2(\phi+\theta) - \frac{1}{2\pi\alpha}\cos 2(\phi+\theta) - \frac{1}{\pi\alpha}\cos 2\theta \tag{4.9}$$

Logarithmic term in the fluctuations can only be induced by $\cos 2\phi$ and $\cos 2\theta$, the two most relevant terms. It leads to

$$\begin{aligned}\sum_{j,j'=0}^{l_\mathcal{A}} \langle n_{j,+} n_{j',+}\rangle_c &\approx \frac{1}{2\pi^2\alpha^2}\int_0^{l_\mathcal{A}}\int_0^{l_\mathcal{A}} dxdy e^{2i\phi(x)-2i\phi(y)} \\ &\approx \frac{1}{2\pi^2}\iint dxdy \frac{1}{(x-y)^2+\alpha^2} \approx -\frac{1}{\pi^2}\ln l_\mathcal{A}\end{aligned} \tag{4.10}$$

$$\begin{aligned}\sum_{j,j'=0}^{l_\mathcal{A}} \langle n_{j,-} n_{j',-}\rangle_c &\approx \frac{1}{2\pi^2\alpha^2}\int_0^{l_\mathcal{A}}\int_0^{l_\mathcal{A}} dxdy e^{2i\theta(x)-2i\theta(y)} \\ &\approx \frac{1}{2\pi^2}\iint dxdy \frac{1}{(x-y)^2+\alpha^2} \approx -\frac{1}{\pi^2}\ln l_\mathcal{A}\end{aligned} \tag{4.11}$$

We recover the quantized coefficient $-\frac{1}{\pi^2}$, as announced in Eq. 4.7.

4.1.3 Bipartite fluctuations and interactions

Up to now, we have left out the interactions. We focus in this section on intra-wire interactions, that therefore leave the two wires uncorrelated. We assume that the interactions do not affect significantly the phase transition between the topological phase and the trivial polarized phase: no intermediate phase opens and the central charge at the critical point is still $c = \frac{1}{2}$ for each wire.

Then, our previous description of the two wires in terms of a free boson must be still valid. The Hamiltonian is in fact still given by:

$$H = \frac{\tilde{v}_F}{2\pi}\left(\frac{1}{\tilde{K}}(\partial_x\phi)^2 + \tilde{K}(\partial_x\theta)^2\right). \tag{4.12}$$

$\tilde{v}_F$ and $\tilde{K}$ are a priori the only two free parameters of the theory[1], $\tilde{v}_F$ is a priori renormalized by the interactions, but one can actually prove that it is pinned to $\tilde{K} = K = 1$ by the absence of correlations between the two wires[2]. Let us compute the bipartite charge fluctuations in each chain to both prove this result and see the evolution of the different terms in presence of interactions.

The form of the bosonized expression of the densities in Eqs. 4.8 and 4.9 are not significantly affected by the presence of interactions. A naive computation for an arbitrary $\tilde{K}$ transforms the logarithmic term in power laws (we only consider the dominant long range behavior for $\tilde{K} < 2$):

$$\langle n_{j,+}n_{j',+}\rangle_c \propto |j-j'|^{-2\tilde{K}} \text{ and } \langle n_{j,-}n_{j',-}\rangle_c \propto |j-j'|^{-2\tilde{K}^{-1}}. \tag{4.13}$$

On the other hand, Eq. 4.7 is still valid as interactions do not couple the two wires. $\mathcal{F}_{n_+}$ and $\mathcal{F}_{n_-}$ must therefore have the same scaling laws, which pins $\tilde{K}$ to 1. The logarithmic term is therefore still present on the $c = \frac{1}{2}$ line of an interacting Kitaev wire, whatever the form of the interactions.
To compute the exact coefficient appearing before the logarithm is actually much more complex. Indeed, even in presence of weak, non-relevant perturbations, the coefficients in front of cosine and sine terms are renormalized[131], such that:

$$n_{+,j} = \frac{A_1}{\pi\alpha}\cos 2\phi + ..., \tag{4.14}$$

with A_1 a non-universal parameter. Finally, it leads to

$$\langle n_{j,\sigma}n_{j+l,\sigma}\rangle_C = -|A_1|^2\left(\frac{1}{2L^2} + (\frac{\mathbf{b}_{\hat{Q}}}{2} + O(\frac{1}{L}))\frac{1}{\left[\frac{L}{\pi}\sin\frac{\pi l_{\mathcal{A}}}{L}\right]^2}\right) + O(\frac{1}{\left[\frac{L}{\pi}\sin\frac{\pi l_{\mathcal{A}}}{L}\right]^4}), \tag{4.15}$$

The fact that the constant and l^{-2} scaling term are multiplied by the same non-universal ratio allows to recover the universality of the logarithmic coefficient. This coefficient can also be understood as the square of a quasi-particle weight induced by the interactions. Note that there is still a cusp in the linear term, though it is quite sensitive to finite-size effects.
We verified numerically this result using MPS simulations. Results are represented in Figure 4.2. We considered a density-density interaction of the form:

$$4U(n_j - \frac{1}{2})(n_{j+1} - \frac{1}{2}). \tag{4.16}$$

This model was thoroughly studied [174–180] and we refer the reader to these articles for a discussion of its phase diagram and properties.

[1]Terms such as $\partial_x\phi$ would break the $\mathbb{Z}_2$ symmetry between the wires.
[2]It is similar to the $SU(2)$ rotation symmetry of the spin sector enforcing $K_\sigma = 1$ in the Hubbard

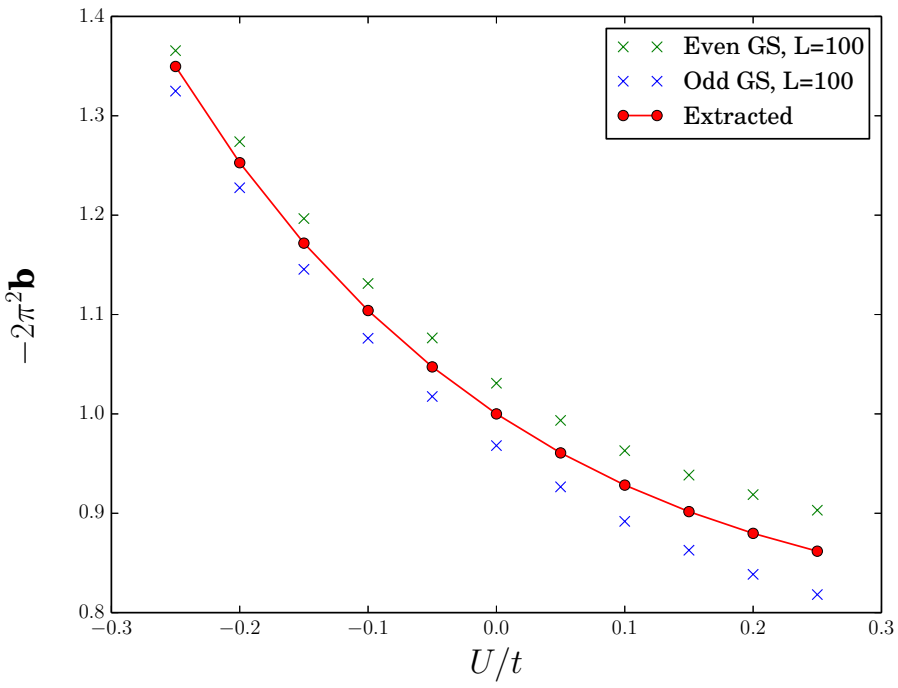

Figure 4.2: Logarithmic coefficient extracted from the correlation functions in a Kitaev's chain with added density-density interactions $4U(n_j - \frac{1}{2})(n_{j+1} - \frac{1}{2})$. We take $t = \Delta$ and consider several values of U (we fix the chemical potential to stay on the critical line). Simulations were performed using MPS codes from the Alps library, for wires with up to 120 sites. The blue and green curves were obtained in the two parity ground states. In red, we extracted the value of the coefficient in the thermodynamic limit.

4.2 Model and simple limiting cases

In this Section, we start by describing with more details the microscopic model of the Kitaev's ladder we consider. We then directly present the phase diagram we obtained, before ending the Section with a brief overview of the Hubbard model, a staple of Condensed Matter, which is the non-superconducting limit of the ladder.

4.2.1 Microscopic model

The model we chose to study is composed of two topological superconducting wires in the presence of Coulomb-like interactions modeled by an on-site repulsion à la Hubbard. It is a generic model, in the sense that these interactions will be present in most systems. Additionally, this ladder is also a step towards building two-dimensional materials.
We take each wire to be described by Kitaev's Hamiltonian described in Section 1.1. The two chains are coupled via a Coulomb interaction:

$$H_{\text{int}} = g \sum_j (n_{j,1} - \frac{1}{2})(n_{j,2} - \frac{1}{2}), \tag{4.17}$$

$n_{j,1/2}$ is the electron number operator in the first/second wire at site j. Interpreting the chain index as a spin index, then this can be identified as the well-known Hubbard interaction, a staple of condensed matter physics thoroughly studied for the last 40 years. This interaction does not break any of the discrete symmetries of the original problem: superconducting induced PHS, parity and TRS are preserved. In this model, we ignore the effect of intra-wire repulsive interactions and assume that the Cooper channel dominates in each wire. This gives a minimal model, which interpolates between Hubbard and Kitaev physics, and displays a competition between topological superconducting ordering and Mott ordering. Reaching the large g limit could be eventually achieved experimentally by placing an insulating material between the wires, forming a capacitance between the two parallel wires. Coupling with a bath could also allow to engineer such an interaction term. More complex interaction terms which allow for exactly solvable points have also been envisioned recently in Refs. [181, 182]. Note that two side gates could be used to screen out the interactions along the two wires. We also note that since a Kitaev superconducting wire can be engineered in ultra-cold atoms through proximity effect [183] or via a Floquet type approach [184], then a controllable interaction could be achieved between and inside the two wires.

This problem can also be expressed in terms of two interacting Ising spin-$\frac{1}{2}$ chains [40] (see Section 1.1.4):

$$-\frac{\mu}{2}\sum_{j,w}\sigma^z_{j,w} + \frac{t-\Delta}{2}\sum_{j,w}\sigma^x_{j,w}\sigma^x_{j+1,w} + \frac{t+\Delta}{2}\sum_{j,w}\sigma^y_{j,w}\sigma^y_{j+1,w} + \frac{g}{4}\sum_{j=1}^{L}\sigma^z_{j,1}\sigma^z_{j,2}, \tag{4.18}$$

where w is a chain index and $\sigma^{x,y,z}$ the Pauli matrices. This model will have the same phase diagram as its fermionic counterpart, but different physical properties [109]. This representation favors another controlled experimental realization with cold atoms [185, 186] or

model.

using Josephson junctions as pseudo two-level systems [187], allowing to access the large g limit. Other Majorana-Josephson models, similar to Ising models in transverse fields have been proposed, see for example Ref. [188]. Such systems would allow us to reach the high coupling limits, and consequently to probe easily the more exotic features of our system. Quantum criticality in a Ising chain has also been observed in real materials [189].

Countless variants of such a model could also be considered. Supplementary terms such as a hopping term between the two wires $-t_\perp c_1^\dagger c_2 + h.c$ or an orthogonal pairing term $\Delta_\perp c_1^\dagger c_2^\dagger + h.c$ [190] could be taken into account. These terms become negligible for a large enough distance d between the wires. The Coulomb repulsion scales like $1/d^2$. The hopping amplitude, scaling as $\exp(-d/\chi)$, with χ being a correlation length, is negligible for $d \gg \chi$. Similarly, if d is larger than the coherence length of the Cooper pair, one can safely ignore $\Delta_\perp$, as long as both these terms do not break the time-reversal symmetry, i.e $t_\perp$ and $\Delta_\perp$ are real. Several interacting terms have been also considered in the case of one wire [174, 175, 177, 179, 191]. Spinless fermionic ladders have also given rise to a plethoric litterature ([192–195] for example).

4.2.2 Phase diagram

In this Section, we directly give the phase diagram we obtained for this model. It will be easier to follow the different approaches used to retrieve it.

The main result of this Chapter is the phase diagram of our model for $\Delta \neq 0$ in Fig. 4.3.

We observe the survival of the SPT phase, called $4MF$, in the presence of finite interactions. This phase is characterized by two free Majorana fermions at each extremity of the ladder. Despite their proximity, the symmetries prevent a direct coupling between the Majorana fermions at each extremity. We consequently observe a four-fold degeneracy of the ground state of the system with open boundary conditions. Each of these ground states has a different combination of fermionic parities. We also observe a widening of the acceptable chemical potential range for weak repulsive interactions ($g > 0$) and a reduction of this range for attractive interactions ($g < 0$), a common feature of these topological superconducting models[191, 196].

At very large coupling and weak chemical potential, two similar phases appear. Both of them are Mott-Ising phases related to the Mott phases of the Hubbard model. For positive g (MI-AF), the corresponding low-energy model is an Antiferromagnetic Ising model, which presents orbital currents and a spontaneous breaking of the time reversal symmetry. For g negative (MI-F), the low-energy model is a Ferromagnetic Ising model in a transverse field, which also breaks time reversal symmetry and exhibits currents between the two wires. At large chemical potential, a polarized trivial phase opens, corresponding to depleted or full wires.

Finally, at finite positive coupling, an intermediate phase opens between $4MF$ and the polarized phase. This is the only gapless phase in this diagram and has a central charge $c = 1$. This phase is an extension of the critical point at $g = 0$, whose critical model is two

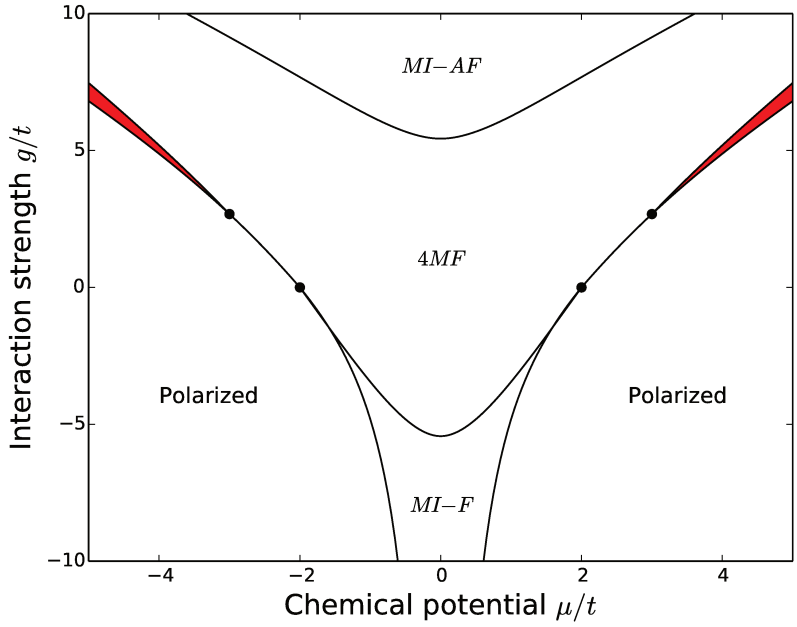

Figure 4.3: Sketch of the phase diagram of the interacting ladder at $\Delta = t$ obtained with analytical (bosonization, exact mappings) and numerical methods (exact diagonalization (ED), Density Matrix Renormalization Group (DMRG)). The chemical potentials of the two chains are taken to be equal. $4MF$ is the SPT gapped phase presenting 2 Majorana fermions at each of the ladder extremities. $MI - AF$ and $MI - F$ are two gapped Mott phases, either antiferromagnetic or ferromagnetic. Polarized corresponds to a trivial phase with a quasi-empty or quasi-full ladder. In red, the gapless DCI phase embodies an extension of the critical point at $g = 0$. It acquires an extension of order t as g goes to $+\infty$.

Ising models. We will denote it Double Critical Ising (DCI). It is nothing but a Luttinger Liquid (LL) of a complex mixture of fermions on the two wires.

4.2.3 The Hubbard model

When $\Delta = 0$, our model reduces to the celebrated and well-studied fermionic Hubbard model through the trivial mapping:

$$c_1 \to c_\uparrow \qquad c_2 \to c_\downarrow.$$

The $U(1)$ symmetry is restored and the Bethe ansatz method is applicable to solve the model at arbitrary chemical potential. In this Section, we present some known results on this stapled model[197]. Its exact phase diagram is displayed in Figure 4.4.
The Hubbard model also has a $SU(2)$ spin symmetry. Introducing $\Delta \neq 0$ breaks this spin

rotation symmetry down to $SO(2) \sim U(1)$ rotations around the y-axis:

$$\begin{pmatrix} c_1 \\ c_2 \end{pmatrix} \to \begin{pmatrix} \cos(\phi) & \sin(\phi) \\ -\sin(\phi) & \cos(\phi) \end{pmatrix} \begin{pmatrix} c_1 \\ c_2 \end{pmatrix} \tag{4.19}$$

which leave the model invariant. The associated conserved charge (Noether's current) is

$$J_y = i \sum_j \left(c^\dagger_{j,1} c_{j,2} - c^\dagger_{j,2} c_{j,1} \right), \tag{4.20}$$

corresponding to the total spin in the y direction. Due to Mermin-Wagner theorem for continuous symmetries[3], it will be pinned to 0 in the different ground states. Despite this constraint, the competition between superconductivity and Mott physics in our model will break time-reversal symmetry and lead to orbital currents.

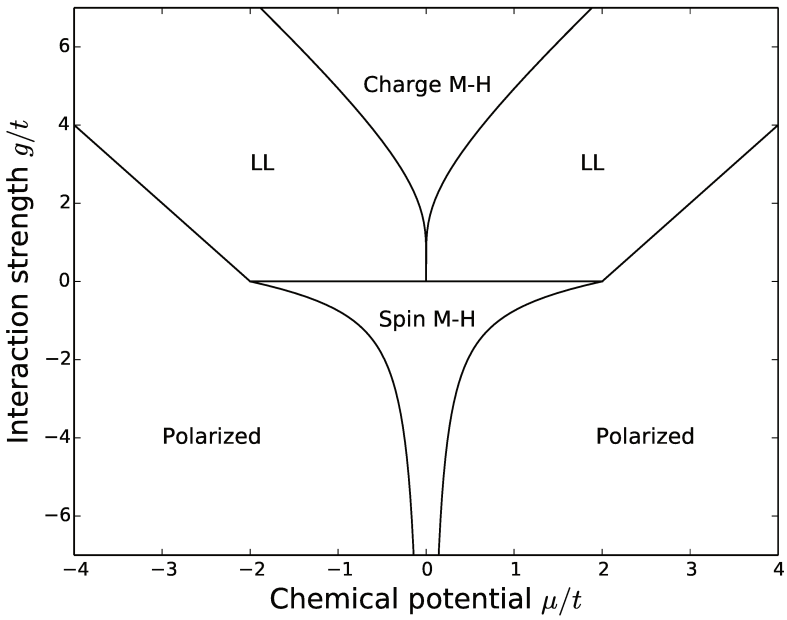

Figure 4.4: Exact phase diagram of the Hubbard model at zero magnetic field, obtained from Bethe Ansatz[197]. Charge M-H corresponds to the celebrated Mott-Heisenberg phase, opening at arbitrarily low $g > 0$. The charge mode is gapped and the electronic density is fixed at half-filling, while the spin mode is free (and its effective model is a $SU(2)$-invariant Heisenberg model). Spin M-H is its equivalent for $g < 0$, inversing the role of the two sectors. Both of them are characterized by a central charge $c = 1$. Luttinger liquid (LL phases) corresponds to two phases of free diluted electrons (with a central charge $c = 2$). Polarized phases are trivial phases with totally empty or full wires.

[3]The Mermin-Wagner theorem states that in one dimension, continuous symmetries cannot be spontaneously broken.

4.3 Close to half-filling: bosonization and RG

In this Section we focus on what happens close to the $\mu = 0$. For $\mu \ll t$, the fermionic density will be close to $\frac{1}{2}$, that is to say the ladder will be half-filled. In this limit, we can make fruitful use of the bosonization methods to perturbatively describe the effects of interactions in the two wires.

4.3.1 Bosonization at half-filling

We proceed to a standard Abelian bosonization scheme [131], considering both Δ and g as perturbations. The notations used for bosonization are summarized in Appendix E.

Assuming that we are close to half-filling and consequently far from the bottom of the energy band in each wire, the free fermion Hamiltonian is given by:

$$H = \sum_{\sigma} \int d\tau dx \frac{v_F}{2\pi} ((\partial_x \theta_\sigma)^2 + (\partial_x \phi_\sigma)^2) \tag{4.21}$$

with σ the index of wire ($\sigma = 1, 2$), $v_F = 2t\alpha \sin(k_F)$ the Fermi velocity and α a short distance cut-off. We take $k_F = \pi/2$ the Fermi momentum to simplify notations.
We then need to derive the different contributions of the pairing Δ and the interaction g. The exact derivation is kept in Appendix E.3.4. We use the representation $U_L^\dagger U_R^\dagger = i$ of the Klein factors.
The contribution of the pairing is given by:

$$\sum_{\sigma=1/2} \frac{2\Delta_\sigma \sin(k_F)}{\pi\alpha} \cos(2\theta_\sigma), \tag{4.22}$$

with $\Delta_\sigma = \Delta$ while the interactions lead to a renormalization of the Luttinger parameters and the additional terms:

$$\sum_{\varepsilon=\pm} \frac{g_\varepsilon}{\alpha^2} \cos(2\sqrt{2}\phi_\varepsilon), \tag{4.23}$$

where we have define $\sqrt{2}\phi_\pm = \phi_1 \pm \phi_2$ and $\sqrt{2}\theta_\pm = \theta_1 \pm \theta_2$. While the wire basis is more convenient for treating the non-interacting Hamiltonian, interactions can be better described in the (charge, pseudo-spin)= $(+, -)$ basis. The total Hamiltonian treated in this basis is given by:

$$H = \sum_{\varepsilon=\pm} \int dx \frac{v_{F,\varepsilon}}{2\pi} (K_\varepsilon (\partial_x \theta_\varepsilon)^2 + K_\varepsilon^{-1} (\partial_x \phi_\varepsilon)^2) + \frac{g_\varepsilon}{\alpha^2} \cos(2\sqrt{2}\phi_\varepsilon) + \frac{\Delta^{(1)}}{\alpha^2} \cos(\sqrt{2}\theta_+) \cos(\sqrt{2}\theta_-). \tag{4.24}$$

K_+ and K_- are the Luttinger parameters. g_+ and g_- appear due to the Coulomb coupling between the two wires. Both are present in Hubbard model and are responsible for the Mott-Heisenberg phases. The pairing Δ plays now the role of a coupling $\Delta^{(1)}$ between the two charge and spin sectors, that cannot be a priori separated. The values of the different parameters before the renormalization group analysis can be found in Table 4.1, as bare values.

Term	Dimension	Bare value
$v_{F,\pm}$	-	$v_F\sqrt{1\pm\frac{g}{\pi v_F}}$
$K_\pm$	-	$K_\pm(0)=\frac{1}{\sqrt{1\pm\frac{g}{\pi v_F}}}$
$\cos 2\theta_\sigma$	K_σ	$\frac{2\Delta\sin(k_F)}{\pi\alpha}$
$\cos(\sqrt{2}\theta_-)\cos(\sqrt{2}\theta_+)$	$\frac{1}{2}(K_+^{-1}+K_-^{-1})$	$\Delta^{(1)}(0)=\frac{4\Delta\alpha}{\pi}$
$\cos(2\sqrt{2}\theta_+)$	$2K_+^{-1}$	$\Delta_+^{(2)}(0)=0$
$\cos(2\sqrt{2}\theta_-)$	$2K_-^{-1}$	$\Delta_-^{(2)}(0)=0$
$\cos(2\sqrt{2}\phi_+)$	$2K_+$	$g_+(0)=\frac{-g}{2\pi^2}$
$\cos(2\sqrt{2}\phi_-)$	$2K_-$	$g_-(0)=\frac{g}{2\pi^2}$

Table 4.1: Dimensions of the different terms of the bosonized model, and bare values in the RG flow.

4.3.2 RG analysis

To be able to solve the Hamiltonian in Eq. 4.24, one needs to proceed to a renormalization group (RG) analysis. A very basic introduction to the philosophy of the RG is kept in Appendix E.3, and we state here the main physical ideas behind it.

As we are interested in the thermodynamic limit, that is to say the long-range behavior of the system, the small scale details of our Hamiltonian should be ignored. The RG procedure selects which operators in the Hamiltonian are important in that limit. Those who are, are called relevant: when increasing the scale at which one looks at the system, their coefficient is renormalized to ∞ at a speed characterized by their "dimension" (here, the lesser, the faster they grow). Others, called irrelevant, vanish in the thermodynamic limit. For the operators we consider in this model, the critical dimension is 2: if their dimension is larger than 2, they are irrelevant. If it smaller than 2, they are relevant.

Table 4.1 also summarizes the dimension of the different operators that appear in Eq. 4.24. The method to determine it is given in Appendix E.3.3. In the absence of interactions, the operators corresponding to Δ_σ are always relevant, and therefore flow to ∞. θ_σ are pinned to $\pm\frac{\pi}{2}$ and the system is gapped as soon as Δ is non-zero. Adding a chemical potential only adds a coupling to the ϕ field, and therefore does not directly affect θ up to the point when we reach the bottom of the band, where the bosonized picture breaks down. Again, it matches qualitatively the exact solution: whatever $\Delta\neq 0$, the phase transition only occurs when $\mu=\pm 2t$, that is to say when the chemical potential indeed reaches the bottom (or top) of the free electron band.

Including the interactions changes the RG equations. We only consider the one-loop RG equations and we do not take into account the renormalization of the Fermi velocities.

An additional term appears in the RG computation that must be taken into account[4]

$$-\sum_{\varepsilon=\pm}\frac{\Delta_\varepsilon^{(2)}}{\alpha^2}\cos(2\sqrt{2}\theta_\varepsilon) \tag{4.25}$$

$\Delta_+^{(2)}$ and $\Delta_-^{(2)}$ are not initially present in the bare Hamiltonian, but are generated under RG by $\Delta^{(1)}$. In a diagrammatic language, they correspond to second order contributions in Δ. The dimensions of the different coefficients are noted in Table 4.1.

We define the renormalization length as: $\alpha(l) = \alpha e^l$. The renormalization flow equations, including all relevant orders, are:

$$\begin{aligned}
\frac{dK_\pm}{dl} &= -\frac{2\pi^2 g_\pm^2}{v_{F,\pm}^2}K_\pm^2 + \frac{2\pi^2(\Delta_\pm^{(2)})^2}{v_{F,\pm}^2} + \frac{\pi^2(\Delta^{(1)})^2}{4v_{F,+}v_{F,-}}\\
\frac{dg_\pm}{dl} &= (2-2K_\pm)g_\pm\\
\frac{d\Delta^{(1)}}{dl} &= (2-\frac{1}{2}(K_+^{-1}+K_-^{-1}))\Delta^{(1)}\\
\frac{d\Delta_\pm^{(2)}}{dl} &= (2-2K_\pm^{-1})\Delta_\pm^{(2)} + \frac{2\pi^2(\Delta^{(1)})^2}{v_{F,\mp}}.
\end{aligned} \tag{4.26}$$

Dimensional analysis of these equations discriminates three different phases at half-filling, to be analyzed below. To qualitatively compare the effects of g_ε and $\Delta^{(1)}$, we compare the bare value of the latter, an a priori strongly relevant coupling, and the effective mass m_g obtained by Bethe-Ansatz in the Hubbard model (in other words the Mott gap in the charge sector), at low coupling [197]

$$\frac{m_g}{t} = -2 + \frac{|g|}{2t} + 2\int_0^\infty d\omega\frac{J_1(\omega)e^{-\frac{|g|\omega}{4t}}}{\omega} \approx \frac{4}{\pi}\sqrt{\frac{|g|}{t}}e^{-\frac{2\pi t}{|g|}} \qquad \text{for } |g| \ll t.,$$

where J_1 is the Bessel function of the first kind.

- If $\Delta \gtrsim |m_g|$, $\Delta^{(1)}$ dominates the $g_\pm\cos(2\sqrt{2}\phi_\pm)$ terms and goes to strong coupling. Both $\theta_\pm$ modes become massive and are locked to the minima of the $\Delta^{(1)}$ term. By continuity with the topological phase at $g = 0$, we expect this strong coupling fixed point to correspond to the SPT phase presenting four Majoranas, or $4MF$ phase.

- If $|m_g| \gtrsim \Delta$ and $g > 0$, g_+ is renormalized to large coupling before $\Delta^{(1)}$ reaches significant values. g_- is irrelevant and renormalized to 0. ϕ_+ is consequently locked to 0 $[\pi/\sqrt{2}]$, corresponding to a Mott ordered phase, and $\Delta^{(1)}$ vanishes at this fixed point. $\Delta_-^{(2)}$ is still relevant and acquires a non-zero value in the initial steps of the renormalization. It consequently gaps the spin sector and both modes (ϕ_+, θ_-) are eventually locked. This fixed point describes the $MI - AF$ phase.

- If $|m_g| \gtrsim \Delta$ and $g < 0$, the reasoning is the same as for $g > 0$ but for an inversion of the charge and the spin sector. (ϕ_-, θ_+) are locked, describing the $MI - F$ phase.

[4]It was actually already generated in the non-interacting case but id not play an important role.

As long as we stay close to half-filling, one can use the same bosonization scheme to determine the effects of a chemical potential. Indeed, one only needs to add a term:

$$-\frac{\mu\sqrt{2}}{\pi}\partial_x\phi_+,$$

in the Hamiltonian. The effect of this term is two-fold: it reduces the effective dimension of $\cos(2\sqrt{2}\phi_+)$ and renormalizes the Fermi velocity [198]. When the renormalized Fermi speed approaches 0, it indicates that we are too far from half-filling and that the spectrum is no longer linear, leading to the breakdown of the bosonization approximation.[5] We summarize the effect of the chemical potential on each of the previously obtained phases:

- If $\Delta \gtrsim |m_g|$, none of the pinned operators includes a ϕ_+ term, meaning that no transition occurs before we reach the bottom of the band and the bosonization procedure breaks down.
- If $|m_g| \gtrsim \Delta$ and $g > 0$, the umklapp term controlled by g_+ starts oscillating. In the Hubbard model occurring at $\Delta = 0$, g_+ is renormalized to zero at a finite ratio $\frac{\mu}{g}$, corresponding to a vanishing charge gap and a commensurate-incommensurate transition to a gapless Luttinger phase [198]. At finite but small Δ, μ weakens g_+ by reducing its dimension until $\Delta^{(1)}$ dominates the RG process and flows to strong coupling. This leads to a resurgence of the 4 Majorana phase at finite μ.
- If $|m_g| \gtrsim \Delta$ and $g < 0$, as with the first phase, a transition does not occur in the bosonization validity range.

4.3.3 Characterization of the 4 Majorana phase

Based on adiabaticity, we expect the topological properties of the $4MF$ phase to be well-described by the $g = 0$, $|\mu| < 2t$ case, *i.e.* two uncoupled Kitaev wires in their topologically non-trivial phases. Hence, four zero-energy Majorana end states should be present and remain uncoupled, corresponding to a four-fold degenerate ground state (each couple of Majorana fermions can form a complex fermion with 0 energy, that leads to a two-fold degeneracy of the ground state). We present in this section a few analytical and numerical arguments that support this claim, beyond the $\mathbb{Z}_8$ classification of Kitaev and Fidkowski[110, 168, 169, 199].

A first approach consists in considering the perturbative effect of g on the extremity of two Kitaev wires in the topological phase. We assume $t = \Delta$ and $\mu = 0$ to get a simpler picture. Using the notation of Section 1.1, we recall that the free Majorana fermions are $\gamma^B_{1,\sigma}$ and $\gamma^A_{L,\sigma}$. The interaction term Eq. (4.17) can be rewritten as: $-g\sum_j \gamma^A_{j,1}\gamma^B_{j,1}\gamma^A_{j,2}\gamma^B_{j,2}$. Only terms at least of order $(\frac{g}{t})^L$ will directly couple the free Majoranas, which translates in exponentially small lifting of the degeneracy. This comes from the fact that the interaction term does not break the PHS symmetry, as was explained in Section 1.3.4. In the

[5] One could recover the results from a bosonized theory, but that would require adding higher order terms that we neglected and cannot treat simply.

thermodynamic limit, we consequently expect the survival of the 4 Majoranas phase.

From a numerical point of view, we have studied several markers for the topological phase. The first is obviously the change in degeneracy going OBC to PBC. While in the latter the ground state present no degeneracies, it is four-times degenerate in the former. The parities of the ground states is a good quantum number, and follows the same rules as in the non interacting case. Introducing the parity operator of each wire:

$$\hat{P}_\sigma = \prod_j (1 - 2n_{j,\sigma}), \tag{4.27}$$

we go from an odd-odd ground state ($\hat{P}_1 = \hat{P}_2 = -1$) with PBC to a ground state in each parity sector ($\hat{P}_1 = \pm 1$, $\hat{P}_2 = \pm 1$) with OBC. Typical behavior for the energy of the first few levels on the line $\mu = 0$ is presented in Figure 4.5.

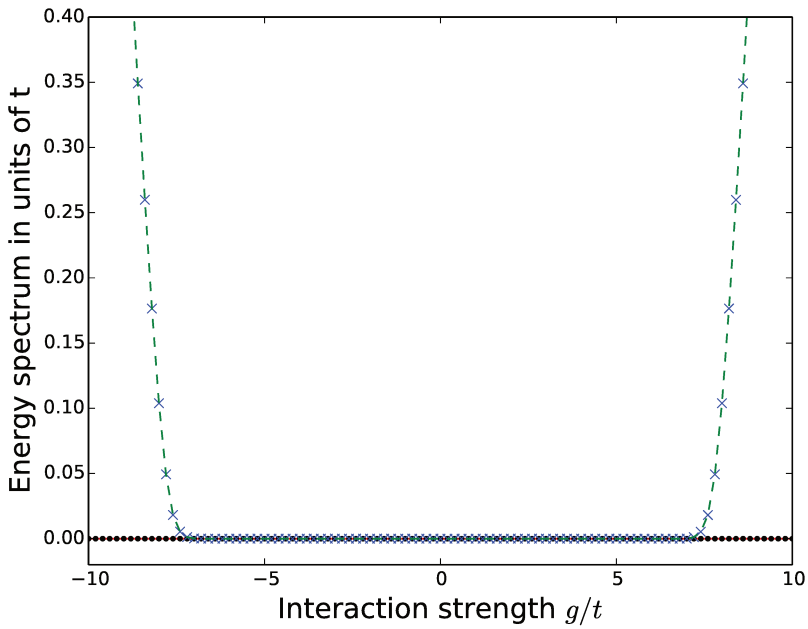

Figure 4.5: The first four levels of the energy spectrum on the line $\mu = 0$ for $t = \Delta$ and with open boundaries for a 60-site ladder. We observe a four-fold degeneracy in the topological phase and a two-fold degeneracy in the Ising phases.

A second good marker for topology is the degeneracy of the entanglement spectrum [102] in the periodic ladder, as explained in Section 2.2.2. The presence of the four Majorana boundary states translates into a four-fold degeneracy in the entanglement spectrum with PBC. This degeneracy can be observed in both ED or MPS simulations. Typical behavior for the entanglement spectrum on the line $\mu = 0$ is presented in Fig. 4.6.

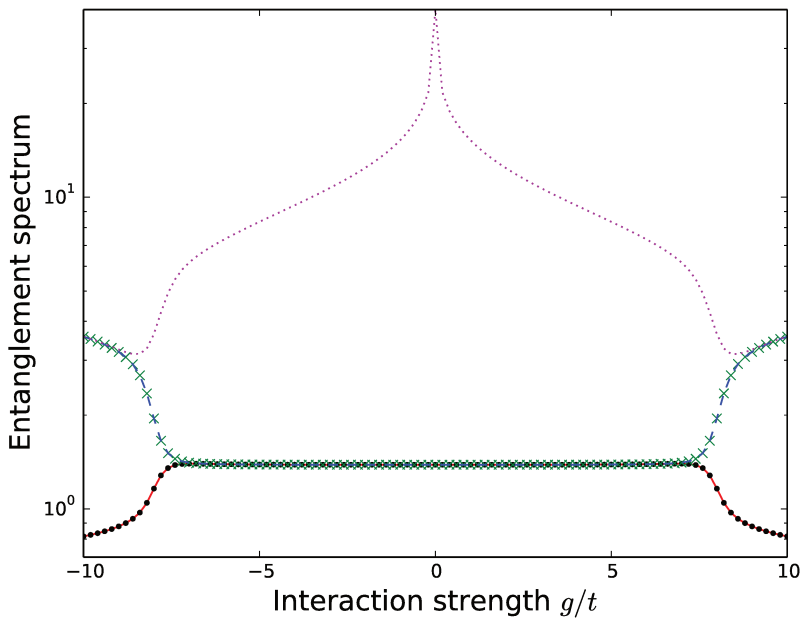

Figure 4.6: The first five levels of the entanglement spectrum on the line $\mu = 0$ for $t = \Delta$ and periodic boundary conditions for a 60-sites ladder. We observe a four-fold degeneracy in the topological phase, and a two-fold degeneracy in the Ising phase due to the degeneracy of the ground state with PBC.

4.3.4 Behavior of the large g phases

The two MI phases at large g are very similar in behavior. For $\Delta_{\pm}^{(2)} = \Delta^{(1)} = 0$, the effective low-energy Hamiltonian is exactly the same as for the Hubbard model, with a gapless spin sector and a charge Mott gap for $g > 0$ (and the opposite for $g < 0$). $\Delta_{-}^{(2)}$ ($\Delta_{+}^{(2)}$) however opens a gap in the spin (charge) sector for $g > 0$ ($g < 0$) and the resulting Mott phases are fully gapped. To obtain the general physical properties of these phases, it is enough to consider a Schrieffer-Wolff transformation into the low-energy subspace at $|g| \gg t, \Delta, \mu$[200]. A Schrieffer-Wolff expansion is simply the computation of a low-energy effective Hamiltonian by using perturbations around a large coefficient. More details on the method and the computation in this model are kept in Appendix D.3

Let us start with the MI-AF phase and $g > 0$. Similar to the Hubbard model, we can define spin operators in a standard way:

$$\begin{aligned}
\sigma_j^z &= c_{j,1}^\dagger c_{j,1} - c_{j,2}^\dagger c_{j,2} \\
\sigma_j^x &= c_{j,1}^\dagger c_{j,2} + c_{j,2}^\dagger c_{j,1} \\
\sigma_j^y &= i(c_{j,2}^\dagger c_{j,1} - c_{j,1}^\dagger c_{j,2}).
\end{aligned}$$

The effective low-energy Hamiltonian is given by:

$$H_{\text{eff},g+} = \frac{t^2-\Delta^2}{g}\sum_j \sigma_j^z\sigma_{j+1}^z + \frac{t^2+\Delta^2}{g}\sum_j \sigma_j^y\sigma_{j+1}^y + \frac{t^2-\Delta^2}{g}\sum_j \sigma_j^x\sigma_{j+1}^x. \tag{4.28}$$

Up to a spin-axis rotation, this effective model is nothing but the standard XXZ model. Δ breaks the $SU(2)$ rotation symmetry of spins of the Hubbard model, preserving only a $U(1)$ rotation invariance around the y-axis that can be directly seen in the Hamiltonian. Moreover, as long as $\Delta \neq 0$, we stay in the Antiferromagnetic Ising phase of this model (the Néel phase, where the anisotropy dominates). Our effective model is consequently gapped in both sectors, and presents a double degeneracy if we have OBC or PBC with an even number of sites. The fermionic density is also fixed at half-filling as long as we stay in this phase. Just as for the Hubbard model, small variations of the chemical potential do not affect the low-energy Hamiltonian, and hence the different observables are left essentially unaffected. A clear physical picture is obtained when $\Delta = t$. The effective model is then a pure Ising model, with trivial ground states: $\bigotimes_j \left|(-1)^j\right\rangle_j^y$, where $\sigma_j^y \left|\pm 1\right\rangle_j^y = \pm \left|\pm 1\right\rangle_j^y$. This peculiar order in the y-direction is characteristic of the formation of orbital (alternating in this case) currents in the ladder. Each of these ground state spontaneously breaks the time reversal symmetry, as the transverse operator current

$$J_\perp^N = i\sum_j (-1)^j (c_{j,1}^\dagger c_{j,2} - c_{j,2}^\dagger c_{j,1}) \tag{4.29}$$

acquires a non-zero expectation value[6]. This spontaneous symmetry breaking is not in contradiction with Mermin-Wagner theorem, as time-reversal is a discrete symmetry ($\mathbb{Z}_2$). We want nonetheless to underline that these orbital currents appear in the absence of an explicit flux, and that they are quite unusual as they correspond to coordinated exchange of 4 fermions between the two wires. Ref. [193] found a similar Orbital Antiferromagnetic phase (OAF), induced by the nearest neighbor interaction $V n_j n_{j+1}$. It is not surprising as $\cos(2\sqrt{2}\theta_-)$, generated by Δ in the RG process, is also a contribution of V. The main difference is in the nature of the spontaneous currents, as direct hopping between the two wires is allowed in Ref. [193]. The occurrence of orbital currents in two dimensions has also attracted some attention in the context of high-Tc superconductors due to the interplay between the magnetism close to the Mott state and the superconductivity[201–204]. They can also be induced through the creation of magnetic fields and orbital effects as in superconductors and through artificial gauge fields [205] in ultra-cold atoms [206]. For recent examples in two-leg ladder systems, see for example Refs. [207–213].
μ does not change perturbatively the effective Hamiltonian Eq. (4.28), as the corresponding term is constant when projected onto the low energy subspace. However, larger μ of order g are responsible for a resurgence of the $4MF$ phase as discussed above.

The case $g < 0$ is very similar in its mathematical structure. We define this time

[6]Note the alternating $(-1)^j$ that differentiates between $J_\perp^N$ and J_y in Eq. 4.20.

anomalous spin operators:

$$\begin{aligned}\mathfrak{s}_j^z &= c_{j,1}^\dagger c_{j,1} + c_{j,2}^\dagger c_{j,2} - 1\\ \mathfrak{s}_j^x &= c_{j,1}^\dagger c_{j,2}^\dagger + c_{j,2} c_{j,1}\\ \mathfrak{s}_j^y &= i(c_{j,2} c_{j,1} - c_{j,1}^\dagger c_{j,2}^\dagger).\end{aligned}$$

The corresponding effective Hamiltonian is:

$$H_{\text{eff},g-} = \frac{t^2-\Delta^2}{|g|}\sum_j \mathfrak{s}_j^z\mathfrak{s}_{j+1}^z - \frac{t^2+\Delta^2}{|g|}\sum_j \mathfrak{s}_j^y\mathfrak{s}_{j+1}^y + \frac{\Delta^2-t^2}{|g|}\sum_j \mathfrak{s}_j^x\mathfrak{s}_{j+1}^x - \mu\sum_j \mathfrak{s}_j^z. \quad (4.30)$$

The physics is the same as for $g > 0$, as we can map one to the other with the transformation: $\mathfrak{s}_j^z \to \sigma_j^z$, $\mathfrak{s}_j^x \to (-1)^j\sigma_j^x$ and $\mathfrak{s}_j^y \to (-1)^j\sigma_j^y$. In term of these anomalous spins, we obtain a gapped Ferromagnetic Ising phase in the $\mathfrak{s}^y$ direction at $\mu = 0$. The ground state is twice-degenerate, and time reversal symmetry is again spontaneously broken, leading to global currents from one wire to the other. The relevant operator $J_\perp^A$ is obtained by considering the case $\Delta = t$:

$$J_\perp^A = i\sum_j (c_{j,1}c_{j,2} - c_{j,2}^\dagger c_{j,1}^\dagger). \quad (4.31)$$

It corresponds to a pair current through the substrate. Ref. [193] does not observe a similar phase, as Vn_jn_{j+1} cannot give a contribution similar to $\Delta_+^{(2)}$.
Its susceptibility to relative chemical potential (a magnetic field in the language of Hubbard model) is zero. The chemical potential now plays the role of a transverse field, leading to a phase transition toward a fully polarized state at μ of order $\frac{t^2+\Delta^2}{g}$.

4.3.5 Nature of the transitions

Finally, we provide numerical and analytical arguments for the nature of the different phase transitions. We start by considering the transition between the MI-AF and $4MF$ phase.

We focus on: $g > 0$ and m_g and Δ are of the same order. First, we argue that the mode (ϕ_-, θ_-) is not affected by the transition. Indeed, θ_- is still locked to $\theta_- = 0\ [\pi/\sqrt{2}]$ and $\Delta_-^{(2)}$ stays relevant at this transition, whether $\Delta^{(1)}$ goes to strong coupling or not. Consequently, the spin sector knows no phase transition. The description of the transition of the charge sector at finite value of Δ is actually a more challenging problem. Let us start by considering the Hubbard model and the commensurate-incommensurate transition between the Mott phase and the liquid phase. We know from exact solutions that, close to the transition, the universal value of the Luttinger parameter for the charge mode is $K_+ = \frac{1}{2}$[214, 215]. We start from this limit and branch a small Δ.

As the spin mode stay gapped, we perform a mean-field approximation in order to separate the two modes:

$$\begin{aligned}\Delta^{(1)}\cos(\sqrt{2}\theta_+)\cos(\sqrt{2}\theta_-) &\to \Delta^{(1)}\cos(\sqrt{2}\theta_+)\langle\cos(\sqrt{2}\theta_-)\rangle\\ &\to \pm\Delta^{(1)}\cos(\sqrt{2}\theta_+).\end{aligned}$$

The sign depends on the ground state of the spin mode, and has no consequences on the picture of the transition. We will consequently consider it positive. We then proceed to a rescaling $\phi_+ \to \phi_+/\sqrt{2}$ to reach the refermionizable point. The effective model close to the Hubbard transition line between the Mott-Heisenberg phase and the LL is:

$$H = \int dx \frac{v_{F,+}}{2\pi}((\partial_x\theta_+)^2 + (\partial_x\phi_+)^2) + \frac{g_+}{\alpha^2}\cos(2\phi_+) + \frac{\Delta^{(1)}}{\alpha^2}\cos(2\theta_+), \tag{4.32}$$

where g_+ is a small effective interacting term, the effective mass. It corresponds to a g term that has been eventually renormalized by the chemical potential. One can then refermionize the Hamiltonian as done for example in Refs. [198, 216, 217]. To that end, we introduce two chiral fermions:

$$\psi_{R/L} = \frac{U_{R/L}}{\sqrt{2\pi\alpha}} e^{\mp i(\phi_+ \pm \theta_+)}, \tag{4.33}$$

where $U_{R/L}$ are Klein factors and α the short distance cut-off of the theory. We place ourselves in the representation where $U_R^\dagger U_L = -i$. We then use the following identification:

$$\cos(2\phi_+) = i\pi\alpha(\psi_R^\dagger\psi_L - \psi_L^\dagger\psi_R)$$
$$\cos(2\theta_+) = i\pi\alpha(\psi_R\psi_L - \psi_L^\dagger\psi_R^\dagger).$$

The effective Hamiltonian is then given by:

$$H = \int dx(-iv_{F,+})(\psi_R^\dagger\partial_x\psi_R - \psi_L^\dagger\partial_x\psi_L) + \frac{ig_+\pi}{\alpha}\int dx(\psi_R^\dagger\psi_L - \psi_L^\dagger\psi_R) + \frac{i\Delta^{(1)}\pi}{\alpha}\int dx(\psi_R\psi_L - \psi_L^\dagger\psi_R^\dagger). \tag{4.34}$$

One can finally introduce Majorana modes and obtain the final expression for our effective Hamiltonian:

$$\psi_{R/L} = \frac{\gamma^0_{R/L} + i\gamma^1_{R/L}}{\sqrt{2}}$$

$$H = \sum_{\sigma=0,1}\int dx \frac{(-iv_{F,+})}{2}\gamma_R^\sigma\partial dx\gamma_R^\sigma - \gamma_L^\sigma\partial dx\gamma_L^\sigma + \int dx \frac{\pi(g_+ + \Delta^{(1)})}{\alpha} i\gamma_R^0\gamma_L^0 + \frac{\pi(g_+ - \Delta^{(1)})}{\alpha} i\gamma_R^1\gamma_L^1. \tag{4.35}$$

The effective model is consequently very simple: two massive Majorana fermions. A phase transition consequently occurs when one of the two masses vanishes, i.e $g_+ \pm \Delta^{(1)} = 0$. At these two points, one of the Majorana wire is free while the other is massive. The transition is therefore an Ising transition instead of a Commensurate-Incommensurate transition, with a central charge $c = \frac{1}{2}$. We argue numerically that this picture is still valid when Δ and g are of the same order by computing the central charge on the transition line.

The transition between the MI-F phase and the $4MF$ phase follows the same physics at $\mu = 0$ by symmetry. Again, numerically the picture is still valid when one branches μ.

Finally the direct transition between the MI-F phase and the Polarized phase is the simplest to describe. As explained in the previous Section, the effective model at large coupling is a Quantum Ising model in a Transverse Field. The critical model is consequently also the critical Ising model, with a central charge $c = \frac{1}{2}$.

4.4 The Double Critical Ising phase

In this Section, we focus on the study of the properties and existence of the Double Critical Ising phase. This phase opens at low-filling, and consequently direct bosonization is not very well suited to describe it. We propose an analytical description of the phase, and some numerical results to confirm its existence.

4.4.1 Mean-field precursor to the DCI

While in one dimension, mean-field computations are usually not reliable, they can give us some insights on the physical properties of a model, and in particular in the existence of phase transitions. In the absence of Coulomb interaction $g = 0$, the transition between the topological and trivial phase is simply given by $\mu = \pm 2t$ and independent of Δ. Due to the conservation of the fermionic parity in each wire, the only partitioning of the interaction that one can introduce without explicitly breaking any symmetry is:

$$g\left(\rho_1(j) - \frac{1}{2}\right) n_{j,2} + g\left(\rho_2(j) - \frac{1}{2}\right) n_{j,1},$$

where $\rho_{1/2}$ is the fermionic density in each wire. Assuming a symmetry between the two wires, we obtain a simple equation for the transition lines:

$$g_\pm = \frac{\mu \mp 2t}{\rho_\pm - \frac{1}{2}} \tag{4.36}$$

where $\rho_\pm$ is the density at the transition point $\mu = \pm 2t$ for the non-interacting Kitaev's wire[155]:

$$\rho_+ - \frac{1}{2} = \begin{cases} \frac{1}{\pi}\frac{\arcsin(\sqrt{1-\Delta^2/t^2})}{\sqrt{1-\Delta^2/t^2}} & \text{if } |\frac{\Delta}{t}| \leq 1 \\ \frac{1}{\pi}\frac{\operatorname{argsh}(\sqrt{\Delta^2/t^2-1})}{\sqrt{\Delta^2/t^2-1}} & \text{else} \end{cases} \tag{4.37}$$

In this limit, the only effect of the transition is a shift of the normal critical points. It can be reformulated as:

$$\mu_\pm = \pm 2t \pm g(\rho_+ - \frac{1}{2}),$$

using $\rho_+ = 1 - \rho_-$. We recover that repulsive interactions widen the range of chemical potential where the topological phase survives, while attractive interactions reduce it. This

equation reproduces well the numerical transition line for weak interaction.

But one can assume the breaking of the expected symmetry between the two wires $c_1 \leftrightarrow c_2$ and allow for different densities. One has now to compare the potential solutions by minimizing the total energy after solving the following two consistency equations:

$$\rho_{1/2} - \frac{1}{2} = -\int_0^{2\pi} \frac{dk}{4\pi} \frac{-(\mu - g(\rho_{2/1} - \frac{1}{2})) - 2t\cos k}{\sqrt{(\mu - g(\rho_{2/1} - \frac{1}{2}) + 2t\cos k)^2 + 4\Delta^2 \sin^2 k}}.$$

There is no simple analytical expression to these solutions but a numerical study reveals the appearance of a set of asymmetrical solutions at finite interaction strength. We find a whole parameter space where there exists an asymmetrical solution whose energy is lower than the symmetrical solution. It is an indicator of the opening of a new phase, and roughly corresponds to the limits of the DCI phase. Nonetheless, as expected, the mean-field argument does not correctly describe its properties. While the mean-field computation predicts a finite difference in densities in each wire even in the thermodynamic limit, numerical simulations assert that the difference in electronic populations between the two wires is only around 2 fermions, whatever the number of sites we consider. Moreover, while the numerical simulations predict a gapless phase, here the phase is necessarily gapped. However, the mean-field approach has the advantage to simply explain the spontaneous breaking of symmetry between the two wires we observe in numerical simulations: instead of having a single ground state, we obtain a doubly degenerate ground state with fermionic parity (even, odd) and (odd, even).

4.4.2 Unraveling the ladder

To find an effective analytical model far from half-filling, we use the same approach as in Section 4.1.2 and build an effective Luttinger Liquid from manipulations of the Majorana fermions. The $U(1)$ symmetry discussed in Section 4.2.3 corresponds to the conservation of the fermionic charge of the d fermions. This charge conservation is extremely convenient for our analytical analysis.

We now take into account the variation of the chemical potential around $\mu = -2t$ that can be written as:

$$-i\delta\mu \sum_{j,\sigma} \alpha_{2j,\sigma}\alpha_{2j-1,\sigma} = \frac{\delta\mu}{2} \sum_j (1 + (-1)^j)(d_j^\dagger d_{j+1} + d_{j+1}^\dagger d_j). \tag{4.38}$$

$\delta\mu$ favors dimerization of the d fermions, as expected.
The new interacting term actually has a simple expression in the basis of the d fermions:

$$-\frac{g}{2} \sum_j (1 + (-1)^j)(n_j - \frac{1}{2})(n_{j+1} - \frac{1}{2}). \tag{4.39}$$

As $\delta\mu$, g also separates into two contributions, one is alternating and the other is constant. The former also favors dimerization (this will appear more clearly below using Bosonization) and competes with $\delta\mu$, while the latter tries to impose a uniform charge distribution

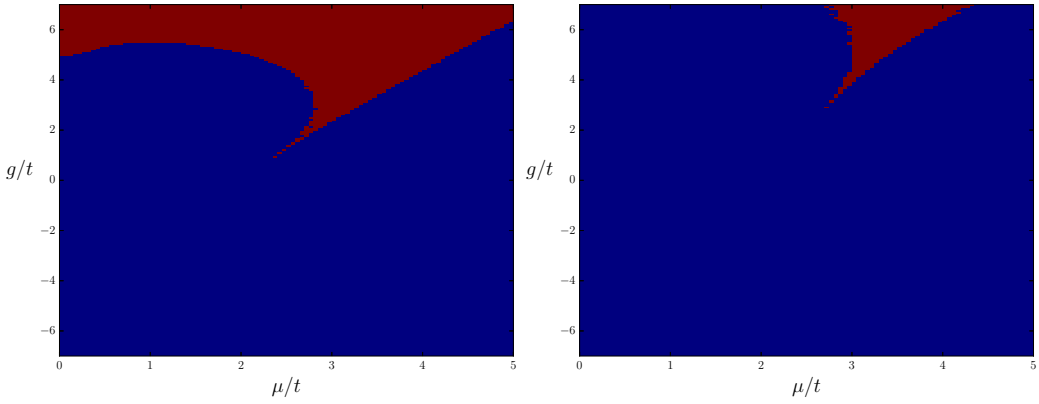

Figure 4.7: Results of the mean-field computations for $d = 0.5t$, $d = t$ and $d = 2t$. We computed the auto-coherent solution of the mean-field equations, and classified them depending on whether they break the symmetry between the two wires (blue for symmetric solutions, red for non-symmetric ones). It also correspond to a change in the degeneracy of the ground state (from no degeneracy to twice degenerate). This criterium does not discriminate between the opening of the Mott-Ising phase and the DCI. Note that there are some signs of the gaplessness of the DCI and of the differences between MI and DCI in the mean-field: presence of several auto-coherent solutions and size of a gap between the different solutions, but these are not enough to conclude.

in competition with the two dimerization schemes.
While most bosonized terms are standard, obtaining the correct contribution for the alternating part of g is actually more challenging. One has to take special care and proceed to do the OPE of the term in order to get the correct expression (see for example Ref. [218] where such terms are included to take into account disorder):

$$(-1)^j n_j n_{j+1} \propto \partial_x \phi_j \sin(2\phi_{j+1}) \to \cos(2\phi_j).$$

The final Hamiltonian is given by:

$$H = \frac{\tilde{v}_F}{2\pi}\left(\frac{1}{K}(\partial_x\phi)^2 + K(\partial_x\theta)^2\right) - g_\phi \cos(2\phi) \tag{4.40}$$

with $\tilde{v}_F = (4t - \delta\mu)\sqrt{1 - \frac{2g}{\pi(4t-\delta\mu)}}$, $g_\phi = (\frac{\delta\mu}{2\pi\alpha} + \frac{g}{2\pi^2\alpha^2})$ and $K = \frac{1}{\sqrt{1-\frac{2g}{\pi(4t-\delta\mu)}}}$. The discussion in this Section is in principle restricted to having $|\delta\mu| \ll t$, as a too large $\delta\mu$ induces a dimerization of the kinetic term, and hence invalidate the bosonization approach.

The dimension of $\cos(2\phi)$ is K. Consequently, as long as $K < 2$, it is always relevant. The topological nature of the transition is given by which dimerization direction is

preferred:

$$-g_\phi \cos(2\phi) \propto g_\phi \sum_j (-1)^j (d_j^\dagger d_{j+1} + d_{j+1}^\dagger d_j)$$
$$= i g_\phi \sum_{j,\sigma} (\gamma_{A,j,\sigma}\gamma_{B,j,\sigma} - \gamma_{B,j+1,\sigma}\gamma_{A,j,\sigma}).$$

The critical line is given by $g_\phi = 0$, which agrees well with the mean-field result (taking α the lattice spacing to be 1).
When $K > 2$, the cosine term stops being relevant: a gapless phase opens around the line $g_\phi = 0$. This phase is a $c = 1$ Luttinger Liquid in the language of the d fermions and therefore an extension of the critical point at $g = 0$. Contrarily to Section 4.1.3, the Luttinger parameter can be different from 1, as the wires are strongly coupled. While there is a parallel with the opening of the phase in the mean field, the latter method can only predict gapped phases.

The opening of this DCI phase can be understood in the following way. $\delta\mu$ and the alternating part of g tend to form two types of contradictory dimerizations that therefore compensate themselves on the critical line. The constant part of g opposes the two dimerization. When g is large enough, it prevents any of them from occurring.

4.4.3 Large g model

An interesting limit to study is the behavior of the DCI when $g \gg t, \Delta$. Indeed, from bosonization, one expects it to survive at infinite coupling, at the vicinity of the point $\mu = \pm\frac{g}{2}$. We focus in this section on $\mu = -\frac{g}{2} + \delta\mu$, with $\delta\mu = O(t)$. At this point, there is either zero or one fermion on each rung of the ladder. It is possible to derive an effective model similar to the $t - J$ model for Hubbard, but we will be interested in the model at 0th order in g.
We define dressed fermions $\tilde{c}_{j,\sigma} = c_{j,\sigma}(1-n_{j,-\sigma})$, where $n_{j,-\sigma}$ is the number operator at site j on the wire 2 if $\sigma = 1$ (and 1 if $\sigma = 2$). These dressed fermions follow a different algebra than usual but allow for a simple writing of the Hamiltonian (and a direct implementation for numerics):

$$\{\bar{c}_{i,\sigma}, \bar{c}_{j,\sigma'}\} = 0 \quad \{\bar{c}_{i,\sigma}, \bar{c}_{j,\sigma}^\dagger\} = \delta_{i,j}(1 - n_{j,-\sigma})$$
$$\{\bar{c}_{i,\sigma}, \bar{c}_{j,-\sigma}^\dagger\} = \delta_{i,j} c_{j,-\sigma}^\dagger c_{j,\sigma} = \delta_{i,j} \bar{c}_{j,-\sigma}^\dagger \bar{c}_{j,\sigma}$$

$$H = -\delta\mu \sum_{j,\sigma} c_{j,\sigma}^\dagger c_{j,\sigma} - t \sum_{j,\sigma} \left(\tilde{c}_{j+1,\sigma}^\dagger \tilde{c}_{j,\sigma} + \tilde{c}_{j,\sigma}^\dagger \tilde{c}_{j+1,\sigma} \right)$$
$$+ \Delta \sum_{j,\sigma} \left(\tilde{c}_{j,\sigma}^\dagger \tilde{c}_{j+1,\sigma}^\dagger + \tilde{c}_{j+1,\sigma} \tilde{c}_{j,\sigma} \right). \quad (4.41)$$

The definition as dressed fermions comes naturally from the restriction to a three dimensional subspace on each site. It is then just as natural to try to find an equivalent

system replacing the fermions under constraints by spin one. It is possible to construct a Jordan-Wigner like transformation that verifies the previous algebra, with S^x, S^y and S^z the usual spin-1 operators.

$$\begin{aligned}\bar{c}^\dagger_{j,\uparrow} &= S^z_j S^+_j e^{i\pi \sum_{k<j} (S^z_k)^2} \\ \bar{c}^\dagger_{j,\downarrow} &= -S^z_j S^-_j e^{i\pi \sum_{k<j} (S^z_k)^2} .\end{aligned} \tag{4.42}$$

After some algebra, one has an alternative expression for the Hamiltonian:

$$\begin{aligned}H = -\mu(S_z)^2 + \frac{\Delta - t}{2}\{S^x_j S^x_{j+1}, S^z_j S^z_{j+1}\} \\ - \frac{\Delta + t}{2}\{S^y_j S^y_{j+1}, S^z_j S^z_{j+1}\} - \frac{t}{2}(S^x_j S^x_{j+1} + S^y_j S^y_{j+1}).\end{aligned} \tag{4.43}$$

Both models can be efficiently treated by numerical means, yet, in contrast to the (solvable) spin-1 chain models[219–222], this Hamiltonian is not easily solvable and the Poisson brackets do not simplify. We will therefore resort to a numerical analysis below showing that the DCI phase becomes well visible in the phase diagram in the limit of large interactions.

4.4.4 Numerical approach

Existence of the DCI phase

While bosonization affirms the existence of the phase for $K > 2$, there exist well-known examples where there is a limiting value for K that is not trivially detectable but appears when one exactly solves the model. A canonical example is, for example, the limit $\frac{1}{2} < K < 2$ in the Hubbard model. With such limit, there would be no opening of the DCI phase at large g. A first numerical approach is to work at fixed g and try to interpolate the boundaries of our supplementary phase in the thermodynamic limit. To determine the boundary of the phase, one can consider either the closing of the gaps or the peak in central charge, as both neighboring phases are gapped. Nevertheless, the most visible numerical marker of the phase will be the degeneracy of the ground state in the case of PBC. In that case, the ground state is doubly degenerate, and the ground states have different fermionic parities: (odd, even) and (even, odd). This spontaneous breakdown of the symmetry between the wires is allowed, as we break only a discrete symmetry, similarly to what happens in the two Mott phases. Mean-field computations allow to intuitively understand this degeneracy. In analogous fermion models (for example the XXZ model), such a degeneracy was observed for PBC when the length of the wire is a multiple of 4 sites[223, 224].

Figure 4.8 presents the results of such a scaling analysis for $\Delta = t$ and $g = 5t$. The width converges towards a finite value $0.06t$.

As another element of answer, one can consider the limiting models for $g \to +\infty$ we previously derived. Figure 4.9 presents the first four levels of the Hamiltonian 4.41 for a range of renormalized chemical potential. The double degeneracy is symptomatic of the DCI phase. The absence of a gap in this phase is also confirmed by both scaling

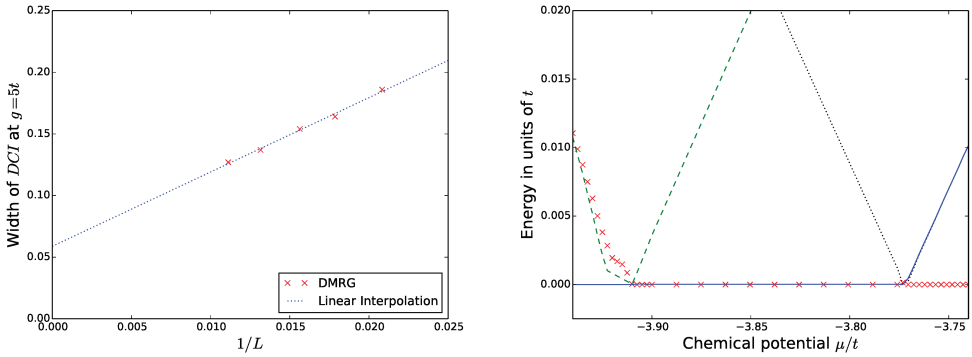

Figure 4.8: Left: linear regression of the width of the DCI phase for $g = 5t$ and $\Delta = t$ based on the analysis of the energy spectrum. This width converges towards a finite non-zero value of order $0.06t$. Right: first four levels of the energy spectrum of the periodic ladder for $g = 5t$ and $\Delta = t$, as a function of the chemical potential for a 76-site wire. On the left, the system is in the polarized phase, on the right it is in the $4FM$ phase. The double degeneracy of the ground state clearly reveals the DCI phase. Symmetry analysis reveals that the parity of the ground states follow the stated rules (even-even in polarized, odd-odd in $4FM$ and (even-odd, odd-even) in DCI.

analysis and entanglement entropy. It also presents the central charge computed from the entanglement entropy of this model, in good agreement with the results at finite g and our theoretical predictions.

We should also discuss the width of the phase in terms of the chemical potential at $g = +\infty$. While it was extremely limited at finite g, it is now of order $3t$ for the system considered in Fig 4.9. On the other hand, at infinite g, the $4MF$ phase has disappeared.

Properties of the DCI phase

First we focus on numerical results obtained using our original model. As in Section IV, we will use different numerical markers: entanglement entropy, entanglement spectrum and spectrum with PBS.

The spectrum for the ladder with PBC is given in Figure 4.8 and we observe for positive and large values of g a gapless phase with an accidental two-fold degeneracy that disappear with OBC. Their parity follow the rules stated in the previous section. Scaling of the finite-sized gap in this phase reveals its gaplessness. We observe also a corresponding two-fold degeneracy in the entanglement spectrum, compared with four-fold for the SPT phase and no degeneracy for the polarized phase in Figure 4.10. Finally, one can compute the central charge from the entanglement entropy: it confirms the gaplessness of the phase and validates our model with the extraction of a charge close to unity in the DCI phase (Figure 4.10).

Finally, computation of the correlation functions confirm that the Luttinger parameter

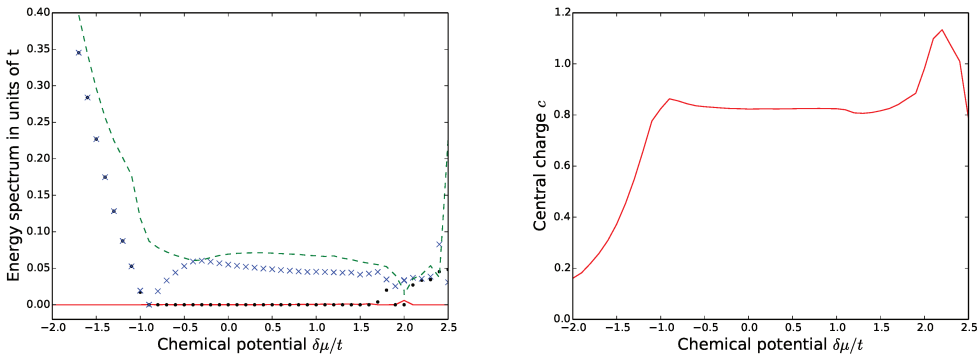

Figure 4.9: Left: first four levels of the energy spectrum at $g = +\infty$ for a 68-site ladder at $\Delta = t$ from DMRG with PBC. The visible double degeneracy of the central phase reveals the survival of the DCI phase. Scaling analysis and entanglement entropy confirms its gaplessness. Right: central charge obtained from entanglement entropy for a 68-site ladder at $\Delta = t$ and $g = +\infty$ from DMRG with PBC, using the model given in Eq 4.41. The results are in qualitative agreement with our theoretical prediction and the results at finite g in Fig 4.10.

has been renormalized to $K > 2$ in the gapless phase. Extraction of a precise value is nonetheless difficult. The sign of the connected correlation function is still positive, as in Kitaev's model at the critical point, and the sub-dominant contribution to the fluctuation stays negative.

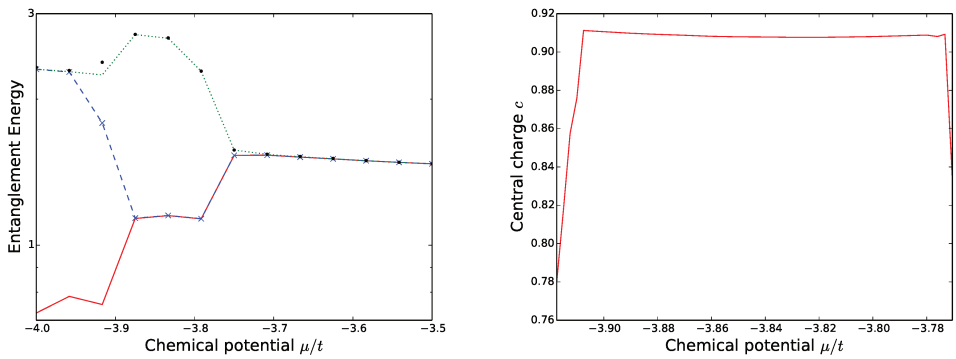

Figure 4.10: Left: entanglement spectrum of the periodic ladder for $g = 5t$ and $\Delta = t$, as a function of the chemical potential for a 90-site wire. On the left, the system is in the polarized phase, on the right it is in the $4FM$ phase. We observe a progressive lifting of the degeneracy from 4 in the $4FM$ to 2 in the DCI and finally no degeneracy in the Polarized phase. Right: central charge extracted from a fit of the entanglement entropy of the periodic ladder for $g = 5t$ and $\Delta = t = 1$, as a function of the chemical potential for a 76-site wire.

Chapter 5

Transport in topological systems

Contents

5.1 Motivation and summary . . . 145
5.1.1 Motivation . . . 145
5.1.2 Summary of the main results . . . 149
5.2 Model and bosonization . . . 151
5.2.1 Model . . . 151
5.2.2 Tunelling term and number of Majoranas . . . 152
5.2.3 Bosonization and Majorana fermions . . . 155
5.3 Quantum Brownian Motion and Topological Kondo model . . . 155
5.3.1 Quantum Brownian Motion . . . 156
5.3.2 Far from charge degeneracy: the Topological Kondo limit . . . 157
5.4 Charge degeneracy point: an exact mapping to the multi-channel Kondo Model . . . 161
5.5 Phase diagram at charge degeneracy . . . 163

5.1 Motivation and summary

5.1.1 Motivation

The realization and manipulation of Majorana bound states in topological superconductors has been the focus of numerous studies[16, 17]. One of the key problems is finding clear experimental signatures of the existence of these elusive quasi-particles: one of the very facts that make them interesting, their resilience, also makes them difficult to observe. It was found that these Majorana fermions have characteristic transport properties.
Indeed, the presence of Majorana fermions at the boundary of a superconductor strongly affects the transport of electrons through the substrate. Depending on what the superconductor is connected to, various effects have been observed. In the following, we briefly review some of them, without trying or hoping to be exhaustive.
First, if one connects the topological superconductor to a trivial metal, the presence of

the zero-energy fermionic mode due to the Majorana fermions allows for single-electron hopping. It in particular leads to local-and cross-Andreev reflections[225, 226]. The local Andreev reflection is a well-known effect of superconductivity: as only Cooper pairs can propagate in the superconductor, when an incident electron from the metallic lead arrives at the boundary, it can tunnel into the superconductor only by combining with another electron. This leads to the appearance of a counter-propagating hole in the lead, and of an additional Cooper pair in the superconductor. This Cooper pair is then dissipated in the electric mass. Such an effect can occur in a normal superconductor, but the self-adjoint character of the Majorana fermion leads to a perfect conduction. This leads to the celebrated[25–33] quantized zero-bias peak, with a quantized conductance:

$$\frac{2e^2}{h}. \tag{5.1}$$

This conductance is nonetheless not a smoking-gun for Majorana fermions, as other type of sub-gap impurities may give similar results[52, 54–57]. As a general rule, not only the peak should be observed, but also its resilience (or lack thereof) to perturbations[53, 58, 59]. The cross-Andreev reflexion appears when connecting two leads (with a voltage bias). The previous hole is reflected in a different lead, which reveals the non-locality of the effective fermion built out of the Majorana fermions of the superconductor. In principle, it is a more robust effect[225–228]. Noise measurement of the different currents carry also information on the fractional nature of the Majorana fermions[229], and connections with quantum dots have also been explored[44].
Secondly, the presence of Majorana fermions affects the Josephson effect[230]. The Josephson effect simply consists in the following. Take two superconductors separated by a small insulator, such that Cooper pairs may tunnel between the two. If their superconducting phase is different, then we observe a current, directly related to the difference in phases:

$$I = I_0 \sin(\chi_1 - \chi_2), \text{ with } \chi_{1/2} \text{ the superconducting phases.} \tag{5.2}$$

In a ring geometry, this difference in phase would be induced by a magnetic flux inside the ring. When varying the magnetic flux, we observe a periodicity of the current every quanta of flux $\frac{\hbar}{2e}$. In the presence of Majorana fermions, single electron tunneling and transport is allowed, leading to the so-called 4π Josephson effect[13, 23, 231–240], where the period is now twice as large. This is simply due to the reduction of the charge of the elementary carriers. The fractional Josephson effect is very resilient due to the Majorana nature of the modes. Variants around this Josephson effect have been considered as probes of the topological nature of the superconducting phase[241].
Theoretically, recent works have also suggested to observe non-Abelian statistics through gate engineering [233, 242].
Combining charging effects with Majorana fermions, or Kondo physics with Majorana fermions [243–245], has already been argued to lead to exotic transport dc [246–249] or ac properties in quantum RC setting [250, 251]. In particular, the device described in Ref. [246] is closely connected to the one we will study in this Chapter. Take a superconducting island, where the total number of electrons is fixed (it is no longer connected to the mass). Then, if one connects two electronic leads to the island close to two Majorana fermions

and apply a small voltage bias, one observe a perfect single channel conductance between the two:

$$\frac{e^2}{h}. \tag{5.3}$$

The incoming electrons effectively transition through the zero-energy delocalized fermion composed of the Majorana fermions which leads to a perfect transmission.

It is therefore natural to study the influence of Majorana fermions on the transport properties of various mesoscopic structures. In this Chapter, we study a device proposed in the seminal works of Refs. [20, 21]: a single floating (not grounded) Majorana island connected to $M \geq 3$ reservoir leads, modeled by Luttinger liquids, through separated Majorana zero modes. It can be understood as a multichannel version of the device proposed in Ref. [246]. The "charge", *i.e.* number of Cooper pairs plus number of fermions in the zero energy Majorana manifold on the islands, can be varied through a gate voltage coupled to the quantum box. Progress in building such mesoscopic boxes have been made recently[252, 253]. In the non-degenerate case where transport occurs through a single charge state, an unconventional Kondo[254] screening, named "Topological Kondo model", has been theoretically explored [20, 21, 255–263] where the $SO(M)$ impurity "spin" is built from the Majorana excitations. Such boxes were proposed as building blocks of a quantum computer[22].

For a normal island without Majorana fermion, Matveev formulated the charge Kondo effect [264, 265] in which two degenerate charge states play the role of an effective spin 1/2 and hybridize with electrons either in contacted reservoirs or on the island, realizing the multichannel Kondo model (M-CKM). Remarkably, in the two-channel Kondo model emulated with two leads, an unscreened Majorana excitation appears at low energy [266–270]. It is however an emergent particle and differs from the proximity-induced Majorana fermions considered in this paper. Recently, the two-channel charge Kondo model has been realized[271] in a GaAs setting with an unprecedented control over the model parameters. Two-channel Kondo screening has also been observed with a real spin [272, 273]. In all cases, it requires fine-tuning which makes its experimental characterization challenging.

The low-energy theory of the Topological Kondo model exhibits non-Fermi liquid exponents captured by a strong coupling quantum Brownian motion (QBM) picture. In this analogy, the effective particle is pinned at the minima of a two-dimensional triangular lattice connected by instantons. Simple expressions for the leading irrelevant operator dimensions can thus be derived in agreement with the more involved Conformal Field Theory approach [274]. The conductance between the different leads is symmetric, fractionnalized and resilient to perturbations.

In contrast with the topological Kondo effect, the multichannel Kondo model does not admit a simple QBM description. The effective particle moves on a honeycomb lattice and the low-energy fixed point is at intermediate (neither weak or strong) coupling which excludes a full analytical QBM analysis. In addition, this infrared intermediate fixed point is not robust and requires fine-tuning whereas the topological Kondo non-Fermi liquid fixed point is at strong coupling and stable against perturbations such as asymmetric lead couplings. This last point seems to favor the experimental observation of the more robust topological Kondo effect over the standard multichannel Kondo model.

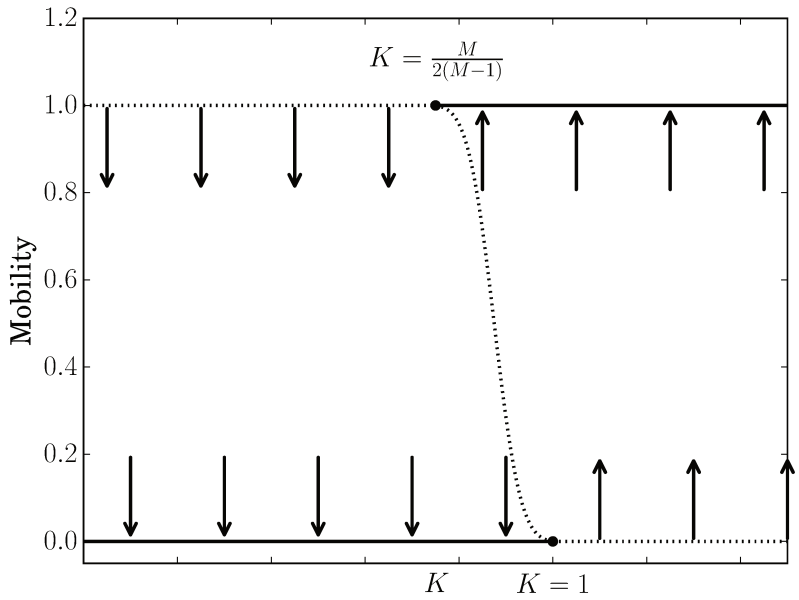

Figure 5.1: Phase diagram and flow for the single Majorana Kondo box far from charge degeneracy. The mobility is defined by: $\mu = \frac{hG_{j,j}}{2e^2}\frac{M}{1-M}$. Solid line describes stable fixed points while pointed lines are unstable. The arrows depict the flow of the most relevant/less irrelevant operators of the corresponding fixed point. K is the Luttinger parameter in all leads, that marks the strength of the interactions. We observe a first-order phase transition between zero and perfect mobility for K between $K = \frac{M}{2(M-1)}$ and $K = 1$.

In this Chapter we focus on the topological Kondo model close to charge degeneracy where the two charge states n and $n+1$ are energetically equivalent and described by a pseudo-spin. We show that the resulting QBM lattice is triangular with a pseudo-spin texture characterized by a Berry phase. The corresponding dual model is a honeycomb lattice. As a result, we recover the multichannel Kondo model but with Luttinger parameters in the leads that are doubled with respect to their bare values. For non-interacting leads, the resulting multichannel Kondo model has effectively strong interacting reservoirs, with the renormalized Luttinger parameter $K = 2$, and the strong coupling QBM fixed point becomes stable in contrast with the standard (non-interacting) Kondo fixed point. The standard multichannel Kondo model is exactly recovered at the bare value $K = 1/2$, *i.e.* for strong electronic repulsion in the leads.
Interestingly, we also show that for a large number of channels, the model is characterized by two stable fixed points in a certain window of Luttinger parameters, at strong and finite coupling, separated by an unstable fixed point, and thereby predicting a quantum phase transition as the electron tunneling amplitude to the lead is varied. The finite coupling fixed point is in fact analytically connected to the infrared fixed point of the multichannel Kondo model, and we thus expect similarly that it is not robust against channel asym-

metries or against lifting the charge degeneracy. Most of our perturbative results are based on the QBM analysis of Kane and Yi [275, 276] which we revisit by focusing on the pseudospin wavefunction. The same model at arbitrary charge degeneracy has been also investigated in Ref. [277] where the resonant peak in the conductance was shown to be strongly enhanced at degeneracy, and the strong coupling point was argued to be robust. We reproduce their main results, except for the fact that the renormalization group (RG) analysis in Ref. [277] is limited to lowest order so that the coexistence of stable fixed points for a number of channels above four is not discussed.
The Chapter is largely based on Ref. [278]. It is organized as follows. In Sec. 5.2, we introduce the problem and its bosonization description. We discuss the QBM picture in Sec. 5.3 and review its application to the topological Kondo model. The charge degenerate point is investigated in Sec. 5.4 where a mapping onto the M-CKM is formulated and in Sec. 5.5 where the evolution of the different fixed points is determined.

5.1.2 Summary of the main results

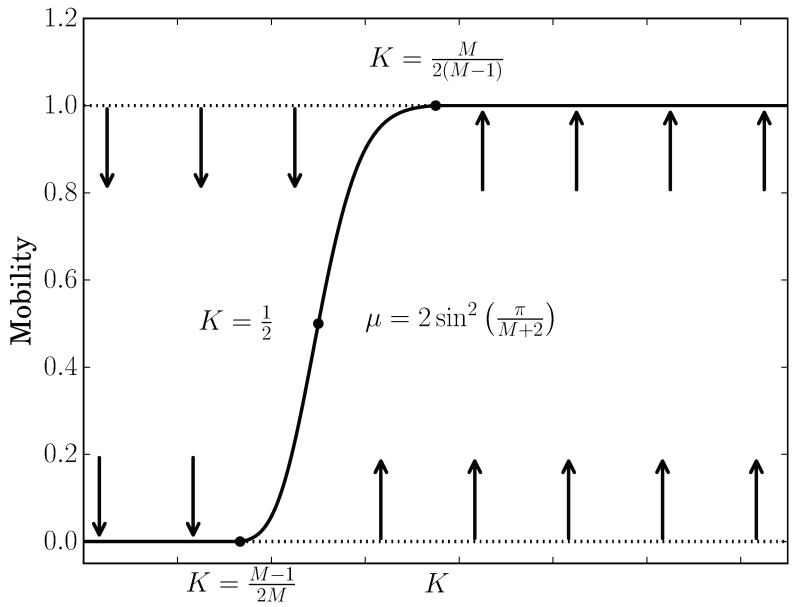

Figure 5.2: Phase diagram and flow for the Majorana Kondo box at charge degeneracy, as a function of the interaction strength, for $M = 3, 4$. The mobility is defined by: $\mu = \frac{hG_{j,j}}{2e^2}\frac{M}{1-M}$. We observe a continuous (second-order) phase transition between an insulating phase and a strong coupling phase with perfect symmetric fractionnalized conductance. In between, there exists a continuous line of stable fixed points.

In summary, we have demonstrated that the transport behaviour of a topological Kondo box hosting Majorana bound states depends sensitively on the proximity to a

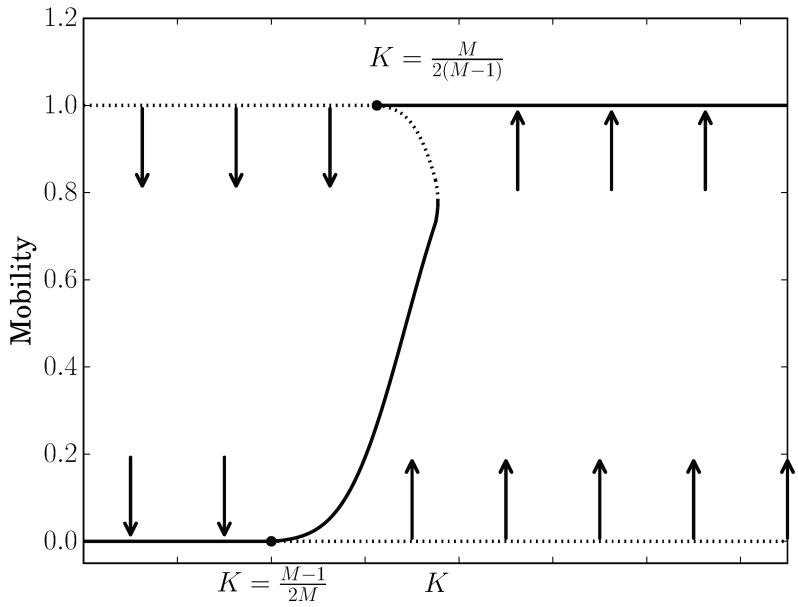

Figure 5.3: Phase diagram and flow for the Majorana Kondo box at charge degeneracy, as a function of the interaction strength for $M \geq 5$. The weak-coupling analysis gives the same results as for $M = 3, 4$, with a continuous stable line of fixed point appearing at a critical $K = \frac{M-1}{2M}$. For K below this critical value, the island is insulating. On the other hand, the strong coupling analysis differs, and is in fact similar to what we observed far from charge degeneracy. An unstable line of fixed points appears for $K = \frac{M}{2(M-1)}$ (with perturbativly the same equation as in the Topological Kondo limit). We postulate the coexistence of the intermediate and the strong coupling fixed points up to some critical value of the interactions where a first-order transition occurs.

charge degeneracy point. Away from charge degeneracy, the box exhibits the well-studied topological Kondo effect, flowing to maximum conductance for non-interacting leads, and displaying a quantum phase transition when the leads form Luttinger liquids, between strong-coupling and insulating regimes. Conductance as a function of the strength of the interactions in the wires is represented in Figure 5.1.

The situation is markedly different when the system is tuned to charge degeneracy. It also depends on the number of leads connected to the topological box and we can identify two situations, represented in Figure 5.2

1. For three or four Luttinger liquid leads, the intermediate Kondo fixed point is stable and exists for $\frac{M-1}{2M} < K < \frac{M}{2(M-1)}$, connecting the weak and strong coupling limits. As a result, the conductance between the leads takes the form

$$G_{j,k} = \frac{2e^2 K \mu(K)}{h} \left(\frac{1}{M} - \delta_{j,k} \right), \tag{5.4}$$

where the mobility $\mu(K)$, shown in Fig. 5.2, varies between 0 and 1. We recover the multichannel Kondo fixed point at $K = 1/2$, with the intermediate mobility $\mu(1/2) = \sin^2[\pi/(M+2)]$.

2. For more than four leads, we recover the critical behaviour of the topological Kondo model at high mobility, which indicates that the pseudo-spin does not play a role if the Majorana fermions are already strongly coupled to the leads. A quantum phase transition thus occurs with maximum conductance on one side. The location of the transition is perturbatively the same as away from charge degeneracy, improving with the number of channels M. The difference at degeneracy is that the insulating phase is replaced by a weakly transmitting phase similar to the continuous line of fixed points observed for $M = 3, 4$, where the conductance decreases with M. This weak coupling regime is in fact analytically connected to a special point at $K = 1/2$ where we recover exactly the multichannel Kondo model.

Our QBM analysis has identified the pseudo-spin, representing the two-state charge degeneracy in the box, as the physical ingredient explaining the difference in behaviour between the charge degenerate and non-degenerate cases. Detuning the system away from charge degeneracy or increasing the number of channels weakens the pseudo-spin component and thus extends topological Kondo physics in the phase diagram. Moreover, the intermediate fixed point (I) is not robust against channel asymmetries, and therefore requires fine-tuning, in contrast with the strong coupling fixed point as discussed in Ref. [277]. We note that the point $K = K_C(M)$ at which the critical line (I) turns over is not known analytically and remains a conjecture.

5.2 Model and bosonization

5.2.1 Model

We consider the device introduced in Refs. [20, 21] and depicted in Figure 5.4 composed of a floating mesoscopic superconductor onto which several topological semi-conducting nanowires have been deposited. They become superconductor by proximity effect (see Section 1.1 and 1.5.3 for examples of tight-binding models describing them). Driven in its topologically non-trivial state, each nanowire hosts a pair of zero-energy Majorana bound states located at its extremities. The superconducting island, also called topological Kondo box, is tunnel-coupled via their Majorana bound states to M normal leads of spinless conduction electrons.

The Hamiltonian describing this device is given by $H = H_{\text{box}} + H_{\text{leads}} + H_t$. We focus on low energies, well below the proximity gap induced by the superconducting island on the nanowires, and keep only the state manifold generated by the Majorana operators. The Hamiltonian for the box thus is simply given by its charging energy

$$H_{\text{box}} = E_C(\hat{N} - n_g)^2 \tag{5.5}$$

with the renormalized backgate voltage n_g. Formally, n_g is the number of holes on the gate. E_C is the charging energy of the box. The number of charges on the box $\hat{N}$, is

written as a sum

$$\hat{N} = 2\hat{N}_c + \hat{n},$$

where $\hat{N}_c$ counts the number of Cooper pairs and $\hat{n}$ the number of fermions in the zero-energy Majorana manifold on the island. $\hat{N}_c$ is conjugate to the superconducting phase χ as expressed by the commutation relation $[\chi, 2\hat{N}_c] = i$. Hence $e^{-2i\chi}$ is an operator shifting the number of Cooper pairs on the island by -1, *i.e.* it annihilates a Cooper pair. The Majorana operators can be paired to define fermionic operators, $d_j = (\gamma_{2j-1} + i\gamma_{2j})/2$. In this fermionic basis, the Majorana occupation number is simply given by $\hat{n} = \sum_{j=1}^{N/2} d_j^\dagger d_j$, where N (even) is the total number of Majorana bound states on island (we consider $N > M$, see the Section 5.2.2). For convenience in the notations but without loss of generality, we assume that the first $j = 1, \ldots, M$ Majorana are tunnel-coupled to the leads. We are mainly interested in $M \geq 3$, where the system is known to present non-trivial Kondo properties.

The electrons in the mesoscopic box have been polarized due to Zeeman effect[23–25, 30]. We then assume that the incoming electrons in the leads can penetrate in the box only if they have the right spin polarization. This justifies the representation as semi-infinite one-dimensional spinless fermions of the electrons in each lead. At low energy, the electron field operator in the lead j is

$$\psi_j(x) = e^{ik_F x}\psi_{R,j}(x) + e^{-ik_F x}\psi_{L,j}(x),$$

introducing right- and left-movers, where k_F is the Fermi momentum. The Hamiltonian has the form

$$H_{\text{leads}} = -iv_F \sum_{j=1}^{M} \int_0^{+\infty} dx \left(\psi_{R,j}^\dagger \partial_x \psi_{R,j} - \psi_{L,j}^\dagger \partial_x \psi_{L,j} \right) + H_{\text{int}} \tag{5.6}$$

where v_F is the Fermi velocity. H_{int} contains electron-electron intra-wire interactions and will be included as a Luttinger parameter K in the bosonization procedure[129–131]. Finally, the coupling between the Majorana bound states and the leads are described by the tunneling Hamiltonian (see Section 5.2.2 for a proper derivation)

$$H_t = -\sum_{j=1}^{M} t_j e^{-i\chi} \psi_j^\dagger(0)\gamma_j + h.c. \tag{5.7}$$

t_j are the tunneling amplitudes, all taken to be real and positive. The symbol (0) refers to the position $x = 0$ of each wire coupled to the island.

5.2.2 Tunelling term and number of Majoranas

In this Section, we detail a rigorous derivation of the tunneling Hamiltonian (5.7). We will prove that we can explicitly build the aforementioned tunneling operator as long as we do not couple to all the Majorana fermions present in the box.

First we consider that each lead is coupled to the extremity of a different nanowire, leading to the existence of at least $2M$ Majoranas. N (even) is the total number of

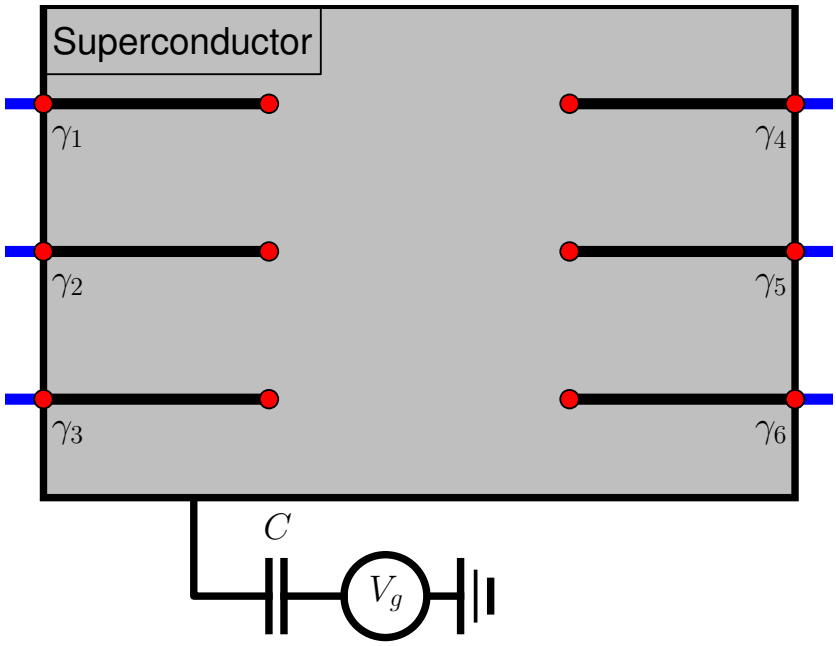

Figure 5.4: Sketch of the Majorana island. A superconducting box (grey) is connected through localized Majorana modes γ_j (red dots) to $M = 6$ normal leads (blue). The Majorana modes are typically realized as boundary bound states of topological nanowires deposited on the superconducting box (in black), and therefore come in pairs. In this proposal, only half the Majoranas are coupled to the leads, but only one uncoupled Majorana is required.

Majorana zero modes on the island. Let $\gamma_{L/R,j}$ be the Majorana fermions at the extremity of each nanowire, and $d_j = \frac{1}{2}(\gamma_{L,j} + i\gamma_{R,j})$ the corresponding delocalized fermion. The tunneling from the lead to the superconducting island can be written:

$$- t_j(d_j^\dagger + d_j e^{2i\chi})\psi_j(0) + h.c. \tag{5.8}$$

While the first term is the usual hopping term of a single fermion, the second one describes an alternative process where an electron of the lead and an electron on the nanowire combine to create a Cooper pair in the bulk of the superconducting island.

We wish to define a new operator $e^{i\tilde{\chi}}$, verifying

$$[\hat{N}, e^{i\tilde{\chi}}] = e^{i\tilde{\chi}}, \tag{5.9}$$

where $\hat{N} = 2\hat{N}_C + \hat{n}$ is the total number of particles in the box, such that all tunneling terms can be written as in Eq. 5.7, with γ_j a Majorana fermion that commutes with $e^{i\tilde{\chi}}$. This operator increases the number of electrons in the box by 1 (and not by 2 as $e^{2i\chi}$ would). For the number of electrons to change by one, the parity of $\hat{n}$ needs to change

as there are necessary an even number of electrons in the condensate. There are an infinite family of operators that invertibly shift this parity and we arbitrarily select the first fermionic number $d_1^\dagger d_1$ to serve as our pivot. We then can build the operator $e^{i\tilde{\chi}}$ explicitly[1].

$$e^{i\tilde{\chi}} = (d_1^\dagger + d_1 e^{2i\chi}) e^{i\pi \sum_{j=2}^{N/2} d_j^\dagger d_j} \times P_{\text{leads}} \tag{5.10}$$

$$= (d_1^\dagger - d_1 e^{2i\chi}) \times P_{\text{tot}} \tag{5.11}$$

where P_{leads} is the fermionic parity in all leads and P_{tot} the total fermionic parity. Their only use is to ensure commutation with all fermionic operators in the leads. $e^{i\tilde{\chi}}$ is unitary (in the limit where $\hat{N}_c \gg 1$) and verifies the desired commutation relation (5.9). From its expression, one checks that

$$e^{i\tilde{\chi}} e^{-2i\chi} = e^{-i\tilde{\chi}} \text{ and } (e^{i\tilde{\chi}})^2 = e^{2i\chi}. \tag{5.12}$$

In addition,

$$[e^{i\tilde{\chi}}, d_j] = [e^{i\tilde{\chi}}, d_j^\dagger] = 0 \quad \forall j > 1 \tag{5.13}$$

From Eq. (5.13), the tunneling term can be rewritten as

$$-t_j \gamma_j e^{i\tilde{\chi}} \psi_j(0) + h.c., \tag{5.14}$$

where

$$\gamma_j = d_j^\dagger e^{-i\tilde{\chi}} + d_j e^{i\tilde{\chi}} \qquad \forall j > 1 \tag{5.15}$$

$$\gamma_1 = e^{i\pi \sum_{j=2}^{N/2} d_j^\dagger d_j} \times P_{\text{leads}}. \tag{5.16}$$

The γ_j operators all commute with $\hat{N}$ (and with the total number of fermions in general), and consequently totally decouple from the charge sector. They can essentially be understood as involutions mapping the $2^{N/2-1}$-dimensional subspace of the states $\prod_{j=1}^{N/2} d_j^{\dagger \nu_j} |0\rangle$, $\nu_j = 0/1$, with even number of fermions on the one with an odd number of fermions, while modifying the number of Cooper pairs so that the total number of electrons in the box is conserved. Finally, they are indeed Majorana fermions as they are self-adjoint and verify the Clifford algebra

$$\{\gamma_j, \gamma_k\} = 2\delta_{j,k} \tag{5.17}$$

They also anti-commute with all fermionic operators in the leads.
Formally, this construction is required because the operator $e^{i\chi}$ is not well-defined[2]. Nonetheless, for all practical reasons, Eq. 5.12 allows us to identify $e^{i\tilde{\chi}}$ and $e^{i\chi}$ in the following. We then recover the Hamiltonian (5.7).

[1] The only requirement on d_1 is that it is connected to only one lead

[2] Not all operators admit a square root, in particular non-diagonalisable ones as $e^{2i\chi}$.

This proof can be generalized to the case where we attach leads at both extremities of the wires, as long as $N > M$. To do so, we choose the following convention for the tunneling term:

$$- t_{2j}(d_j^\dagger + e^{2i\chi} d_j)\psi_{2j}(0) - t_{2j-1} i(d_j^\dagger - e^{2i\chi} d_j)\psi_{2j-1}(0) + h.c. \quad \forall j \geq 1, \tag{5.18}$$

with $t_1 = 0$ (*i.e.* we choose that an uncoupled Majorana is in the lead 1). Then, the expression for the operator $e^{i\tilde{\chi}}$ is unchanged.

For $N = M$, one can no longer find enough independent hermitian matrices in the $2^{M/2-1}$-dimensional subspace and the γ matrices no longer verify the Clifford algebra: following the previous convention, γ_1 and γ_2 commute. We then cannot apply the reasoning we derive in this Chapter, and the device will have a different response.

5.2.3 Bosonization and Majorana fermions

We take advantage of the one-dimensional character of lead electrons and apply Abelian bosonization[129–131]. The Klein factors introduced in the bosonization procedure can be combined with the impurity Majorana fermions to derive a purely bosonic Hamiltonian. The ensuing technical analysis is considerably simplified.

Introducing a short-distance length α, we use the standard Abelian bosonization[131] summarized in Appendix E (for semi-infinite leads) such that:

$$\psi_{R/L,j} = \frac{U_{R/L,j}}{\sqrt{2\pi\alpha}} e^{-i(\pm\phi_j - \theta_j)}, \tag{5.19}$$

In this representation, the lead Hamiltonian (5.6) is written as

$$H_{\text{leads}} = \sum_j \int_0^{+\infty} dx \frac{v_F}{2\pi}(K(\partial_x\theta_j)^2 + \frac{1}{K}(\partial_x\phi_j)^2). \tag{5.20}$$

$$= \sum_j H_0\{\phi_j, \theta_j, K\} \tag{5.21}$$

The Luttinger parameter accounts for the electron-electron interactions in the leads. If they are repulsive, $K < 1$. The leads stop at $x = 0$ in the vicinity of the island, imposing the Dirichlet boundary condition $\psi_{R,j}(0) = \psi_{L,j}(0)$. Hence there is a single Klein factor per lead, $U_{R,j} = U_{L,j}$, and $\phi_j(0) = 0$. This can also be understood the following way: instead of considering a wire only from $-\infty$ to 0, we separate the left- and right-moving modes and consider only a single chiral fermionic wire going from $-\infty$ to ∞, with the box/impurity at $x = 0$.

5.3 Quantum Brownian Motion and Topological Kondo model

Before studying the Topological Kondo box at charge degeneracy, we introduce the formalism we will use throughout this Chapter: the quantum brownian motion. The one-dimensional problem of transport with an impurity is mapped to the movement of a

quantum particle in a $M-1$ dimensional lattice. It is an effective 0-dimensional (in the many-body sense) problem that can be efficiently treated using the Renormalisation Group. In a second step, we summarize the results obtained by Refs. [20, 21] as a reference point for our study.

5.3.1 Quantum Brownian Motion

The quantum impurity model we derived in the previous section is a boundary one-dimensional model. By integrating all modes with $x > 0$ except the operator at $x = 0$ in the action formalism, it can be formulated as a zero-dimensional spatial problem with one temporal dimension. The integration of these Gaussian bosonic modes[131] transforms the Euclidean action into

$$S = \sum_{\omega_m} \sum_j \frac{|\omega_m| K}{2\pi\beta} |\theta_j(\omega_m)|^2 + \int_0^\beta d\tau H_{\mathrm{P}}(\tau) \tag{5.22}$$

where β is the inverse temperature and all bosonic fields $\theta_j(\omega_m)$ are implicitly taken at $x = 0$, and

$$H_{\mathrm{P}} = H_{\mathrm{box}} + H_t. \tag{5.23}$$

We have introduced the bosonic Matsubara frequencies ω_m over which the action is summed. The first term in this expression $\sim |\omega_m|$ describes dissipation caused by electron-hole excitations in the leads. As we will show in the following, the global mode (Φ, Θ), $\Theta/\Phi = \frac{1}{\sqrt{M}} \sum_j \theta_j/\phi_j$, separates from the other modes. In a general fashion, we introduce the $M-1$ dimensional bosonic modes $\vec{r}$ and $\vec{k}$ defined by $(\vec{r}, \Theta) = R\vec{\theta}$, $(\vec{k}, \Phi) = R\vec{\phi}$, R being an orthogonal matrix.

Indeed, the transformation used to decouple the total mode $\frac{1}{\sqrt{M}} \sum\limits_j \theta_j$ must satisfy two criteria. First, it must be an orthogonal transformation to respect the commutation relations of the bosonic fields. Second, it must generate the total mode within the new coordinates. For M leads, a convenient matrix R that we shall use is

$$R_{i,j} = 0, \ \forall\ i > j+1 \qquad R_{i,j} = \frac{1}{\sqrt{i(i+1)}}, \ \forall\ i \leq j < M \tag{5.24}$$

$$R_{i,i+1} = \frac{-i}{\sqrt{i(i+1)}}, \ \forall i < M \qquad R_{M,i} = \frac{1}{\sqrt{M}}, \tag{5.25}$$

and $(R_{M,i})_{1 \leq i \leq M}$ generates the global modes (Φ, Θ). While such matrices R lead to the same result, this choice simplify some evaluations. We introduce the vectors $\vec{w}_j$ defined by:

$$\vec{w}_j = (R_{1,j}, ..., R_{M-1,j}) \tag{5.26}$$

Dropping the global mode, the action can be rewritten as

$$S = \sum_{\omega_m} \sum_j^{M-1} \frac{|\omega_m| K}{2\pi\beta} |r_j(\omega_m)|^2 + \int_0^\beta d\tau H_{\mathrm{P}}(\tau) \tag{5.27}$$

The action can be identified with the QBM model[275, 276] where a massless particle subject to dissipation moves in a $M-1$ dimensional space with coordinates $\vec{r}$. The potential $H_{\rm P}$ seen by the particle depends not only on the coordinate $\vec{r}$ but also on the charge configuration $\hat{N}$. Depending on the gate voltage, we shall restrict the charge to a single value, in which case we have a scalar potential, or two degenerate values represented by a ficticious spin attached to the particle. Following the seminal approaches of Refs. [275, 276] with the dual action of instanton tunneling [279, 280], we shall use this analogy to describe the low energy properties of the model in the strong coupling limit.

5.3.2 Far from charge degeneracy: the Topological Kondo limit

Before discussing the degenerate case, let us shortly review the topological Kondo model [20, 21, 255–263] and its QBM solution. This will introduce concepts and notations that will be useful in the analysis of the degenerate case.

We begin by assuming that the charging energy is the dominant energy scale $E_C \gg T, t_j^2/v_F$ such that only one or two charge states are relevant for transport. We further assume that n_g is close to an integer value n and project the model onto the charge quantized configuration $\hat{N}=n$. Given that H_t changes the number of electrons on the island by ± 1, the Schrieffer-Wolff expansion (see Appendix D.3) allows us to take into account virtual processes through the neighbouring charge states $n+1$ and $n-1$. To second order, we obtain the exchange term

$$H_{SW} = \sum_{j\neq k}^{M,M} \tilde{\lambda}_{j,k} \psi_k^\dagger(0)\psi_j(0)\gamma_j\gamma_k, \tag{5.28}$$

with $\tilde{\lambda}_{j,k} = \tilde{t}_j\tilde{t}_k\left(\frac{1}{\Delta E(n+1)} - \frac{1}{\Delta E(n-1)}\right)$ and

$$\Delta E(n') = E_C(n'-n)(n+n'-2n_g) \tag{5.29}$$

the difference in energy $H_{\rm box}$ between the charge value n' and n. The Schrieffer-Wolff transformation also produces small scattering potential terms $\sim \psi_j^\dagger\psi_j$ that do not change under renormalization group and can be discarded. We note that the tunneling amplitudes in the Schrieffer-Wolff Hamiltonian (5.28) are in fact renormalized [247] by the RG process between the short-time cutoff $\tau_c = \alpha/v_F$ and the charging energy E_C where they increase with the scaling exponent $1-1/(2K)$ such that $\tilde{t}_j = \sqrt{E_C/\tau_c}\, t_j(\tau_c/E_C)^{1-1/(2K)}$.

The appellation Topological Kondo model can be understood from this expression[227]. One can build out of the M leads and M Majorana fermions two pseudo-spins:

$$J_{{\rm leads},j,k} = \frac{i}{2}(\psi_j^\dagger\psi_k - \psi_k^\dagger\psi_j) \text{ and } J_{{\rm Majorana},j,k} = i\gamma_j\gamma_k \text{ for } j\neq k, \tag{5.30}$$

such that the Schrieffer-Wolff Hamiltonian can be rewritten in the isotropic limit as:

$$H_{SW} = -\lambda \vec{J}_{\rm leads}.\vec{J}_{\rm Majorana}. \tag{5.31}$$

The symmetry group of the Majorana-based pseudo-spin differs slightly from the usual $SU(M)$: as Majorana fermions are real fields, it is limited to $SO(M)$.

In terms of our bosonized fields, the exchange term is reexpressed as

$$H_{SW} = \sum_{j\neq k}^{M,M} \lambda_{j,k} U_k U_j \gamma_j \gamma_k e^{i(\theta_j - \theta_k)}, \tag{5.32}$$

with the notation $\theta_j \equiv \theta_j(0)$ and $\lambda_{j,k} = \frac{\tilde{\lambda}_{j,k}}{\pi\alpha}$. The product $p_j = i\gamma_j U_j$ is the parity operator associated with the Majorana fermions γ_j and U_j. The different p_j commute between themselves and with the Hamiltonian, have eigenvalues ± 1, but do not conserve the full parity operator. However, the $M-1$ independent products $p_j p_k = \pm 1$ can be diagonalized simultaneously[21, 257]. The sign of $p_j p_k$ can be changed by shifting the bosonic fields by π, we thus fix it arbitrarily to $+1$. With these conventions and choice of gauge, the exchange term assumes a fully bosonic form

$$H_{SW} = -\sum_{j\neq k}^{M,M} \lambda_{j,k} \cos(\theta_j - \theta_k), \tag{5.33}$$

The global mode (Φ, Θ), $\Phi/\Theta = \frac{1}{\sqrt{M}} \sum \phi_j/\theta_j$, decouples from H_{SW} as anticipated.

One can compute the poor man's scaling equations for this problem[281], and the renormalization group (RG) analysis is straightforward

$$\frac{d\lambda_{j,k}}{d\ell} = \left(1 - \frac{1}{K}\right)\lambda_{j,k} + 2\sum_{m\neq j,k}^{M} \lambda_{j,m}\lambda_{m,k}, \tag{5.34}$$

with the flow parameter $\ell = \ln \tau_c$. Appendix G.1.1 presents a detailed derivation of these equations.[3] Channel asymmetry between the different electron hopping terms $\lambda_{j,k}$ is not relevant and the RG flow points to a symmetric combination $\lambda_{j,k} \to \lambda(1-\delta_{j,k})$. Assuming channel symmetry reduces the RG equation to

$$\frac{d\lambda}{d\ell} = \left(1 - \frac{1}{K}\right)\lambda + 2(M-2)\lambda^2, \tag{5.35}$$

where three fixed points can be identified. Figure 5.5 represents a typical RG flow for $\lambda_{j,k}$.

First, the weak coupling fixed point with $\lambda = 0$, noted (O), corresponding to decoupled leads between which no electric current flows, or, using the Kubo formula detailed in Appendix G.2,

$$G_{j,k}^{(O)} = 0, \tag{5.36}$$

where $G_{j,k}$ is the conductance between the leads j and k. This is an attractive point for $K < 1$.

For $K \geq 1$, the growth of λ under renormalization suggests to study a strong coupling limit $\lambda = +\infty$ noted (S). In this limit, the fields θ_j are pinned to one of the minima of

[3] Note the difference with the RG equations of the previous Chapter: the linear term is now proportional to $1 - d_g$, d_g the dimension of the operator, instead of $2 - d_g$. The difference comes from the fact that it is a boundary term, and therefore the cosine operators are only integrated over imaginary time.

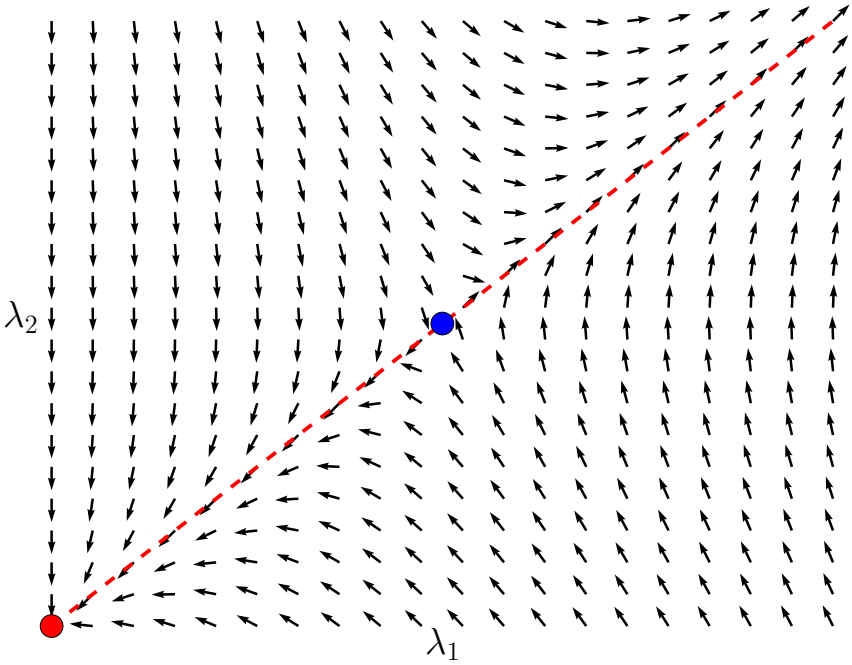

Figure 5.5: Example of normalized vector field induced by the RG equations 5.34. We consider $M = 3$ leads, and assume $\lambda_{1,2} = \lambda_{1,3} = \lambda_1$, and $\lambda_{2,3} = \lambda_2$ for $K = 0.8$. The blue point is the intermediate instable fixed point(I) for $\lambda_1 = \lambda_2 = \frac{K^{-1}-1}{2(M-2)}$. The red line is the fixed attractive stable line $\lambda_1 = \lambda_2$. There are two stable fixed points where all flows converge: the red point (O) with $\lambda_1 = \lambda_2 = 0$ that corresponds to uncoupled leads, and the Topological Kondo Model fixed point $\lambda_1 = \lambda_2 = +\infty$.

the potential described by H_{SW}. Using the Kubo formula, the conductance[275, 276] $G_{j,k}$ is now given by (Appendix G.2 for a derivation)

$$G_{j,k}^{(S)} = \frac{2e^2K}{h}\left(\frac{1}{M} - \delta_{j,k}\right). \tag{5.37}$$

In agreement with the physical picture of strong coupling, this is the maximum conductance one can reach with the constraint of charge conservation. It indeed corresponds to a perfect symmetric transmission of incoming electrons. For $M = 2$, we recover that the Majorana Kondo box maps onto a problem of resonant tunneling, where the conductance is simply $\frac{e^2K}{h}$ for spinless fermions. The factor $\left(\frac{1}{M} - \delta_{j,k}\right)$ can be understood in the following way: due to the isometry of the fixed point, an electron arriving on the impurity is scattered uniformly in all leads, imposing

$$G_{j,k}^{(S)} = G - \delta_{j,k}G_0, \tag{5.38}$$

where $G_0 = 2e^2K/h$. Conservation of the current leads to $\sum_j G_{j,k} = 0$, that is to say $G_0/G = M$, giving us the aforementioned factor. We note that in practice the Luttinger

liquid wires are ultimately in contact to Fermi liquid reservoirs which has the effect of renormalizing [282, 283] the Luttinger parameter to $K = 1$ in Eq. (5.37).

A third fixed point, noted (I), is identified for $K < 1$ corresponding to the intermediate coupling

$$\lambda^I = \frac{K^{-1} - 1}{2(M-2)}. \tag{5.39}$$

It is unstable against both weak (O) and strong coupling (S) fixed points. The perturbative RG equation (5.35) justifies the existence of this intermediate unstable point only for K close but below 1, such that λ^I remains small.

To check the stability of (S), one can perform an instanton analysis. Given the simple structure of the potential, the more relevant/less irrelevant operators at (S) are operators translating one minimum of the potential described by H_{SW} to one of its neighbours. The variable Θ does not appear in H_{SW} and therefore has a free evolution reflecting charge quantization [259] on the island. For clarity, we henceforth set $\Theta = 0$. In terms of the variable $\vec{r}$, the minima of the potential described by H_{SW} form a (hyper)triangular lattice, and we can explicitly construct the operators connecting them. For simplicity, we write these minima in the θ_j basis. A minimum, R_0, and all its nearest-neighbours R_k, $(k = 1...M)$ are given by

$$\begin{aligned} R_0 : &\quad \theta_j = 0 \quad \forall j \\ R_k : &\quad \theta_k = \frac{2\pi(M-1)}{M}, \quad \theta_j = -\frac{2\pi}{M} \quad \forall j \neq k \end{aligned} \tag{5.40}$$

In a semi-classical analysis, quantum fluctuations around these minima are neglected and the only low energy processes are instanton solutions connecting them. Introducing the variable ϕ_k (the charge in lead k) canonically conjugated to θ_k/π,

$$[\phi_j, \theta_k] = i\pi\delta_{j,k}, \tag{5.41}$$

it is then possible to explicitly construct the instanton operators. The shift from R_0 to R_k is thus realized by the translation operator

$$\hat{O}_k = \exp\left[2i\left(\phi_k - \frac{1}{\sqrt{M}}\Phi\right)\right] \tag{5.42}$$

where $\Phi = \frac{1}{\sqrt{M}}\sum_k \phi_k$ is the total charge field. Identifying ϕ_k with the field $\phi_k(0)$, we obtain the following dual action describing the vicinity of (S)

$$S = \sum_{\omega_m}\sum_j \frac{|\omega_m|}{2\pi K\beta}|\phi_j(\omega_m)|^2 - v\int_0^\beta d\tau \sum_k \hat{O}_k(\tau), \tag{5.43}$$

where v describes weak backscattering of electrons coming from reservoirs.

The stability of (S) is controlled by the dimension of the operators $\hat{O}_k$. Using the free part of the action (5.43), one obtains the dimension $2K(M-1)/M$. This result can also be understood in the QBM picture [275, 276] where the product between the dimension of the original perturbation $e^{i(\theta_j - \theta_k)}$ (here $1/K$) and the leading irrelevant operator at

strong coupling is fixed to $2(M-1)/M$ for a hypertriangular lattice in $M-1$ dimension. We therefore find that (S) is stable for $K > \frac{M}{2(M-1)}$, and unstable towards (O) for smaller values of K. Computing the one-loop RG equation, one obtains [276] that the unstable fixed point (I) departs from (S) for $K > \frac{M}{2(M-1)}$ and disappears below.

The whole phase diagram for the topological Kondo model is summarized in Fig. 5.1. For $\frac{M}{2(M-1)} < K < 1$, a first order transition between zero and maximum conductance is predicted [20] to occur as the coupling to the reservoir is varied. The Kondo temperature is evaluated from the RG equation (5.35),

$$T_K \simeq E_c e^{-\frac{1}{2(M-2)\nu\lambda}}, \tag{5.44}$$

where ν is the density of states in the wires. T_K sets the crossover energy scale between weak and strong coupling.

5.4 Charge degeneracy point: an exact mapping to the multichannel Kondo Model

We now turn to the charge degenerate case where the gate voltage is fixed to a half-integer value $n_g = n + 1/2$. The two charge states n and $n+1$ are energetically equivalent and define a low energy sector akin to a spin-1/2 Hilbert space. Further assuming a large charging energy $E_C \gg T, t_j^2/v_F$, we project to this subspace and rewrite the full bosonized Hamiltonian as

$$H = H_{\text{leads}} - \sum_{j=1}^{M} \frac{2t_j}{\sqrt{2\pi\alpha}} \left(\tau_- U_j \gamma_{j,r} e^{-i\theta_j} + h.c. \right), \tag{5.45}$$

with the pseudo-spin operator $\tau_-|n+1\rangle = |n\rangle$. Similarly to Eq. 5.28, the hopping terms are renormalized when reducing the charge sector to an effective pseudo-spin. In terms of the original bare values of the tunneling, they can be reexpressed as: $\tilde{t}_j \approx t_j \left(\tau_c/E_c\right)^{1-\frac{1}{2K}}$. In the following, for simplicity, we drop the tilde on t_j.

We show in the following that this Hamiltonian can be exactly mapped onto the M-CKM. First, one can rescale the bosonic fields in order to obtain the correct dimension for the operators coupled to the pseudo-spin, namely

$$\tilde{K} = 2K, \quad \tilde{\theta}_j = \frac{\theta_j}{\sqrt{2}}, \quad \tilde{\phi}_j = \sqrt{2}\phi_j \tag{5.46}$$

Second, we use the trick presented in the previous section to fuse the Majorana fermions and the Klein factors. We introduce the operators $p_j = i\gamma_j U_j$ and fix them to 1. Shifting the θ_j variables by $\pi/2$ to absorb an i factor, we obtain the bosonized form

$$H = H_{\text{leads}}\{\tilde{\phi}, \tilde{\theta}, \tilde{K}\} - \sum_{j=1}^{M} \left(\frac{J_{\perp,j}}{2} \tau_+ e^{i\sqrt{2}\tilde{\theta}_j} + h.c \right) + \frac{v_F}{\sqrt{2}} J_z \tau_z \sum_{j=1}^{M} \partial_x \tilde{\phi}_j, \tag{5.47}$$

where $J_{\perp,j} = \frac{4t_j}{\sqrt{2\pi\alpha}}$ and $J_z = 0$, corresponding to the spin sector of the anisotropic M-CKM (the charge mode decouples from the impurity spin). Alternatively, contact with

the M-CKM can be made from Eq. (5.45) with the analogy

$$U_{j,\uparrow} = U_j, \quad U_{j,\downarrow} = \gamma_j. \tag{5.48}$$

We note that the Luttinger parameter $\tilde{K}$ in Eq. (5.47) characterizes the spin sector and requires in the M-CKM the SU(2) spin symmetry to be broken in the leads to be different from one. By constrast, here, no such symmetry-breaking is necessary as Eq. (5.47) emerges as an effective model with $\tilde{K} \neq 1$ as a general case. For non-interacting leads for example, where $K = 1$, one has $\tilde{K} = 2$.

The effective Kondo model (5.47) is strongly anisotropic since $J_z = 0$. A finite J_z is nevertheless generated in the RG process. We consider for simplicity the channel-isotropic case $J_{\perp,j} = J_\perp$, and derive the corresponding RG equations following Anderson, Yuval and Hamman [284] (see Appendix G.1.2) extended to the interacting case $\tilde{K} \neq 1$,

$$\frac{dJ_z}{d\ell} = J_\perp^2 \left(\frac{1}{\tilde{K}} - \frac{M}{2} J_z \right), \tag{5.49}$$

$$\frac{dJ_\perp}{d\ell} = \left(1 - \frac{1}{\tilde{K}}\right) J_\perp + J_z J_\perp \left(1 - \frac{M\tilde{K}}{4} J_z\right). \tag{5.50}$$

These equations are perturbative in $J_\perp$ and exact in J_z. Studying these equations, one sees that the longitudinal coupling J_z is attracted by the fixed point value $J_z = \frac{2}{M\tilde{K}}$ at which J_z ceases to be generated and the RG evolution of $J_\perp$ decouples. An example of such RG flow is given in Figure 5.6. It corresponds in fact to the standard Emery-Kivelson[266] (or Toulouse[285]) limit in the M-CKM [275, 276, 286]. It is reached by the RG flow even if the initial value of J_z is zero. Therefore, it makes sense to start with the model (5.47) directly at $J_z = \frac{2}{M\tilde{K}}$ and perform the unitary transformation

$$U = \exp\left(i \frac{\tilde{K} J_z \sqrt{M}}{\sqrt{2}} \tilde{\Theta}(0) \tau_z \right), \tag{5.51}$$

to eliminate the J_z term from Eq. (5.47). The resulting Hamiltonian is

$$\hat{U}^\dagger H \hat{U} = H_{\text{leads}}\{\phi, \theta, K\} - \sum_{j=1}^{M} \left(\frac{J_{\perp,j}}{2} \tau_+ e^{i(\theta_j - \frac{1}{\sqrt{M}}\Theta)} + h.c \right) \tag{5.52}$$

when written again in terms of the old fields, see Eq. (5.46). The use of the unitary transformation is not only for mathematical convenience but also possesses a physical significance. The model (5.52) is now invariant under a global shift of all fields θ_j which implies that the total mode $\Theta = \frac{1}{\sqrt{M}} \sum_j \theta_j$ decouples as in the previous section. Although the present degenerate case does not satisfy a strict charge quantization, the flow of incoming electrons must exactly compensate the flow of outgoing electrons since there can be no charge accumulation in the floating quantum box. As a result, current conservation also holds as reflected by the free mode Θ.

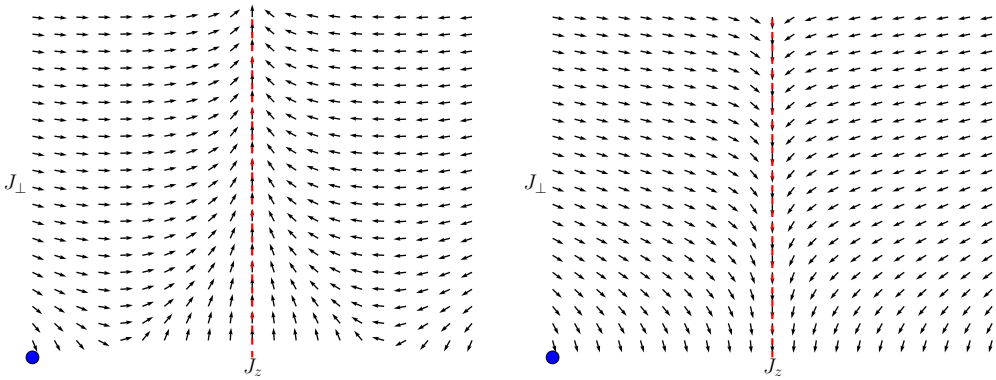

Figure 5.6: Normalized RG flow for the M-CKM model at weak coupling based on equations 5.49 and 5.50. In both graphs, we consider $M = 3$ leads. The unstable point (O) at $J_\perp = J_z = 0$, in blue, is always there. In red, the fixed attractive line $J_z = \frac{2}{M\tilde{K}}$. Depending on the value pf $\tilde{K}$, once the red line is reached, $J_\perp$ is renormalized to either 0 or ∞. Left: $\tilde{K} = 0.8$. Then $J_\perp$ has an effective dimension of $\frac{5}{6}$ and is therefore relevant and renormalized to $+\infty$/ Right: $\tilde{K} = 0.5$. $J_\perp$ has an effective dimension $\frac{4}{3} > 1$ and is therefore irrelevant and renormalized to 0.

5.5 Phase diagram at charge degeneracy

The pertubation operators in Eq. (5.52) have dimension $\frac{M-1}{2MK}$ after the unitary transformation. Hence, for $K < \frac{M-1}{2M}$, the system flows towards the uncoupled fixed point (O), with $J_\perp = 0$, and the conductance is zero as in Eq. (5.36). For $K > \frac{M-1}{2M}$, (O) is unstable and the RG equations (5.49), (5.50) must be supplemented by the next order in $J_\perp$. Eq. (5.49) is unchanged whereas Eq. (5.50) becomes

$$\frac{dJ_\perp}{d\ell} = \left(1 - \frac{1}{2K}\right) J_\perp + J_z J_\perp \left(1 - \frac{MK}{2} J_z\right) - C_M(K) J_\perp^3, \tag{5.53}$$

where $C_M(K) = \mathcal{O}(1)$ depends on K and the number of channels M. The coefficient $C_M^* = C_M[(M-1)/(2M)]$ can be evaluated at the threshold for the instability of the uncoupled point (O) and shown to be always positive [276], demonstrating an intermediate RG-stable fixed point at $J_z^I = 1/(MK)$ and

$$J_\perp^I = \sqrt{\frac{K - \frac{M-1}{2M}}{K C_M^*}}, \tag{5.54}$$

valid for K close to $\frac{M-1}{2M}$. Figure 5.7 gives an example of such RG flow. At the fixed point (I), the conductance is non-vanishing, $\propto (J_\perp^I)^2$ for small $J_\perp^I$. It increases continuously with the Luttinger parameter K. The way (I) connects with the strong coupling fixed point (O) depends on the value of M and shall be discussed below where the strong coupling limit is investigated. At the specific point where $K = 1/2$, then $\tilde{K} = 1$ and Eq. (5.52)

represents exactly the non-interacting M-CKM. From conformal theory[274, 287–289], it is known that the conductance is given in that case by

$$G_{j,k} = \frac{2e^2K}{h}\sin^2(\frac{\pi}{M+2})\left(\frac{1}{M} - \delta_{j,k}\right). \tag{5.55}$$

The conductance for other values of K is not known analytically.

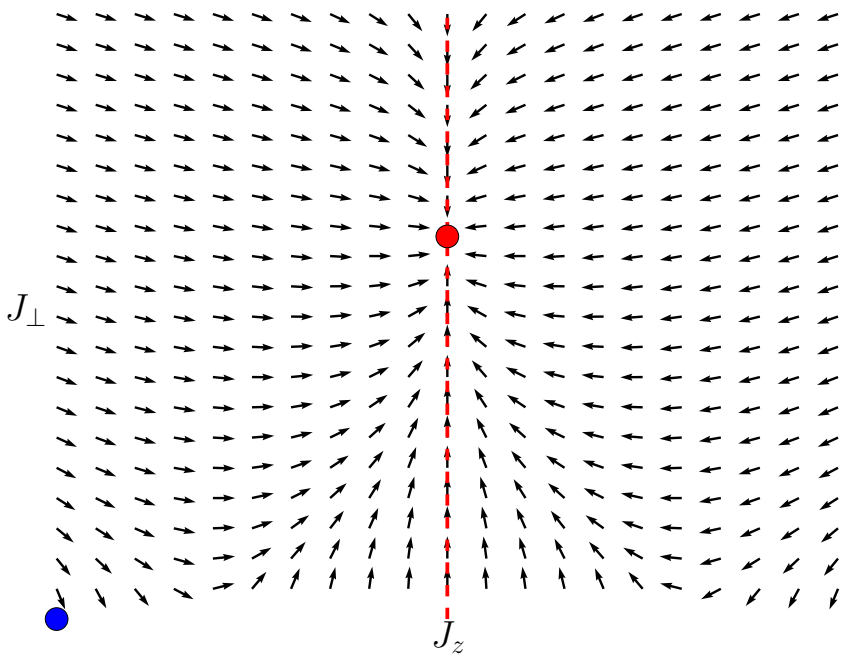

Figure 5.7: RG flow for the M-CKM model at weak coupling based on Eq. 5.53. We take $M = 3$, $\tilde{K} = 0.8$, and fix $C_M = 0.15$ for convenience of representation. The unstable point (O) and the fixed line for J_z are present, but the additional stable fixed point (I), in red, appears due to the third order term.

Let us study the model at strong coupling. In Ref. [276], Eq. (5.52) was argued to be the dual model of a particle moving in a hyperhoneycomb lattice formed by two interpenetrating triangular lattices between which the operators $\tau_\pm$ alternate. We discuss here directly the strong coupling limit, noted (0), $J_{\perp,j} = +\infty$ of Eq. (5.52) and construct explicitely its dual action by taking into account the pseudo-spin wavefunction. In the spirit of a semi-classical approach, we minimize Eq. (5.52) (without the lead term) with respect to the fields θ_j and the spin configuration, whereas the total field Θ factorizes (set to zero for simplicity) and is free. In the channel-isotropic case, $J_{\perp,j} = J_\perp$, the energy to minimize has the form

$$-J_\perp \begin{pmatrix} 0 & \mathcal{S} \\ \mathcal{S}^* & 0 \end{pmatrix} \qquad \mathcal{S} = \sum_j e^{i(\theta_j - \frac{1}{\sqrt{M}}\Theta)} \tag{5.56}$$

Interestingly, the minima are located at exactly the same field θ_j positions as in the topological Kondo model, R_0 and its neighbours R_k as given in Eq. (5.40), forming a triangular lattice in a $M-1$ dimensional space orthogonal to the total mode $(1,1,\ldots,1)$ direction. But the problem is nevertheless different since there is an additional pseudo-spin degree of freedom, and each minimum is characterized by a certain spin wavefunction, $(|+\rangle+|-\rangle)$ for R_0, and $(e^{-i\pi/M}|+\rangle+e^{i\pi/M}|-\rangle)$ for R_k. The conductance at strong coupling is still given by Eq. (5.37).

Technically, moving from one minimum to its neighbour rotates the spin direction by an angle $2\pi/M$ around the z axis. Hence, performing a loop starting and ending at R_0 exhausting the different neighbour directions, one obtains a rotation of 2π coming with an overall phase $e^{i\pi}=-1$ resulting from the pseudo-spin Berry phase [4]. This sign is in fact responsible for the change of sign of the second order term in the RG flow for $M=3$ (and the third order term for $M=4$), leading to differing phase diagrams for the triangular and honeycomb lattices. The dual action, representing the instanton solutions connecting the minima of Eq. (5.52), is constructed in the same way as in Sec. 5.3.2. The leading irrelevant operators at low energy are thus given by the translations

$$\hat{O}_k^{(h)} = \exp\left[2i\left(\phi_k - \frac{1}{\sqrt{M}}\Phi\right)\right]\exp\left(-\frac{i\pi}{M}\tau_z\right), \tag{5.57}$$

where the second part accounts for the spin rotation between two consecutives minima, *e.g.* R_0 and R_k. Its dimension is the same as $\hat{O}_k$ in Eq. (5.42), $2K(M-1)/M$. We note that the minima of the potential $H_{\text{dual}} = -v\sum_j \hat{O}_k^{(h)}$ form a hyperhoneycomb lattice for a given spin projection $\tau_z=+1$ or -1. The RG analysis of the model at strong coupling, or $v \ll 1$, depends on the dimension M [276]. For $M=3$, the RG equation is

$$\frac{dv}{d\ell} = (1-4K/3)v - 2v^2 \tag{5.58}$$

where the last term sign has its origin in the pseudo-spin Berry phase as discussed in the appendix G.1.2. As a result, the intermediate coupling fixed point (I) occurs for $K<3/4$, with $v^{(I)} = \frac{1-4K/3}{2}$ valid for $1-4K/3 \ll 1$, and is stable. Its is continuously connected to the intermediate fixed point (I) found at weak coupling. For $M=4$, one obtains

$$\frac{dv}{d\ell} = (1-3K/2)v - (A_4-B_4)v^3, \qquad A_4 > B_4 \tag{5.59}$$

leading to (I) for $K<2/3$ and $v^{(I)} = \sqrt{\frac{1-3K/2}{A_4-B_4}}$. In both situations, $M=3$ and 4, the phase diagram has the form shown in the upper panel of Fig. 5.2 and the stable intermediate point (I) connects the weak and strong coupling fixed points as K is varied.

This is in contrast with $M \geq 5$ where the RG equation takes the form

$$\frac{dv}{d\ell} = \left(1 - \frac{2(M-1)K}{M}\right)v + B_M v^3, \tag{5.60}$$

[4] The -1 factor was also interpreted as an effective and alternating $\pm\pi$ flux threading each plaquette of the triangular lattice [276].

with $B_M > 0$. The intermediate fixed point exists for $K > 2(M-1)/M$ and is unstable. This suggests the phase diagram represented in the lower panel of Fig. 5.2. Comparing with the non-degenerate case, or topological Kondo model, one observes that exactly the same RG equation (5.60) holds [276]. The first reason is that the fields θ_j are pinned at the same positions irrespective of charge degeneracy. Moreover, the spin wavefunction, and the corresponding Berry phase, plays a role for a product of at least $M-1$ $\hat{O}_k^{(0)}$ operators such that perturbation theory differs only for orders above $M-2$. The result is that the critical line (I) is the same at high mobility in both non-degenerate and degenerate cases for sufficiently large M, *i.e.* the departures of the dotted lines in Figure 5.1 and Figure 5.2 (lower panel) from strong coupling (mobility $\mu = 1$) are identical. The two curves start to differ at larger v (or smaller mobility) where the line (I) at charge degeneracy is below the topological Kondo case [5]. At even smaller mobility, the effect of the pseudo-spin Berry phase becomes prominent: the line (I) eventually turns over and connects with the stable fixed-point line (I) originating from weak coupling and containing the multichannel Kondo fixed point at $K = 1/2$, see Figure 5.2 (lower panel).

The spin wavefunction also provides a physical picture to understand the effect of a small charge degeneracy $\delta \ll 1$, with

$$n_g = n + 1/2 + \delta. \tag{5.61}$$

For example, at strong coupling, the semi-classical energy to minimize is

$$-J_\perp \begin{pmatrix} 2\delta E_C & \mathcal{S} \\ \mathcal{S}^* & -2\delta E_C \end{pmatrix}, \tag{5.62}$$

with eigenvalues $\pm\sqrt{4(\delta E_C)^2 + |\mathcal{S}|^2}$. The fields θ_j are thus pinned at the same positions $R_{0,k}$ but the spin wavefunction is polarized by $\delta \neq 0$ along the z direction, thereby reducing the impact of the Berry phase. Since δ is relevant on the (I) critical line, as we know from the M-CKM at $K = 1/2$, this implies that the system flows at low energy towards the non-degenerate case, or Figure 5.1. At finite energy (temperature), we expect a continuous crossover for the (I) critical line between the two limiting cases represented by Figure 5.1 and Figure 5.2.

Finally, from Eq. 5.53, one can evaluate the one-loop Kondo temperature:

$$T_K \approx \nu t^{\frac{2K}{2K-1}}, \tag{5.63}$$

where ν is the density of states and t is the typical bare value of the tunneling term. For $\frac{1}{2} < K < K_c$, it corresponds to the Kondo temperature of the MCKM intermediate fixed point, while for $K > K_c$, it characterizes the strong coupling limit. When the leads are non-interacting ($K = 1$), we obtain the very physical expression: $T_K \approx \nu t^2$, characteristic of a resonant tunneling transport through the superconducting island, in agreement with Ref. [277].

Up to know we only considered flavor isotropic tunneling, *i.e.* $t_j = t\ \forall j$. While flavor anisotropy was irrelevant in the Topological Kondo model, it is no longer the case at charge

[5] Nothing prevents the curve at charge degeneracy to cross above the topological Kondo line (non-degenerate case) for even lower mobility before turning over.

degeneracy[290, 291] where we are dealing with an intermediate fixed point. Indeed, the critical model goes from M-CKM to M'-CKM, where M' is the number of channels with the largest value of $J_{\perp,j}$ (generally $M' = 1$). Consequently, observing the fractional non-trivial conductance of M-CKM will require fine-tuning [292] and be experimentally more challenging than far from charge degeneracy.

Conclusion

We have studied in this thesis various properties of topological materials, from entanglement markers in correlation functions to their transport properties.
First, we have seen that in one- and two-dimensional non-interacting topological models, the bipartite fluctuations in typical critical phases are characterized by universal scaling laws that mimic those of the von Neumann entropy. Due to the absence of charge conservation, an additional volume law is present, with non-analyticities that mark the different phase transitions. At the critical point, logarithmic terms arise, with a universal coefficient, independent of any microscopic parameter. In one dimension, it is truly invariant, and its value and sign show the gap inversion that occurs at a topological phase transition. In two dimensions, we were able to extract its dependency on the geometry of the considered subsystem, and we have shown that one can directly recover the winding number of the different Dirac cones, and probe the topological nature of the transition. The same quantification can be extracted directly from the connected correlation functions or from the mutual fluctuations (the analogous of the mutual information). Here, we chose to limit ourselves to the study of the BDI and D classes, but these observations can be straightforwardly generalized to the other non-trivial classes. It is for example particularly relevant for the DIII class of Hamiltonian whose gapless phases are topologically protected in two dimensions[41].
Still, many questions on the bipartite fluctuations, with or without charge conservation, are left open. Those quantifications and universalities are possible due to the fact that the Fermi surface is a zero-dimensional manifold. A similar treatment may therefore be directly applied to three-dimensional gapless phases, and in particular to Weyl semi-metals[293, 294]. These materials are characterized by a point-like Fermi surface, with chiral nodes, *i.e.* the direct equivalent of Dirac cones in three dimensions. It would be interesting to check whether one can directly probe the chiral charge associated to each node in the same way we are able to probe the winding number of the Dirac cones. It would be a direct, unambiguous, measurement of the topological nature of the Weyl semi-metals. The effect of Fermi arcs on the boundaries of the materials would also be interesting, and perhaps an even more exciting prospect would be the case of the superconducting Weyl semi-metals with Majorana nodes and arcs[295]. On a more theoretical side, we have observed a very good agreement between the scaling of the fluctuations and the entropy. Yet, the usual bounds on mutual information obtained from mutual fluctuations are far from exhaustion: it would be interesting to see whether one can build better bounds in the specific case of the charge fluctuations. That would allow for a direct measurement of entanglement in experiments. Finally, it would also be particularly interesting to general-

ize our results to the typical critical points that separate trivial phases from parafermionic phases[296, 297]. The change in critical model should also be seen directly in the fluctuations, which then may lead to a way of directly measuring these exotic quasi-particles.
In a second step, we have included interactions in our description. The interplay of topology and interactions leads to rich physics. We have studied the influence of interactions on a typical topological superconductor and shown that only the coefficient of the logarithmic contribution to the fluctuations was renormalized, while its sign, and the fact that there is a logarithmic term at the phase transition between trivial and polarized phase survive. We then have introduced and discussed a model of two topological superconductors coupled by Coulomb interactions. We have shown that, while the topological phase survives the presence of weak interactions, new phases may open. In particular, we have seen that Mott phases appear close to half-filling, with unusual orbital currents that spontaneously break the time reversal symmetry, despite the absence of direct tunnelling from a wire to the other. We have also shown the opening of an exotic gapless phase, a direct extension from the standard topological critical point, a rare feature in these models. In a general fashion, it would be interesting to get a systematic understanding of the interplay of large interactions and topological superconductivity: we know for example that orbital currents are not an unusual occurrence when mixing them. Another possible extension, in relation with the bipartite fluctuations is simply the generalisation to arbitrary systems, and in particular, the question whether one can truly recover universality of the logarithmic coefficient from more concrete observables.
Finally, we have studied an hetero-structure composed of a floating superconducting island carrying Majorana fermions as impurities, connected to several leads. We have computed its transport properties and shown that one recovers the physics of the standard multichannel Kondo model, yet at an initially very interacting point. The conductance then takes a symmetric fractionalized form. We have used the Quantum Brownian Motion formalism, that allows to tackle both weak- and strong-coupling limits. The existence (and a description) of a critical interaction strength at which the box undergoes a first-order transition between the multichannel Kondo fixed point and the strong coupling fixed point for large number of leads is an interesting still-open question, where more numerics methods may help. Additionally, as this model is thought to be a potential building block for a quantum computer, we are currently studying the physics of several such boxes coupled together, which makes very interesting links with still open problems such as the multi-impurity, multichannel Kondo model. Variants of this box replacing the Majorana fermions by parafermions or other anyons would also be particularly interesting to investigate[298]. The effect of the Majorana fermions can be understood as a change in statistics compared to the standard transport problem. Parafermions and anyons would then strongly affect the transport properties of the box.

This thesis now reaches its conclusion, and my final words will be a simple

Thank you.

Appendix A

Résumé en français

Introduction

Classifier les différentes phases de la matière est l'un des principaux objectifs de la physique. Que cela soit dans des exemples de la vie réelle tels que l'évaporation ou la fusion de l'eau ou pour les études théoriques les plus abstraites de matériaux exotiques, les propriétés de ces différentes phases et des transitions de l'une à l'autre revêtent une importance fondamentale pour comprendre notre monde. La physique de la matière condensée se concentre sur l'étude des propriétés des liquides et des solides. Celles-ci ont, la plupart du temps, comme origine le comportement collectif des nombreux atomes et électrons qui les composent. Ce comportement est émergent : les propriétés du système macroscopique ne peuvent pas toutes être comprises à partir de la description des particules individuelles.
Le paradigme historique pour décrire les phases et les transitions de phase, pour les systèmes quantiques et classiques, a été formulé par Ginzburg et Landau. Au lieu de partir d'une parfaite description microscopique, et donc d'un modèle insoluble, il repose sur la construction de théories effectives simples. Les symétries du système, c'est-à-dire les transformations qui doivent le laisser invariant, limitent les termes qui peuvent apparaître dans le modèle. On peut alors définir une observable physique locale, le paramètre d'ordre, dont la valeur change et devient non nulle dans les états fondamentaux (les états de plus basse énergie) ou les états thermiques à la transition de phase, alors que certaines de ces symétries imposent que sa moyenne doit être nulle. Ce phénomène est appelé brisure spontanée de symétrie, car certains états semblent violer les symétries du système. Bien sûr, les symétries sont toujours respectées, mais le niveau auquel elles sont appliquées change. Dans la phase désordonnée, les symétries sont appliquées directement sur les états et le paramètre d'ordre est nul pour tous les états fondamentaux, tandis que dans la phase ordonnée, elles sont maintenant appliquées sur l'espace (vectoriel) des états: le paramètre d'ordre peut être différent de zéro dans certains états, mais s'annulera toujours en moyenne. Cela conduit habituellement à un changement de la dégénérescence (nombre) d'états fondamentaux. L'exemple le plus simple est le suivant: prenez une quantité réelle ou complexe telle que la polarisation de spin ou la phase supraconductrice ϕ et une énergie potentielle qui ne dépend que de la norme de celle-ci : $V(\phi) = r|\phi|^2 + |\phi|^4$. Le système possède certaines symétries: V est invariant sous la transformation $\phi \to -\phi$ si ϕ est réel (resp. $\phi \to e^{i\theta}\phi$ si ϕ est complexe). On parle d'une symétrie $\mathbb{Z}_2$ (resp. $U(1)$),

d'après leur représentation de groupe. En ignorant toute dynamique, minimiser l'énergie du système revient à minimiser V. Si r est positif, le minimum de V est atteint pour $\phi = 0$, point laissé invariant par les transformations susmentionnées: il correspond à une phase désordonnée. À l'inverse, si r est négatif, le minimum est atteint pour $|\phi| = \frac{\sqrt{|r|}}{2}$ et maintenant deux fois (resp. infiniment) dégénéré. Cela correspond à une phase ordonnée: les symétries ne laissent pas les états invariants, mais transforment un état en un autre.
La description de Landau des transitions de phase a eu un incroyable succès dans une grande variété de modèles et de matériaux, et a permis d'expliquer de nombreuses transitions de phase différentes. Pourtant, entre 1971 et 1973, Berezinskii [1, 2], Kosterlitz et Thouless [3, 4] ont décrit une nouvelle transition de phase qui ne pouvait être expliquée par une brisure de symétrie, dans un aimant classique bidimensionnel . Un tel aimant peut être décrit de manière minimale par un réseau bidimensionnel de spins ferromagnétiques (porté par les atomes) qui interagissent entre eux et tendent à s'aligner. À température nulle, les spins sont parfaitement alignés, mais lorsque la température augmente, des excitations, consistant en paires de vortex et anti-vortex commencent à apparaître et forment un gaz dilué. À une température critique, une transition de phase se produit, alors que le célèbre théorème de Mermin-Wagner empêche toute brisure des symétries continues pertinentes dans ce modèle. Les paires se divisent et des vortex isolés apparaissent. Ces travaux, récompensé par le prix Nobel en 2016, partagé avec F. Haldane, sont le premier exemple d'une transition de phase topologique et d'une phase où les défauts topologiques (les vortex) jouent un rôle fondamental.
Les Effets Hall Quantiques Entier et Fractionnaire (I / FQHE), découverts en 1980 [5] et 1982 [6] sont des exemples peut-être encore plus connus de phases topologiques. Ils apparaissent lorsque l'on confine un gaz d'électrons en deux dimensions, à basse température, et en présence d'un fort champ magnétique normal au plan. Lorsque l'on applique une tension à travers le plan, un courant perpendiculaire est généré. Si l'on varie l'intensité du champ magnétique, on peut mesurer des plateaux parfaits de la conductivité transversale de Hall, correspondant à des annulations de la conductivité longitudinale. Sur chaque plateau, la conductivité est égale au quantum de conductance $\frac{e^2}{h}$ multiplié par un entier (un rationnel pour le FQHE) avec une remarquable précision de 10^{-9}, bien au-delà de ce que les impuretés et les défauts permettraient normalement. Cette conductance est maintenant utilisée en métrologie pour définir la constante hyperfine. Le courant est purement porté par les bords de l'échantillon tandis que le coeur du système reste isolant. Aucune observable physique locale ne peut différencier, dans le coeur du système, ces isolants de Hall d'un isolant atomique (où les électrons sont simplement localisés sur leurs atomes). Néanmoins, cette quantification de la conductance a été directement liée par Thouless *et al* [7] aux propriétés des bandes électroniques dans le coeur du système. Le terme quantifié qui apparaît dans la conductance correspond à un invariant topologique global de la structure de bandes (ou de la fonction d'onde à n corps [8]), qui peut être utilisé pour classifier ces phases (et s'annule dans un isolant atomique). Par définition, cet invariant est largement indépendant des détails microscopiques du système et très résistant à la présence de défauts et d'impuretés, comme cela a été observé expérimentalement. Dans le cas de l'IQHE, l'invariant topologique, appelé nombre de Chern, correspond également au nombre de modes de bord transportant le courant électrique. Un isolant atomique ordinaire n'a pas de modes de bord. Cette correspondance sous-jacente entre le coeur du

système et ses bords est à la base de l'étude des matériaux topologiques.
La découverte de ces premiers isolants topologiques a mené à une révolution de la matière condensée. En quelques décennies, de plus en plus de matériaux topologiques différents ont été découverts. Avec la réalisation que des phases similaires à l'IQHE pouvaient être créées en l'absence de champs magnétiques forts [9], ou la construction de supraconducteurs topologiques [10], la topologie est devenue omniprésente en physique de la matière condensée théorique (et expérimentale) . Toutes les phases topologiques fermioniques sans interactions ont été classifiées selon la dimension (spatiale) du système et leurs symétries [11, 12]. La classification des phases topologiques en interaction est, quant à elle, un problème beaucoup plus complexe. Le FQHE a été le premier exemple d'une phase où les interactions permettent l'émergence de nouvelles quasi-particules exotiques. Ces excitations se comportent comme des fractions d'électrons appelées anyons. Leur charge est une fraction de la charge électronique, et leurs statistiques d'échange ne sont ni celles d'un boson ni celle d'un fermion. Cette fractionnalisation conduit à une dégénérescence robuste de l'état fondamental, qui dépend uniquement du genre (de sa topologie) du système, et non des détails microscopiques.
Au cours de la dernière décennie, le poids grandissant de l'information quantique, et surtout la course pour la réalisation d'un ordinateur et de simulateurs quantiques ont entrainé un surcroit d'intérêt pour ces états de bord ou excitations fractionnalisés. Comme exemple typique, dans les supraconducteurs topologiques (avec ou sans interactions), des fermions de Majorana d'énergie nulle apparaissent sur les bords du système ou au cœur des vortex (excitations) [10, 13]. Ces fermions de Majorana ont d'abord été proposés par Ettore Majorana [14] en 1937 comme solutions particulières de l'équation de Dirac: des particules qui seraient leurs propres antiparticules. Initialement pensés pour la physique des hautes énergies, c'est la matière condensée qui a finalement vu leur première apparition. L'obstacle principal à la construction d'un ordinateur quantique est la décohérence : l'environnement tend à se coupler aux degrés de liberté quantiques d'un système. L'information quantique est ensuite dissipée dans un nombre macroscopique de degrés de liberté, laissant le système dans un état effectivement classique. La nature topologique et fractionnaire des fermions de Majorana limiterait fortement ces couplages et en principe les rendrait idéals pour réaliser des bits quantiques [15]: comme aucune observable locale ne peut distinguer entre des états différant uniquement par la présence ou l'absence d'une telle quasi-particule, l'environnement ne peut pas être fortement couplé au système. Plusieurs structures ont été proposées permettant de réaliser des ensembles complets de portes logiques, ainsi que des mémoires quantiques, en utilisant des fils supraconducteurs avec des fermions de Majorana à chaque extrémité [16–19]. Obtenir une preuve expérimentale directe et décisive de l'existence de ces fermions de Majorana reste cependant un problème essentiellement ouvert.

Dans cette thèse

Dans cette thèse, nous étudions d'un point de vue théorique différents aspects de la matière topologique: la criticalité et les marqueurs des transitions de phase topologiques dans les modèles génériques unidimensionnels, puis bidimensionnels, l'effet des interactions fortes

dans les supraconducteurs topologiques et le transport électronique médié par les fermions de Majorana.

Ce manuscrit est organisé comme suit. Les chapitres 1 et 2 sont des chapitres introductifs sur la topologie et l'intrication en physique de la matière condensée. Dans le chapitre 1, après une description détaillée de la chaîne de Kitaev [13] que nous utiliserons comme exemple tout au long de cette thèse, nous présentons une introduction générale aux systèmes topologiques. Le chapitre 2 est ensuite consacré à l'intrication, concept fondamental de la mécanique quantique et en particulier dans la description des matériaux fortement corrélés. Nous introduisons l'entropie d'intrication de von Neumann et le spectre d'intrication. Ils ont été fondamentaux dans l'étude théorique des systèmes topologiques, et plus généralement des phases libres. Il est cependant difficile de les mesurer expérimentalement. L'étude des fluctuations de charge bipartites, aussi définies dans ce Chapitre, a été proposée afin de remédier à ce problème. Celles-ci permettent une mesure faible de l'intrication, en particulier pour des modèles unidimensionnels libres (Liquides de Luttinger).

Le reste de la thèse est ensuite consacré à nos travaux. Nous généralisons dans le chapitre 3 les précédents travaux sur les Liquides de Luttinger à des familles génériques de supraconducteurs et isolants topologiques en une et deux dimensions, systèmes dans lesquels la charge observée n'est plus conservée. Nous montrons que les transitions de phases topologiques sont caractérisées par certains coefficients universels dans les fluctuations et les fonctions de corrélations. Les systèmes bidimensionnels que nous étudions présentent des cônes de Dirac, et ces coefficients dépendent de leur enroulement. Cela nous permet de caractériser la topologie de ces points critiques. Dans tous les cas, les fluctuations suivent une loi de volume, qui a un comportement non-analytique aux transition de phase.
Dans le chapitre 4, nous nous intéressons aux systèmes en interactions. Nous montrons tout d'abord que certaines des signatures des transitions topologiques survivent en leur présence, dans les supraconducteurs topologiques. Nous étudions ensuite le diagramme de phase de deux fils supraconducteurs couplés par une interaction Coulombienne. Celle-ci mène à la création de phases exotiques grâce à la compétition avec la supraconductivité non-conventionnelle. Nous montrons en particulier l'apparition de phases de Mott brisant spontanément la symétrie de renversement du temps et présentant des courant orbitaux non-triviaux, ainsi que celle d'une phase de fermions libres, qui est l'extension de deux chaînes de Majorana critiques en interaction.
Enfin, le chapitre 5 est consacré à l'étude des effets de la présence de fermions de Majorana sur le transport électronique. Nous étudions un îlot supraconducteur où plusieurs de ces fermions existent. Ce système pourrait être l'un des composants élémentaires d'un éventuel ordinateur quantique. Les fermions de Majorana changent les statistiques d'échange des porteurs de charges, ce qui se traduit par une fractionnalisation de la conductance. Celle-ci se révèle très robuste face aux anisotropies et autres perturbations. Nous étendons les études précédentes au cas où le nombre d'électrons dans la boîte peut fluctuer, et montrons l'équivalence de ce problème avec le modèle Kondo à plusieurs canaux. Nous réinterprétons alors ce modèle en terme du déplacement d'une particule dans un réseau

fictif dissipatif.

Chapitre 1

L'objectif de ce chapitre est de fournir une introduction simple et concise à différents aspects fondamentaux de la topologie en physique de la matière condensée, à l'aide de divers exemples. Cette thèse se concentre essentiellement sur les travaux théoriques à température nulle. De façon générale, un système quantique peut être décrit par son Hamiltonien, un opérateur ou une forme intégrale qui définit son énergie. Un état quantique est une état-propre de cet opérateur. À température finie, le système sera décrit par une somme pondérée de ces états propres, tandis qu'à température nulle, il suffit d'étudier l'état fondamental (l'état d'énergie la plus basse) de l'Hamiltonien, qui peut être dégénéré. Dans ce chapitre, nous nous concentrons sur les propriétés de ces états fondamentaux, qui peuvent également être directement déduites de celles de l'Hamiltonien lui-même. Nous commençons par une brève présentation du fil de Kitaev[13], un exemple paradigmatique de supraconducteur topologique que nous utiliserons comme modèle de référence tout au long du manuscrit. Nous continuons avec le formalisme générique que nous utilisons pour décrire les systèmes sans interactions, en mettant l'accent sur les modèles à deux bandes. Ensuite, l'essentiel de ce chapitre est une introduction à la topologie dans ces systèmes sans interaction, en suivant la classification des Réfs. [12, 23]. Grace à la description simple permise par l'absence d'interactions, nous faisons un lien entre systèmes physiques topologiques et la notion de classe d'homotopie (topologie des lacets). Nous définissons aussi les divers invariants topologiques pertinents dans ce manuscrit, et abordons rapidement la correspondance entre les bords et le coeur d'un système, liant les propriétés topologiques de l'Hamiltonien à la présence ou à l'absence d'états de bord est brièvement abordée.
Nous concluons ce chapitre avec une description des différents modèles, en une et deux dimensions, qui seront utilisés dans cette thèse. Les deux dernières sections peuvent être ignorées en première lecture, et consultées quand les modèles présentés sont étudiés.

Chapitre 2

Dans le premier chapitre, nous n'avons pas fait référence à l'intrication. Pourtant, ces corrélations non-locales sont la différence fondamentale entre les systèmes quantiques et classiques, et sont responsables de la topologie des états que nous étudions. Historiquement, l'étude de l'intrication était initialement réservée à l'information quantique, et aux études des conséquences de la mécanique quantique en tant que théorie physique. Les premières expériences, basées sur la vérification des inégalités de Bell, illustrant le paradoxe d'Einstein-Podolsky-Rosen, visaient à vérifier la validité de la mécanique quantique. Néanmoins, le rapide développement de l'informatique quantique au cours des dernières décennies a permis une meilleure compréhension des propriétés de l'intrication, y compris dans les systèmes mésoscopiques. L'étude de la structure de l'intrication s'est révélée inestimable pour décrire les transitions de phase (topologiques) à température nulle et les états fondamentaux (topologiques) correspondants. En effet, pour de telles transitions et de tels

états, l'étude des fonctions de corrélation ne permet généralement pas de décrire correctement les changements subis par le système et ses propriétés globales. Les corrélations quantiques ne suffisent pas à discriminer entre des phases aux propriétés topologiques différentes, tandis que l'étude de l'intrication, par exemple l'entropie d'intrication ou le spectre d'intrication, révèle leur nature.
Ce chapitre est donc une introduction à la notion d'intrication dans les systèmes quantiques, et plus précisément dans la physique à n corps. La section 2.1 définit l'entropie d'intrication de von Neumann, ainsi que d'autres mesures fondamentales d'intrication. Après avoir décrit leurs propriétés générales, nous donnons un aperçu des principales idées sous-jacentes dans l'étude de l'intrication pour les systèmes à n corps, en mettant l'accent sur les modèles non gappés. La section 2.2 est dédiée au spectre d'intrication. Il est particulièrement utile pour caractériser les états topologiques qui possèdent des états de bord, car sa mesure repose sur la création de bords artificiels. Enfin, nous présentons dans la section 2.3 une introduction au concept de fluctuations bipartites. Ces fluctuations peuvent être utilisées comme une sonde faible de l'intrication, qui a l'avantage d'être expérimentalement mesurable. Pour une observable locale $\hat{O}$ et une sous-région $\mathcal{A}$ du système total, elles sont définies par:

$$\mathcal{F}_{\hat{O}}(\mathcal{A}) = \langle (\sum_{\vec{r}\in\mathcal{A}} \hat{O}_{\vec{r}})^2 \rangle - \left(\sum_{\vec{r}\in\mathcal{A}} \langle \hat{O}_{\vec{r}} \rangle \right)^2 \tag{A.1}$$

Nous donnons une brève présentation des travaux précédents sur ce sujet, centrés sur les liquides de Luttinger où la charge totale est conservée, avant de consacrer le prochain chapitre à notre extension aux modèles topologiques.

Chapitre 3

Ce chapitre est consacré à notre travail sur les fluctuations bipartites dans les systèmes topologiques sans interactions. Plus précisément, nous nous concentrons sur les fluctuations bipartites à et à proximité des phases critiques qui apparaissent habituellement dans de tels systèmes, car les fluctuations bipartites apportent plus d'informations pour les phases non-gappées. Trouver de telles phases critiques n'est pas une garantie de transition de phase topologique, car il est toujours possible de construire des modèles complexes où elles apparaissent sans changement dans la topologie du système, mais est néanmoins une signature importante de ces transitions. En outre, certains systèmes libres sont eux-mêmes protégés topologiquement [41] (par exemple, la classe DIII pour $d = 2$): les fluctuations bipartites sont alors un outil parfait pour leur étude.
Dans ce chapitre, nous nous concentrons sur des systèmes critiques uni- et bidimensionnels typiques des transitions de phase topologiques. Nous considérons les fluctuations des bilinéaires fermioniques locaux tels que la charge ou les différentes polarisations de pseudo-spin. Nous commençons dans la section 3.1 par un aperçu des propriétés mathématiques des fluctuations de ces systèmes à une dimension. En utilisant le théorème de Wick, on peut commodément exprimer les fluctuations en tant que simple produit scalaire des fonctions de Green modulé par un noyau, le noyau de Fejér. Cette fonction a des propriétés

très intéressantes qui nous permettent de déterminer la forme générale des fluctuations pour les systèmes sans interactions:

$$\mathcal{F}_{\hat{O}}(\mathcal{A}) = i_{\hat{O}} l_{\mathcal{A}} + \mathbf{b}_{\hat{O}} \ln l_{\mathcal{A}} + \mathcal{O}(1), \tag{A.2}$$

avec $\hat{O}$ l'opérateur considéré et $l_{\mathcal{A}}$ la longueur du sous-système $\mathcal{A}$. Nous prouvons également que $i_{\hat{O}}$ est lié à la densité d'information quantique de Fisher [144] (QFID)[1]. La QFID, objet initialement défini pour la métrologie et l'information quantique, est une borne de la reproductibilité des systèmes quantiques. Pour les supraconducteurs et les isolants à deux bandes que nous étudions ici, nous obtenons la limite suivante pour ce coefficient:

$$i_{\hat{O}} \leq \frac{q_e}{2} \text{avec } q_e \text{ la charge dans la cellule unitaire.} \tag{A.3}$$

Le terme logarithmique n'apparait que si le système est non-gappé et la valeur de $\mathbf{b}_{\hat{O}}$ est directement liée aux symétries de l'Hamiltonien et à l'amplitude des discontinuités des fonctions de corrélation aux moments où le gap se ferme.
Dans la section 3.2, nous appliquons le formalisme dérivé précédemment à la famille de modèles topologiques BDI, à laquelle appartient le modèle de Kitaev. Nous calculons les fluctuations pour une base complète des bilinéaires fermioniques locaux dans les système à deux bandes. Nous montrons que, à la transition de phase, le coefficient linéaire a des cusps caractéristiques qui permettent une détection facile des transitions de phase. La discontinuité de la dérivée peut être reliée à la vitesse des différentes composantes de l'Hamiltonien. Pour des transitions de phase simples, où le gap se ferme à un seul moment, nous montrons que les symétries de particules-trous (PHS) et de renversement de temps (TRS) imposent que le coefficient logarithmique des fluctuations de charge est universel et donné par:

$$\mathbf{b}_{\hat{Q}} = -\frac{q_e}{2\pi^2}. \tag{A.4}$$

Le signe négatif prouve que ces fluctuations ne peuvent pas être décrites en termes de fluctuations de densité d'un liquide de Luttinger. Pour les supraconducteurs, $q_e = 1$, et $|\mathbf{b}_{\hat{Q}}|$ est la moitié de ce qu'il serait pour les fermions libres. Ce facteur deux est directement analogue à celui apparaissant dans la charge centrale.

Lorsqu'on envisage des transitions de phase plus complexes, où le gap se ferme à plusieurs moments, la valeur du coefficient n'est plus universelle, tandis que le cusp du terme linéaire survit généralement. Pour identifier exactement la transition de phase, nous introduisons le facteur de structure des fluctuations bipartites:

$$\mathcal{SF}_{\hat{O}}(\mathcal{A}, \psi) = \langle | \sum_{j \in \mathcal{A}} e^{i\psi j} \hat{O}_j |^2 \rangle - | \langle \sum_{j \in \mathcal{A}} e^{i\psi j} \hat{O}_j \rangle |^2 \tag{A.5}$$

Cet objet nous permet de déterminer le nombre exact de points de fermeture du gap et leurs propriétés. Dès que ψ est différent de zéro, le terme logarithmique disparait.

[1] L'information quantique de Fisher, définie comme les fluctuations liées d'une observable pour un état pur, mesure la productibilité de la fonction d'onde, c'est-à-dire la séparabilité de l'état dans un espace où l'observable est locale.

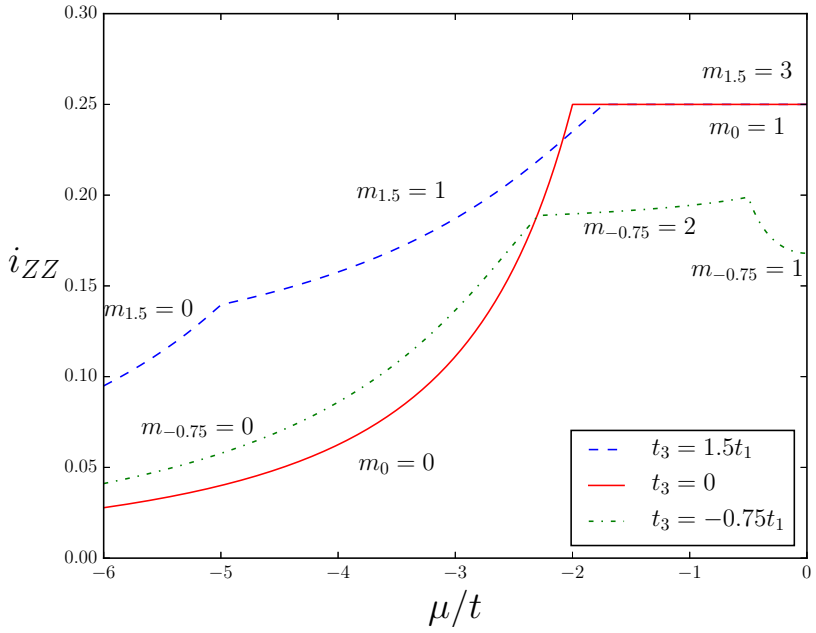

Figure A.1: Terme linéaire des fluctuations bipartite de charge dans une variante étendue du modèle de Kitaev (avec des sauts et un appariement au troisième plus proche voisin), en fonction du potentiel chimique μ pour plusieurs valeurs du ratio $\frac{t_3}{t_1}$ with $\Delta_l = t_l$. Les cusps marquent chaque transition de phase. m est le nombre d'enroulement associé à chaque phase, et correspond au nombre de fermions de Majorana protégés à chaque extrémités.

Lorsque ψ est égal à $k_j - k_{j'}$, avec k_j les moments où le gap se ferme, le terme logarithmique réapparait et reprend une valeur universelle.
Enfin, nous discutons également les corrections de température et de taille finie. Ces dernières sont particulièrement importantes dans les simulations numériques de supraconducteurs topologiques, car il faut prendre en compte précisément les modes 0 et π. Nous trouvons la forme exacte des corrections pour le modèle de Kitaev et vérifions la convergence numérique des fluctuations grâce à des simulations de type Matrix Product States.
La Section 3.3 est consacrée à l'étude des fluctuations bipartites dans les Hamiltoniens de classe D. Nous vérifions que la plupart des propriétés précédemment dérivées sont toujours valides: cusps aux transitions de phase, coefficients logarithmiques quantifiés... Nous prenons également le temps de traiter, à titre d'exemple de systèmes au-delà du paradigme à deux bandes, le modèle des fils supraconducteur de Rashba introduit dans la section 1.5.3. Nous trouvons qu'un choix approprié de la charge observée mène aux mêmes résultats que dans le modèle plus simple de Kitaev.
Enfin, nous étudions des modèles typiques de fermions non gappés en deux dimensions dans la Section 3.4. Plus précisément, nous nous concentrons sur des modèles présentant des cônes de Dirac, caractéristiques des transitions de phase dans les modèles topologiques bidimensionnels. Nous nous concentrons sur les fluctuations de charge dans les modèles à

deux bandes. Nous montrons d'abord, en utilisant l'analogue 2D du noyau de Fejér, que les fluctuations vérifient:

$$i_{\hat{O}} A_{\mathcal{A}} + c_{\hat{O}} R_{\mathcal{A}} + \mathbf{b}_{\hat{O}} \ln l_{\mathcal{A}} + O(1), \tag{A.6}$$

où $A_{\mathcal{A}}$ est l'aire de la région considére, et $R_{\mathcal{A}}$ et $l_{\mathcal{A}}$ sont deux longueurs caractéristiques ($R_{\mathcal{A}}$ est généralement le périmètre). Nous prouvons alors que le coefficient $i_{\hat{O}}$ est toujours donné par la QFID associée à la charge électronique. Il ne présente pas de cusps aux transitions de phase, mais une divergence logarithmique de sa dérivée seconde. Nous pouvons étendre ce résultat à des dimensions plus élevées : pour une surface de Fermi de dimension nulle et une dispersion linéaire, on s'attend à une discontinuité de la dérivée $d^{\text{ème}}$ en dimension impaire et à une divergence logarithmique de celle-ci en dimension paire.

Nous nous concentrons ensuite sur le terme logarithmique pour un seul cône de Dirac isotrope. $\mathbf{b}$ est non-nul seulement si le système est non gappé et dépend du nombre d'enroulement m du cône de Dirac. Nous montrons également que, comme pour la vNEE, il n'apparait que si la région $\mathcal{A}$ présente des coins. Chaque coin contribue indépendamment, avec une amplitude:

$$\frac{q_e m^2}{32\pi^2}(1 + (\pi - \psi)\cot\psi)\ln l_{\mathcal{A}}, \text{avec } \psi \text{ l'angle du coin.} \tag{A.7}$$

La fonction $\psi \to 1+(\pi-\psi)\cot\psi$ est appelé fonction de coin (corner function). Elle ne correspond pas celle qui apparaît dans l'entropie des fermions de Dirac en deux dimensions, mais à celle du modèle d'information mutuelle étendue (Extended Mutual Information model). Ces résultats ne dépendent pas de la forme du réseau. Il est aussi intéressant de souligner le signe positif du terme logarithmique, qui est opposé à celui apparaissant dans la vNEE des systèmes concernés.

Nous généralisons ensuite à des systèmes plus complexes. Tout d'abord, nous considérons ensuite l'effet de l'anisotropie des cônes sur les fluctuations. Nous montrons que des anisotropies dans l'espace des moments sont équivalents à des anisotropies dans l'espace réel: les fluctuations dépendent maintenant de la direction de $\mathcal{A}$, et la fonction de coin est déformée. Finalement, nous concluons ce chapitre en étudiant des phases critiques présentant plusieurs cônes de Dirac. Nous montrons que le facteur de structure des fluctuations nous permet de distinguer entre une phase triviale telle que le graphène, présentant deux cônes avec un nombre d'enroulement opposé, et la phase $\mu = 0$ d'un supraconducteur $p + ip$ où les deux cônes ont le même nombre d'enroulement.

La plupart des résultats de ce chapitre ont été dérivés directement pour des Hamiltoniens spécifiques, en utilisant les différentes symétries pour minimiser les effets des détails microscopiques des modèles considérés. Les mêmes résultats peuvent être obtenus en utilisant directement la théorie conforme, donnant une description de basse énergie de ces familles de modèles critiques. Nous avons choisi de ne pas présenter ce type de dérivation car, d'un point de vue pratique et expérimental, la manière dont les observables se projettent sur les champs conformes est tout aussi importante que le comportement des champs conformes à basse énergie. Le traitement des observables physiques permet de ne pas avoir à traiter la question complexe de cette projection. Il est aussi important de souligner que la quantification des fluctuations peut également être réinterprétée en termes de quantification des

termes dominants des fonctions de corrélation. Par exemple, l'universalité du coefficient logarithmique en une dimension pour les fluctuations de charge dans les supraconducteurs topologiques se traduit par:

$$\langle n_j n_{j'} \rangle_c = -\frac{\mathbf{b}_{\hat{Q}}}{2} \frac{1}{(j-j')^2} + o(\frac{1}{(j-j')^2}). \tag{A.8}$$

Ce chapitre reprend des résultats publiés dans la Réf. [145], ainsi que d'autres travaux en cours de préparation.
Méthodes utilisées: solutions exactes et calcul intégral, espaces de Hilbert-Sobolev (Fourier), diagonalisation exacte

Chapitre 4

Le chapitre 4 s'intéresse aux effets des interactions dans les systèmes topologiques. La première partie du chapitre se concentre sur la construction d'une description fiable du point critique topologique pour un supraconducteur topologique en interaction et sur l'effet des interactions sur les fluctuations bipartites étudiées précédemment. Quand interactions et topologie sont présents, de nouvelles phases exotiques peuvent apparaître. L'effet Hall fractionnel en est un exemple parfait: c'est un analogue direct de l'IQHE, où un courant quantifié circule sur les bords du système, mais la conductivité prend maintenant des valeurs rationnelles bien précises plutôt que des valeurs entières. Cet effet, expérimentalement découvert en 1982 [6] et expliqué théoriquement en 1983[100], a depuis été le sujet de nombreuses études. En effet, la nature non-entière de la conductance est un symptôme de l'existence de porteurs de charge fractionnaires. Ces quasi-particules ne vérifient pas les relations de commutation bosonique ou celles d'anticommutation fermionique, mais des règles d'échange plus complexes.
Une autre conséquence non triviale de l'ajout d'interactions est la réduction des groupes d'homotopie des différentes classes d'Hamiltoniens et par conséquent la réduction des invariants topologiques. Peut-être l'exemple le plus célèbre est celui découvert par Fidkowski et Kitaev: la reduction $\mathbb{Z}_8$ [110, 168, 169]. Alors que les différentes classes d'Hamiltoniens restent bien définies en présence d'interactions, il a été démontré que l'invariant topologique de la classe BDI n'est plus un élément de $\mathbb{Z}$ mais de $\mathbb{Z}_8$, tout comme il se réduit à $\mathbb{Z}_2$ lors de la rupture de la symétrie de renversement du temps. Illustrons brièvement la signification physique de cette réduction. Si nous prenons $n < 8$ fils de Kitaev dans leur phase topologique avec des conditions aux bords ouvertes, il n'est pas possible de coupler les modes de Majorana de bords d'énergie nulle en ajoutant des interactions arbitrairement faibles, du moment qu'elles préservent les symétries de renversement du temps et particule-trou. Les fermions de Majorana sont protégés par les symétries. Cependant, si nous considérons 8 fils de Kitaev côte à côte, il est possible de créer une interaction qui donne une énergie finie à tous les modes d'énergie nulle, qui ne sont donc plus protégés.
Alors que le FQHE est un effet des interactions fortes, la classification modulo $\mathbb{Z}_8$ limite les comportements possibles de nos systèmes lorsque les interactions sont plus faibles que le gap du système sans interactions. Dans ce Chapitre, nous étudions un régime intermédiaire: partant d'un système topologique protégé par la classification $\mathbb{Z}_8$, nous

nous intéressons à ce qui se produit lorsque les interactions sont suffisamment importantes pour que la protection topologique soit brisée, et en particulier aux phases exotiques (non topologiques) qui peuvent apparaître. Dans la Section 4.1, nous présentons, en tant qu'introduction, des méthodes permettant de résoudre une version avec interactions du fil de Kitaev. En particulier, nous proposons un schéma de bosonisation qui permet de décrire le point critique $c = \frac{1}{2}$ en termes de liquide de Luttinger. Nous utilisons ensuite cette représentation pour déterminer l'effet des interactions sur les fluctuations de charge bipartite. Nous démontrons analytiquement et numériquement que le terme logarithmique survit en présence d'interactions mais qu'il est renormalisé. Une analyse des corrections de taille finie permet néanmoins de retrouver la valeur universelle du coefficient et donc de déterminer la classe d'équivalence du point critique à l'aide des fluctuations y compris en présence d'interactions.

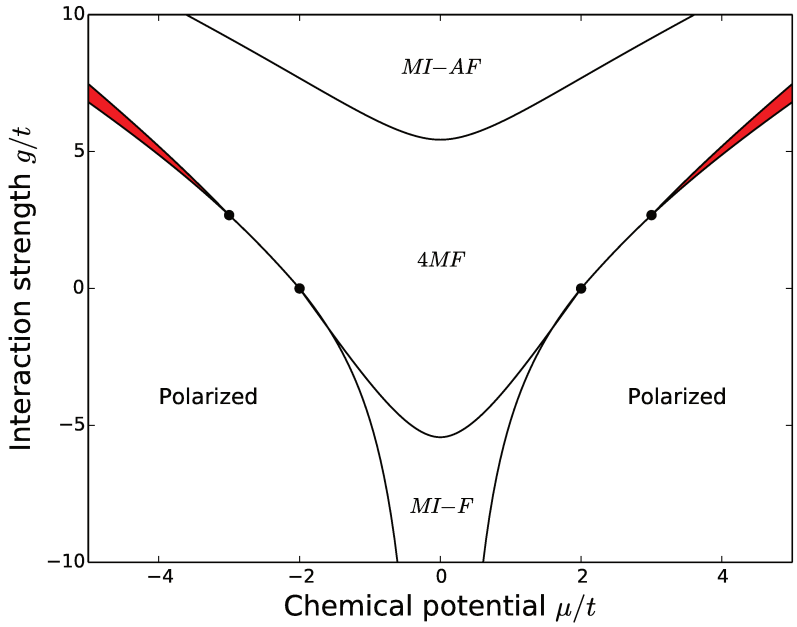

Figure A.2: Diagramme de phase schématique de deux fils de Kitaev en interaction, obtenu par des méthodes analytiques (bosonisation) et numériques (diagonalisation exacte et DMRG). Les potentiels chimiques dans les deux scènes sont supposés égaux. $4FM$ est la phase topologique, avec deux fermions de Majorana présents à chaque extrémité du fil. $MI-AF$ et $MI-F$ sont deux phases de Mott gappées, soit antiferromagnétique, soit ferromagnetique. Les phases polarisées ("Polarized") correspondent à la phase triviale du modèle de Kitaev. En rouge, la phase gappée DCI est une extension du point critique en l'absence d'interactions.

Le reste du chapitre est consacré à l'étude d'un autre modèle de supraconducteurs en interaction que nous avons étudié dans la Réf. [155]. Il est basé sur deux fils de Kitaev,

couplés par une interaction densité-densité, correspondant à une description minimale de l'interaction Coulombienne. La section 4.2 présente le modèle et son Hamiltonien. Après une discussion approfondie du modèle, nous proposons un aperçu de son diagramme de phase (Figure A.2). Comme les symmétries de renversement du temps et la symétrie particule-trou sont respectées, la phase topologique survit même à des interactions fortes. À faible potentiel chimique et large couplage, deux phases de Mott apparaissent, présentant des courants orbitaux exotiques. La section 4.3 présente une étude complète de ces deux phases, ainsi que la preuve de leur existence. Pour un fort potentiel chimique, le système est polarisé. Enfin, dans un régime intermédiaire, où les interactions et le potentiel chimique sont comparables, une nouvelle phase non gappée s'ouvre. Cette phase, que nous dénommons phase critique d'Ising double (Double Critical Ising), est étudiée dans la section 4.4, et est une extension des deux points critiques $c = \frac{1}{2}$ des chaines de Kitaev sans interactions. Ce chapitre détaille des résultats publiés dans la Réf. [155], ainsi que quelques nouveaux résultats complémentaires.
Méthodes utilisées: bosonisation, groupe de renormalisation, diagonalisation exacte, DMRG basée sur les MPS

Chapitre 5

Enfin, nous nous intéressons dans ce dernier chapitre aux effets de la présence de fermions de Majorana sur le transport électronique. La manipulation des états de Majorana liés dans les supraconducteurs topologiques a fait l'objet de nombreuses études [16, 17]. L'une des principales questions restant à résoudre est de trouver des signatures expérimentales claires de l'existence de ces quasi-particules insaisissables : la résilience de ces fermions de Majorana à la décohérence les rend également difficiles à observer. Une façon de détecter ces fermions de Majorana est de s'intéresser au transport électronique. En effet, la présence de fermions de Majorana aux extrémités d'un supraconducteur affecte fortement le transport d'électrons à travers le substrat. Selon à quoi est couplé le supraconducteur, différents effets peuvent être mesurés: effet Josephson anormal[13, 23, 230–240], reflexions d'Andreev parfaites locales[25–33, 53, 58, 59, 225, 226] et transversales[225–228]. Cependant, ces signaux ne sont pas univoques: les valeurs des conductances et des périodicités anormales peuvent être obtenues dans des systèmes sans Majoranas. C'est la résilience de ces valeurs aux perturbations qui marque l'aspect topologique de ces quasi-particles. D'autres travaux ont également suggéré d'observer directement les statistiques non-abéliennes des Majoranas à l'aide de portes quantiques[233, 242].
Combiner des effets de charge avec la présence des fermions de Majorana, c'est à dire la physique de Kondo avec celle des fermions de Majorana [243–245], conduit à des propriétés de transport exotiques dans les régimes continus [246–249] ou alternatifs [250, 251]. Dans ce chapitre, nous étudions une généralisation de la structure décrite dans la Réf. [246]. Nous considérons un îlot supraconducteur, où le nombre total d'électrons est fixé par une capacitance (l'îlot n'est pas directement relié à la masse). Sur cet îlot est déposé un fil semi-conducteur, de façon à réaliser un supraconducteur topologique par proximité. On connecte alors une électrode à chaque extrémité du fil, et donc à un fermion de Majorana et nous appliquons une faible tension. On peut alors observer une conductivité parfaite quantifiée entre les deux électrodes, correspondant à un canal unique de

transmission:

$$\frac{e^2}{h}. \tag{A.9}$$

Un électron entrant va en fait se délocaliser dans le fermion virtuel d'énergie nulle composé des deux fermions de Majorana.
Dans ce chapitre, nous étudions le dispositif proposé dans les travaux pionniers des Refs. [20, 21]: un seul îlot supraconducteur, où plusieurs fils topologiques ont été déposés, de façon à connecter $M \geq 3$ fermions de Majorana à autant d'électrodes, modélisées par des liquides de Luttinger. La "charge" de l'îlot, c'est-à-dire le nombre de paires de Cooper plus le nombre de fermions dans l'espace des Majoranas, peut être modifiée par une tension de grille. Dans le cas non-dégénéré, où la charge de l'îlot est fixée et unique, un effet Kondo [254] non conventionnel, appelé "modèle topologique de Kondo", a été théoriquement exploré [20, 21, 255–263] avec apparition d'un "spin" $SO(M)$ construit à partir des fermions de Majorana. De telles boîtes ont été proposées comme éléments constitutifs d'un ordinateur quantique[22] et de nombreux progrès ont été faits pour les réaliser expérimentalement[252, 253].

Pour une île non-supraconductrice, en l'absence de fermions de Majorana, Matveev a démontré un effet Kondo de charge[264, 265] dans lequel deux états de charge dégénérés jouent le rôle d'un spin 1/2 effectif et s'hybridisent avec les électrons des électrodes ou de l'îlot. Le modèle effectif est appelé modèle Kondo multicanal(M-CKM). Remarquablement, dans le modèle Kondo à deux canaux, une excitation de Majorana apparaît à faible énergie [266–270]. Il s'agit cependant d'une particule émergente et diffère des fermions Majorana induits par supraconductivité par proximité considérés dans ce chapitre. Récemment, le modèle de Kondo de charge à deux canaux a été réalisé [271] dans un système de GaAs avec un contrôle sans précédent sur les paramètres du modèle; ou encore avec un spin ordinaire [272, 273]. Dans tous les cas, la caractérisation expérimentale est difficile du fait de l'instabilité du modèle. A basse énergie, le modèle Kondo topologique présente des exposants caractéristiques des non-liquides de Fermi, et qui peuvent être décrits par un mouvement brownien quantique (QBM) de couplage fort. Dans cette analogie, une particule effective se déplace d'un minimum à l'autre d'un potentiel, ceux-ci formant un réseau triangulaire bidimensionnel (modèle d'instanton). Les dimensions des principaux opérateurs non pertinents peuvent donc être dérivées, en accord avec une approche de théorie des champs conformes[274]. La conductance entre les différents fils est symétrique, fractionnalisée et résistante aux perturbations. Contrairement à l'effet Kondo topologique, le modèle Kondo multicanal n'admet pas une description simple en terme de QBM. La particule effective se déplace sur un réseau en nid d'abeille et le point fixe de faible énergie correspond à un couplage intermédiaire, ce qui exclut un traitement analytique perturbatif complet. De plus, ce point fixe infrarouge intermédiaire n'est pas robuste alors que le point fixe de Kondo topologique correspond à un couplage fort et est stable contre les perturbations, telles que les asymétries dans les couplages. Ce dernier point semble favoriser l'observation expérimentale de l'effet Kondo topologique au lieu de l'effet multicanal standard.
Dans ce chapitre, nous nous concentrons sur le modèle de Kondo topologique proche de la dégénérescence de charge, où deux états de charge consécutifs n et $n+1$ sont énergiquement équivalents et forment un pseudo-spin. Nous montrons que le réseau QBM qui en résulte

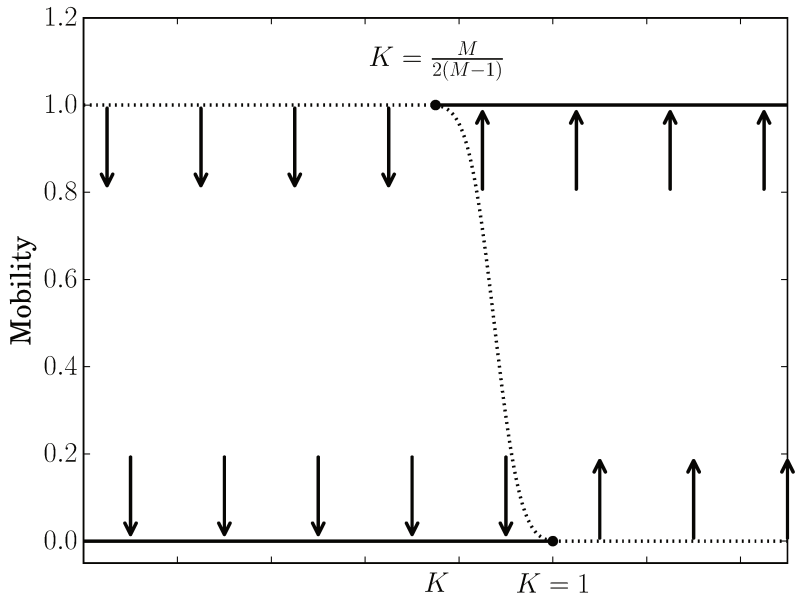

Figure A.3: Diagramme de phase et renormalisation pour une boîte de Kondo-Majorana loin de la dégénérescence de charge. La mobilité correspond ici à: $\mu = \frac{hG_{j,j}}{2e^2}\frac{M}{1-M}$. La ligne continue décrit des points fixes stables du courant de renormalisation tandis que les lignes pointillées correspondent à des points fixes instables. Les flèches représentent le courant des opérateurs les plus pertinents/moins pertinents. K est le paramètre Luttinger dans toutes les électrodes, qui quantifie la force des interactions dans celles-ci. Nous observons une transition de phase du premier ordre entre une phase où l'îlot est isolant ($\mu = 0$) et une phase où le courant est parfaitement transmis ($\mu = 1$) pour K entre $K = \frac{M}{2(M-1)}$ et $K = 1$.

est un réseau triangulaire, mais avec une texture de spin non triviale: chaque plaquette porte une phase de Berry de π. Le modèle dual est un réseau en nid d'abeille. Par conséquent, le modèle effectif est un modèle Kondo multicanal mais où le paramètre de Luttinger est doublé. Ainsi, pour des électrodes sans interactions, le modèle Kondo multicanal qui en résulte possède des réservoirs en interactions fortes, avec le paramètre Luttinger renormalisé $K = 2$, et le point fixe QBM à couplage fort devient stable. Le modèle Kondo multicanal standard correspond à une valeur initiale de $K = 1/2$, c'est à dire une forte répulsion électronique dans les électrodes.

Pour un grand nombre de canaux, le modèle admet deux points fixes stables dans une certaine fenêtre des paramètres de Luttinger, à couplage fort et intermédiaire, séparés par un point fixe instable, et prédire ainsi une transition de phase quantique à mesure que l'amplitude du tunnel électronique au plomb varie. Le point fixe du couplage intermédiaire est en fait connecté de manière analytique au point fixe infrarouge du modèle Kondo multicanal, et nous nous attendons donc à ce qu'il ne soit pas robuste contre les asymétries de canal ou contre la levée de la dégénérescence de charge. La plupart de nos résultats sont

basés sur l'analyse QBM de Kane et Yi[275, 276] que nous examinons en nous concentrant sur la fonction d'onde pseudospin.

Le même modèle a été étudié indépendamment par Michaeli *et al*[277], où le pic de résonance de la conductance est fortement amélioré à la dégénérescence, et le point de couplage fort est robuste. Nous reproduisons leurs principaux résultats, bien que l'analyse du courant de renormalisation dans la Ref. [277] est restreinte à l'ordre le plus bas, et par conséquent la coexistence de points fixes stables pour un nombre de canaux supérieur à 4 n'est pas discutée. Dans la Sec. 5.2, nous présentons la structure étudiée, et discutons de sa bosonisation. Nous présentons le formalisme QBM dans la Sec. 5.3 et détaillons son application au modèle de Kondo topologique. Le point de dégénérescence de charge est étudié dans la Sec. 5.4 où nous détaillons la projection sur le modèle M-CKM. Dans la Sec. 5.5, nous analysons le modèle grâce au groupe de renormalisation.

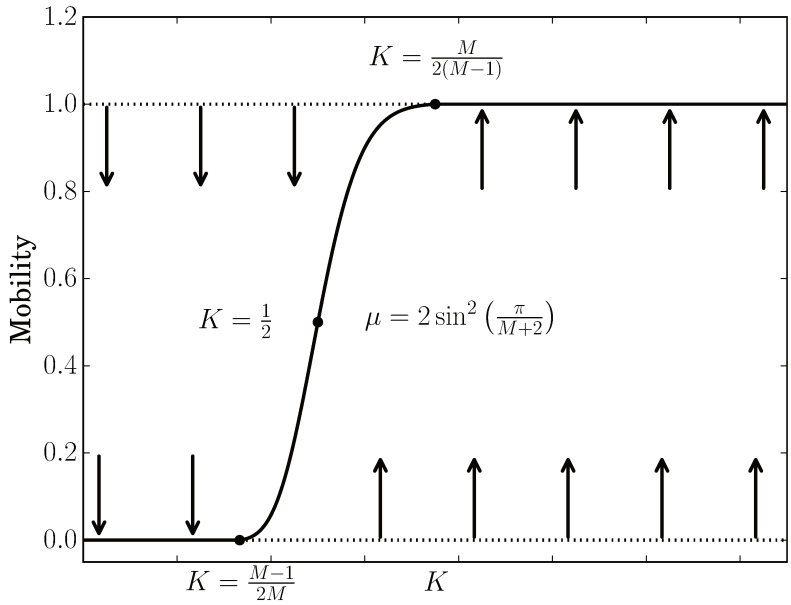

Figure A.4: Diagramme de phase de la boîte de Kondo-Majorana à la dégénérescence de charge, en fonction du paramètre de Luttinger dans les électrodes, pour $M = 3, 4$. La mobilité est définie par: $\mu = \frac{hG_{j,j}}{2e^2}\frac{M}{1-M}$. Nous observons une transition de phase du second ordre entre une phase isolante, et une phase de couplage fort avec une conductance fractionnalisée et symétrique. Une ligne continue de points fixes stables relie les deux phases.

Nous démontrons que les propriétés de transport d'une boîte Kondo topologique qui héberge des états liés de Majorana dépendent sensiblement de la proximité d'un point de dégénérescence de charge. Quand il y a un unique état de charge de basse énergie, l'effet dominant est l'effet Kondo topologique, avec une transition de phase quantique du premier ordre entre un régime fortement couplé où la conductivité est maximale et symétrique entre

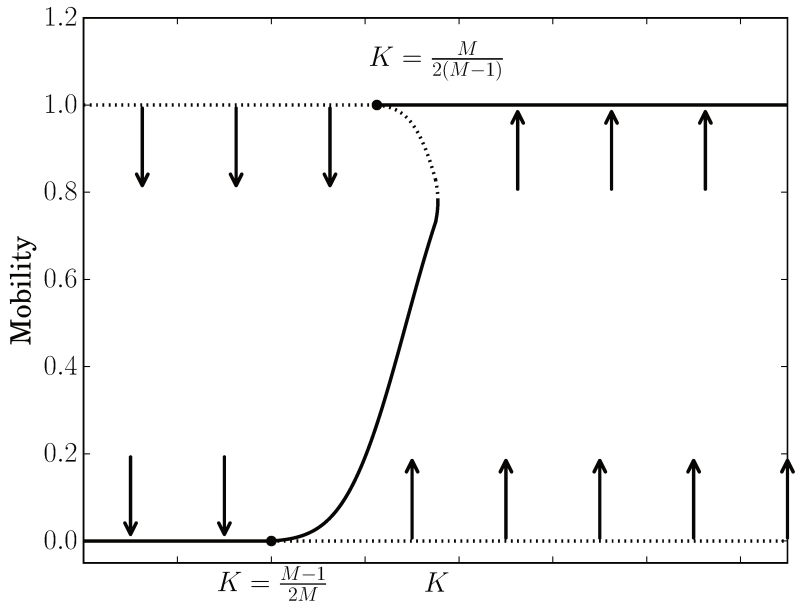

Figure A.5: Diagramme de phase de la boîte de Kondo-Majorana à la dégénérescence de charge, en fonction du paramètre de Luttinger dans les électrodes, pour $M \geq 5$. L'analyse de couplage faible donne les mêmes résultats que pour $M = 3, 4$, avec une ligne continue de points fixes apparaissant à $K_c = \frac{M-1}{2M}$. Pour $K \leq K_c$, l'îlot est isolant. L'analyse de couplage fort est cependant différente et est en fait semblable à ce que nous avions observé dans le modèle Kondo topologique. Une ligne instable de points fixes apparaît à $K = \frac{M}{2(M-1)}$ (vérifiant perturbativement la même équation que dans la limite Kondo topologique). Nous postulons la coexistence de points fixes intermédiaire et de couplage fort jusqu'à une valeur critique du paramètre de Luttinger où la transition devient du premier ordre.

les électrodes, et un régime parfaitement isolant. Le diagramme de phase et la conductivité en fonction de la force des interactions dans les électrodes sont représentés dans la Figure A.3. La situation est nettement différente lorsque le système est à la dégénérescence de charge, et dépend aussi du nombre d'électrodes connectés à l'îlot. Nous identifions deux situations, représentées dans les Figures A.4 et A.5.

1. Pour trois ou quatre électrodes, le point fixe de Kondo intermédiaire est stable et existe pour $\frac{M-1}{2M} < K < \frac{M}{2(M-1)}$, et connecte les régimes de couplage fort et faible. Par conséquent, la conductance entre les électrodes est égale à

$$G_{j,k} = \frac{2e^2 K \mu(K)}{h} \left(\frac{1}{M} - \delta_{j,k} \right), \tag{A.10}$$

où la mobilité $\mu(K)$, montrée dans la Figure A.4, varie entre 0 et 1. Nous récupérons

le point fixe Kondo multicanal pour $K = 1/2$, avec une mobilité intermédiaire $\mu(1/2) = \sin^2[\pi/(M+2)]$.

2. Pour plus de quatre fils (Figure A.5), nous récupérons le comportement critique du modèle Kondo topologique à large mobilité, ce qui indique que le pseudo-spin de charge peut-être ignoré si les fermions de Majorana sont déjà fortement couplés aux électrodes. Comparé au modèle Kondo topologique, la principale différence est l'existence d'une ligne point fixe intermédiare stable qui remplace la phase isolante, et est similaire à celle obtenue pour $M = 3, 4$.

Notre analyse QBM révèle que le pseudo-spin, représentant les deux états de charge, est l'ingrédient physique principal expliquant la différence de comportement entre les cas dégénéré et non-dégénéré. S'éloigner du point dégénéré ou augmenter le nombre de canaux réduit l'importance de ce pseudo-spin et permet l'appararition de la physique du modèle Kondo topologique. De plus, le point fixe intermédiaire n'est pas robuste vis à vis des asymétries de couplage, et nécessite donc un réglage fin des paramètres expérimentaux, contrairement au point fixe de couplage fort tel que décrit dans Ref.[277]. Nous notons que le paramètre critique pour lequel la ligne intermédiaire stable tourne et devient instable n'est pas connu analytiquement et son existence reste une conjecture.

Ce chapitre repose en grande partie sur les résultats publiés dans la Réf. [278].
Méthodes utilisées: bosonisation, groupe de renormalisation

Conclusions

Nous avons étudié dans cette thèse diverses propriétés des matériaux topologiques, allant des marqueurs d'intrication dans les fonctions de corrélation à leurs propriétés de transport.
Tout d'abord, nous avons vu que, dans les phases critiques typiques des modèles topologiques sans interactions à une ou deux dimensions, les fluctuations bipartites sont caractérisées par des lois d'échelle universelles qui imitent celles de l'entropie de von Neumann. En raison de l'absence de conservation des charges étudiées, le coefficient dominant est une loi de volume, dont les non-analyticités marquent les différentes transitions de phase. Aux points critiques, des termes logarithmiques apparaissent, avec un coefficient universel, indépendent de tout paramètre microscopique. A une dimension, ce coefficient est invariant, et sa valeur et son signe montrent l'inversion du gap qui se produit lors d'une transition de phase topologique. En deux dimensions, nous avons pu extraire sa dépendance en la géométrie du sous-système considéré, et nous avons montré que l'on peut récupérer directement le nombre d'enroulement des différents cônes de Dirac et donc sonder la transition. Une quantification similaire peut être directement extraite des fonctions de corrélation connectées ou des fluctuations mutuelles (analogues de l'information mutuelle). Ici, nous avons choisi de nous limiter à l'étude des classes BDI et D, mais ces observations peuvent être directement généralisées aux autres classes non-triviales. Ceci est particulièrement pertinent pour la classe d'Hamiltoniens DIII dont les phases non-gappées sont protégées topologiquement en deux dimensions [41].

Pourtant, de nombreuses questions sur les fluctuations bipartites, avec ou sans conservation de la charge, restent ouvertes. Ces quantifications et universalités sont possibles car la surface de Fermi est de dimension nulle. Un traitement similaire peut donc être directement appliqué à des phases non-gappées tridimensionnelles, et en particulier aux semi-métaux de Weyl [293, 294]. Ces matériaux sont caractérisés par une surface de Fermi présentant des points chiraux, c'est-à-dire l'équivalent direct des cônes de Dirac en trois dimensions. Il serait intéressant de vérifier si l'on peut directement sonder la charge chirale associée à chaque nœud de la même manière que nous avons pu sonder le nombre d'enroulement des cônes de Dirac. Ce serait une mesure directe, sans ambiguïté, de la nature topologique des semi-métaux de Weyl. Etudier l'effet des arcs de Fermi sur les limites des matériaux serait également intéressant, et peut-être une perspective encore plus excitante serait l'étude des semi-métaux Weyl supraconducteurs qui présentent des nœuds et des arcs de Majorana[295]. Sur un plan plus théorique, nous avons observé un très bon accord entre les lois d'échelle des fluctuations et celles de l'entropie. Pourtant, les limites habituelles sur l'information mutuelle obtenue à partir des fluctuations mutuelles sont loin d'être saturées: il serait intéressant de voir si l'on peut construire de meilleures limites dans le cas particulier des fluctuations de charge. Cela permettrait une mesure directe de l'intrication dans les expériences. Enfin, il serait particulièrement intéressant de généraliser nos résultats aux points critiques typiques qui séparent les phases triviales des phases parafermioniques [296, 297]. La modification du modèle critique devrait également être observée directement dans les fluctuations, ce qui peut conduire à une mesure directe de ces quasi-particules exotiques.

Dans un second temps, nous avons inclus les interactions dans notre description des supraconducteurs. La présence conjointe de la topologie et des interactions conduit à une physique riche. Nous avons étudié l'influence des interactions sur un supraconducteur topologique typique et montré que le coefficient de la contribution logarithmique aux fluctuations a été seulement renormalisé (son signe et son existence sont conservés). Nous avons ensuite présenté et discuté un modèle de deux supraconducteurs topologiques couplés par des interactions coulombiennes. Nous avons montré que, bien que la phase topologique survive à la présence d'interactions faibles, de nouvelles phases peuvent s'ouvrir. En particulier, nous avons vu que des phases de Mott apparaissent à et près du demi-remplissage. Elles présentent des courants orbitaux inhabituels qui brisent spontanément la symétrie de renversement du temps, malgré l'absence de saut direct d'un fil à l'autre. Nous avons également montré l'ouverture d'une phase critique exotique, une extension directe du point critique topologique standard. D'une manière générale, il serait intéressant d'avoir une compréhension systématique de l'effet des interactions sur la supraconductivité topologique. Une autre extension possible, en relation avec les fluctuations bipartites, est simplement la généralisation à des systèmes arbitraires et, en particulier, la question de savoir si l'on peut réellement récupérer l'universalité du coefficient logarithmique et donc identifier les phases critiques à partir d'observables mesurables.

Enfin, nous avons étudié une hétéro-structure composée d'un îlot supraconducteur portant des fermions de Majorana, reliée à plusieurs électrodes. Nous avons déterminé ses propriétés de transport et montré que l'on récupère la physique du modèle Kondo multicanal standard, au prix d'une renormalisation des interactions. La conductance prend alors une forme fractionnée symétrique. Nous avons utilisé le formalisme du movement

brownien quantique, qui permet d'aborder à la fois les limites de couplage faible et fort. L'existence (et une description) du point critique auquel la boîte subit une transition de premier ordre entre le point fixe de Kondo multicanal et le point fixe de couplage fort pour un grand nombre d'électrodes reste un problème ouvert, qu'il serait particulièrement intéressant d'étudier numériquemnt. De plus, comme ce modèle pourrait être un des blocs élémentaires d'un éventuel ordinateur quantique, nous étudions actuellement la physique de plusieurs boîtes de ce genre couplées entre elles, une physique très similaire à celle d'anciens problèmes encore ouverts tels que le modèle Kondo multi-impureté, multicanal. Des variantes de cette boîte où l'on aurait remplacé les fermions de Majorana par des parafermions seraient aussi particulièrement intéressantes, y compris d'un point de vue purement mathématique[298]. L'effet des fermions de Majorana peut être compris comme un changement de statistiques des porteurs de charge. Parafermions et anyons affecteraient par conséquent fortement les propriétés de transport de la boîte.

Appendix B

Brief summary of abbreviations

- B(C)F: Bipartite (Charge) Fluctuations: see 2.3.2
- BZ: Brillouin Zone: see Appendix D.1.
- ES: Entanglement spectrum: see Section 2.2
- LL: Luttinger Liquids: see Appendix E
- MCKM: Multichannel Kondo model: see Section 5.4
- OBC: Open Boundary Conditions: the system is taken to be open, *i.e.* it has boundaries at which it stops.
- PBC: Periodic Boundary Conditions: the system is taken to be periodic.
- QBM: Quantum Brownian Motion: see Section 5.3.1
- QCP: Quantum Critical Point: point in parameter space where a phase transition occurs.
- QPT: Quantum Phase Transition: (sudden) change in the long-range properties of the ground state of a quantum system.
- RG: Renormalization Group: see Appendix E.3
- TKM: Topological Kondo Model: see Section 5.3.2
- vNEE: von Neumann Entanglement Entropy: see Section 2.1

Appendix C

Brief summary on Hilbert-Sobolev spaces

It is interesting to present an alternate and more complete mathematical point of view on the different terms that arise in the bipartite fluctuations. In this Appendix, we introduce the notion of Hilbert-Sobolev spaces[299], which is the proper mathematical characterization for classifying the different scaling laws and scaling terms in the fluctuations. We define the Hilbert-Sobolev space $H^m(\mathbb{T}^d)$ on the d-dimensional torus as the space of the functions on $\mathbb{T}^d$ such that:

$$f \in H^m(\mathbb{T}^d) \Leftrightarrow \sum_{\vec{n}\in\mathbb{Z}^d} |\mathcal{FT}\{f\}(\vec{n})|^2(1+|\vec{n}|^2)^m < +\infty \tag{C.1}$$

These spaces basically categorize the convergence speed of $|\mathcal{FT}\{f\}(\vec{n})|^2$.
Now, recall the expression of the fluctuations in one and two dimensions. For fluctuations generated by the correlation function f, they are given by:

$$\langle\langle f, f\rangle\rangle_{1D} = l\sum_{n=-l}^{l} |\mathcal{FT}\{f\}(n)|^2 - \sum_{n=-l}^{l} |n||\mathcal{FT}\{f\}(n)|^2 \tag{C.2}$$

$$\begin{aligned}\langle\langle f, f\rangle\rangle_{2D} = l_x l_y \sum_{n_x,n_y} |\mathcal{FT}\{f\}(n_x,n_y)|^2 - l_x \sum_{n_x,n_y} |n_y||\mathcal{FT}\{f\}(n_x,n_y)|^2 \\ - l_y \sum_{n_x,n_y} |n_x||\mathcal{FT}\{f\}(n_x,n_y)|^2 + \sum_{n_x,n_y} |n_x||n_y||\mathcal{FT}\{f\}(n_x,n_y)|^2\end{aligned} \tag{C.3}$$

Classifying the different terms in Eqs. C.2 and C.3 is equivalent to identifying in which space the function f lives.

Starting with the one-dimensional case, the parallel with the Hilbert-Sobolev space definition is immediate. Gapped functions are continuous, and therefore in $H^{\frac{1}{2}}(\mathbb{T})$, while in the gapless case, they belonged to $H^{\frac{1}{2}-\varepsilon}(\mathbb{T})$ for all $\varepsilon > 0$ but not to $H^{\frac{1}{2}}(\mathbb{T})$. This leads to the appearance of a logarithmic term at the gapless points.

A similar classification can be made in two dimensions. For gapped phases, the Green functions that appear in the fluctuations are continuous everywhere, and therefore belong to $H^1(\mathbb{T}^2)$. For such a function f, all four sums in Eq. C.3 therefore converge, and we trivially obtain:

$$\langle\langle f, f\rangle\rangle = i_f l_x l_y + c_x l_x + c_y l_y + \mathcal{O}(1) = i_f A_{\mathcal{A}} + c_f R_{\mathcal{A}} + \mathcal{O}(1), \tag{C.4}$$

where $R_{\mathcal{A}}$ is a characteristic length of the region $\mathcal{A}$ (usually the perimeter). Contribution to c_f can arise both from finite-sum corrections to the first sum, and directly from the second and third summation. It is therefore non-universal.
For gapless Hamiltonians, singularities can appear in the different Green functions at the gap-closing momenta. Let us define the Fermi surface as the manifold $\delta\Gamma = \{\vec{k} \in \mathcal{BZ}, E_{\vec{k}} = 0\}$, where $E_{\vec{k}}$ is the energy of the quasi-particle with momentum $\vec{k}$. Depending on its dimensions and the order of singularities, f will belong to different Hilbert-Sobolev spaces, and therefore the scaling terms will change. For $\delta\Gamma$ of dimension 1 (free fermions for example), Green functions will usually exhibit discontinuities on the one-dimensional manifold. They will therefore belong to $H^{\frac{1}{2}-\varepsilon}(\mathbb{T}^2)$ but not to $H^{\frac{1}{2}}(\mathbb{T}^2)$. This in turn leads to sub-dominant scaling terms such that:

$$\langle\langle f, f\rangle\rangle = i_f A_{\mathcal{A}} + b_f l_{\mathcal{A}} \ln l_{\mathcal{A}} + \mathcal{O}(l_{\mathcal{A}}), \tag{C.5}$$

which have been observed for free fermions[133, 142]. This $l \ln l$ scaling term is also found in the entanglement entropy for such models as was explained in Chapter 2.
For the models we are interested in, $\delta\Gamma$ consists only in a finite number of points. There will only be point-like singularities, that are not always removable. Then the Green functions will belong to $H^{1-\varepsilon}(\mathbb{T}^2)$ but not necessarily to $H^1(\mathbb{T}^2)$. Then the fourth sum may give rise to logarithmic terms such that the scaling laws will be:

$$\langle\langle f, f\rangle\rangle = i_f A_{\mathcal{A}} + c_f R_{\mathcal{A}} + \mathbf{b}_f \ln l_{\mathcal{A}} + \mathcal{O}(1), \tag{C.6}$$

For completeness, we point out that logarithmic terms could appear from the finite-sum corrections of the first three sums. In practice, it is not the case for Dirac fermions.

This classification can be naturally extended to any dimension. In general, a Fermi Surface of dimension d_F in physical dimension d, we expect that the largest logarithmic contribution is of order:

$$l^{d_F-1} \ln l, \tag{C.7}$$

and the relevant correlation functions are in $H^{\frac{d-d_F}{2}-\varepsilon}(\mathbb{T}^d)$ but not $H^{\frac{d-d_F}{2}-\varepsilon}(\mathbb{T}^d)$.

Appendix D

Details on microscopic computations

D.1 Brillouin Zone and reciprocal lattice

We present here a quick definition of the Brillouin Zone (BZ), and how to determine it on an arbitrary two-dimensional lattice. The Brillouin Zone, as we introduce it here, is entirely dependent on the existence of a lattice.
Let us consider a system defined on an arbitrary infinite simple Bravais lattice $\mathcal{L}$ in d-dimensions, such that there exist d vectors $\vec{x}_j$ verifying:

$$\vec{r} \in \mathcal{L} \text{ if and only if } \vec{r} = \sum_{j=1}^{d} n_j \vec{x}_j, \text{ with } n_j \in \mathbb{Z}$$

Each site can consist in a single fermion, as in the case of Kitaev's wire or the $p + ip$ superconductor, or it can include several, as in the graphene or the SSH model. We generically define the unit-cell in order to have this simple structure, and an invariance by translation of the system that leads to a simplification of the computations in momentum space.
We then define the reciprocal lattice by the lattice spanned by the vectors $\vec{k}_j$ that verifies:

$$\vec{x}_j.\vec{k}_{j'} = 2\pi\delta_{j,j'} \tag{D.1}$$

Though there exist several families of such vectors, the lattice they span is unique. The reciprocal lattice $\mathcal{RL}$ has the simple expression:

$$\vec{k} \in \mathcal{RL} \Leftrightarrow \exists(n_1, ...n_d) \in \mathbb{Z}^d,\ \vec{k} = \sum_{j=1}^{d} n_j \vec{k}_j$$

The first Brillouin Zone is then simply the unit-cell of $\mathcal{RL}$ centered in $\vec{0}$, that can also be defined by:

$$\vec{k} \in \mathcal{BZ} \Leftrightarrow ||\vec{k}|| = \min_{\vec{k}_0 \in \mathcal{RL}} ||\vec{k} - \vec{k}_0||$$

The relation D.1 guarantees that

$$V_{\mathcal{BZ}} V_{\mathcal{UC}} = (2\pi)^d,$$

where $V_{\mathcal{BZ}}$ (resp. $V_{\mathcal{UC}}$) is the size of the BZ (resp. of the unit-cell), that is to say the length in one-dimension, area in two dimensions, etc...

For a finite, periodic lattice, the actual definition of the Brillouin Zone may be slightly more complex and it depends on the exact boundaries imposed. It corresponds to the momenta of the previously defined BZ that are compatible with the finite size of the lattice. Assume that there exists a family of vectors $\vec{x}_j$ that spans the real-space lattice, such that

$$\vec{r} \in \mathcal{L} \Leftrightarrow \exists (n_1, ..., n_d) \in \prod_j [0, l_j[\cap \mathbb{Z},\ \vec{r} = \sum_{j=1}^{d} n_j \vec{x}_j$$

and where we identify $\vec{r}$ and $\vec{r} + l_j \vec{x}_j$ (periodic boundary conditions). Then defining $\vec{k}_k$ as previously, we take the Brioullin Zone to be:

$$\vec{k} \in \mathcal{BZ} \Leftrightarrow \exists (n_1, ..., n_d) \in \prod_j [0, l_j[\cap \mathbb{Z},\ \vec{k} = \sum_{j=1}^{d} \frac{n_j - \lfloor \frac{l_j - 1}{2} \rfloor}{l_j}) \vec{k}_j$$

These momenta are the one appearing in the proper finite Fourier transform on the lattice.

We conclude with a few relevant examples:

- One-dimensional lattices.
  The lattice is spanned by the vector $\vec{x}_1 = a$. The corresponding reciprocal vector $\vec{k}_1$ is simply $\frac{2\pi}{a}$, and the lattice is also one-dimensional. The BZ is simply the segment $]-\frac{\pi}{a}, \frac{\pi}{a}]$.

- Rectangular lattices.
  The lattice is spanned by the vector $\vec{x}_1 = a_x(1,0)$ and $\vec{x}_2 = a_y(0,1)$. Then, we take $\vec{k}_1 = \frac{2\pi}{a_x}(1,0)$ and $\vec{k}_2 = \frac{2\pi}{a_y}(0,1)$. The BZ is the square $]-\frac{\pi}{a_x}, \frac{\pi}{a_x}] \times]-\frac{\pi}{a_y}, \frac{\pi}{a_y}]$

- Triangular lattices.
  The triangular lattice appears in this thesis as the Bravais formulation of the honeycomb lattice. As such, it is spanned by the vectors $\vec{x}_1 = a(1,0)$ and $\vec{x}_2 = -a(\frac{1}{2}, \frac{\sqrt{3}}{2})$. The corresponding momenta are $\vec{k}_1 = \frac{2\pi}{a}(1, -\frac{1}{\sqrt{3}})$ and $\vec{k}_2 = \frac{2\pi}{a}(0, -\frac{2}{\sqrt{3}})$. The BZ is a regular hexagon, represented in Figure 1.11.

D.2 Diagonalization and correlation functions of the Rashba nanowires

In this section, we simply expose the main computation steps for diagonalizing the Rashba nanowire model[23, 24], and the expression for the various correlation functions that appear in the computation of the BCF.

The real-space Hamiltonian for the Rashba model for topological superconductor is (summations on j are implicit):

$$H = -\mu c^\dagger_{j,\sigma} c_{j,\sigma} - t(c^\dagger_{j,\sigma} c_{j+1,\sigma} + h.c.) + V c^\dagger_{j,\alpha} \sigma^z_{\alpha,\beta} c_{j,\beta} \\ - i\lambda(c^\dagger_{j,\alpha} \sigma^y_{\alpha,\beta} c_{j+1,\beta} + h.c.) + \Delta(c^\dagger_{j,\uparrow} c^\dagger_{j,\downarrow} + c_{j,\downarrow} c_{j,\uparrow}), \quad \text{(D.2)}$$

where c are spin-$\frac{1}{2}$ fermionic annihilation operator, μ is a chemical potential, t a hopping term, V a Zeeman field, λ a Rashba spin-orbit coupling and Δ a s-wave pairing obtained by proximity.
The model can be exactly diagonalized in the Nambu basis $\Psi_k = (c_{k,\uparrow}, c_{k,\downarrow}, c^\dagger_{-k,\downarrow}, c^\dagger_{-k,\uparrow})^T$. In this basis, the Hamiltonian can be rewritten as:

$$H = \sum_k \Psi^\dagger_k h(k) \Psi_k$$

with

$$h(k) = \begin{pmatrix} \varepsilon(k) + V & -i\varepsilon_2(k) & \Delta & 0 \\ i\varepsilon_2(k) & \varepsilon(k) - V & 0 & -\Delta \\ \Delta & 0 & -\varepsilon(k) + V & -i\varepsilon_2(k) \\ 0 & -\Delta & i\varepsilon_2(k) & -\varepsilon(k) - V \end{pmatrix}, \quad \text{(D.3)}$$

with $\varepsilon(k) = -\mu - 2t\cos(k)$ and $\varepsilon_2(k) = 2\lambda\sin(k)$. Defining the Pauli matrices,

$$\tau_z = \begin{pmatrix} \mathbb{I}_2 & 0_2 \\ 0_2 & -\mathbb{I}_2 \end{pmatrix}, \qquad \tau^x = \begin{pmatrix} 0_2 & \mathbb{I}_2 \\ \mathbb{I}_2 & 0_2 \end{pmatrix}, \qquad \sigma^z = \begin{pmatrix} \sigma^z & 0_2 \\ 0_2 & \sigma^z \end{pmatrix}$$

the system is diagonalized by:

$$e^{-i\frac{\gamma_+}{2}R_+} e^{-i\frac{\gamma_-}{2}R_-} e^{i\frac{\beta}{2}\tau^y\sigma^z} e^{-i\frac{\alpha}{2}\sigma^x} h(k) e^{i\frac{\alpha}{2}\sigma^x} e^{-i\frac{\beta}{2}\tau^y\sigma^z} e^{i\frac{\gamma_+}{2}R_+} e^{i\frac{\gamma_-}{2}R_-} \\ = \begin{pmatrix} E_+ & 0 & 0 & 0 \\ 0 & E_- & 0 & 0 \\ 0 & 0 & -E_- & 0 \\ 0 & 0 & 0 & -E_+ \end{pmatrix}, \quad \text{(D.4)}$$

where the energy spectrum is given by:

$$E^2_\pm = \Delta^2 + \varepsilon(k)^2 + \varepsilon_2^2(k) + V^2 \pm 2\sqrt{V^2\varepsilon(k)^2 + \varepsilon(k)^2\varepsilon_2(k)^2 + \Delta^2 V^2}, \quad \text{(D.5)}$$

the diagonalizing angles by: and the two rotation matrix by:

$$X_+ = \begin{pmatrix} 0 & 0 & 0 & 1 \\ 0 & 0 & 0 & 0 \\ 0 & 0 & 0 & 0 \\ 1 & 0 & 0 & 0 \end{pmatrix}, \qquad X_- = \begin{pmatrix} 0 & 0 & 0 & 0 \\ 0 & 0 & 1 & 0 \\ 0 & 1 & 0 & 0 \\ 0 & 0 & 0 & 0 \end{pmatrix}.$$

We can express the original fermion in the Bogoliubov basis:

$$\begin{pmatrix} c_{k,\uparrow} \\ c_{k,\downarrow} \\ c^\dagger_{-k,\downarrow} \\ c^\dagger_{-k,\downarrow} \end{pmatrix} = e^{i\frac{\alpha}{2}\sigma^x} e^{-i\frac{\beta}{2}\tau^y\sigma^z} e^{i\frac{\gamma_+}{2}R_+} e^{i\frac{\gamma_-}{2}R_-} \begin{pmatrix} \eta_{k,+} \\ \eta_{k,-} \\ \eta^\dagger_{-k,-} \\ \eta^\dagger_{-k,+} \end{pmatrix}, \quad \text{(D.6)}$$

such that $H = E_{k,+}\eta^\dagger_{k,+}\eta_{k,+} + E_{k,-}\eta^\dagger_{k,-}\eta_{k,-}$. Computation of the relevant two-fermions correlator in the ground state is straightforward, albeit tedious.

$$\langle c^\dagger_{k,\uparrow} c_{q,\uparrow}\rangle = \frac{1}{4}\delta_{k,q}\,(2 - \cos(\beta)(\cos(\gamma_+) + \cos(\gamma_-)) \\ + \cos(\alpha)\,(\cos(\gamma_-) - \cos(\gamma_+)) + \sin(\alpha)\sin(\beta)(\sin(\gamma_+) + \sin(\gamma_-)))$$

$$\langle c^\dagger_{k,\downarrow} c_{q,\downarrow}\rangle = \frac{1}{4}\delta_{k,q}\,((2 - \cos(\beta)(\cos(\gamma_+) + \cos(\gamma_-)) \\ + \cos(\alpha)\,(\cos(\gamma_+) - \cos(\gamma_-)) - \sin(\alpha)\sin(\beta)(\sin(\gamma_+) + \sin(\gamma_-)))$$

$$\langle c^\dagger_{k,\uparrow} c^\dagger_{q,\uparrow}\rangle = \frac{-i}{4}\delta_{k,-q}\,(\cos(\beta)(\sin(\gamma_-) + \sin(\gamma_+)) \\ + \cos(\alpha)\,(\sin(\gamma_+) + \sin(\gamma_-)) + \sin(\alpha)\sin(\beta)(\cos(\gamma_-) + \cos(\gamma_+)))$$

$$\langle c^\dagger_{k,\downarrow} c^\dagger_{q,\downarrow}\rangle = \frac{-i}{4}\delta_{k,-q}\,(\cos(\beta)(\sin(\gamma_-) + \sin(\gamma_+)) \\ + \cos(\alpha)\,(\sin(\gamma_-) - \sin(\gamma_+)) - \sin(\alpha)\sin(\beta)(\cos(\gamma_-) + \cos(\gamma_+)))$$

$$\langle c^\dagger_{k,\uparrow} c_{q,\downarrow}\rangle = \frac{-i}{4}\delta_{k,q}\,(\cos(\alpha)\sin(\beta)(\sin(\gamma_-) + \sin(\gamma_+)) + \sin(\alpha)(\cos(\gamma_+) - \cos(\gamma_-)))$$

$$\langle c^\dagger_{k,\uparrow} c^\dagger_{q,\downarrow}\rangle = -\frac{1}{4}\delta_{k,-q}\,(\cos(\alpha)\sin(\beta)(\cos(\gamma_+) + \cos(\gamma_-)))$$

The BCF for the different charges can be safely computed using Wick's theorem and the previous expressions. We focus on the topological transition that occur for $-2t < \mu < 0$ and $V = \sqrt{\Delta^2 + (\mu + 2t)^2}$. For large Zeeman field, the system is in a topological phase, while it is a trivial superconductor at low V. None of the angles gives a good winding number, but a discontinuity at $k = 0$ appear in γ_- at the phase transition, marking the topological change.

D.3 Schrieffer-Wolff transformation in Kitaev's ladder

In this Section, we present the main ideas behind the Schrieffer-Wolff transformation, and details on the computation for the Kitaev's ladder in Section 4.3.4. We refer the readers to Ref. [200] for a complete and detailed review.

The Schrieffer-Wolff transformation is nothing but a variant around degenerate perturbation theory. Given an Hamiltonian H_0 with a degenerate low-energy subspace $\mathbb{E}_0$, and a small perturbation V, such that $||V|| \ll \Delta E$, where ΔE is the gap in energy between $\mathbb{E}_0$ and the next energy subspace, one can derive a systematic expansion of an effective

Hamiltonian that will act only on $\mathbb{E}_0$.
This effective Hamiltonian is given, at second order in V, by:

$$H_{\text{eff}} = P_0 H_0 + V P_0 - \frac{1}{2} \sum_{|n\rangle,|m\rangle \in \mathbb{E}_0} \sum_{|l\rangle \notin \mathbb{E}_0} \left(\frac{1}{E_l - E_m} + \frac{1}{E_l - E_n} \right) \langle n|V|l\rangle \langle l|V|m\rangle \, |n\rangle \langle m| \,, \tag{D.7}$$

where the vectors $\{|n\rangle\}$ form an orthogonal eigenbasis of H_0 with eigenvalue E_n, and P_0 is the projector on $\mathbb{E}_0$.

Now we can apply this method to the Kitaev's ladder of Chapter 4. We take as H_0 the interacting term

$$g \sum_j (n_{j,1} - \frac{1}{2})(n_{j,2} - \frac{1}{2}),$$

and consider the rest of the Hamiltonian to be a small perturbation.
Let us start with $g > 0$, $g \gg t, \Delta\mu$. Then the low-energy subspace E_0 is spanned by the local vectors

$$|+\rangle_j = c^\dagger_{j,1} |0\rangle_c \text{ and } |-\rangle_j = c^\dagger_{j,2} |0\rangle_c \,. \tag{D.8}$$

For the many-body states, our convention is to take the c operators by ascending order of sites. All states generated by this basis have an energy $-\frac{g}{4}$. The first order correction $P_0 H_{\mathcal{K}} P_0$ vanishes. The second order correction can be straightforwardly extracted. The contribution of the tunnel terms is:

$$\begin{aligned} H_{\text{eff},t} = -\frac{t^2}{2g} \sum_j & |+\rangle_j |-\rangle_{j+1} \langle +|_j \langle -|_{j+1} + |-\rangle_j |+\rangle_{j+1} \langle -|_j \langle +|_{j+1} \\ & - |-\rangle_j |+\rangle_{j+1} \langle +|_j \langle -|_{j+1} - |+\rangle_j |-\rangle_{j+1} \langle -|_j \langle +|_{j+1}) \end{aligned} \tag{D.9}$$

The contribution of the pairing terms is:

$$\begin{aligned} H_{\text{eff},d} = \frac{\Delta^2}{2g} \sum_j & |+\rangle_j |+\rangle_{j+1} \langle +|_j \langle +|_{j+1} + |-\rangle_j |-\rangle_{j+1} \langle -|_j \langle -|_{j+1} \\ & + |+\rangle_j |+\rangle_{j+1} \langle -|_j \langle -|_{j+1} + |-\rangle_j |-\rangle_{j+1} \langle +|_j \langle +|_{j+1}) \end{aligned} \tag{D.10}$$

The chemical potential is a constant on $\mathbb{E}_0$ and can be ignored. Then, we can point out the following correspondence (it is a true operator equality when restraining ourselves to $\mathbb{E}_0$):

$$\begin{aligned} |+\rangle \langle +| &= \frac{1+\sigma^z}{2} \\ |-\rangle \langle -| &= \frac{1-\sigma^z}{2} \end{aligned}$$

$$\begin{aligned} |+\rangle_j |-\rangle_{j+1} \langle -|_j \langle +|_{j+1} + |-\rangle_j |+\rangle_{j+1} \langle +|_j \langle -|_{j+1} &= \frac{1}{2}(\sigma^x_j \sigma^x_{j+1} + \sigma^y_j \sigma^y_{j+1}) \\ |+\rangle_j |+\rangle_{j+1} \langle -|_j \langle -|_{j+1} + |-\rangle_j |-\rangle_{j+1} \langle +|_j \langle +|_{j+1} &= \frac{1}{2}(\sigma^x_j \sigma^x_{j+1} - \sigma^y_j \sigma^y_{j+1}) \end{aligned}$$

to obtain, up to constant terms:

$$H_{\text{eff},g+} = \frac{t^2-\Delta^2}{g}\sum_j \sigma_j^z\sigma_{j+1}^z + \frac{t^2+\Delta^2}{g}\sum_j \sigma_j^y\sigma_{j+1}^y + \frac{t^2-\Delta^2}{g}\sum_j \sigma_j^x\sigma_{j+1}^x \tag{D.11}$$

The same approach can be used for $g<0$. The local energy subspace is now given by:

$$|+\rangle_j = c_{j,1}^\dagger c_{j,2}^\dagger |0\rangle_c \text{ and } |-\rangle_j = |0\rangle_c\,, \tag{D.12}$$

with the same convention for the low-energy subspace. Defining the operators,

$$\begin{aligned}
\mathfrak{s}_j^z &= c_{j,1}^\dagger c_{j,1} + c_{j,2}^\dagger c_{j,2} - 1\\
\mathfrak{s}_j^x &= c_{j,1}^\dagger c_{j,2}^\dagger + c_{j,2}c_{j,1}\\
\mathfrak{s}_j^y &= i(c_{j,2}c_{j,1} - c_{j,1}^\dagger c_{j,2}^\dagger).
\end{aligned}$$

we can similarly derive an effective Hamiltonian. The main difference is that the chemical potential now has a non-trivial effect at first order in perturbation, such that:

$$H_{\text{eff},g-} = \frac{t^2-\Delta^2}{|g|}\sum_j \mathfrak{s}_j^z\mathfrak{s}_{j+1}^z - \frac{t^2+\Delta^2}{|g|}\sum_j \mathfrak{s}_j^y\mathfrak{s}_{j+1}^y + \frac{\Delta^2-t^2}{|g|}\sum_j \mathfrak{s}_j^x\mathfrak{s}_{j+1}^x - \mu\sum_j \mathfrak{s}_j^z. \tag{D.13}$$

Appendix E

Luttinger liquids, bosonization and RG

E.1 Basics of Luttinger Liquids theory

Luttinger Liquids theory was developed to treat perturbatively interacting fermionic problems in one dimension. It relies in the equivalence between density and spin wave excitations in these models and some bosonic models. It will be of use to us when defining fluctuations in the standard charge conserving model in Section 2.3.3. We will also use the formalism throughout Chapters 4 and 5, as it is a convenient way to address interacting models, and compute transport properties. This section is meant to be a quick cheat sheet for bosonization. We also refer to [129–131] for an in-depth introduction to abelian bosonization in condensed matter physics. We follow the conventions of the latter reference.

Formally, we consider fermionic systems whose kinetic energy is a linear function of the momenta, such as the kinetic part of the Hamiltonian is given by:

$$v_f|k - k_f|c_k^\dagger c_k. \tag{E.1}$$

Free fermions on a lattice can be expressed in this form by linearizing the hopping terms close to the Fermi momenta $\pm k_F = \pm \arccos \frac{\mu}{2t}$ as long as $\mu \ll 2t$. The fermions are then separated in two "subspecies", the left moving part with momenta close to $-k_F$ noted c_L and the right moving part (momenta close to k_F) noted c_R.

$$c_j = e^{ik_F j} c_{R,j} + e^{-ik_F j} c_{L,j}. \tag{E.2}$$

We then introduce two real bosonic fields, conjugate to each other. They therefore verify the commutation relations:

$$[\phi(x), \theta(x')] = i\frac{\pi}{2}\mathrm{sgn}(x' - x) \quad \text{and} \quad [\phi(x), \phi(x')] = [\theta(x), \theta(x')] = 0. \tag{E.3}$$

Finally, to ensure commutation relations between different species of fermions, and to take care of potential change in the number of fermions, we introduce ladder operators U_R and

U_L that decrease the number of right- or left-moving fermions. In the thermodynamic limit, these operators can safely be replaced by Majorana operators that verify.

$$\{U_r, U_{r'}^\dagger\} = 2\delta_{r,r'} \quad \text{and} \quad \{U_r, U_{r'}\} = \{U_r^\dagger, U_{r'}^\dagger\} = 0. \tag{E.4}$$

The well-known mapping between the fermions and the bosonic fields is given, in the thermodynamic limit, by:

$$c_{R,j} = \frac{U_{R,\sigma}}{\sqrt{2\pi\alpha}} e^{-i(\phi_{j,\sigma}-\theta_{j,\sigma})} \quad \text{and } c_{L,j} = \frac{U_{L,\sigma}}{\sqrt{2\pi\alpha}} e^{i(\phi_{j,\sigma}+\theta_{j,\sigma})}, \tag{E.5}$$

where α is cut-off distance that corresponds to the lattice spacing. The bosonic LL theory will be treated as a continuum theory and a cut-off is required to avoid unphysical divergences.

The Hamiltonian in the continuum theory can be expressed in terms of the linearized fermions:

$$-iv_F \int dx \left(c_{R,\sigma}^\dagger(x)\partial_x c_{R,\sigma}(x) - c_{L,\sigma}^\dagger(x)\partial_x c_{L,\sigma}(x) \right), \tag{E.6}$$

where $v_F = 2t\alpha \sin(k_F)$ is the Fermi velocity. It leads to the final expression in terms of the bosonic fields:

$$H_0 = \int dx \frac{v_F}{2\pi} ((\partial_x\theta_\sigma)^2 + (\partial_x\phi_\sigma)^2) \tag{E.7}$$

The Hamiltonian H_0 is the basic form of a bosonized Hamiltonian. As will be further detailed in Chapter 4 and Appendix E.3.4, interacting terms can be treated in the same way. The supplementary interacting terms are replaced by a corresponding expression in terms of ϕ and θ. Without entering into details for now, weak interactions that do not affect the nature of the gapless phase lead to an effective Hamiltonian given by:

$$H_{LL} = \int dx \frac{v_F}{2\pi} (K(\partial_x\theta)^2 + \frac{1}{K}(\partial_x\phi)^2), \tag{E.8}$$

where K is the so-called Luttinger parameter that quantify the strength of the interactions. For non-interacting systems, $K = 1$, for repulsive interactions, $K < 1$ and for attractive interactions $K > 1$.

E.2 Bipartite charge fluctuations of a critical $c = m$ bosonic model

Let us consider a n-channel fermionic wire. Let $(\phi_p, \theta_p)_{1\leq p\leq n}$ be the corresponding modes obtained by bosonization [131]. Suppose that the critical model of the wire is characterized by a central charge $c = m$, with m integer, and that we can find m independent real bosonic modes $(\phi_\alpha, \theta_\alpha)_{1\leq\alpha\leq m}$, linear combination of (ϕ_p, θ_p), whose effective Hamiltonian is free. The $n-m$ other orthogonal modes are of course necessarily gapped. Then, the logarithmic contribution to the bipartite charge fluctuations in any of the p-channel is positive and can be expressed in terms of the Luttinger parameters of the α modes. We present a quick proof for $n = 2$ and $m = 1$. The generalization, if fastidious, is self-explanatory.
Let (ϕ_1, θ_1) and (ϕ_2, θ_2) be the "good" bosonic modes to describe the system, with (ϕ_1, θ_1)

free while (ϕ_2, θ_2) is gapped in ϕ_2. Let $F_1(l)$ and $F_2(l)$ be their bipartite charge fluctuations. The typical Hamiltonian, closed to the fixed point, will be given by $H_c = H_1 + H_2$, with:

$$H_1 = \frac{v_{F,1}}{2\pi} \int \frac{1}{K_1} (\nabla \phi_1)^2 + K_1 (\nabla \theta_1)^2$$

$$H_2 = \frac{v_{F,2}}{2\pi} \int \frac{1}{K_2} (\nabla \phi_2)^2 + K_2 (\nabla \theta_2)^2 + g \cos(\alpha \phi_2)$$

with K_2, g and α such that $g\cos(\alpha\phi_2)$ is a relevant term that is flowing to strong coupling. A standard computation[131] gives:

$$\begin{aligned}
\langle e^{i\phi_1(l)} e^{-i\phi_1(0)} \rangle &\approx e^{-\frac{K_1}{2} C(l)} \\
\langle e^{i\theta_1(l)} e^{-i\theta_1(0)} \rangle &\approx e^{-\frac{K_1^{-1}}{2} C(l)} \\
\langle (\phi_2(l) - \phi_2(0))^2 \rangle &= O(1) \\
\langle e^{i\theta_2(l)} e^{-i\theta_2(0)} \rangle &\approx e^{-\tilde{\Delta} l}
\end{aligned}$$

with $\tilde{\Delta}$ a non-universal quantity corresponding to the gap of the system, and C a function defined by[131]:

$$C(l) = \frac{1}{2} \log \left(\frac{l^2 + \alpha^2}{\alpha^2} \right).$$

α is a short distance cut-off. Other correlators are zero at the fixed RG point. Using the following equality $\langle e^{i\phi(l)} e^{-i\phi(0)} \rangle = e^{-1/2 \langle (\phi(l) - \phi(0))^2 \rangle}$, valid for Gaussian modes, one can obtain F_1 and F_2. Consequently, $F_1(l)$ scale logarithmically with the length of A, while F_2 is globally constant.

Now let $(\phi_{a/b}, \theta_{a/b})$ be two bosonic modes whose charge fluctuations $\mathcal{F}_{a/b}$ we can actually access. Assume there exists a unitary hermitian transform mapping the "good" modes to those measured. Let $\phi_{a/b} = \sum_i u_{i,a/b} \phi_i + v_{i,a/b} \theta_i$. One can easily express $\mathcal{F}_{a/b}$ as a sum of correlators of $\phi_{1/2}$ and $\theta_{1/2}$. We introduce the quantity $\mathcal{J}_i(l) = \frac{1}{\pi^2} \langle (\theta_i(l) - \theta_i(0))^2 \rangle$. $\mathcal{J}_i$ is the analogous of $\mathcal{F}_i$, replacing the field ϕ by its conjugate θ. It corresponds to the bipartite current fluctuations. It has similar properties. As all cross-correlators cancel close to the Renormalization Group fixed point, we obtain

$$\mathcal{F}_{a/b}(l_{\mathcal{A}}) = \sum_i u_{i,a/b}^2 F_i + v_{i,a/b}^2 J_i$$

$$\mathcal{F}_{a/b}(l_{\mathcal{A}}) = (u_{1,a/b}^2 \frac{K_1}{\pi^2} + v_{1,a/b}^2 \frac{K_1^{-1}}{\pi^2}) \log l + v_{2,a/b}^2 \tilde{\Delta} l + \mathcal{O}(1).$$

As all present bosonic modes are real, all coefficients must also be real. As the transformations must be invertible, $u_{1,a/b}$ and $v_{1,a/b}$ cannot be all zeros.

Then, there is a logarithmic contribution in at least one of the two observed channels and it must be positive.

Instead of considering the field (ϕ_2, θ_2) gapped in ϕ_2, one can also gap the mode by fixing θ_2. The role of $\mathcal{F}_2$ and $\mathcal{J}_2$ is then inverted and our conclusion is still valid.

E.3 RG analysis in bosonized theories

In this Section, we give an overview of the renormalization group procedure, and, through a simple example, we give the tools for deriving the RG equations in Luttinger Liquids.

E.3.1 Overview

The main idea behind renormalization is the idea of scaling: if we consider a system in the thermodynamic limit, we are interested in its long-range properties and behavior. The details of what happens at very small scale are not necessarily relevant to the long-range physics. To abstract ourselves of these details, instead of considering what happens at a length scale α, we could consider a minimal length scale $\alpha' = \alpha e^l$ with $l > 0$. One can then integrate out all the degrees of freedom at a scale smaller than α', in order to get a potentially simpler Hamiltonian. A simple lattice based example is:

Initial model	$\rightarrow$ Length scale separation	$\rightarrow$ Large scale effective Hamiltonian
$H(1) = \sum_{j\in L} H_j$	$\sum_{j\in\frac{L}{3}}\sum_{x=1}^{3} H_{3j+x}$	$H(3) = \sum_{j\in\frac{L}{3}} \tilde{H}_j$

In this example, we change our length scale by a factor of 3. Then we (usually) reduce the Hamiltonian $\tilde{H}_j$ by keeping only the relevant low-energy states and discarding the others, such that the dimension of its Hilbert space is the same as H_j's. By iterating this procedure, we establish effective differential equations in Hamiltonians' space as a function of the RG length l, and try to compute their limit when $l \rightarrow +\infty$. In practice, we identify a set of relevant operators that compose the Hamiltonians, and derive differential equations on their coefficients.

This approach can be generalized to other type of systems, but also other type of cut-off: one can proceed to a similar renormalization scheme in momentum space or frequency space by integrating out large momenta (which correspond to small distances). In this thesis, we will mostly focus on real space and imaginary time renormalization.

E.3.2 Derivation for the sine-Gordon model

The staple model to study how RG behaves in Luttinger Liquids is the sine-Gordon model[130, 131] described by the Hamiltonian:

$$H_{SG} = \frac{v_f}{2\pi}\iint dxd\tau \frac{1}{K}(\partial_x\phi)^2 + K(\partial_x\theta)^2 + \frac{g}{\alpha^2}\iint dxd\tau \cos(a\phi) \tag{E.9}$$

There are several ways to derive the RG equations of such a model. Following the method in Ref. [131], we derive the value of an arbitrary correlator at second order in g, neglecting the renormalization of the Fermi speed. We note $\langle ... \rangle_{\tilde{g}}$ the average taken in the ground state of Eq. E.9 with $g = \tilde{g}$. We note $\vec{r} = (x, \tau)$ the coordinate in real space and imaginary

time.

$$\langle e^{ib\phi(\vec{r}_1)}e^{-ib\phi(\vec{r}_2)}\rangle_g = \langle e^{ib\phi(\vec{r}_1)}e^{-ib\phi(\vec{r}_2)}\rangle_0 + \frac{g^2}{8v_F^2}\sum_{\varepsilon_1,\varepsilon_2=\pm 1}\int d\vec{r}d\vec{r}'\langle e^{ib\phi(\vec{r}_1)}e^{-ib\phi(\vec{r}_2)}e^{ia\varepsilon_1\phi(\vec{r})}e^{a\varepsilon_2\phi(\vec{r}_2)}\rangle_{c,0} \quad \text{(E.10)}$$

Then one can use the standard result from the Gaussian theory to compute the previous correlator:

$$\langle\prod_j e^{i\sum_j A_j\phi(\vec{r}_j)+B_j\theta(\vec{r}_j)}\rangle_0 = \delta_{\sum_j A_j=\sum_j B_j=0} e^{\frac{1}{2}\sum_{j<j'}(A_jA_{j'}K+B_jB_{j'}K^{-1})F_1(\vec{r}_j-\vec{r}_{j'})-(A_jB_{j'}+B_jA_{j'})F_2(\vec{r}_j-\vec{r}_{j'})}, \quad \text{(E.11)}$$

with F_1 and F_2 the functions

$$F_1(x,\tau) = \frac{1}{2}\log(\frac{x^2+(v_f|\tau|+\alpha)^2}{\alpha^2}) \text{ and } F_2(x,\tau) = -i\text{Arg}(v_f\tau+\alpha\text{sign}(\tau)+ix). \quad \text{(E.12)}$$

After some lengthy computations, in the limit $||\vec{r}_1-\vec{r}_2|| \gg \alpha$, one obtains:

$$\langle e^{ib\phi(\vec{r}_1)}e^{-ib\phi(\vec{r}_2)}\rangle_g = e^{-\frac{b^2K}{2}F_1(\vec{r}_1-\vec{r}_2)}\left(1+\frac{\pi K^2a^2b^2g^2}{16v_F^2\alpha^4}\int_{r>\alpha} d^2r^2e^{-\frac{a^2K}{2}F_1(r)}\right). \quad \text{(E.13)}$$

This form can be interpreted as an expansion of the exponential $e^{-\frac{b^2K}{2}F_1(\vec{r}_1-\vec{r}_2)}$, *i.e.* the correlator at $g=0$, with an effective Luttinger parameter given by:

$$K_{\text{eff}} = K - \frac{g^2\pi^2a^2K^2}{4v_F^2}\int_\alpha^\infty \frac{dr}{\alpha}\left(\frac{r}{\alpha}\right)^{3-\frac{a^2K}{2}} \quad \text{(E.14)}$$

From this expression, we can apply the RG procedure. The effective Luttinger parameter should be left invariant by a change in the cut-off of the integral, as it governs the long range properties of the system. Let $\alpha' = \alpha + d\alpha$, changing the integral cut-off leads to:

$$K_{\text{eff}} = K - \frac{g^2\pi^2a^2K^2}{4v_F^2}\frac{d\alpha}{\alpha} - \frac{g^2\pi^2a^2K^2}{4v_F^2}\int_{\alpha'}^\infty \frac{dr}{\alpha}\left(\frac{r}{\alpha}\right)^{3-\frac{a^2K}{2}}. \quad \text{(E.15)}$$

To absorb the change, one can redefine

$$K(\alpha') = K(\alpha) - \frac{g^2\pi^2a^2K^2}{4v_F^2}\frac{d\alpha}{\alpha} \quad \text{(E.16)}$$

$$g(\alpha')^2 = g(\alpha)^2\left(\frac{\alpha'}{\alpha}\right)^{4-\frac{a^2K}{2}} \quad \text{(E.17)}$$

Finally, we parametrize the cut-off evolution such that $\alpha' = \alpha e^l$, which leads to the celebrate equations:

$$\frac{dg}{dl} = (2 - \frac{|a|^2}{4}K)g \tag{E.18}$$

$$\frac{dK}{dl} = -\frac{g^2\pi^2a^2}{4v_F^2}K^2 \tag{E.19}$$

We see that, in the presence of a cosine term, typically generated by interactions, both the Luttinger parameter and g are renormalized. $\frac{|a|^2}{4}K$ is the (RG) dimension of the operator $\iint dxd\tau \cos(a\phi)$. Defining $D = \frac{a^2}{4}K$ the dimension and $\tilde{g} = \frac{g\pi}{v_F}$ the renormalized coefficient, the equations take the simple, universal form:

$$\frac{d\tilde{g}}{dl} = (2 - D)\tilde{g} \tag{E.20}$$

$$\frac{dD}{dl} = -\tilde{g}^2D^2 \tag{E.21}$$

The flow of these equations is depicted and analysed in Figure E.1. We call bare values the initial values in the original Hamiltonian of the different parameters. Starting from an infinitesimal $\tilde{g}$, one can distinguish two cases: if $D > 2$, the dimension of the operator is larger than the critical dimension $D_c = 2$, and is therefore renormalized to 0. The operator is said to be irrelevant, and in the thermodynamic limits, the Hamiltonian is equivalent to one with $\tilde{g} = 0$, with some (weakly) renormalized Luttinger parameter. If $D < D_c$, then the operator is relevant, and $\tilde{g}$ is renormalized to ∞. To obtain the ground state of the Hamiltonian, one therefore has to minimize $\tilde{g}\cos a\phi$. For $g > 0$, $\phi(x,\tau) = \frac{\pi}{a}$ $[\frac{2\pi}{a}]$: the ϕ field becomes a constant. We say it is pinned. Due to the commutation relation with θ, the θ field wildly fluctuates. Finally, the system is gapped as one has to break the cosine term to obtain an excited state.
The case of an operator $\cos a\theta$ can be simply obtained by replacing K by K^{-1}.

E.3.3 Beyond the simple sine-Gordon model

To take into account several (competing) cosine and sine operators, one has to be more careful: operators can feed and help generate others at higher order in the perturbation. In a formally correct renormalization procedure, one needs to work with a closed family of operators, such as no new operators appear. In practice, we can usually discard the strongly irrelevant terms. We will treat three simple examples to illustrate the mechanisms involved and how to obtain the RG equations.

- A single operator can generate higher-order terms. In fact, our previous analysis was not absolutely complete: an operator $\cos(a\phi)$ is going to generate all higher-order harmonics in the RG procedure. Indeed, if $\alpha < |x-y| < \alpha'$, the product $\cos(a\phi(x))\cos(a\phi(y))$ is no longer separable after the rescaling, and it will contribute to the appearance of an effective operator $\cos(2a\phi(x))$. To derive the RG equations in such a case, one formally has to add this operator from scratch (with a coefficient g_2) and compute the third order terms:

$$\frac{g^2g_2}{\alpha^6}\langle e^{ia(\phi(x)+\phi(y)-2\phi(z))}\rangle_0 = \frac{g^2g^{(2)}}{\alpha^6}e^{\frac{a^2}{2}(F_1(x-y)-2F_1(x-z)-2F_1(y-z))}, \tag{E.22}$$

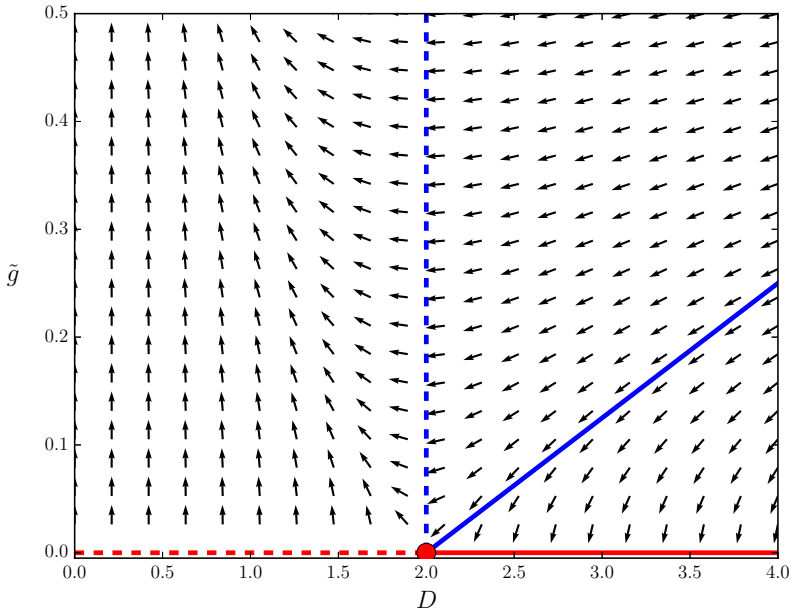

Figure E.1: Normalized flow of Eqs. E.20. The continuous red line marks the continuum of fixed points with $D \geq 2$, where $\tilde{g}$ is renormalized to 0 and the bosons are free. The discontunous red line marks the unstable non-interacting fixed points. The blue line is the separatrix and the horizontal black line marks the critical dimension $D_c = 2$. When the bare values of $\tilde{g}$ and D are below the separatrix, $\tilde{g}$, the cosine operator is irrelevant and renormalized to 0. When the bare values are on the left of the vertical discontinuous blue line, the cosine is relevant and $\tilde{g}$ is therefore renormalized to $+\infty$. The boson is then gapped and the field ϕ pinned to the minima of $\cos a\phi$. Finally, the region between the separatrix and the horizontal line is an intermediate regime where the cosine is irrelevant, but large enough so D is renormalized beyond D_c, which lead to g being, in the end, renormalized to infinity. The system is then gapped.

for $|x-y| < \alpha'$ (and also for $|y-z| < \alpha'$) and comparing it with either $e^{-2a^2 F_1(x-z)}$ (or $e^{-\frac{a^2}{2} F_1(x-z)}$. The RG equations will then be of the form:

$$\frac{dg}{dl} = (2 - \frac{|a|^2}{4}K)g + A_2 g g_2 \tag{E.23}$$

$$\frac{dg_2}{dl} = (2 - |a|^2 K)g_2 + B_2 g^2 \tag{E.24}$$

$$\frac{dK}{dl} = -\left(\frac{g^2\pi^2 a^2}{4v_F^2} + \frac{g_2^2\pi^2 a^2}{v_F^2}\right)K^2 \tag{E.25}$$

The coefficient A_2 and B_2 are (usually non-universal) coefficients obtained from the computation of the correlation functions (in this simple case, $A_2 > 0$ and $B_2 < 0$: the second order term generated by g only should not oppose g). A detailed computation

for the Kondo problem is given in Appendix G. Even though it is not initially present, the g_2 term will be generated by the source term g^2.

- Several independent terms can be present, the seminal example being $\cos a\phi$ and $\cos b\theta$. In such a case, if limiting ourselves to first-loop computations, one can simply treat their contribution separately.

- In a general setting though, if several terms are present, they will lead to the appearance in the RG flow of their product. Following the previous example, one will generate the entire family:

$$\cos(na\phi + mb\theta), \text{ with } n, m \in \mathbb{Z}^2 \tag{E.26}$$

Their RG dimension is simply $\frac{n^2a^2K}{4} + \frac{m^2b^2K^{-1}}{4}$. In this simple example, the more relevant operators are the initial ones, and it will (except at some fine tuning points) be not necessary to include the higher harmonics. On the other hand, if the original operators were $\cos a\phi$ and $\cos(a\phi + b\theta)$, the RG flow would generate the exact same family of operators and one therefore should take into account the generated $\cos b\theta$, more relevant than the original $\cos(a\phi + b\theta)$.

E.3.4 Bosonization of the Kitaev-Hubbard model

In this Section, we derive the bosonized form of the different terms that appear in the Hamiltonian of Section 4.2 and 4.3. We recall that we separate a spinless fermionic operator $c_{j,\sigma}$, j being a site index and σ the wire index, into its left and right components:

$$c_{j,\sigma} = e^{-ik_F j} c_{R,j,\sigma} + e^{ik_F j} c_{L,j,\sigma}, \tag{E.27}$$

with k_F the Fermi momentum (that will be taken to $\frac{\pi}{2}$, i.e. half-filling), that can then be bosonized by introducing the fields $(\phi_\sigma, \theta_\sigma)$ (that depends on j and τ the imaginary time), the four Klein factors $U_{L/R,\sigma}$ (taken to be effective Majorana operators) and α a cut-off length:

$$c_{R,j,\sigma} = \frac{U_{R,\sigma}}{\sqrt{2\pi\alpha}} e^{-i(\phi_{j,\sigma} - \theta_{j,\sigma})} \text{ and } c_{L,j,\sigma} = \frac{U_{L,\sigma}}{\sqrt{2\pi\alpha}} e^{i(\phi_{j,\sigma} + \theta_{j,\sigma})}. \tag{E.28}$$

We also recall the useful Naker-Campbell-Hausdorff(-Zassenhaus) formula. For two operators A and B such that $[A, B]$ commutes with both A and B, then:

$$e^A e^B = e^{A+B} e^{\frac{1}{2}[A,B]}. \tag{E.29}$$

and the definition of the charge and pseudo-spin basis $(+, -)$:

$$\phi_\pm = \frac{1}{\sqrt{2}}(\phi_1 \pm \phi_2) \text{ and } \theta_\pm = \frac{1}{\sqrt{2}}(\theta_1 \pm \theta_2) \tag{E.30}$$

From there, we will sequentially bosonized the different contributions. The hopping term has been treated previously:

$$-t \sum_j c_j^\dagger c_{j+1} + c_{j+1}^\dagger c_j \to \frac{v_F}{2\pi} \iint dx d\tau (\partial_x \phi)^2 + (\partial_x \theta)^2, \text{ with } v_F = 2t \sin(k_F)$$

The chemical potential transforms into:

$$-\mu c^\dagger_{j,\sigma} c_{j,\sigma} = -\mu\rho_0 + \frac{\mu}{\pi}\partial_x\phi_{j,\sigma} - \frac{\mu}{\pi\alpha}\cos(2\phi_{j,\sigma} - 2k_F j)$$

ρ_0 is the average density (a constant we discard). The cosine term is oscillating, and can be discarded. In the $(+,-)$ basis, the expression is simply

$$\mu\frac{\sqrt{2}}{\pi}\partial_x\phi_{j,+} \tag{E.31}$$

The pairing term is given by:

$$\begin{aligned}
\Delta c^\dagger_{j,\sigma} c^\dagger_{j+1,\sigma} + h.c. &= \frac{\Delta}{2\pi\alpha}(U^\dagger_{L,\sigma} e^{-i(\phi_{j,\sigma}+\theta_{j,\sigma}-k_F j)} + U^\dagger_{R,\sigma} e^{i(\phi_{j,\sigma}-\theta_{j,\sigma}-k_F j)}) \\
&\qquad (U^\dagger_{L,\sigma} e^{-i(\phi_{j,\sigma}+\theta_{j,\sigma}-k_F (j+1))} + U^\dagger_{R,\sigma} e^{i(\phi_{j,\sigma}-\theta_{j,\sigma}-k_F (j+1))}) \\
&= \frac{\Delta}{2\pi\alpha}(\left(U^\dagger_{L,\sigma} U^\dagger_{R,\sigma} e^{-2i\theta - ik_F} + U^\dagger_{R,\sigma} U^\dagger_{L,\sigma} e^{-2i\theta + ik_F} + h.c.\right) \\
&\qquad + 2\cos(2\phi_{j,\sigma} - 2\theta_{j,\sigma} - 2k_F j) + 2\cos(2\phi_{j,\sigma} + 2\theta_{j,\sigma} - 2k_F j) \\
&= \frac{\Delta}{2\pi\alpha}(4\sin k_F \cos(2\theta_{j,\sigma}) + 2\cos(2\phi_{j,\sigma} - 2\theta_{j,\sigma} - 2k_F j) \\
&\qquad + 2\cos(2\phi_{j,\sigma} + 2\theta_{j,\sigma} - 2k_F j)),
\end{aligned}$$

where we have taken $U^\dagger_{L,\sigma} U^\dagger_{R,\sigma} = i$ (it is a product of two Majorana fermions that will commute with the Hamiltonian) and neglected higher-order terms. The last two contributions are far less relevant than the first one and are strongly oscillating for $k_F \approx \frac{\pi}{2}$. We consequently discard them. In the $(+,-)$ basis, the pairing contribution is:

$$\frac{4\Delta \sin k_F}{\pi\alpha}\cos\sqrt{2}\theta_+ \cos\sqrt{2}\theta_- \tag{E.32}$$

Finally, the interactions have the traditional Hubbard form $g(n_{j,1} - \frac{1}{2})(n_{j,2} - \frac{1}{2})$. Using the previous expression for the density, we obtain:

$$\begin{aligned}
&g\left(-\frac{1}{\pi}\partial_x\phi_{j,1} + \frac{1}{\pi\alpha}\cos(2\phi_{j,1} - 2k_F j)\right)\left(-\frac{1}{\pi}\partial_x\phi_{j,2} + \frac{1}{\pi\alpha}\cos(2\phi_{j,2} - 2k_F j)\right) \\
&\quad = \frac{g}{\pi^2}\partial_x\phi_{j,1}\partial_x\phi_{j,2} + \frac{g}{\pi^2\alpha^2}\cos(2\phi_{j,1} - 2k_F j)\cos(2\phi_{j,2} - 2k_F j) \\
&\quad = \frac{g}{\pi^2}\partial_x\phi_{j,1}\partial_x\phi_{j,2} + \frac{g}{2\pi^2\alpha^2}\cos(2\phi_{j,1} - 2\phi_{j,2}) + \frac{g}{2\pi^2\alpha^2}\cos(2\phi_{j,1} + 2\phi_{j,2} - 4k_F j)
\end{aligned}$$

In the $(+,-)$ basis, it can be written as:

$$\frac{g}{2\pi^2}\left((\partial_x\phi_{j,+})^2 - (\partial_x\phi_{j,-})^2\right) + \frac{g}{2\pi^2\alpha^2}\cos(2\sqrt{2}\phi_{j,-}) + \frac{g}{2\pi^2\alpha^2}\cos(2\sqrt{2}\phi_{j,+} - 4k_F j) \tag{E.33}$$

We have discarded all the oscillating term except for $\cos(2\sqrt{2}\phi_{j,+} - 4k_F j)$. Close to half-filling, $4k_F \to 2\pi$ and therefore it is actually not oscillating. When moving away from half-filling, oscillations progressively make the cosine irrelevant and will renormalize it to

zero[131]. It is the so-called umklapp term. The first contribution renormalizes the Fermi speeds and the Luttinger parameters, such that:

$$v_{F,\pm} = v_F\sqrt{1 \pm \frac{g}{\pi v_F}} \text{ and } K_\pm = \frac{1}{\sqrt{1 \pm \frac{g}{\pi v_F}}}. \tag{E.34}$$

Finally, given that the pairing induced term is by far more relevant than the other contributions, we need to take into account higher order contributions (only the second order will be relevant). In particular, care has to taken has the second harmonic

$$\begin{aligned}\cos(\sqrt{2}\theta_+(x))\cos(\sqrt{2}\theta_-(x))\cos(\sqrt{2}\theta_+(y))\cos(\sqrt{2}\theta_-(y))\\ = \frac{1}{4}(\cos(\sqrt{2}(\theta_+(x)-\theta_+(y)) + \cos(\sqrt{2}(\theta_+(x)+\theta_+(y)))\\ \times(\cos(\sqrt{2}(\theta_-(x)-\theta_-(y)) + \cos(\sqrt{2}(\theta_-(x)+\theta_-(y)))\end{aligned}$$

In the RG, when $\alpha < x - y < \alpha'$, the terms $\cos(\sqrt{2}(\theta_\pm(x) - \theta_\pm(y))$ can be essentially replaced by $1 + O(\alpha^2)$, which indeed will generate the two terms

$$-\frac{\Delta_\pm^{(2)}}{\alpha^2}\cos(2\sqrt{2}\theta_\pm)$$

The minus sign comes from the change of order in the expansion of the partition function. The exact source term in the RG equations, proportional to $(\Delta^{(1)})^2$, can be obtained with the methods described in the Appendix G. Its exact value is not relevant for our treatment of the problem.

Appendix F

Conformal Theory computations

F.1 Bipartite charge fluctuations for a $c = \frac{1}{2}$ model

We are now interested in computing the charge fluctuations in the case of a $c = \frac{1}{2}$ model. We are interested in proving using CFT arguments that the sign of the logarithmic contribution to the charge fluctuations is negative in such a model. The change in the behavior of these fluctuations comes both from the different underlying critical theory, but also from the difference on how to express the fermionic density in terms of the primary fields. Indeed, the difference will subsist in the case of a $c = 2 \times \frac{1}{2}$ theory. The critical conformal theory of Quantum Ising can be expressed as a theory of a free real (Majorana) fermions ψ. We only consider the point $t = \Delta$ for simplicity, but the analysis stands at all $\Delta \neq 0$.

We can reformulate the Hamiltonian in the following way:

$$H_K = 2it \sum_j \gamma_{j,B}(\gamma_{j+1,A} - \gamma_{j,A}) - i\delta\mu \sum_j \gamma_{j,A}\gamma_{j,B}. \tag{F.1}$$

We first go to continuous limit $\gamma_{j,A/B} \to \sqrt{\alpha}\gamma_{A/B}(x)$, where α is the lattice spacing. Then we introduce two chiral fermions:

$$\gamma_R = \frac{\gamma_B - \gamma_A}{\sqrt{2}}$$
$$\gamma_L = \frac{\gamma_A + \gamma_B}{\sqrt{2}}.$$

Posing $v = 2t\alpha$ and $m = \alpha\delta\mu$, the Hamiltonian of the system is now given by:

$$H_K = \int dx \frac{iv}{2} \left(\gamma_L \partial_x \gamma_L - \gamma_R \partial_x \gamma_R\right) - im\gamma_L\gamma_R. \tag{F.2}$$

m is the mass of the Majorana field. At $m = 0$, one can identify this Hamiltonian with its conformal action counterpart. Introducing $z = \tau + ix$, γ_L and γ_R corresponds to the holomorphic and anti-holomorphic part of the conformal field. The action is given by:

$$S = \varepsilon \int dz d\bar{z} \gamma_L \partial_{\bar{z}} \gamma_L + \gamma_R \partial_z \gamma_R. \tag{F.3}$$

$\varepsilon > 0$ is a normalization factor. It will be fixed to 1 (at least in non-interacting systems) by the correlation functions and commutation relations. The fermionic density operator (i.e the σ^z field for the spins) can be written in terms of primary fields as $i\gamma_L(z)\gamma_R(\bar{z})$, up to constant terms that will disappear because we are interested in the connected correlators. One can consequently rewrite:

$$F_A(l) = -\iint_{[0,l]^2} dxdy \langle \gamma_L(ix)\gamma_R(-ix)\gamma_L(iy)\gamma_R(-iy)\rangle_c \tag{F.4}$$

Using the Operator Product Expansion (OPE)[81, 130] $\gamma_L(z)\gamma_L(w) = \frac{1}{2\pi\varepsilon}\frac{1}{z-w}$ for the Majorana field directly yields the result:

$$\begin{aligned} F_A(l) &= \iint_{[0,l]^2} dxdy \frac{1}{4\pi^2\varepsilon^2}\frac{1}{|x-y|^2} \\ &\approx -\frac{1}{2\pi^2\varepsilon^2}\log l + \alpha l + \beta. \end{aligned} \tag{F.5}$$

The minus sign in front of the logarithmic contribution can be understood from the $(i)^2 = -1$ pre-factor in Eq. (23) stemming from the definition of the (electron) density operator as $i\gamma_L(z)\gamma_R(\bar{z})$. α and β are non-universal constants that arise from the integration, and are linked to the cut-off of our theory. The results coincide with the expression obtained in the microscopic computations for $\varepsilon = 1$. This can be confirmed by the computation of the correlation function corresponding to $i\gamma_L(ix)\gamma_L(iy)$ in the original Bogoliubov particles language. One can show that the coefficient of the leading term corresponding to the OPE expansion of the CFT corresponds indeed to $\varepsilon = 1$ and, moreover, that it does not depend on Δ/t. In Kitaev's wire, the logarithmic contributions to the bipartite charge fluctuations are actually independent from the ratio Δ/t as long as $\Delta \neq 0$.

F.2 Bipartite charge fluctuations for a $c = 1$ boson

For reference, we introduce in a few lines the computations of the logarithmic fluctuations for a free boson, *i.e.* a Luttinger Liquid, using CFT. Without entering into any details, the charge density is now given by:

$$\rho = \rho_0 - \frac{1}{\pi}\partial_x\phi, \tag{F.6}$$

where ϕ is the bosonic field and ρ_0 the average density. The primary fields of the CFT theory are $\partial_z\phi(z)$, with $z = \tau + ix$, and of correlators

$$\partial_z\phi(z)\partial_w\phi(w) = -\frac{1}{4\pi\varepsilon}\frac{1}{(z-w)^2}$$

and therefore the fluctuations are given by:

$$\mathcal{F}_\rho(\mathcal{A}) = \frac{1}{\pi^2} \iint\limits_{[0,l_\mathcal{A}]^2} \langle \partial_x \phi \partial_y \phi \rangle = -\frac{1}{\pi^2} \iint\limits_{[0,l_\mathcal{A}]^2} \langle \partial_z \phi(z) \partial_w \phi(w) \rangle \tag{F.7}$$

$$= -\frac{1}{\pi^2} \frac{1}{4\pi\varepsilon} \iint\limits_{[0,l_\mathcal{A}]^2} \frac{1}{(x-y)^2} \approx \frac{1}{\pi^2} \frac{1}{2\pi\varepsilon} \ln l_\mathcal{A} + ..., \tag{F.8}$$

where we have neglected the non-universal term. ε, the normalization factor, must be fixed using either the correlation functions, or the compressibility[126], but its sign is always positive. In the end, we recover:

$$\mathcal{F}_\rho(\mathcal{A}) = \frac{K}{\pi^2} \ln l_\mathcal{A} \tag{F.9}$$

Appendix G

Topological Kondo model

G.1 RG flow

In this appendix, we recall the main steps of the derivation the RG equations for the M-CKM and the Topological Kondo model. To do so, we use a systematic expansion of the partition function, following Ref. [276].

G.1.1 RG equations for the Topological Kondo model

Weak coupling

Let us start with the easier case of the Topological Kondo model. We first consider the topological Kondo model corresponding to the absence of charge degeneracy. We use the QBM formalism for simplicity. We define the vectors $\vec{w}_j$ such that $\theta_j = \vec{w}_j.\vec{r} + \frac{1}{\sqrt{M}}\Theta$. They verify $\vec{w}_j.\vec{w}_k = \delta_{j,k} - \frac{1}{M}$. Explicit expressions can be found in Section 5.3.1. The action governing the model at weak coupling is

$$S = \sum_{\omega_m} \sum_{j}^{M-1} \frac{|\omega_m| K}{2\pi\beta} |r_j(\omega_m)|^2 - \sum_{j\neq k}^{M,M} \lambda_{j,k} \int_0^\beta \frac{d\tau}{\tau_c} \cos((\vec{w}_j - \vec{w}_k).\vec{r}), \tag{G.1}$$

where τ_c is a short distance imaginary time cut-off. One can then proceed to a systematic expansion of the partition function using $\lambda_{j,k}$ as a small parameter. At order n, we obtain the contribution

$$\int_{\tau_1<..<\tau_l} \langle \prod_{l=1}^{n} \frac{d\tau_l}{\tau_c} \sum_{j_l\neq k_l}^{M,M} \lambda_{j_l,k_l} \cos((\vec{w}_{j_l} - \vec{w}_{k_l}).\vec{r}(\tau_l))\rangle_0, \tag{G.2}$$

where $\langle ... \rangle_0$ is the average value with the unperturbed action. We proceed then to real-space renormalization in imaginary time, i.e. we increase the cut-off τ_c to $\tau_c' = \tau_c e^\ell$, and fuse operators closer than τ_c'. Using the invariance of the action upon renormalization of the cut-off, we derive the different RG equations. We recall the correlation functions for

the free bosons (we include an infrared cut-off in the integrals):

$$\langle \prod_j e^{i\vec{w}_{k_j}.\vec{r}(\tau_j)} \rangle_0 = \delta_{\sum_j \vec{w}_{k_j}=0} \prod_{j<l} \left(\frac{\tau_c^2}{(\tau_j - \tau_l)^2} \right)^{-\frac{\vec{w}_{k_j}.\vec{w}_{k_l}}{2K}} \tag{G.3}$$

A first contribution is generic: when $\tau_2 - \tau_1 \gg \tau_c'$,

$$\lambda_{j,k}\lambda_{k,j} \int_{\tau_1<\tau_2} \frac{d\tau_1 d\tau_2}{\tau_c^2} \langle \cos((\vec{w}_j - \vec{w}_k).\vec{r}(\tau_1)) \cos((\vec{w}_k - \vec{w}_j).\vec{r}(\tau_2)) \rangle_0$$
$$= \lambda_{j,k}\lambda_{k,j} \int_{\tau_1<\tau_2} \frac{d\tau_1 d\tau_2}{\tau_c^2} \left(\frac{\tau_c^2}{(\tau_1 - \tau_2)^2} \right)^{\frac{1}{K}}$$

This last expression must be cut-off independent, imposing $\lambda_{j,k}(\ell)\lambda_{k,j}(\ell) = e^{(2-\frac{2}{K})\ell}\lambda_{j,k}\lambda_{k,j}$, or by symmetry, $\lambda_{j,k}(\ell) = e^{(1-\frac{1}{K})\ell}\lambda_{j,k}$

When $\tau_2 - \tau_1 < \tau_c'$, the operators are no longer taken separately and fuse together. In particular, if $j_1 = k_2$, $k_1 \neq j_2$, we generate additional terms $\cos((\vec{w}_{j_2} - \vec{w}_{k_1}).\vec{r}(\tau_1))$ (alternatively for $j_2 = k_1$, $k_2 \neq j_1$). To rigorously compute the exact coefficient for this contribution, we use the third order terms $\lambda_{j_1,k_1}\lambda_{k_1,k_2}\lambda_{k_2,j_1}$, with $\tau_3 - \tau_1 \gg \tau_c'$. We need to evaluate, for $j \neq k \neq l \neq j$:

$$\int_{\tau_c<\tau<\tau_c e^\ell} \langle e^{i(\vec{w}_j - \vec{w}_k).\vec{r}(\tau_1)} e^{i(\vec{w}_k - \vec{w}_l).\vec{r}(\tau_1+\tau)} e^{i(\vec{w}_l - \vec{w}_j).\vec{r}(\tau_3)} \rangle_0 \tag{G.4}$$

$$= \left(\frac{\tau_c^2}{(\tau_3 - \tau_1)^2} \right)^{\frac{1}{2K}} \int_{\tau_c<\tau<\tau_c e^\ell} \left(\frac{\tau_c^2}{\tau^2} \frac{\tau_c^2}{(\tau_3 - \tau_1 - \tau)^2} \right)^{\frac{1}{2K}} = \left(\frac{\tau_c^2}{(\tau_3 - \tau_1)^2} \right)^{\frac{1}{K}} \ell \qquad \text{if } \ell \ll 1 \tag{G.5}$$

We finally obtain for $\ell \ll 1$,

$$\lambda_{j,k}(\ell) = \lambda_{j,k} + (1 - \frac{1}{K})\ell\lambda_{j,k} + 2\ell \sum_{m\neq j,k} \lambda_{j,m}\lambda_{m,k},$$

leading to the RG equation (5.34).

Strong coupling

At strong coupling, the action describing instanton excitations is given by Eq. (5.43) reproduced here,

$$S = \sum_{\omega_m} \sum_j \frac{|\omega_m|}{2\pi K\beta} |\phi_j(\omega_m)|^2 - v \int_0^\beta d\tau \sum_k \hat{O}_k(\tau), \tag{G.6}$$

with the operators $\hat{O}_k = e^{2i(\phi_k - \frac{1}{\sqrt{M}}\Phi)}$ connecting the lattice of minima. Proceeding with an expansion in powers of v, the calculation is similar as at weak coupling except for the replacement $K \to \frac{1}{K}$.

For $M = 3$, we note that $\hat{O}_1\hat{O}_2 = \hat{O}_3^\dagger$. The computation of the third order coefficient is identical to Eq. (G.5) and the RG equation is given by

$$\frac{dv}{d\ell} = \left(1 - \frac{4K}{3}\right) v + 2v^2 \tag{G.7}$$

For $M > 3$, the first non-zero terms are at third order in v. The two types contributions one has to take into account are: $\hat{O}_1\hat{O}_2\hat{O}_2^\dagger = \hat{O}_1$ and, for $M = 4$ only, $\hat{O}_1\hat{O}_2\hat{O}_3 = \hat{O}_4^\dagger$. The computation of the corresponding terms lead to the RG equation [276]

$$\frac{dv}{d\ell} = \left(1 - \frac{2(M-1)K}{M}\right) v + (B_M + A_4\delta_{M,4})v^3 \tag{G.8}$$

where B_M is a positive coefficient, see also Eq. (G.18). Eqs. (G.7) and (G.8) predict that for all $M \geq 3$, the strong coupling fixed point is unstable for $K \leq \frac{M}{2(M-1)}$, while for $K > \frac{M}{2(M-1)}$, an unstable fixed point (I) emerges at finite v.

G.1.2 RG equations for the M-CKM

Weak coupling

The Hamiltonian obtained after the unitary transformation (5.51) is given by Eq. (5.47), and can also be written as

$$\hat{U}^\dagger H \hat{U} = H_{\text{leads}}\{\tilde{\phi}, \tilde{\theta}, \tilde{K}\} - \sum_{j=1}^{M} \left(\frac{J_{\perp,j}}{2} \tau_+ e^{i\sqrt{2}\vec{w}_j.\tilde{r}_j + \sqrt{2}\left(\frac{1}{\sqrt{M}} - \frac{\tilde{K}J_z\sqrt{M}}{2}\right)\tilde{\Theta}} + h.c \right). \tag{G.9}$$

We introduce the notation $M_z = \frac{1}{\sqrt{M}} - \frac{\tilde{K}J_z\sqrt{M}}{2}$ and compute the RG equations for both $J_\perp$ and M_z.

We proceed with a similar expansion of the partition function using $J_\perp$ as a small parameter. The contribution of order n is

$$\left(\frac{J_\perp}{2}\right)^n \int\limits_{\tau_1<\ldots<\tau_n} \frac{d\tau_1 \ldots d\tau_n}{\tau_c^n} \sum_{\text{n-loops}} \exp\left(\sum_{j<k}^{n,n} V_{j,k}\right) + h.c., \tag{G.10}$$

where $\sum\limits_{\text{n-loops}}$ signify that we sum over all n-uplets (a_j) such that $\sum(-1)^j \vec{w}_{a_j} = 0$ and (using Eq. (G.3))

$$V_{j,k} = 2\frac{(-1)^{j+k}}{\tilde{K}} \left(M_z^2 + \vec{w}_{a_j}.\vec{w}_{a_k}\right) \log\left(\frac{\tau_k - \tau_j}{\tau_c}\right) \tag{G.11}$$

The alternating signs take into account the spin operators. Similarly, we increase the cut-off τ_c to $\tau_c' = \tau_c e^\ell$, and fuse the operators when needed. To lowest order, only two consecutive operators can fuse. The most relevant contribution appears when these two

contributions have the same $\vec{w}_{a_j}$. Let us assume that this happens for the lth and $l^{\text{th}}+1$ operators and define $\tau = \tau_{l+1} - \tau_l < \tau_c'$ and

$$V_d(\tau_l, \tau, a_l) = \sum_{j<l} V_{j,l} + V_{j,l+1} + \sum_{j>l+1} V_{l,j} + V_{l+1,j}$$
$$\approx 2 \sum_{j\neq l,l+1} \frac{(-1)^{j+l}}{\tilde{K}} \left(M_z^2 + \vec{w}_{a_j}.\vec{w}_{a_l}\right) \tau \partial_{\tau_l} \log(\frac{|\tau_l - \tau_j|}{\tau_c})$$

Integrating over the two variables τ_l and τ reduces the n-loop to a n-2 loop and consequently, at order n, we have an additional contribution coming from the order n+2,

$$\left(\frac{J_\perp}{2}\right)^2 \sum_{j=0}^{n} \sum_a \int_{\tau_j}^{\tau_{j+1}} \frac{d\tau'}{\tau_c} \int_{\tau_c}^{\tau_c e^\ell} \frac{d\tau}{\tau_c} e^{V_d(\tau',\tau,a)}$$
$$\approx \left(\frac{J_\perp}{2}\right)^2 \sum_{j=0}^{n} \sum_a \int_{\tau_j}^{\tau_{j+1}} \frac{d\tau'}{\tau_c} \int_{\tau_c}^{\tau_c e^\ell} \frac{d\tau}{\tau_c} 1 + V_d(\tau',\tau,a)$$
$$\approx \left(\frac{J_\perp}{2}\right)^2 \left(\frac{M\beta(e^\ell - 1)}{\tau_c} - 8M \frac{M_z^2(e^\ell - 1)}{\tilde{K}} \sum_{j<k} (-1)^{j+k} \log(\frac{\tau_k - \tau_j}{\tau_c}) \right),$$

where $\tau_0 = 0$ and $\tau_{n+1} = \beta$. While the first term can be ignored, as it corresponds to a rescaling of the ground state energy, the second term indeed renormalizes the partition function. Reexponentiation leads to a correction of $V_{p,q}$ given by

$$V_{p,q} \to V_{p,q} - \frac{MJ_\perp^2(e^\ell - 1)}{K} M_z^2 (-1)^{p+q} \log(\frac{\tau_q - \tau_p}{\tau_c}) \tag{G.12}$$

For small ℓ, we have

$$M_z(\ell)^2 = M_z^2 - MJ_\perp^2 M_z^2 \ell, \tag{G.13}$$

or

$$\frac{dJ_z}{dl} = J_\perp^2 \left(\frac{1}{\tilde{K}} - \frac{MJ_z}{2}\right), \tag{G.14}$$

which is the first RG equation. To obtain the RG equations for $J_\perp$, we simply rescale τ_c in both the integrals and $V_{j,k}$ and extract the n dependency. We obtain

$$J_\perp^n = J_\perp^n(\ell) e^{-n\ell} e^{-2\ell \sum_{j<k} \frac{(-1)^{j+k}}{\tilde{K}} (M_z^2 + \vec{w}_{a_j}.\vec{w}_{a_k})} = J_\perp^n(\ell) e^{-n\ell} e^{\frac{n}{\tilde{K}}\ell(M_z^2 + \frac{M-1}{M})}$$
$$\frac{dJ_\perp}{d\ell} = \left(1 - \frac{M-1}{M\tilde{K}} - \frac{M_z^2}{\tilde{K}}\right) J_\perp = \left(1 - \frac{1}{\tilde{K}} + J_z[1 - \frac{\tilde{K}J_z M}{4}]\right) J_\perp$$

Strong coupling

In this case, the vicinity of the strong coupling fixed point (S) is governed by the action

$$S = \sum_{\omega_m} \sum_j \frac{|\omega_m|}{2\pi K\beta} |\phi_j(\omega_m)|^2 - v \int_0^\beta d\tau \sum_k \hat{O}_k^{(h)}(\tau), \tag{G.15}$$

where the $\hat{O}_k^{(h)}$ operators, with dimension $\frac{2K(M-1)}{M}$, are given in Eq. (5.57). The difference with the operators $\hat{O}_k$ encountered in the topological Kondo model, see Eq. (G.6), is in the pseudo-spin rotation $e^{-i\pi\tau_z/M}$.

For $M = 3$, $\hat{O}_1^{(h)}\hat{O}_2^{(h)} = -\hat{O}_3^{(h)\dagger}$, where the minus sign stems from the Berry phase of the spin wavefunction, $e^{-i\pi\tau_z} = -1$. The calculation of the RG equation is this almost identical to (G.5),

$$\frac{dv_2}{d\ell} = (1 - 4K/3)v - 2v^2 \tag{G.16}$$

except for the sign change in the last term. In general for $M > 3$, the first non-zero contribution to the RG equation (apart from a linear term) is third order in v. For $M = 4$, there is a competition between two contributions, the contraction $\hat{O}_1^{(h)}\hat{O}_2^{(h)}\hat{O}_2^{(h)\dagger} = \hat{O}_1^{(h)}$ in which the spin plays no role, leading to the coefficient

$$B_4 = 6\int_0^1 dx \left[\frac{x^{2/3} + x^{-2/3} - 2}{(1-x)^2} + \left(\frac{x}{1-x}\right)^{2/3} - 1\right] \tag{G.17}$$

and the contribution $\hat{O}_1^{(h)}\hat{O}_2^{(h)}\hat{O}_3^{(h)} = -\hat{O}_4^{(h)\dagger}$, carrying the spin Berry phase, associated to the coefficient

$$A_4 = 6\int_0^1 dx \frac{1}{x^{2/3}(1-x)^{2/3}} \tag{G.18}$$

The RG equation takes the form

$$\frac{dv_3}{d\ell} = \left(1 - \frac{3K}{2}\right)v - (A_4 - B_4)v^3 \tag{G.19}$$

with $A_4 - B_4 > 0$ such that the spin wavefunction eventually governs the transition. We obtain a phase diagram similar to $M = 4$ as explained in the main text.

For $M \geq 5$, only $\hat{O}_1^{(h)}\hat{O}_2^{(h)}\hat{O}_2^{(h)\dagger} = \hat{O}_1^{(h)}$ contributes to third order in v. The RG equation takes the form (5.60) in the main text, exactly the same as in the charge non-degenerate case Eq. (G.8), and the phase diagram differs from $M \leq 4$.

G.2 Kubo approach to conductance

To compute the conductance in the Majorana island, we will use Kubo formula. We present in this Appendix a short derivation of the Kubo formula for our model, before an example of application far from charge degeneracy (see for example Ref [258] for an alternative derivation). We express the conductance as a correlation function of the initial bosonic field first, and then as a correlation function of the $(\vec{k}, \Phi)$ fields.

G.2.1 Kubo formula

We start from linear response theory. Given a small perturbation $H'(t)$ switched on adiabatically, the change for the average value of the observable A is:

$$\langle \Delta A(t)\rangle = \frac{-i}{\hbar}\int_{-\infty}^{t} e^{-\eta(t-t')}\langle [A(t), H'(t')]\rangle dt' \tag{G.20}$$

with $\eta \to 0^+$. Let $C^R_{A,B}(t-t') = -\frac{i}{\hbar}\theta(t-t')\langle[A(t),B(t')]\rangle$. To compute $C^R_{A,B}(\omega)$, we compute another correlation function and do an analytic continuation. Let $C_{A,B}(\tau) = -\langle T_\tau A(\tau)B(0)\rangle$. Starting with:

$$A(\tau) = \frac{1}{\beta}\sum_{n=-\infty}^{n=+\infty} e^{-i\omega_n\tau}A(i\omega_n) \tag{G.21}$$

$$B(0) = \frac{1}{\beta}\sum_{n=-\infty}^{n=+\infty} B(i\omega_n) \tag{G.22}$$

we obtain:

$$C_{A,B}(i\omega_n) = -\int_0^\beta d\tau e^{i\omega_n\tau}\frac{1}{\beta^2}\sum_{m,k} e^{-i\omega_n\tau}\langle A(i\omega_m)B(i\omega_k)\rangle \tag{G.23}$$

$$C_{A,B}(i\omega_n) = -\frac{1}{\beta}\sum_k \langle A(i\omega_n)B(i\omega_k)\rangle. \tag{G.24}$$

In particular,

$$C_{\dot{A},B}(i\omega_n) = -\frac{1}{\beta}\sum_k i\omega_n\langle A(i\omega_n)B(i\omega_k)\rangle. \tag{G.25}$$

The current operator for the wire j is given by $e\partial_t N_j$, where N_j is the total charge in the wire. The linear conductance $G_{j,k}$, corresponding to the current in the jth wire due to a potential in the kth wire is $\frac{\partial\langle\Delta e\partial_t N_j\rangle}{\partial V_k}$, where V_k is the potential in the wire k. Given $A = eN_j$ and $B = eV_kN_k$, we finally obtain the conductance $G(\omega)$:

$$G_{j,k}(\omega) = -\frac{e^2}{h}\int d\nu\omega\langle N_j(\omega)N_k(\nu)\rangle \tag{G.26}$$

Finally, as we are interested in the DC conductance, we obtain:

$$G = -\frac{e^2}{h}\lim_{\omega\to 0}\int d\nu\omega\langle N_j(\omega)N_k(\nu)\rangle \tag{G.27}$$

As our action is diagonal in the Matsubara frequencies, it simplifies to:

$$G_{j,k} = -\frac{e^2}{h}\lim_{\omega\to 0}\omega\langle N_j(\omega)N_k(\omega)\rangle \tag{G.28}$$

G.2.2 Application for the strong coupling limit far from charge degeneracy

For semi-infinite LL wires, $N = \frac{\phi(x=0)}{\pi}$. We want to express N_j as a function of $(\vec{k},\Phi)$, dual to $(\vec{r},\Theta)$.

$$G_{j,k} = -\frac{e^2}{\pi^2 h}\lim_{\omega\to 0}\omega\langle\phi_j(i\omega)\phi_k(i\omega)\rangle \tag{G.29}$$

$$G_{j,k} = -\frac{e^2}{\pi^2 h}\sum_{l,m}^{M-1}\vec{w}_k(l)\vec{w}_j(m)\lim_{\omega\to 0}\omega\langle k_l(i\omega)k_m(i\omega)\rangle, \tag{G.30}$$

where $\vec{w}_k(l)$ is the lth component of $\vec{w}_k$. The global mode does not intervene as it is pinned due to charge conservation, and consequently does not contribute. $\vec{k}$ being the dual of $\vec{r}$, when the latter are pinned in the strong coupling limit, $\vec{k}$ is free and one obtains:

$$\lim_{\omega \to 0} \omega \langle k_l(i\omega) k_m(i\omega) \rangle = 2\pi^2 K \delta_{l,m}, \tag{G.31}$$

leading to the celebrated conductance:

$$G_{k,j} = -\frac{2Ke^2}{h} \vec{w}_k . \vec{w}_j = \frac{2Ke^2}{h} (\frac{1}{M} - \delta_{k,j}). \tag{G.32}$$

Bibliography

[1] V. L. Berezinskii. Destruction of long-range order in one-dimensional and two-dimensional systems having a continuous symmetry group i. classical systems. *Soviet Journal of Experimental and Theoretical Physics*, 32(493), 1971.

[2] V. L. Berezinskii. Destruction of long-range order in one-dimensional and two-dimensional systems having a continuous symmetry group ii. quantum systems. *Soviet Journal of Experimental and Theoretical Physics*, 34(610), 1972.

[3] J. M. Kosterlitz and D. J. Thouless. Long range order and metastability in two dimensional solids and superfluids (application of dislocation theory). *Journal of Physics C: Solid State Physics*, 5 (11)(L124), 1972.

[4] J. M. Kosterlitz and D. J. Thouless. Ordering, metastability and phase transitions in two-dimensional systems. *Journal of Physics C: Solid State Physics*, 6 (7)(1181), 1973.

[5] K. v. Klitzing, G. Dorda, and M. Pepper. New method for high-accuracy determination of the fine-structure constant based on quantized hall resistance. *Phys. Rev. Lett.*, 45:494–497, Aug 1980.

[6] D. C. Tsui, H. L. Stormer, and A. C. Gossard. Two-dimensional magnetotransport in the extreme quantum limit. *Phys. Rev. Lett.*, 48:1559–1562, May 1982.

[7] D. J. Thouless, M. Kohmoto, M. P. Nightingale, and M. den Nijs. Quantized hall conductance in a two-dimensional periodic potential. *Phys. Rev. Lett.*, 49:405–408, Aug 1982.

[8] Q. Niu, D. J. Thouless, and Y.-S. Wu. Quantized hall conductance as a topological invariant. *Phys. Rev. B*, 31:3372–3377, Mar 1985.

[9] F. D. M. Haldane. Model for a quantum hall effect without landau levels: Condensed-matter realization of the "parity anomaly". *Phys. Rev. Lett.*, 61:2015–2018, Oct 1988.

[10] N. Read and D. Green. Paired states of fermions in two dimensions with breaking of parity and time-reversal symmetries and the fractional quantum hall effect. *Phys. Rev. B*, 61:10267–10297, Apr 2000.

[11] A. P. Schnyder, S. Ryu, A. Furusaki, and A. W. W. Ludwig. Classification of topological insulators and superconductors in three spatial dimensions. *Phys. Rev. B*, 78:195125, Nov 2008.

[12] A. Kitaev. Periodic table for topological insulators and superconductors. In V. Lebedev and M. Feigel'Man, editors, *American Institute of Physics Conference Series*, volume 1134 of *American Institute of Physics Conference Series*, pages 22–30, May 2009.

[13] A. Kitaev. Unpaired majorana fermions in quantum wires. *Physics Uspekhi*, 44(10S):131, 2001.

[14] E. Majorana. *Nuevo Cimento 5*, 1937.

[15] C. Nayak, S. H. Simon, A. Stern, M. Freedman, and S. Das Sarma. Non-abelian anyons and topological quantum computation. *Rev. Mod. Phys.*, 80:1083–1159, Sep 2008.

[16] J. Alicea. New directions in the pursuit of majorana fermions in solid state systems. *Rep. Prog. Phys. 75, 076501*, 2012.

[17] C. W. J. Beenakker. Search for majorana fermions in superconductors. *Annual Review of Condensed Matter Physics*, 4(1):113–136, 2013.

[18] T. Hyart, B. van Heck, I. C. Fulga, M. Burrello, A. R. Akhmerov, and C. W. J. Beenakker. Flux-controlled quantum computation with majorana fermions. *Phys. Rev. B*, 88:035121, Jul 2013.

[19] D. Aasen, M. Hell, R. V. Mishmash, A. Higginbotham, J. Danon, M. Leijnse, T. S. Jespersen, J. A. Folk, C. M. Marcus, K. Flensberg, and J. Alicea. Milestones toward majorana-based quantum computing. *Phys. Rev. X*, 6:031016, Aug 2016.

[20] B. Béri and N. R. Cooper. Topological kondo effect with majorana fermions. *Phys. Rev. Lett.*, 109:156803, Oct 2012.

[21] A. Altland and R. Egger. Multiterminal coulomb-majorana junction. *Phys. Rev. Lett.*, 110:196401, May 2013.

[22] S. Plugge, L. A. Landau, E. Sela, A. Altland, K. Flensberg, and R. Egger. Roadmap to majorana surface codes. *Phys. Rev. B*, 94:174514, Nov 2016.

[23] R. M. Lutchyn, J. D. Sau, and S. Das Sarma. Majorana fermions and a topological phase transition in semiconductor-superconductor heterostructures. *Phys. Rev. Lett. 105, 077001*, 2010.

[24] Y. Oreg, G. Refael, and F. von Oppen. Helical liquids and majorana bound states in quantum wires. *Phys. Rev. Lett. 105, 177002*, 2010.

[25] A. Das, Y. Ronen, Y. Most, Y. Oreg, M. Heiblum, and H. Shtrikman. Zero-bias peaks and splitting in an al–inas nanowire topological superconductor as a signature of majorana fermions. *Nat. Phys.*, 8(12):887–895, 2012.

[26] M. T. Deng, C. L. Yu, G. Y. Huang, M. Larsson, P. Caroff, and H. Q. Xu. Anomalous zero-bias conductance peak in a nb–insb nanowire–nb hybrid device. *Nano Letters*, 12(12):6414–6419, 2012. PMID: 23181691.

[27] V. Mourik, K. Zuo, S. M. Frolov, S. R. Plissard, E. P. A. M. Bakkers, and L. P. Kouwenhoven. Signatures of majorana fermions in hybrid superconductor-semiconductor nanowire devices. *Science 336, 1003*, 2012.

[28] H. O. H. Churchill, V. Fatemi, K. Grove-Rasmussen, M. T. Deng, P. Caroff, H. Q. Xu, and C. M. Marcus. Superconductor-nanowire devices from tunneling to the multichannel regime: Zero-bias oscillations and magnetoconductance crossover. *Phys. Rev. B*, 87:241401, Jun 2013.

[29] A. D. K. Finck, D. J. Van Harlingen, P. K. Mohseni, K. Jung, and X. Li. Anomalous modulation of a zero-bias peak in a hybrid nanowire-superconductor device. *Phys. Rev. Lett.*, 110:126406, Mar 2013.

[30] S. M. Albrecht, A. P. Higginbotham, M. Madsen, F. Kuemmeth, T. S. Jespersen, J. Nygård, P. Krogstrup, and C. M. Marcus. Exponential protection of zero modes in Majorana islands. *Nature*, 531:206–209, March 2016.

[31] J. Chen, P. Yu, J. Stenger, M. Hocevar, D. Car, S. R. Plissard, E. P. A. M. Bakkers, T. D. Stanescu, and S. M. Frolov. Experimental Phase Diagram of a One-Dimensional Topological Superconductor. *ArXiv e-prints*, October 2016.

[32] M. T. Deng, S. Vaitiekenas, E. B. Hansen, J. Danon, M. Leijnse, K. Flensberg, J. Nygård, P. Krogstrup, and C. M. Marcus. Majorana bound state in a coupled quantum-dot hybrid-nanowire system. *Science*, 354(6319):1557–1562, 2016.

[33] H. Zhang, Ö. Gül, S. Conesa-Boj, K. Zuo, V. Mourik, F. K. de Vries, J. van Veen, D. J. van Woerkom, M. P. Nowak, M. Wimmer, D. Car, S. Plissard, E. P. A. M. Bakkers, M. Quintero-Pérez, S. Goswami, K. Watanabe, T. Taniguchi, and L. P. Kouwenhoven. Ballistic Majorana nanowire devices. *ArXiv e-prints*, March 2016.

[34] J. Li, H. Chen, I.K. Drozdov, A. Yazdani, B.A. Bernevig, and A.H. MacDonald. Topological superconductivity induced by ferromagnetic metal chains. *Phys. Rev. B*, 90(23):235433, December 2014.

[35] S. Nadj-Perge, I. K. Drozdov, J. Li, H. Chen, S. Jeon, J. Seo, A. H. MacDonald, B. A. Bernevig, and A. Yazdani. Observation of Majorana fermions in ferromagnetic atomic chains on a superconductor. *Science*, 346:602–607, October 2014.

[36] C.-E. Bardyn, M. A. Baranov, C. V. Kraus, E. Rico, A. İmamoğlu, P. Zoller, and S. Diehl. Topology by dissipation. *New Journal of Physics*, 15(8):085001, August 2013.

[37] C.V. Kraus, M. Dalmonte, M.A. Baranov, A.M. Läuchli, and P. Zoller. Majorana edge states in atomic wires coupled by pair hopping. *Phys. Rev. Lett.*, 111:173004, Oct 2013.

[38] J. Ruhman, E. Berg, and E. Altman. Topological states in a one-dimensional fermi gas with attractive interactions. *Phys. Rev. Lett. 114, 100401*, 2015.

[39] J. Bardeen, L. N. Cooper, and J. R. Schrieffer. Microscopic theory of superconductivity. *Phys. Rev.*, 106:162–164, Apr 1957.

[40] S. Sachdev. *Quantum Phase Transitions.* 2001.

[41] C.-K. Chiu, J. C. Y. Teo, A. P. Schnyder, and S. Ryu. Classification of topological quantum matter with symmetries. *Rev. Mod. Phys.*, 88:035005, Aug 2016.

[42] A. Bernevig and T. Neupert. Topological Superconductors and Category Theory. *ArXiv e-prints*, June 2015.

[43] B. A. Dubrovin, A. T. Fomenko, and S. P. Novikov. *Modern Geometry-Methods and Applications.* 1985.

[44] S. Tewari and J. D. Sau. Topological invariants for spin-orbit coupled superconductor nanowires. *Phys. Rev. Lett.*, 109:150408, Oct 2012.

[45] D. Sticlet, C. Bena, and P. Simon. Josephson effect in superconducting wires supporting multiple majorana edge states. *Phys. Rev. B 87, 104509*, 2013.

[46] Z. Wang, X.-L. Qi, and S.-C. Zhang. Equivalent topological invariants of topological insulators. *New Journal of Physics*, 12(6):065007, 2010.

[47] D. Sticlet, F. Piéchon, J.-N. Fuchs, P. Kalugin, and P. Simon. Geometrical engineering of a two-band chern insulator in two dimensions with arbitrary topological index. *Phys. Rev. B*, 85:165456, Apr 2012.

[48] M. F. Atiyah and I. M. Singer. The index of elliptic operators on compact manifolds. *Bull. Amer. Math. Soc.*, 69:422–433, 1963.

[49] R. Jackiw and C. Rebbi. Solitons with fermion number 1/2. *Phys. Rev. D*, 13:3398–3409, Jun 1976.

[50] W. P. Su, J. R. Schrieffer, and A. J. Heeger. Solitons in polyacetylene. *Phys. Rev. Lett.*, 42(25):1698–1701, Jun 1979.

[51] Y. Niu, S. B. Chung, C.-H. Hsu, I. Mandal, S. Raghu, and S. Chakravarty. Majorana zero modes in a quantum ising chain with longer-ranged interactions. *Phys. Rev. B 85, 035110*, 2012.

[52] D. Bagrets and A. Altland. Class d spectral peak in majorana quantum wires. *Phys. Rev. Lett.*, 109:227005, Nov 2012.

[53] S. Das Sarma, J. D. Sau, and T. D. Stanescu. Splitting of the zero-bias conductance peak as smoking gun evidence for the existence of the majorana mode in a superconductor-semiconductor nanowire. *Phys. Rev. B*, 86:220506, Dec 2012.

[54] G. Kells, D. Meidan, and P. W. Brouwer. Near-zero-energy end states in topologically trivial spin-orbit coupled superconducting nanowires with a smooth confinement. *Phys. Rev. B*, 86:100503, Sep 2012.

[55] X. Lee, E. J. H. and Jiang, R. Aguado, G. Katsaros, C. M. Lieber, and S. De Franceschi. Zero-bias anomaly in a nanowire quantum dot coupled to superconductors. *Phys. Rev. Lett.*, 109:186802, Oct 2012.

[56] J. Liu, A. C. Potter, K. T. Law, and P. A. Lee. Zero-bias peaks in the tunneling conductance of spin-orbit-coupled superconducting wires with and without majorana end-states. *Phys. Rev. Lett.*, 109:267002, Dec 2012.

[57] D. I. Pikulin, J. P. Dahlhaus, M. Wimmer, H. Schomerus, and C. W. J. Beenakker. A zero-voltage conductance peak from weak antilocalization in a majorana nanowire. *New Journal of Physics*, 14(12):125011, 2012.

[58] T. D. Stanescu and S. Tewari. Majorana fermions in semiconductor nanowires: fundamentals, modeling, and experiment. *Journal of Physics: Condensed Matter*, 25(23):233201, 2013.

[59] C.-X. Liu, J. D. Sau, T. D. Stanescu, and S. Das Sarma. Andreev bound states versus Majorana bound states in quantum dot-nanowire-superconductor hybrid structures: Trivial versus topological zero-bias conductance peaks. *ArXiv e-prints*, May 2017.

[60] G. E. Volovik. *Universe in a Helium Droplex*. Oxford University Press, 2003.

[61] A. C. Potter and P. A. Lee. Engineering a $p+ip$ superconductor: Comparison of topological insulator and rashba spin-orbit-coupled materials. *Phys. Rev. B*, 83:184520, May 2011.

[62] V. Gurarie, L. Radzihovsky, and A. V. Andreev. Quantum phase transitions across a p-wave feshbach resonance. *Phys. Rev. Lett.*, 94:230403, Jun 2005.

[63] M. Stone and S.-B. Chung. Fusion rules and vortices in $p_x + ip_y$ superconductors. *Phys. Rev. B*, 73:014505, Jan 2006.

[64] K. S. Novoselov. Nobel lecture: Graphene: Materials in the flatland. *Rev. Mod. Phys.*, 83:837–849, Aug 2011.

[65] C. L. Kane and E. J. Mele. Z_2. *Phys. Rev. Lett.*, 95:146802, Sep 2005.

[66] C. L. Kane and E. J. Mele. Quantum spin hall effect in graphene. *Phys. Rev. Lett.*, 95:226801, Nov 2005.

[67] A. B. Bernevig and S.-C. Zhang. Quantum spin hall effect. *Phys. Rev. Lett.*, 96:106802, Mar 2006.

[68] N. Laflorencie. Quantum entanglement in condensed matter systems. *Physics Reports*, 646:1 – 59, 2016. Quantum entanglement in condensed matter systems.

[69] L. Susskind. The world as a hologram. *Journal of Mathematical Physics*, 36:6377–6396, November 1995.

[70] P. Calabrese and J. Cardy. Entanglement entropy and quantum field theory. *Journal of Statistical Mechanics: Theory and Experiment*, 2004(06):P06002, 2004.

[71] S. Furukawa, V. Pasquier, and J. Shiraishi. Mutual information and boson radius in a $c = 1$ critical system in one dimension. *Phys. Rev. Lett.*, 102:170602, Apr 2009.

[72] P. Calabrese, J. Cardy, and E. Tonni. Entanglement entropy of two disjoint intervals in conformal field theory. *Journal of Statistical Mechanics: Theory and Experiment*, 2009(11):P11001, 2009.

[73] M. B. Hastings. An area law for one-dimensional quantum systems. *Journal of Statistical Mechanics: Theory and Experiment*, 2007(08):P08024, 2007.

[74] M. M. Wolf, F. Verstraete, M. B. Hastings, and J. I. Cirac. Area laws in quantum systems: Mutual information and correlations. *Phys. Rev. Lett.*, 100:070502, Feb 2008.

[75] D. N. Page. Average entropy of a subsystem. *Phys. Rev. Lett.*, 71:1291–1294, Aug 1993.

[76] T. Barthel, M.-C. Chung, and U. Schollwöck. Entanglement scaling in critical two-dimensional fermionic and bosonic systems. *Phys. Rev. A*, 74:022329, Aug 2006.

[77] D. Gioev and I. Klich. Entanglement entropy of fermions in any dimension and the widom conjecture. *Phys. Rev. Lett.*, 96:100503, Mar 2006.

[78] Michael M. Wolf. Violation of the entropic area law for fermions. *Phys. Rev. Lett.*, 96:010404, Jan 2006.

[79] B. Swingle. Entanglement entropy and the fermi surface. *Phys. Rev. Lett.*, 105:050502, Jul 2010.

[80] W. Ding, A. Seidel, and K. Yang. Entanglement entropy of fermi liquids via multi-dimensional bosonization. *Phys. Rev. X*, 2:011012, Mar 2012.

[81] P. Di Francesco, P. Matthieu, and D. Senechal. *Conformal Field Theory.* 1996.

[82] C. Holzhey, F. Larsen, and F. Wilczek. Geometric and renormalized entropy in conformal field theory. *Nuclear Physics B*, 424(3):443 – 467, 1994.

[83] G. Vidal, J. I. Latorre, E. Rico, and A. Kitaev. Entanglement in quantum critical phenomena. *Phys. Rev. Lett.*, 90:227902, Jun 2003.

[84] V. E. Korepin. Universality of entropy scaling in one dimensional gapless models. *Phys. Rev. Lett.*, 92:096402, Mar 2004.

[85] E. Fradkin and J. E. Moore. Entanglement entropy of 2d conformal quantum critical points: Hearing the shape of a quantum drum. *Phys. Rev. Lett.*, 97:050404, Aug 2006.

[86] M. A. Metlitski, C. A. Fuertes, and S. Sachdev. Entanglement entropy in the $o(n)$ model. *Phys. Rev. B*, 80:115122, Sep 2009.

[87] H. Casini and M. Huerta. Entanglement entropy in free quantum field theory. *Journal of Physics A: Mathematical and Theoretical*, 42(50):504007, 2009.

[88] P. Bueno, R. C. Myers, and W. Witczak-Krempa. Universality of corner entanglement in conformal field theories. *Phys. Rev. Lett.*, 115:021602, Jul 2015.

[89] P. Bueno and R. C. Myers. Corner contributions to holographic entanglement entropy. *Journal of High Energy Physics*, 2015(8):68, 2015.

[90] H. Elvang and M. Hadjiantonis. Exact results for corner contributions to the entanglement entropy and rényi entropies of free bosons and fermions in 3d. *Physics Letters B*, 749:383 – 388, 2015.

[91] R.-X. Miao. A holographic proof of the universality of corner entanglement for cfts. *Journal of High Energy Physics*, 2015(10):38, 2015.

[92] T. Faulkner, R. G. Leigh, and O. Parrikar. Shape dependence of entanglement entropy in conformal field theories. *Journal of High Energy Physics*, 2016(4):88, 2016.

[93] H. Osborn and A. Petkou. Implications of conformal invariance in field theories for general dimensions. *Annals of Physics*, 231(2):311 – 362, 1994.

[94] J. Helmes, L. E. Hayward Sierens, A. Chandran, W. Witczak-Krempa, and R. G. Melko. Universal corner entanglement of dirac fermions and gapless bosons from the continuum to the lattice. *Phys. Rev. B*, 94:125142, Sep 2016.

[95] H. Casini and M. Huerta. Remarks on the entanglement entropy for disconnected regions. *Journal of High Energy Physics*, 2009(03):048, 2009.

[96] A. Kitaev and J. Preskill. Topological entanglement entropy. *Phys. Rev. Lett.*, 96:110404, Mar 2006.

[97] M. Levin and X.-G. Wen. Detecting topological order in a ground state wave function. *Phys. Rev. Lett.*, 96:110405, Mar 2006.

[98] A. Kitaev. Anyons in an exactly solved model and beyond. *Annals of Physics*, 321(1):2 – 111, 2006. January Special Issue.

[99] A. Hamma, R. Ionicioiu, and P. Zanardi. Bipartite entanglement and entropic boundary law in lattice spin systems. *Phys. Rev. A*, 71:022315, Feb 2005.

[100] R. B. Laughlin. Anomalous quantum hall effect: An incompressible quantum fluid with fractionally charged excitations. *Phys. Rev. Lett.*, 50:1395–1398, May 1983.

[101] S. Furukawa and G. Misguich. Topological entanglement entropy in the quantum dimer model on the triangular lattice. *Phys. Rev. B*, 75:214407, Jun 2007.

[102] H. Li and F. D. M. Haldane. Entanglement spectrum as a generalization of entanglement entropy: Identification of topological order in non-abelian fractional quantum hall effect states. *Phys. Rev. Lett.*, 101:010504, Jul 2008.

[103] N. S. Williams, K. Le Hur, and A. N. Jordan. Effective thermodynamics of strongly coupled qubits. *Journal of Physics A: Mathematical and Theoretical*, 44(38):385003, 2011.

[104] A. Sterdyniak, N. Regnault, and B. A. Bernevig. Extracting excitations from model state entanglement. *Phys. Rev. Lett.*, 106:100405, Mar 2011.

[105] M. Haque, O. Zozulya, and K. Schoutens. Entanglement entropy in fermionic laughlin states. *Phys. Rev. Lett.*, 98:060401, Feb 2007.

[106] R. Thomale, D. P. Arovas, and B. A. Bernevig. Nonlocal order in gapless systems: Entanglement spectrum in spin chains. *Phys. Rev. Lett.*, 105:116805, Sep 2010.

[107] B. Swingle and T. Senthil. Geometric proof of the equality between entanglement and edge spectra. *Phys. Rev. B*, 86:045117, Jul 2012.

[108] X.-L. Qi, H. Katsura, and A. W. W. Ludwig. General relationship between the entanglement spectrum and the edge state spectrum of topological quantum states. *Phys. Rev. Lett.*, 108:196402, May 2012.

[109] M. Greiter, V. Schnells, and R. Thomale. The 1D Ising model and the topological phase of the Kitaev chain. *Annals of Physics*, 351:1026–1033, December 2014.

[110] A. M. Turner, F. Pollmann, and E. Berg. Topological phases of one-dimensional fermions: An entanglement point of view. *Phys. Rev. B*, 83:075102, Feb 2011.

[111] R. Islam, R. Ma, P. M. Preiss, M. E. Tai, A. Lukin, M. Rispoli, and M. Greiner. Measuring entanglement entropy in a quantum many-body system. *Nature*, 528(7580):77–83, December 2015.

[112] J. Cardy. Measuring entanglement using quantum quenches. *Phys. Rev. Lett.*, 106:150404, Apr 2011.

[113] D. A. Abanin and E. Demler. Measuring entanglement entropy of a generic many-body system with a quantum switch. *Phys. Rev. Lett.*, 109:020504, Jul 2012.

[114] H. Pichler, G. Zhu, A. Seif, P. Zoller, and M. Hafezi. Measurement protocol for the entanglement spectrum of cold atoms. *Phys. Rev. X*, 6:041033, Nov 2016.

[115] I. Peschel. Calculation of reduced density matrices from correlation functions. *Journal of Physics A: Mathematical and General*, 36(14):L205, 2003.

[116] I. Klich, G. Refael, and A. Silva. Measuring entanglement entropies in many-body systems. *Phys. Rev. A*, 74:032306, Sep 2006.

[117] H. F. Song, S. Rachel, and K. Le Hur. General relation between entanglement and fluctuations in one dimension. *Phys. Rev. B*, 82:012405, 2010.

[118] A. Komnik and H. Saleur. Full counting statistics of chiral luttinger liquids with impurities. *Phys. Rev. Lett.*, 96:216406, Jun 2006.

[119] B. Hsu, E. Grosfeld, and E. Fradkin. Quantum noise and entanglement generated by a local quantum quench. *Phys. Rev. B*, 80:235412, Dec 2009.

[120] I. Klich and L. Levitov. Quantum noise as an entanglement meter. *Phys. Rev. Lett.*, 102:100502, Mar 2009.

[121] P. Nataf, M. Dogan, and K. Le Hur. Heisenberg uncertainty principle as a probe of entanglement entropy: Application to superradiant quantum phase transitions. *Phys. Rev. A*, 86:043807, Oct 2012.

[122] G. C. Levine, M. J. Bantegui, and J. A. Burg. Full counting statistics in a disordered free fermion system. *Phys. Rev. B*, 86:174202, Nov 2012.

[123] D. J. Luitz, N. Laflorencie, and F. Alet. Many-body localization edge in the random-field heisenberg chain. *Phys. Rev. B*, 91:081103, Feb 2015.

[124] R. Singh, J. H. Bardarson, and F. Pollmann. Signatures of the many-body localization transition in the dynamics of entanglement and bipartite fluctuations. *New Journal of Physics*, 18(2):023046, 2016.

[125] J.-M. Stéphan and F. Pollmann. Full counting statistics in the haldane-shastry chain. *Phys. Rev. B*, 95:035119, Jan 2017.

[126] H. F. Song, S. Rachel, C. Flindt, I. Klich, N. Laflorencie, and K. Le Hur. Bipartite fluctuations as a probe of many-body entanglement. *Physical Review B*, 85(3):035409, 2012.

[127] J. Smith, A. Lee, P. Richerme, B. Neyenhuis, P. W. Hess, P. Hauke, M. Heyl, D. A. Huse, and C. Monroe. Many-body localization in a quantum simulator with programmable random disorder. *Nature Physics*, 12:907–911, October 2016.

[128] A. Mazurenko, C. S. Chiu, G. Ji, M. F. Parsons, M. Kanász-Nagy, R. Schmidt, F. Grusdt, E. Demler, D. Greif, and M. Greiner. Experimental realization of a long-range antiferromagnet in the Hubbard model with ultracold atoms. *Nature*, 545:462–466, December 2016.

[129] F. D. M. Haldane. Luttinger liquid theory of one-dimensional quantum fluids. i. properties of the luttinger model and their extension to the general 1d interacting spinless fermi gas. *J. Phys. C 14 2585*, 1981.

[130] A. O. Gogolin, A. A. Nersesyan, and A. M. Tsvelik. *Bosonization and strongly correlated systems.* 1998.

[131] T. Giamarchi. *Quantum Physics in One Dimension.* 2004.

[132] N. Laflorencie, E. S. Sørensen, M.-S. Chang, and I. Affleck. Boundary effects in the critical scaling of entanglement entropy in 1d systems. *Phys. Rev. Lett.*, 96:100603, Mar 2006.

[133] P. Calabrese, M. Mintchev, and E. Vicari. Exact relations between particle fluctuations and entanglement in fermi gases. *EPL (Europhysics Letters)*, 98(2):20003, 2012.

[134] V. Eisler and I. Peschel. Surface and bulk entanglement in free-fermion chains. *Journal of Statistical Mechanics: Theory and Experiment*, 2014(4):P04005, 2014.

[135] M. Dalmonte, E. Ercolessi, and L. Taddia. Critical properties and rényi entropies of the spin-$\frac{3}{2}$ xxz chain. *Phys. Rev. B*, 85:165112, Apr 2012.

[136] S. Rachel, N. Laflorencie, H. F. Song, and K. Le Hur. Detecting quantum critical points using bipartite fluctuations. *Phys. Rev. Lett.*, 108:116401, Mar 2012.

[137] N. Laflorencie and S. Rachel. Spin-resolved entanglement spectroscopy of critical spin chains and luttinger liquids. *Journal of Statistical Mechanics: Theory and Experiment*, 2014(11):P11013, 2014.

[138] A. Purkayastha and V. Subrahmanyam. Block entanglement and fluctuations in finite-size correlated electron systems. *Phys. Rev. B*, 89:195125, May 2014.

[139] I. Frérot, P. Naldesi, and T. Roscilde. Entanglement and fluctuations in the xxz model with power-law interactions. *Phys. Rev. B*, 95:245111, Jun 2017.

[140] J. S. Bell. Fluctuation compressibility theorem and its application to the pairing model. *Phys. Rev.*, 129:1896–1900, Feb 1963.

[141] A. Petrescu, H. F. Song, S. Rachel, Z. Ristivojevic, C. Flindt, N. Laflorencie, I. Klich, N. Regnault, and K. Le Hur. Fluctuations and entanglement spectrum in quantum hall states. *Journal of Statistical Mechanics: Theory and Experiment*, 2014(10):P10005, 2014.

[142] B. Swingle. Rényi entropy, mutual information, and fluctuation properties of fermi liquids. *Phys. Rev. B*, 86:045109, Jul 2012.

[143] H. F. Song, N. Laflorencie, S. Rachel, and K. Le Hur. Entanglement entropy of the two-dimensional heisenberg antiferromagnet. *Phys. Rev. B*, 83:224410, Jun 2011.

[144] C. W. Helstrom. *Quantum Detection and Estimation Theory.* 1976.

[145] L. Herviou, C. Mora, and K. Le Hur. Bipartite charge fluctuations in one-dimensional F_2 superconductors and insulators. *Phys. Rev. B*, 96:121113(R), Sep 2017.

[146] T.-L. Wang, L.-N. Wu, W. Yang, G.-R. Jin, N. Lambert, and F. Nori. Quantum fisher information as a signature of the superradiant quantum phase transition. *New Journal of Physics*, 16(6):063039, 2014.

[147] P. Hauke, M. Heyl, L. Tagliacozzo, and P. Zoller. Measuring multipartite entanglement through dynamic susceptibilities. *Nature Physics*, 12:778–782, August 2016.

[148] W. Wu and J.-B. Xu. Geometric phase, quantum fisher information, geometric quantum correlation and quantum phase transition in the cavity-bose–einstein-condensate system. *Quantum Information Processing*, 15(9):3695–3709, 2016.

[149] E.-J. Ye, Z.-D. Hu, and W. Wu. Scaling of quantum fisher information close to the quantum phase transition in the xy spin chain. *Physica B: Cond Mat, 502*, pages 151–154, 2016.

[150] S. Pappalardi, A. Russomanno, A. Silva, and R. Fazio. Multipartite entanglement after a quantum quench. *Journal of Statistical Mechanics: Theory and Experiment*, 2017(5):053104, 2017.

[151] F. Benatti, R. Floreanini, and U. Marzolino. Entanglement in fermion systems and quantum metrology. *Phys. Rev. A*, 89:032326, Mar 2014.

[152] G. Tóth and I. Apellaniz. Quantum metrology from a quantum information science perspective. *Journal of Physics A: Mathematical and Theoretical*, 47(42):424006, 2014.

[153] P. Hyllus, W. Laskowski, R. Krischek, C. Schwemmer, W. Wieczorek, H. Weinfurter, L. Pezzé, and A. Smerzi. Fisher information and multiparticle entanglement. *Phys. Rev. A*, 85:022321, Feb 2012.

[154] G. Tóth. Multipartite entanglement and high-precision metrology. *Phys. Rev. A*, 85:022322, Feb 2012.

[155] L. Herviou, C. Mora, and K. Le Hur. Phase diagram and entanglement of two interacting topological kitaev chains. *Phys. Rev. B, 93, 165142*, 2016.

[156] B. M. McCoy. Spin correlation functions of the $x-y$ model. *Phys. Rev.*, 173:531–541, Sep 1968.

[157] P. Pfeuty. The one-dimensional ising model with a transverse field. *Annals of Physics*, 57(1):79–90, 1970.

[158] B. Bauer, L. D. Carr, H. G. Evertz, A. Feiguin, J. Freire, S. Fuchs, L. Gamper, J. Gukelberger, E. Gull, S. Guertler, A. Hehn, R. Igarashi, S. V. Isakov, D. Koop, P. N. Ma, P. Mates, H. Matsuo, O. Parcollet, G. Pawłowski, J. D. Picon, L. Pollet, E. Santos, V. W. Scarola, U. Schollwöck, C. Silva, B. Surer, S. Todo, S. Trebst, M. Troyer, M. L. Wall, P. Werner, and S. Wessel. The alps project release 2.0: open source software for strongly correlated systems. *Journal of Statistical Mechanics: Theory and Experiment*, 2011(05):P05001, 2011.

[159] M. Dolfi, B. Bauer, S. Keller, A. Kosenkov, T. Ewart, A. Kantian, T. Giamarchi, and M. Troyer. Matrix product state applications for the alps project. *Computer Physics Communications*, 185(12):3430–3440, 2014.

[160] M. Trif and Y. Tserkovnyak. Resonantly tunable majorana polariton in a microwave cavity. *Phys. Rev. Lett.*, 109:257002, Dec 2012.

[161] A. Cottet, T. Kontos, and B. Douçot. Squeezing light with majorana fermions. *Phys. Rev. B*, 88:195415, Nov 2013.

[162] T. L. Schmidt, A. Nunnenkamp, and C. Bruder. Microwave-controlled coupling of majorana bound states. *New Journal of Physics*, 15(2):025043, 2013.

[163] O. Dmytruk, M. Trif, and P. Simon. Cavity quantum electrodynamics with mesoscopic topological superconductors. *Phys. Rev. B*, 92:245432, Dec 2015.

[164] K. Yavilberg, E. Ginossar, and E. Grosfeld. Fermion parity measurement and control in majorana circuit quantum electrodynamics. *Phys. Rev. B*, 92:075143, Aug 2015.

[165] M. C. Dartiailh, T. Kontos, B. Douçot, and A. Cottet. Direct cavity detection of majorana pairs. *Phys. Rev. Lett.*, 118:126803, Mar 2017.

[166] D. Nozadze and N. Trivedi. Compressibility as a probe of quantum phase transitions in topological superconductors. *Phys. Rev. B*, 93:064512, Feb 2016.

[167] S. N. Kempkes, A. Quelle, and C. Morais Smith. Universalities of thermodynamic signatures in topological phases. *Scientific Reports*, 6:38530–, December 2016.

[168] L. Fidkowski and A. Kitaev. Effects of interactions on the topological classification of free fermion systems. *Phys. Rev. B*, 81:134509, Apr 2010.

[169] L. Fidkowski and A. Kitaev. Topological phases of fermions in one dimension. *Phys. Rev. B*, 83:075103, Feb 2011.

[170] I. P. McCulloch. From density-matrix renormalization group to matrix product states. *Journal of Statistical Mechanics: Theory and Experiment*, 2007(10):P10014, 2007.

[171] F. Verstraete, V. Murg, and J. I. Cirac. Matrix product states, projected entangled pair states, and variational renormalization group methods for quantum spin systems. *Advances in Physics*, 57(2):143–224, 2008.

[172] U. Schollwöck. The density-matrix renormalization group in the age of matrix product states. *Annals of Physics*, 326(1):96 – 192, 2011. January 2011 Special Issue.

[173] D. Allen, P. Azaria, and P. Lecheminant. A two-leg quantum ising ladder: a bosonization study of the annni model. *Journal of Physics A: Mathematical and General*, 34(21):L305, 2001.

[174] S. Gangadharaiah, B. Braunecker, P. Simon, and D. Loss. Majorana edge states in interacting one-dimensional systems. *Phys. Rev. Lett.*, 107:036801, Jul 2011.

[175] E. Sela, A. Altland, and A. Rosch. Majorana fermions in strongly interacting helical liquids. *Phys. Rev. B*, 84:085114, Aug 2011.

[176] F. Hassler and D. Schuricht. Strongly interacting majorana modes in an array of josephson junctions. *New Journal of Physics*, 14(12):125018, 2012.

[177] R. Thomale, S. Rachel, and P. Schmitteckert. Tunneling spectra simulation of interacting majorana wires. *Phys. Rev. B*, 88:161103, Oct 2013.

[178] H. Katsura, D. Schuricht, and M. Takahashi. Exact ground states and topological order in interacting kitaev/majorana chains. *Phys. Rev. B*, 92:115137, Sep 2015.

[179] Y.-H. Chan, C.-K. Chiu, and K. Sun. Multiple signatures of topological transitions for interacting fermions in chain lattices. *Phys. Rev. B*, 92:104514, Sep 2015.

[180] N. M. Gergs, L. Fritz, and D. Schuricht. Topological order in the kitaev/majorana chain in the presence of disorder and interactions. *Phys. Rev. B*, 93:075129, Feb 2016.

[181] F. Iemini, L. Mazza, D. Rossini, R. Fazio, and S. Diehl. Localized majorana-like modes in a number-conserving setting: An exactly solvable model. *Phys. Rev. Lett.*, 115:156402, Oct 2015.

[182] N. Lang and H.P. Buechler. Topological states in a microscopic model of interacting fermions. *Phys. Rev. B 92, 041118*, 2015.

[183] Karyn Le Hur. Andreev scattering in the asymmetric ladder with preformed bosonic pairs. *Phys. Rev. B*, 64:060502, Jul 2001.

[184] A. C. Potter, T. Morimoto, and A. Vishwanath. Classification of interacting topological floquet phases in one dimension. *Phys. Rev. X*, 6:041001, Oct 2016.

[185] U. Dorner, P. Fedichev, D. Jaksch, M. Lewenstein, and P. Zoller. Entangling Strings of Neutral Atoms in 1D Atomic Pipeline Structures. *Physical Review Letters*, 91(7):073601, August 2003.

[186] J. Simon, W. S. Bakr, R. Ma, M. E. Tai, P.M. Preiss, and M. Greiner. Quantum simulation of antiferromagnetic spin chains in an optical lattice. *Nature*, 472(7343):307–312, 2011.

[187] L.S. Levitov, T.P. Orlando, J.B. Majer, and J.E. Mooij. Quantum spin chains and majorana states in arrays of coupled qubits. *arXiv:cond-mat/0108266*, 2001.

[188] B. M. Terhal, F. Hassler, and D. P. DiVincenzo. From Majorana fermions to topological order. *Physical Review Letters*, 108(26):260504, June 2012.

[189] R. Coldea, D. A. Tennant, E. M. Wheeler, E. Wawrzynska, D. Prabhakaran, M. Telling, K. Habicht, P. Smeibidl, and K. Kiefer. Quantum Criticality in an Ising Chain: Experimental Evidence for Emergent E_8 Symmetry. *Science*, 327:177, January 2010.

[190] A. C. Potter and P. A. Lee. Multichannel generalization of kitaev's majorana end states and a practical route to realize them in thin films. *Physical Review Letters*, 105(22):227003, November 2010.

[191] E. M. Stoudenmire, J. Alicea, O. A. Starykh, and M. P. A. Fisher. Interaction effects in topological superconducting wires supporting majorana fermions. *Phys. Rev. B*, 84:014503, Jul 2011.

[192] U. Ledermann and K. Le Hur. Phases of the two-band model of spinless fermions in one dimension. *Phys. Rev. B 61, 2497*, 2000.

[193] S. T. Carr, B. N. Narozhny, and A. A. Nersesyan. Spinless fermionic ladders in a magnetic field: Phase diagram. *Phys. Rev. B*, 73:195114, May 2006.

[194] J. S. Meyer, K. A. Matveev, and A. I. Larkin. Transition from a one-dimensional to a quasi-one-dimensional state in interacting quantum wires. *Phys Rev Lett. 98, 126404*, 2007.

[195] G. Roux, E. Orignac, S. R. White, and D. Poilblanc. Diamagnetism of doped two-leg ladders and probing the nature of their commensurate phases. *Phys. Rev. B 76, 195105*, 2007.

[196] H. Guo and S.-Q. Shen. Topological phase in a one-dimensional interacting fermion system. *Phys. Rev. B*, 84:195107, Nov 2011.

[197] F. H. L. Essler, H. Frahm, F. Göhmann, A. Klümper, and V. E. Korepin. *The one-dimensional Hubbard model*. Cambridge University Press, 2005.

[198] H. J. Schulz. Critical behavior of commensurate-incommensurate phase transitions in two dimensions. *Phys. Rev. B*, 22:5274–5277, Dec 1980.

[199] F. Pollmann, A. M. Turner, E. Berg, and M. Oshikawa. Entanglement spectrum of a topological phase in one dimension. *Phys. Rev. B*, 81:064439, Feb 2010.

[200] S. Bravyi, D. P. DiVincenzo, and D. Loss. Schrieffer-wolff transformation for quantum many-body systems. *Ann. Phys. Vol. 326, no 10, pp.2793-2826*, 2011.

[201] T. C. Hsu, J. B. Marston, and I. Affleck. Two observable features of the staggered-flux phase at nonzero doping. *Phys. Rev. B*, 43:2866–2877, Feb 1991.

[202] S. Chakravarty, R. B. Laughlin, D. K. Morr, and C. Nayak. Hidden order in the cuprates. *Phys. Rev. B*, 63:094503, Jan 2001.

[203] C. M. Varma. Proposal for an experiment to test a theory of high-temperature superconductors. *Phys. Rev. B*, 61:R3804–R3807, Feb 2000.

[204] A. Kaminski, S. Rosenkranz, H. M. Fretwell, J. C. Campuzano, Z. Li, H. Raffy, W. G. Cullen, H. You, C. G. Olson, C. . Varma, and H. Höchst. Spontaneous breaking of time-reversal symmetry in the pseudogap state of a high-T_c superconductor. *Nature*, 416:610–613, April 2002.

[205] J. Dalibard, F. Gerbier, G. Juzeliūnas, and P. Öhberg. Colloquium: Artificial gauge potentials for neutral atoms. *Reviews of Modern Physics*, 83:1523–1543, October 2011.

[206] I. Bloch, J. Dalibard, and W. Zwerger. Many-body physics with ultracold gases. *Rev. Mod. Phys.*, 80:885–964, Jul 2008.

[207] M. Atala, M. Aidelsburger, M. Lohse, J. T. Barreiro, B. Paredes, and I. Bloch. Observation of the meissner effect with ultracold atoms in bosonic ladders. *Nature Physics 10, 588-593*, 2014.

[208] A. Dhar, M. Maji, T. Mishra, R. V. Pai, S. Mukerjee, and A. Paramekanti. Bose hubbard model in a strong effective magnetic field: Emergence of a chiral mott insulator ground state. *Phys. Rev. A 85, 041602 (R)*, 2012.

[209] A. Petrescu and K. Le Hur. Bosonic mott insulator with meissner currents. *Phys. Rev. Lett. 111, 150601*, 2013.

[210] A. Petrescu and K. Le Hur. Chiral mott insulators, meissner effect, and laughlin states in quantum ladders. *Phys. Rev. B 91, 054520*, 2015.

[211] M. Piraud, F. Heidrich-Meisner, I. P. McCulloch, S. Greschner, T. Vekua, and U. Schollwoeck. Vortex and meissner phases of strongly-interacting bosons on a two-leg ladder. *Phys. Rev. B 91, 140406(R)*, 2015.

[212] A. Tokuno and A. Georges. Ground states of a bose-hubbard ladder in an artificial magnetic field: Field-theoretical approach. *New J. Phys. 16, 073005*, 2015.

[213] E. Cornfeld and E. Sela. Chiral currents in one-dimensional fractional quantum hall states. *Phys. Rev. B 92, 115446*, 2015.

[214] H. J. Schulz. Correlation exponents and the metal-insulator transition in the one-dimensional hubbard model. *Phys. Rev. Lett.*, 64:2831–2834, Jun 1990.

[215] Y. Ren and P. W. Anderson. Asymptotic correlation functions in the one-dimensional hubbard model with applications to high-t_c superconductivity. *Phys. Rev. B*, 48:16662–16672, Dec 1993.

[216] K. Le Hur. Critical ising modes in low-dimensional kondo insulators. *Phys. Rev. B, 60 9116*, 1999.

[217] P. Lecheminant and E. Orignac. Magnetization and dimerization profiles of the cut two-leg spin ladder. *Phys. Rev. B*, 65:174406, Apr 2002.

[218] E. Orignac and T. Giamarchi. Weakly disordered spin ladders. *Phys. Rev. B*, 57:5812–5829, Mar 1998.

[219] F. D. M. Haldane. Nonlinear field theory of large-spin heisenberg antiferromagnets: Semiclassically quantized solitons of the one-dimensional easy-axis néel state. *Phys. Rev. Lett.*, 50:1153–1156, Apr 1983.

[220] I. Affleck, T. Kennedy, E. H. Lieb, and H. Tasaki. Rigorous results on valence-bond ground states in antiferromagnets. *Phys. Rev. Lett.*, 59:799–802, Aug 1987.

[221] L.A. Takhtajan. The picture of low-lying excitations in the isotropic Heisenberg chain of arbitrary spins. *Physics Letters A*, 87:479–482, February 1982.

[222] H. M. Babujian. Exact solution of the one-dimensional isotropic Heisenberg chain with arbitrary spins S. *Physics Letters A*, 90:479–482, August 1982.

[223] B. Sutherland. *Beautiful Models: 70 Years of Exactly Solved Quantum Many-body Problems*. World Scientific, 2004.

[224] D. Loss. Parity effects in a luttinger liquid: Diamagnetic and paramagnetic ground states. *Phys. Rev. Lett.*, 69:343–346, Jul 1992.

[225] J. Nilsson, A. R. Akhmerov, and C. W. J. Beenakker. Splitting of a cooper pair by a pair of majorana bound states. *Phys. Rev. Lett.*, 101:120403, Sep 2008.

[226] K. T. Law, Patrick A. Lee, and T. K. Ng. Majorana fermion induced resonant andreev reflection. *Phys. Rev. Lett.*, 103:237001, Dec 2009.

[227] B. Béri. Nonlocal conductance reveals helical superconductors. *Phys. Rev. B*, 85:140501, Apr 2012.

[228] L. Fang, D. Schmeltzer, J.-X. Zhu, and A. Saxena. Tunneling Current Measurement Scheme to Detect Majorana Zero Mode Induced Crossed Andreev Reflection. *ArXiv e-prints*, May 2017.

[229] C. J. Bolech and E. Demler. Observing majorana bound states in p-wave superconductors using noise measurements in tunneling experiments. *Phys. Rev. Lett.*, 98:237002, Jun 2007.

[230] B. D. Josephson. Possible new effects in superconductive tunnelling. *Physics Letters*, 1(7):251 – 253, 1962.

[231] K. Kwon, H.-J.and Sengupta and V. M. Yakovenko. Fractional ac josephson effect in p- and d-wave superconductors. *The European Physical Journal B - Condensed Matter and Complex Systems*, 37(3):349–361, 2004.

[232] L. Fu and C. L. Kane. Josephson current and noise at a superconductor/quantum-spin-hall-insulator/superconductor junction. *Phys. Rev. B*, 79:161408, Apr 2009.

[233] J. Alicea, Y. Oreg, G. Refael, F. von Oppen, and M. P. A. Fisher. Non-Abelian statistics and topological quantum information processing in 1D wire networks. *Nature Physics*, 7:412–417, May 2011.

[234] P. A. Ioselevich and M. V. Feigel'man. Anomalous josephson current via majorana bound states in topological insulators. *Phys. Rev. Lett.*, 106:077003, Feb 2011.

[235] K. T. Law and P. A. Lee. Robustness of majorana fermion induced fractional josephson effect in multichannel superconducting wires. *Phys. Rev. B*, 84:081304, Aug 2011.

[236] L. P. Rokhinson, X. Liu, and J. K. Furdyna. The fractional a.c. Josephson effect in a semiconductor-superconductor nanowire as a signature of Majorana particles. *Nature Physics*, 8:795–799, November 2012.

[237] M. Veldhorst, M. Snelder, M. Hoek, T. Gang, V. K. Guduru, X. L. Wang, U. Zeitler, W. G. van der Wiel, A. A. Golubov, H. Hilgenkamp, and A. Brinkman. Josephson supercurrent through a topological insulator surface state. *Nature Materials*, 11:417–421, May 2012.

[238] D. M. Badiane, L. I. Glazman, M. Houzet, and J. S. Meyer. Ac josephson effect in topological josephson junctions. *Comptes Rendus Physique*, 14(9):840 – 856, 2013.

[239] J. B. Oostinga, L. Maier, P. Schüffelgen, D. Knott, C. Ames, C. Brüne, G. Tkachov, H. Buhmann, and L. W. Molenkamp. Josephson Supercurrent through the Topological Surface States of Strained Bulk HgTe. *Physical Review X*, 3(2):021007, April 2013.

[240] J. Wiedenmann, E. Bocquillon, R. S. Deacon, S. Hartinger, O. Herrmann, T. M. Klapwijk, L. Maier, C. Ames, C. Brüne, C. Gould, A. Oiwa, K. Ishibashi, S. Tarucha, H. Buhmann, and L. W. Molenkamp. 4π-periodic Josephson supercurrent in HgTe-based topological Josephson junctions. *Nature Communications*, 7:10303, January 2016.

[241] K. N. Nesterov, M. Houzet, and J. S. Meyer. Anomalous josephson effect in semiconducting nanowires as a signature of the topologically nontrivial phase. *Phys. Rev. B*, 93:174502, May 2016.

[242] B. I. Halperin, Y. Oreg, A. Stern, G. Refael, J. Alicea, and F. von Oppen. Adiabatic manipulations of majorana fermions in a three-dimensional network of quantum wires. *Phys. Rev. B*, 85:144501, Apr 2012.

[243] A. Golub, I. Kuzmenko, and Y. Avishai. Kondo correlations and majorana bound states in a metal to quantum-dot to topological-superconductor junction. *Phys. Rev. Lett.*, 107:176802, Oct 2011.

[244] M. Lee, J. S. Lim, and R. López. Kondo effect in a quantum dot side-coupled to a topological superconductor. *Phys. Rev. B*, 87:241402, Jun 2013.

[245] M. Cheng, M. Becker, B. Bauer, and R. M. Lutchyn. Interplay between kondo and majorana interactions in quantum dots. *Phys. Rev. X*, 4:031051, Sep 2014.

[246] L. Fu. Electron teleportation via majorana bound states in a mesoscopic superconductor. *Phys. Rev. Lett.*, 104:056402, Feb 2010.

[247] A. Zazunov, A. Levy Yeyati, and R. Egger. Coulomb blockade of majorana-fermion-induced transport. *Phys. Rev. B*, 84:165440, Oct 2011.

[248] B. van Heck, R. M. Lutchyn, and L. I. Glazman. Conductance of a proximitized nanowire in the coulomb blockade regime. *Phys. Rev. B*, 93:235431, Jun 2016.

[249] Z.-Q. Bao and F. Zhang. Topological Two-Channel Kondo Effect in Majorana Transistor. *ArXiv e-prints*, 2016.

[250] A. Golub and E. Grosfeld. Charge resistance in a majorana *rc* circuit. *Phys. Rev. B*, 86:241105, Dec 2012.

[251] M. Lee and M.-S. Choi. Quantum resistor-capacitor circuit with majorana fermion modes in a chiral topological superconductor. *Phys. Rev. Lett.*, 113:076801, Aug 2014.

[252] P. Krogstrup, N. L. B. Ziino, W. Chang, S. M. Albrecht, M. H. Madsen, E. Johnson, J. Nygård, C. M. Marcus, and T. S. Jespersen. Epitaxy of semiconductor-superconductor nanowires. *Nature Materials*, 14:400–406, April 2015.

[253] F. Buccheri, G. D. Bruce, A. Trombettoni, D. Cassettari, H. Babujian, V. E. Korepin, and P. Sodano. Holographic optical traps for atom-based topological kondo devices. *New Journal of Physics*, 18(7):075012, 2016.

[254] P. Nozières and A. Blandin. Kondo effect in real metals. *J. Phys (Paris)*, 41 (3):pp.193–211, 1980.

[255] E. Eriksson, A. Nava, C. Mora, and R. Egger. Tunneling spectroscopy of majorana-kondo devices. *Phys. Rev. B*, 90:245417, Dec 2014.

[256] E. Eriksson, C. Mora, A. Zazunov, and R. Egger. Non-fermi-liquid manifold in a majorana device. *Phys. Rev. Lett.*, 113:076404, Aug 2014.

[257] B. Béri. Majorana-klein hybridization in topological superconductor junctions. *Phys. Rev. Lett.*, 110:216803, May 2013.

[258] M. R. Galpin, A. K. Mitchell, J. Temaismithi, D. E. Logan, B. Béri, and N. R. Cooper. Conductance fingerprint of majorana fermions in the topological kondo effect. *Phys. Rev. B*, 89:045143, Jan 2014.

[259] A. Zazunov, A. Atland, and R. Egger. Transport properties of the coulomb-majorana junction. *New Journal of Physics*, 16(1):015010, 2014.

[260] A. Altland, B. Béri, R. Egger, and A. M. Tsvelik. Multichannel kondo impurity dynamics in a majorana device. *Phys. Rev. Lett.*, 113:076401, Aug 2014.

[261] A. Altland, R. Béri, R. Egger, and A. M. Tsvelik. Bethe ansatz solution of the topological kondo model. *Journal of Physics A: Mathematical and Theoretical*, 47(26):265001, 2014.

[262] F. Buccheri, H. Babujian, V. E. Korepin, P. Sodano, and A. Trombettoni. Thermodynamics of the topological Kondo model. *Nuclear Physics B*, 896:52–79, July 2015.

[263] S. Plugge, A. Zazunov, E. Eriksson, A. M. Tsvelik, and R. Egger. Kondo physics from quasiparticle poisoning in majorana devices. *Phys. Rev. B*, 93:104524, Mar 2016.

[264] K. A. Matveev. Quantum fluctuations of the charge of a metal particle under the coulomb blockade conditions. *Zh. Eksp. Teor. Fiz.*, 99:1598–1611, May 1991. [*Sov. Phys. JETP* **72,** 892 (1991)].

[265] K. A. Matveev. Coulomb blockade at almost perfect transmission. *Phys. Rev. B*, 51:1743–1751, Jan 1995.

[266] V. J. Emery and S. Kivelson. Mapping of the two-channel kondo problem to a resonant-level model. *Phys. Rev. B*, 46:10812–10817, Nov 1992.

[267] D. G. Clarke, T. Giamarchi, and B. I. Shraiman. Curie and non-curie behavior of impurity spins in quantum antiferromagnets. *Phys. Rev. B*, 48:7070–7076, Sep 1993.

[268] A. M. Sengupta and A. Georges. Emery-kivelson solution of the two-channel kondo problem. *Phys. Rev. B*, 49:10020–10022, Apr 1994.

[269] P. Coleman, L. B. Ioffe, and A. M. Tsvelik. Simple formulation of the two-channel kondo model. *Phys. Rev. B*, 52:6611–6627, Sep 1995.

[270] C. Mora and K. Le Hur. Probing dynamics of majorana fermions in quantum impurity systems. *Phys. Rev. B*, 88:241302, Dec 2013.

[271] Z. Iftikhar, S. Jezouin, A. Anthore, U. Gennser, F. D. Parmentier, A. Cavanna, and F. Pierre. Two-channel Kondo effect and renormalization flow with macroscopic quantum charge states. *Nature*, 526:233–236, October 2015.

[272] R. M. Potok, I. G. Rau, H. Shtrikman, Y. Oreg, and D. Goldhaber-Gordon. Observation of the two-channel kondo effect. *Nature*, 446(7132):167–171, 2007.

[273] A. J. Keller, L. Peeters, C. P. Moca, I. Weymann, D. Mahalu, V. Umansky, G. Zaránd, and D. Goldhaber-Gordon. Universal Fermi liquid crossover and quantum criticality in a mesoscopic system. *Nature*, 526:237–240, October 2015.

[274] I. Affleck and A. W. W. Ludwig. Exact conformal-field-theory results on the multichannel kondo effect: Single-fermion green's function, self-energy, and resistivity. *Phys. Rev. B*, 48:7297–7321, Sep 1993.

[275] H. Yi and C. L. Kane. Quantum brownian motion in a periodic potential and the multichannel kondo problem. *Phys. Rev. B*, 57:R5579–R5582, Mar 1998.

[276] H. Yi. Resonant tunneling and the multichannel kondo problem: Quantum brownian motion description. *Phys. Rev. B*, 65:195101, Apr 2002.

[277] K. Michaeli, L. Aviad Landau, E. Sela, and L. Fu. Electron Teleportation in Multi-Terminal Majorana Islands: Statistical Transmutation and Fractional Quantum Conductance. *ArXiv e-prints*, August 2016.

[278] L. Herviou, K. Le Hur, and C Mora. Many-terminal majorana island: From topological to multichannel kondo model. *Phys. Rev. B*, 94:235102, Dec 2016.

[279] A. Schmid. Diffusion and localization in a dissipative quantum system. *Phys. Rev. Lett.*, 51:1506–1509, Oct 1983.

[280] C. L. Kane and M. P. A. Fisher. Transmission through barriers and resonant tunneling in an interacting one-dimensional electron gas. *Phys. Rev. B*, 46:15233–15262, Dec 1992.

[281] P. W. Anderson. A poor man's derivation of scaling laws for the kondo problem. *Journal of Physics C: Solid State Physics*, 3(12):2436, 1970.

[282] I. Safi and H. J. Schulz. Transport in an inhomogeneous interacting one-dimensional system. *Phys. Rev. B*, 52:R17040–R17043, Dec 1995.

[283] D. L. Maslov and M. Stone. Landauer conductance of luttinger liquids with leads. *Phys. Rev. B*, 52:R5539–R5542, Aug 1995.

[284] P. W. Anderson, G. Yuval, and D. R. Hamann. Exact results in the kondo problem. ii. scaling theory, qualitatively correct solution, and some new results on one-dimensional classical statistical models. *Phys. Rev. B*, 1:4464–4473, Jun 1970.

[285] G. Toulouse. Infinite-u anderson hamiltonian for dilute alloys. *Phys. Rev. B*, 2:270–277, Jul 1970.

[286] K. A. Matveev. Charge fluctuations under the coulomb blockade conditions. *Physica B*, 203 3-4:404–408, 1994.

[287] I. Affleck. Conformal Field Theory Approach to the Kondo Effect. *Acta Phys. Polon.*, B26:1869–1932, December 1995.

[288] I. Affleck, M. Oshikawa, and H. Saleur. Quantum brownian motion on a triangular lattice and /c=2 boundary conformal field theory. *Nuclear Physics B*, 594:535–606, February 2001.

[289] I. Affleck, M. Oshikawa, and H. Saleur. Boundary critical phenomena in su (3) 'spin' chains. *Journal of Physics A: Mathematical and General*, 34(6):1073, 2001.

[290] I. Affleck, A. W. W. Ludwig, H.-B. Pang, and D. L. Cox. Relevance of anisotropy in the multichannel kondo effect: Comparison of conformal field theory and numerical renormalization-group results. *Phys. Rev. B*, 45:7918–7935, Apr 1992.

[291] G. Zarand, G. T. Zimanyi, and F. Wilhelm. Is the Multichannel Kondo Model Appropriate to Describe the Single Electron Transistor? *eprint arXiv:cond-mat/0003013*, March 2000.

[292] K. Le Hur and G. Seelig. Capacitance of a quantum dot from the channel-anisotropic two-channel kondo model. *Phys. Rev. B*, 65:165338, Apr 2002.

[293] S. Murakami. Phase transition between the quantum spin hall and insulator phases in 3d: emergence of a topological gapless phase. *New Journal of Physics*, 9(9):356, 2007.

[294] S. Murakami. Phase transition between the quantum spin hall and insulator phases in 3d: emergence of a topological gapless phase. *New Journal of Physics*, 10(2):029802, 2008.

[295] A. Chen and M. Franz. Superconducting proximity effect and majorana flat bands at the surface of a weyl semimetal. *Phys. Rev. B*, 93:201105, May 2016.

[296] P. Fendley. Parafermionic edge zero modes in z n -invariant spin chains. *Journal of Statistical Mechanics: Theory and Experiment*, 2012(11):P11020, 2012.

[297] P. Fendley. Free parafermions. *Journal of Physics A: Mathematical and Theoretical*, 47(7):075001, 2014.

[298] K. Snizhko, R. Egger, and Y. Gefen. Measurement and Control of Coulomb-Blockaded Parafermion Box. *ArXiv e-prints*, April 2017.

[299] G. Leoni. *A first course in Sobolev spaces.* Providence, RI: American Mathematical Society (AMS), 2009.

ÉCOLE DOCTORALE
Physique en Île-de-France (EDPIF)
université PARIS-SACLAY

Titre : Phases topologiques et Fermions de Majorana

Mots clefs : Topologie, supraconducteurs, fermions de Majorana, intrication, Kondo

Résumé : Dans cette thèse, nous étudions d'un point de vue théorique différents aspects de la matière topologique. Ces systèmes présentent des propriétés résistantes aux éventuelles perturbations grâce à une topologie non-triviale de leur structure de bandes. Des excitations exotiques, par exemple des fermions de Majorana, peuvent apparaitre à leurs bords. L'étude des marqueurs d'intrication a été fondamentale dans la compréhension de ces systèmes, et des phases libres en général. Il est cependant difficile de les mesurer. Les fluctuations de charge bipartites, permettant une mesure faible de l'intrication, ont été proposées comme alternative. Nous généralisons les précédents travaux sur les Liquides de Luttinger à des familles génériques de supraconducteurs et isolants topologiques en une et deux dimensions. Les fluctuations suivent une loi de volume, liée à l'Information Quantique de Fisher et non-analytique aux transition de phase. Leurs points critiques sont caractérisés par des coefficients universels, qui révèlent leur topologie.
Dans un second temps, nous considérons des systèmes en interactions. Certaines des signatures des transitions topologiques survivent dans les supraconducteurs topologiques. Nous étudions ensuite le diagramme de phase de deux fils supraconducteurs couplés par une interaction Coulombienne, présentant des phases exotiques grâce à la compétition avec la supraconductivité non-conventionnelle. Des courants orbitaux brisant spontanément la symétrie de renversement du temps peuvent apparaître, ainsi qu'une phase de fermions libres, extension de deux chaînes de Majorana critiques. Enfin, nous nous intéressons aux effets des fermions de Majorana sur le transport électronique. Nous étudions un îlot supraconducteur où plusieurs de ces fermions existent, pouvant être l'un des composants élémentaires d'un éventuel ordinateur quantique. Ces impuretés changent les statistiques des porteurs de charges, menant à une fractionalisation robuste de la conductance. Nous étendons les études précédentes au cas où le nombre d'électrons dans la boîte peut fluctuer, et montrons l'équivalence de ce problème avec le modèle Kondo à plusieurs canaux. Nous réinterprétons alors ce modèle en terme du déplacement d'une particule dans un réseau fictif dissipatif.

Title : Topological phases and Majorana fermions

Keywords : Topology, superconductors, Majorana fermions, entanglement, Kondo

Abstract : In this thesis, we study theoretically different aspects of topological systems. These models present resilient properties due to a non-trivial topology of their band structures, and in particular exotic edge excitations such as Majorana fermions. Entanglement markers have been fundamental to the study of these systems and of gapless systems in general, but are challenging to measure. Bipartite charge fluctuations were proposed as a weak measurement of entanglement entropy. We extend results on standard Luttinger Liquids to generic families of one- and two-dimensional non-interacting topological systems. A volume law arises, and is linked to the Quantum Fisher information, with non-analyticities at the phase transitions. Critical points are characterized by universal coefficients that reveal the topological aspect of the transitions.
In a second time, we include interactions and show that some of these signatures are preserved in interacting topological superconductors. Through analytical and numerical methods, we study two Coulomb-coupled topological superconducting wires. The interplay between unconventional superconductivity and strong interactions leads to exotic phases. We show the appearance of orbital currents spontaneously breaking the time-reversal symmetry, and of an unusual gapless phase that is the extension of two critical Majorana modes.
Finally, we focus on electronic transport mediated by Majorana fermions. We study a floating superconducting island carrying several such impurities, a potential building block for a quantum computer. The Majorana fermions affect the statistics of the charge carriers, which leads to very resilient fractionalized transport. We extend previous studies to the charge degenerate case and map it to the Multi-Channel Kondo model at large interaction, reinterpreted in terms of a particle moving in a high-dimensional, dissipative lattice.

Université Paris-Saclay
Espace Technologique / Immeuble Discovery
Route de l'Orme aux Merisiers RD 128 / 91190 Saint-Aubin, France